Deltares

Enabling Delta Life

Sediment transport in a fringing reef environment

Analysis using laboratory experiments and numerical modelling

Deltares

Sediment transport in a fringing reef environment

Analysis using laboratory experiments and numerical modelling

Willem Bodde

1202362-015

Keywords
Fringing reef, XBeach, hydrodynamics, morphodynamics, sediment transport, infragravity wave, seiching, flume experiment, FOSLIM, wave-induced set-up, bed friction

Summary
Coral reefs are highly valuable structures in many respects and it is increasingly important to understand hydrodynamics and morphodynamics around reefs to be able to better protect them and their hinterland. This study focused on fringing reefs and is part of a larger research program by the University of Western Australia. Flume experiments were performed on a scaled fringing reef in the laboratory facilities of Deltares in Delft. The objective of this thesis was to analyse the measurements from the morphological part of the study and to model the experiments using the numerical model XBeach in order to improve understanding of wave dynamics and sediment dynamics over reefs by analysing laboratory data and numerical modelling and to assess the ability of XBeach to model sediment transport in this case.

The hydrodynamic data was analysed and the specific conditions in a fringing reef environment(steep slope and high bed roughness) were shown to have influence on many processes such as short wave breaking, infragravity(IG) wave generation, IG wave transformation, seiching, wave-induced setup and wave reflection. The measurements showed that long waves dominate the short waves in the lagoon. The flow velocities in the rough cases were lower than that in the smooth cases as a result of the bed friction.

It was found that the specific hydrodynamics of a fringing reef environment are reflected in the sediment transport and in the bed profile development. The result of the sediment data analysis paints a very consistent picture in which both the short and the long waves play a role, but the long waves appear to be the dominant factor in sediment transport and bed profile development especially close to the beach. Also the effect of the bed roughness becomes visible, mainly in the shape of a swash bar which is different for rough and smooth cases. This shows that the dominance of long waves in a fringing reef lagoon results in different sediment dynamics than for example on a regular sandy beach.

The XBeach modelling reproduced the short wave height, flow velocity and the breakpoint mechanism rather well. The results for the long wave height and reef flat seiching agreed reasonably with the data. The effect of bed roughness on wave-induced set-up was found to be complex. In the experiments the roughness had no influence on the set-up while in XBeach the set-up increased significantly when using a high bed roughness value. This can possibly be solved by adding an extra force according to Dean and Bender (2006) to account for a shear stress exerted by the roughness elements on the water column counter to the direction of wave propagation. This could increase the application range of XBeach.

The use of XBeach and its default sediment transport formulation resulted in very little sediment suspension in the sandy lagoon which was in disagreement with the data. Also the development of the beach profile was not correctly predicted by XBeach. Further research is recommended to increase the ability of XBeach to model these processes.

Version	Date	Author	Initials	Review	Initials	Approval	Initials
	Sep 2013	W.P Bodde BSc		A.R. van Dongeren PhD		F.M.J. Hoozemans MSc	

State
final

Deltares

Sediment transport in a fringing reef environment

An analysis using laboratory experiments and numerical modelling

By Willem Bodde

A thesis submitted in partial fulfilment of the requirements for the degree of

Master of Science

in the field of

Civil Engineering

at

Delft University of Technology

Delft, The Netherlands

Graduation committee:

Prof.dr.ir. M.J.F. Stive	Chairman, Delft University of Technology
Dr.ir. M. Zijlema	Delft University of Technology
Dr.ir. A.R. Van Dongeren	Deltares
Dr.ir. J.S.M. Van Thiel De Vries	Deltares/Delft University of Technology
Ir. A.W.M. Pomeroy	University of Western Australia

Preface

This thesis was written as the conclusion of my education at the Faculty of Civil Engineering at the Delft University of Technology and was the final requirement to complete the master Hydraulic Engineering. Within this master I have followed the track of Coastal Engineering inspired by my passion for the sea and its coasts and the highly dynamic phenomena that come with them, of which the beauty and pure power of breaking waves remains unrivalled.

With this thesis I hope to extend the available knowledge about these phenomena in general and their interaction with coral reefs in particular in order to make a modest contribution to the protection and conservation of these valuable and magnificent structures.

The research for this thesis was conducted at the offices and laboratory facilities of Deltares in Delft, where I was involved in physical model experiments on a scaled coral reef in November 2012. The experiments were designed by the University of Western Australia as part of the PhD research projects of Mark Buckley and Andrew Pomeroy under the supervision of Ryan Lowe. The data collected during the experiments forms the basis of my thesis and I would like to thank the University of Western Australia, Mark Buckley, and Ryan Lowe, for financing this research and for the chance to work with their data and to discuss my results.

I would like to thank my supervisors at Deltares, Jaap van Thiel de Vries and especially Ap van Dongeren, for their enthusiastic, inspired and skilled supervision and input that made this thesis possible. I would also like to thank the other members of the graduation committee, chairman Marcel Stive and Marcel Zijlema. And many thanks to the one member residing overseas, Andrew Pomeroy, for answering my many e-mails and supplying me with all the data I needed.

Thanks to my fellow students at Deltares, who made me feel at home and with who I enjoyed many lunch breaks, coffee breaks and an occasional drink or two. I would also like to thank my friends for their support and the good times we have enjoyed, also during the writing of this thesis. A special thanks goes to Annemarie for all the good moments we had, for always being there for me and for teaching me many valuable lessons.

Finally I would like to thank my family for believing in me and supporting me throughout my study and my life. Thank you, Mathijs, for the many hours we spent together and for your advice on numerous subjects.

Willem Pieter Bodde,

Delft, September 2013

Acknowledgements:
The laboratory experiment forms part of a PhD study by A. Pomeroy and is supported by a Robert and Maude Gledden Postgraduate Research Award and The Gowrie Trust Fund. The experiment was funded by an ARC Future Fellowship Grant to Ryan Lowe and a UWA Research Collaboration Award to Andrew Pomeroy and Ryan Lowe. This work was funded in part by Deltares Strategic Research in the Event-driven Hydro- and Morphodynamics program (1202362.015).

Summary

Coral reefs are natural structures that have grown along stretches of coast in tropical and subtropical waters and as atolls encircling a lagoon in the open ocean. Coral reefs are highly valuable structures in many respects: they represent great ecological value, they often play a role in protecting the coast and beaches behind them and they offer many possibilities for recreation and tourism. It is increasingly important to understand hydrodynamics and morphodynamics around reefs to be able to better predict them, for example to assess the impact of sea level rise and dredging activities on the ecology and the protective function of coral reefs.

This study focused on coral reefs of the fringing type, which are reefs with a land backing that stretch along a coast and that often have a lagoon and a beach at their lee side. The study is part of a larger research program by two PhD students of the University of Western Australia into fringing coral reefs. In the context of this research, flume experiments were performed on a scaled fringing reef in the laboratory facilities of Deltares in Delft. The objective of this thesis was to analyse the measurements from the morphological part of the study and to model the experiments using the numerical model XBeach in order to:

'Improve understanding of wave dynamics and sediment dynamics over reefs by analysing laboratory data and numerical modelling'

The two main differences between a fringing reef coast and a regular sandy beach coast are the steep slope of the reef, followed by a reef flat and the high bed roughness of a coral reef. This study was particularly intended to understand the effect of these specific fringing reef features on hydrodynamics and in turn, of the hydrodynamics on sediment dynamics.

The experiments were performed on a scale 1:15 generic fringing reef in one of the flumes of Deltares. The flume dimensions were 55 x 1 x 1.2 m (LxBxH). The shape and dimensions of the reef, some terminology and the conditions used are presented in the figure below. In total four different runs of seven hours were performed, with and without roughness on the green dashed area and with 'deep' or 'shallow' water on the reef. The roughness was created by gluing concrete cubes of 1.8 cm to the smooth plywood covers. The lagoon and beach area had a sandy bottom. Measurements were performed of surface elevation, flow velocity, suspended sediment concentrations and bed profile development.

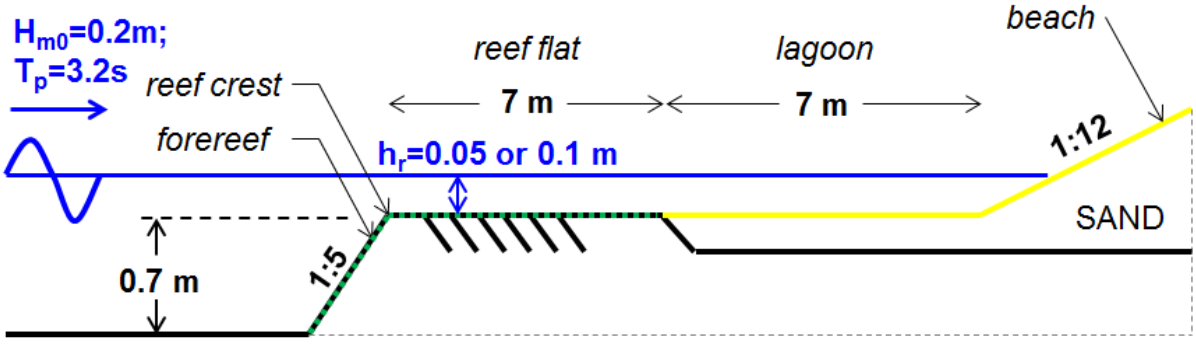

The hydrodynamic data was analysed and the specific conditions in a fringing reef environment were shown to have influence on many processes such as wave breaking, infragravity (IG) wave generation, IG wave transformation, seiching, wave-induced setup and wave reflection. The measurements showed that long waves dominate the short waves in the lagoon and that near the beach the short wave height for the different cases is grouped by water depth and the long wave height is grouped by bed roughness. The grouping by bed roughness was mainly related to the seiching on the reef flat, as the seiching was less strong for the cases with bed roughness. The flow velocities in the rough cases were lower than that in the smooth cases as a result of the bed friction.

For detailed analysis the long waves were separated into IG waves and very low frequency (VLF) waves. The VLF waves were found to consist of a reef flat seiching component and a component related to a very low frequency variation of the short wave height offshore. This could for example be relevant for understanding transient rip currents. The analysis also showed the importance of the breakpoint mechanism for generation of long waves at the breakpoint. In general the findings from the data analysis agree well with existing literature about long waves and hydrodynamics on reefs.

Also the concentration and profile measurements have been analysed and combined with the hydrodynamic data. It was found that the specific hydrodynamics of a fringing reef environment are reflected in the sediment transport and suspension and in the bed profile development. The effect of bed friction on long waves and of long waves themselves on sediment transport was shown in this report by analysing the third order flow velocity moment, which is related to wave skewness and sediment transport, by analysing correlations between hydrodynamic and sediment concentration time series and by analysing the bed profile development.

The result of these analyses paints a very consistent picture in which both the short and the long waves play a role, but the long waves appear to be the dominant factor in sediment transport and bed profile development especially close to the beach. Also the effect of the roughness elements becomes visible, mainly in the shape of a swash bar, which is different for rough and smooth cases. This shows that the dominance of long waves in a fringing reef lagoon indeed results in different sediment dynamics than for example on a regular sandy beach.

The concentration measurements as such were also analysed and showed that the optical concentration meters (FOSLIMs) were very sensitive to turbidity in the water, so it was decided to subtract a value from the measurements to account for this background turbidity. The resulting concentrations measured with the optical devices were approximately half of the values measured using a sediment suction sampler. All concentrations were depth-averaged and averaged over a simulation. Because of the high uncertainties regarding concentration measurements and the differences between the optical and the sampled concentrations, an order of magnitude agreement with the model XBeach was the goal of the numerical modelling part.

The flume experiments were modelled using XBeach to assess the ability of XBeach to model the hydrodynamics and morphodynamics. The calibration was based on the measured short wave height and the parameters of the breaker model of Daly et al. (2012) were used to reproduce the short wave transformation. The bed roughness was calibrated separately and it was shown that the best results were obtained for the current friction factor $c_f = 0.1$ and wave friction factor $f_w = 0.3$.

The XBeach modelling reproduced the short wave height, flow velocity and the breakpoint mechanism rather well. The results for the long wave height and reef flat seiching agreed reasonably with the data. The effect of bed roughness on wave-induced set-up was found to be rather complex. In the experiments the bed roughness had no influence on the set-up while in XBeach the set-up increased significantly when a high bed roughness value was used. According to Dean and Bender (2006) an extra force should be introduced that accounts for a shear stress exerted by the roughness elements on the water column counter to the direction of wave propagation. This force is caused by nonlinearity of the near-bed particle velocities. It is recommended to study this theory to implement it in XBeach. Their theory also included effects of vegetation on set-up, so this could increase the suitability of XBeach to model different cases.

The use of XBeach and its default sediment transport formulation resulted in very little sediment suspension in the sandy lagoon, which was in total disagreement with the data. Three solutions were proposed of which application of a current efficiency factor reducing the critical velocity to account for the effect of bed ripples was shown to be effective in increasing sediment suspension. Further research is needed to investigate whether it is physically correct to use such a factor, since it is rather obvious that reducing the critical velocity by any factor would increase sediment suspension. It is also recommended to look into other approaches to model sediment transport, such as the energetics approach, and to check whether the extra stirring by the oscillating flow velocity is sufficiently accounted for.

Besides the lack of suspension, the second issue that was found is that XBeach does not reproduce the formation of the swash bar. The swash bar is formed as waves run up the beach and carry sediment upslope. The experiment data shows that during run down not all of this sediment is moved down again and a bar is formed. Apparently XBeach is not capable of modelling this process as in the model sand is only eroded from the beach and a typical dune erosion slope is created. If the application of XBeach is to be extended to a wider range of application areas it is recommended to include the processes underlying swash bar formation in the model.

Contents

1 Introduction

1.1 Background

Coral reefs are natural structures that have grown along stretches of coast in tropical and subtropical waters and as atolls encircling a lagoon in the open ocean. Coral reefs are highly valuable structures in many ways. In the ecological sense they provide a strongly varied habitat to support a wide variation of species. They also have a function in protecting the coast and beaches behind them because they act as a natural breakwater as they dissipate the major part of the incoming wave energy. This wave energy can be significant during local storms and in case of the arrival of swells generated at longer distance. Another function of reefs is recreational as it often offers an environment that is attractive for divers and surfers.

Based on topography reefs have since long been categorised in three main categories (Darwin, 1842):

- Fringing corals reefs; consist of a reef with a land backing and sometimes a lagoon at the lee side of the reef.
- Barrier reefs; are detached from land and have large lagoons in their lee such as the Great Barrier Reef.
- Atolls; are reefs in the open ocean surrounding or partially surrounding a lagoon.

All three types of reef have in common that they have very steep slopes coming from deep water on the seaward side compared to sandy beaches with the crest of the reef usually around or just below mean sea level. The physical structure of the reef with the organisms living there is very rough, with the quadratic bottom friction coefficient K 20-70 times larger than on a sandy bed (Lugo-Fernandez et al., 1998).

Much of the hydrodynamic studies to date have been focussing on typical sandy beaches with mild slopes and smooth beds (Komar (1998) as cited in Lowe et al. (2005)) and not on coral reefs. Also very little research has been done in the area of morphodynamics and sediment transport on and behind a coral reef. Sandy beaches are quite different from the rough and steep sloped coral reefs. Therefore the dominant hydrodynamic and morphodynamic processes on and behind reefs might differ from those on beaches.

Morphodynamics are not so much related to change of the actual shape of the reef itself, as to the lagoon and sandy beach behind the reef. A good understanding of these processes on reefs is important because resulting currents play an important role in cross-reef transport of nutrients and sediment and because wave-induced forces play a role in determining ecology on the coral reef (Lowe et al., 2005). Better understanding morphodynamics and sediment transport on a reef can for example be important to improve environmental impact assessments for nearby dredging activities and to understand the effect of sea level rise.

1.1.1 Waves on coral reefs

Munk and Sargent (1948) were the first to report observations about setup over the coral reef of Bikini Atoll caused by wave breaking. They also identified the biological significance of the resulting wave-driven currents on coral reefs by creating different environments suitable for

different species, by supplying mineral nutrients and gases and by refreshing the water in the lagoon. Wave attenuation due to wave breaking over coral reefs is very strong and measurements show a large decrease in wave height from locations seaward of the reef to locations on the reef flat. The resulting large change in radiation stress causes significant setup over the reef (Young, 1989). A linear relation (with significant scatter) was shown between the incoming wave height and the current velocity on the reef. The current velocity is also related to the water depth over the reef. When the water is very shallow the currents will be weak, because the friction is strong and when the water is deep the currents will also be weak, because wave breaking is limited and the gradients in radiation stress will be small. Somewhere in between is a water depth for which maximum current velocities occur (Hearn, 1999).

Another finding of Young (1989) was a significant change in the shape of the wave spectra on the reef. The energy on the reef is redistributed across all frequencies. The observation that the wave spectra transform strongly over the coral reef was consistent with the findings of Lee and Black (1978) who found an increase of energy in the low frequency range during a field experiment on the coral reef of Oahu, Hawaii. The source of redistribution of energy towards the lower frequency is unclear, but it appears to be similar to surf beats observed elsewhere. Surf beat is a phenomenon which was first described by Munk (1949) who observed irregular oscillations of the near-shore water level that were correlated to fluctuations in the height and period of incoming waves. These oscillations were long waves moving offshore with periods in the order of 2-3 minutes. Later these waves were explained using the theory of Longuet-Higgins and Stewart (1962) about radiation stress, which explained the formation of *bound* long waves under wave groups. These waves are generated by the variation of wave height and therefore radiation stress under wave groups with waves of different frequencies. This variation causes a small set down of the water level under the higher waves in the group and a small setup under lower waves. This creates a long wave that travels with, and is bound to, the wave group. These long waves are released from the wave group at the short wave breakpoint and propagate towards the beach as free long waves where they reflect and propagate back in a seaward direction.

The generation mechanism of freely propagating long waves, or infragravity (IG) waves, in the nearshore is shown to be particularly strong for beaches with mild slopes and mild wave conditions (low short wave steepness) (Baldock, 2012). However, Baldock (2012) also showed that for steep slopes and steep waves another mechanism causes the generation of IG waves. On steep slopes there is insufficient time for the progressive release of the long forced waves. In that case IG waves can be generated by a breakpoint mechanism as proposed by Symonds et al. (1982). According to this theory long waves are generated by the temporal variation in breakpoint location of the short waves that travel in groups. The breakpoint moves up and down in onshore and offshore direction because the higher waves break farther offshore than the lower waves in a group. The moving breakpoint causes a varying forcing on the water column, which behaves comparable to a wave maker and will generate waves at the group period and its harmonics. Baldock (2012) proposed a surf beat similarity parameter to indicate the type of surf beat that is likely to dominate in different conditions. This parameter depends on the relative beach slope and the wave steepness.

Using a field study performed on the Ningaloo Reef in Western Australia Pomeroy et al. (2012) looked into the generation of free IG waves on the reef. The steep forereef slope of 1:20 resulted in a high value for the surf beat similarity parameter indicating that the breakpoint mechanism should be dominant for this situation. The presence of the breakpoint mechanism was confirmed with numerical modelling so the results are consistent with the

research done by Baldock (2012). Because coral reefs in general have very steep forereef slopes it would be likely that the breakpoint mechanism is the dominant mechanism generating IG waves on most reefs.

The early observations by Lee and Black (1978) and Young (1989) of energy redistribution towards lower frequencies already indicated that IG waves play a part in the hydrodynamics on a coral reef. Recent research by Van Dongeren et al. (2013) and the research of Pomeroy et al. (2012) is consistent with this and shows that the IG waves become dominant over the reef flat and in the lagoon. In the Ningaloo Reef field study the bottom shear stress caused by the IG waves accounts for up to 50% of the total shear stress and therefore it dominates over shear stress generated by short waves (<40%) and mean currents (up to 20%). For their research the numerical model XBeach (Roelvink et al., 2009) was used and it was shown that the model shows good skill in predicting IG waves on a fringing coral reef in 2DH mode. It was also shown that bottom friction dissipation is much lower for IG waves than for short waves and the presence of IG waves is strongly modulated by the tide, mostly due to friction dissipation rates varying with the water level. The last observation is consistent with the theory of Hearn (1999), that IG wave activity depends on the depth over the reef.

A challenge in modelling wave transformation over a coral reef is to find a good parameterization for wave dissipation due to wave breaking and bottom friction (Lowe et al., 2005). In their paper Lowe et al. (2005) investigated how to model bottom friction on a coral reef and they investigated the contribution of wave breaking and bottom friction to the total wave energy dissipation over the reef. They showed that the dissipation on the reef flat was dominated by friction rates that are much higher than those observed on sandy beaches. The frictional dissipation at different frequency components could be described using a spectral wave friction model using a single hydraulic roughness length scale. The energy dissipation increases as the wave frequency increases so low frequency waves experience less bottom friction. The hydraulic roughness length scale was shown to agree quite well with the physical roughness measured at the site. It became clear that dissipation on the forereef is dominated by bottom friction and wave breaking, with their contributions being comparable in magnitude. They even showed that under typical wave conditions the bulk of the dissipation of wave energy over the entire reef width is caused by bottom friction and not by wave breaking. Lowe et al. (2007) continued the research into bottom friction over a reef by looking into spectral wave flow attenuation within submerged canopies (very rough surfaces). Short period motions turned out to be more effective at driving a flow within a canopy than longer period motions. The rate of wave energy dissipation is linked to this flow structure within a canopy and is stronger for the shorter-period wave components. The dissipation by canopies is a function of the horizontal wave excursion amplitude A_{∞}. This again shows that the longer period, IG motions experience less bottom friction than short wave motions on a coral reef.

1.1.2 Sediment transport on and behind reefs

With high roughness values, steep slopes and IG motions dominating the bed shear stress over the flat, the dominant hydraulic processes on a coral reef are different than those on sandy beaches. This difference can be expected to have an impact on the morphodynamics of coral reefs, however little research has been conducted in this area.

Several sediment transport formulations have been proposed for bedload and suspended transport under combined wave-current action. For these formulations it is commonly thought that the waves stir up the sediment and the current transports it. They are generally applied to model sediment transport for cases with sandy beaches and their applicability to coral reefs is yet to be investigated. Below a short overview will be given of available sediment transport

formulations using the Delft3D-Flow manual (Deltares, 2012d) and the book of Soulsby (1997):

Van Rijn (1993)
This is the default transport formulation used in Delft3D. In this formulation a distinction is made between sediment transport above and below a reference height. Transport below the reference height is treated as bedload transport and transport above the reference height is treated as suspended load.

The concentration of suspended sediment in the water column is calculated from a reference concentration at the reference height. This concentration is determined using a critical bed shear stress calculated according to the Shields curve. Shear stress due to currents and waves is taken into account.

The bedload transport consists of a contribution by waves, currents and suspended sediment transport due to wave asymmetry effects. The wave and current contribution is calculated from a critical depth-averaged velocity based on the Shields curve.

Soulsby/Van Rijn (1997)
An adapted form of this formulation is used in the model XBeach, but is not the default formulation. It uses a velocity calculated from the depth-averaged current velocity and the root-mean-square wave orbital velocity, which is compared to a threshold critical velocity. The difference is multiplied by a factor consisting of a part for suspended transport and a part for bedload transport. Also slope effects can be taken into account in the formula.

The transport volumes calculated with this formula agree quite well with the Van Rijn formula. The values of Soulsby/Van Rijn are somewhat higher in the presence of wave action (Soulsby, 1997). The formula should be used for rippled beds only.

Van Rijn (2007)
This formulation is an updated version of Soulsby/Van Rijn and is the default transport formulation in XBeach. The formulation was updated based on more recent and more detailed datasets and the contributions of bed load and suspended load transport were separated. The option to include near-bed turbulence was also added.

Bijker (1971)
The formula of Bijker is still widely used in coastal areas. Bedload and suspended load are treated separately and depend on the wave orbital velocity amplitude and the depth-averaged current velocity. This formula does not use a critical velocity threshold for initiation of motion.

Soulsby (1997)
This is a transport relation based on different formulations provided in Soulsby (1997). It calculates non-dimensional transport as a function of a mean and an oscillating component for the Shields parameter, where the currents determine the mean and the waves the oscillating component.

Bailard (1981)
The total transport in the Bailard formula is made up of the sum of four terms: bedload transport on horizontal bed, slope effect on bedload transport, suspended load transport on horizontal bed and slope effect on suspended transport. For his formula Bailard uses the energetics approach in which the work done in transporting sediment is a fixed proportion of

the total energy dissipated by the flow. The formula gives the transport in one point and has to be integrated over the surf zone to get the total transport.

The formula gives better agreement with measurements for wave-dominated than for current-dominated conditions.

Grass (1981)
The formula of Grass was derived for sediment transport by looking at the turbulent kinetic energy caused by the waves and the currents. It uses empirical coefficients to fit the equation to site-specific data. The general form of the equation is $A*u^n$ and is basically the velocity to a certain power n. It should only be used for rippled beds and when $U_{rms}<U_{da}$.

The sediment transport formulae discussed above are for a large part empirically derived and a formula is thought to be useful when it predicts the transport order of magnitude correctly. The Bailard formula for example was shown to predict transport generally within a factor 5 and often within a factor 2 of the observed values (Soulsby, 1997).

In Storlazzi et al. (2009) the relevance of sediment for coral reefs becomes clear. High sediment concentrations and resulting turbidity can lead to decreased light availability for photosynthesis and can eventually lead to coral mortality. The accumulation of sediment at certain locations could stress the corals and coral colonies can be buried. In their research they show that due to the complex morphology of the coral reef strong hydrodynamic gradients occur which can cause large differences in deposition, re-suspension and advection of sediment on short spatial and temporal scales. They observed that potentially the most harm to the coral can be done by re-suspension of sediment by wave action due to its proximity to the corals and the long duration of the impact.

To further understand sediment dynamics on a coral reef Storlazzi et al. (2011) used Delft3D to model sediment transport over the Molokai fringing reef in Hawaii. They investigated the effect of sea level rise on the hydrodynamics and resulting sediment dynamics under the assumption that the water level over the reef would increase (the coral cannot keep up with rates of sea level rise). As a consequence of sea level rise they identified the following changes:

- Higher waves because of greater water depth over the reef. The waves can penetrate more easily on the reef flat moving the zone of primary wave breaking and high turbulence more shorewards.
- Increased current speeds, because of greater wave-driven flow from the larger waves and reduced hydrodynamic roughness.
- Greater resuspension of sediment because of the increased wave action on the reef. This will lead to higher and longer persistence of turbidity because the increased shear stress and turbulence inhibit sediment from settling. Another effect on sediment dynamics is that more wave energy reaches the coastline, which can lead to coastal erosion and additional sediment being added to the reef flat.

The research by Storlazzi et al. (2011) shows the importance of understanding hydrodynamic and morphodynamic processes on a coral reef and shows that the resulting suspended and settled sediment can have strong effects on coral reef organisms and ecology. They used the sediment transport formula of Van Rijn (1993) to compare sediment transport under different hydrodynamic conditions and various sea level rise scenarios. The results were not compared with measurements and were only used for comparison between scenarios.

The challenge for coral reefs is to find out how the high bottom friction values influence the (IG) waves on the reef and how these waves in turn affect the sediment transport. This would for example be possible by looking at the correlation between IG wave activity and suspended sediment concentrations in a flume experiment. Subsequently to model morphodynamics and sediment transport on and behind reefs, a suitable sediment transport formulation will have to be selected from the existing ones or possibly a new formulation will have to be worked out.

1.2 Objectives of this thesis

The aim of the research project of which this thesis is a part, is to further enhance the understanding of wave transformation over a coral reef and to increase the ability to model and parameterize processes such as wave breaking, bottom friction and sediment transport on reefs. This will eventually attribute to better predictions of waves, currents, sediment transport and ecological developments on a reef. The ability to predict is increasingly important to assess the impact of sea level rise and dredging activities on the ecology and the protective function of fringing coral reefs.

The research project is divided into a hydrodynamic and a morphodynamic part and is one of the first attempts to understand and model sediment transport on a coral reef. As part of the larger research project the objective of this thesis, which focuses on sediment dynamics, is to:

'Improve understanding of wave dynamics and sediment dynamics over fringing reefs by analysing laboratory data and numerical modelling'

The objective can be subdivided into the following parts:

- Analyse and process the data obtained from the experiments in the Eastern Scheldt Flume at Deltares, focussing on:
    - Low frequency spectral distribution and evolution over the reef
    - Correlation between incoming short waves and long waves on the reef
    - Suspended sediment concentrations
    - Correlation between IG wave activity and suspended sediment concentrations

- Setup and calibrate the numerical model XBeach to reproduce the hydrodynamics from the experiments

- Assess the ability of XBeach to simulate suspended sediment concentrations in the lagoon behind the reef using the default sediment transport formulation by comparing model results with the dataset from the flume experiments

- Use the simulations and data to identify relevant physical parameters for sediment transport in the lagoon, their relative contribution and to investigate the role of bottom friction through its effect on the IG wave climate

- Determine why the model reproduces the experiments well or not well

The research questions that will be answered are:

- How do waves transform over a smooth and rough fringing reef?

- How do the measured sediment concentrations and bed-profile developments relate to the hydrodynamics?

- How does the model XBeach with its default sediment transport formulas compare to the data?

- What improvements should be made to XBeach to improve the suitability to model cases comparable to the experiments?

1.3 Methodology

This thesis is part of a larger study into wave transformation and sediment transport over fringing coral reefs by the University of Western Australia in cooperation with Deltares. Experiments were conducted in the Eastern Scheldt flume at Deltares in Delft to obtain an accurate dataset of waves breaking, propagating and transforming and suspended sediment concentrations over a fringing coral reef. Laboratory conditions allow for very detailed measurements to be performed such that the processes over the reef can be studied in great detail. The flume experiments are also suitable to perform measurements in the surf zone where the waves are breaking, which can be difficult in field experiments because of the energetic conditions at that location. The aim of this study is to use the dataset from the experiments to better understand and describe wave transformation and sediment transport over a fringing coral reef.

Below the methodology for this thesis is outlined. The methodology describes the steps that were undertaken in order to achieve the goals as mentioned in the previous section. This research consists of three major parts:

- **Part 1: Literature review**
  Existing literature on wave transformation over coral reefs and sediment transport in general and on a reef was reviewed.

- **Part 2: Flume experiments and data analysis**
  Flume experiments in the Eastern Scheldt Flume at Deltares were performed with a setup representing a generic form of a fringing coral reef, see Figure 1.1. The experiments consisted of a hydrodynamic and a morphology part but only the morphology part is considered for this report, which are the two lower panels in the figure. The experiments consisted of 4 runs with varying water level and bed roughness. The bed roughness was created by placing concrete cubes on the smooth ‘reef’ surface in the flume.

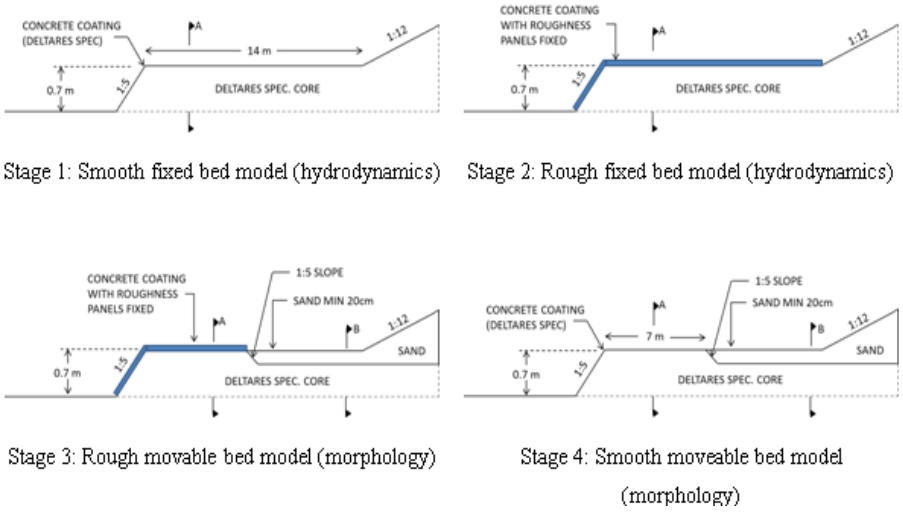

Figure 1.1 Set-up of experiments in the Eastern Scheldt Flume

During the experiment measurements were done on wave height, current velocity, sediment concentration and bed level development. This data was analysed and processed to be able to look at the processes that are happening on the reef, e.g. the incoming and the reflected signal were separated and wave spectra were generated to look at spectral evolution over the reef and phenomena such as resonance. The generation and transformation of IG waves was analysed in detail. To investigate the role of IG waves on sediment transport the correlation between measured IG wave activity and sediment concentrations is investigated. Also the development of the long and short wave flow velocity over the reef and the development of the bed profile is assessed.

- **Part 3: XBeach modelling**
  - **Part 3a: Compare XBeach with flume experiment**
    The first part of the modelling work with XBeach was to model the flume setup and conditions and compare the results with the results from the experiments. The comparison is made based on measured and simulated hydrodynamics, sediment concentrations and morphodynamics. The modelling is one-dimensional and assessed the performance of XBeach on sediment transport and concentrations.

  - **Part 3b: Identify relevant processes and influence of bottom friction**
    From the XBeach results and the flume results an analysis was performed to identify the processes that determine the suspended sediment concentration and to look at the effect of bottom friction on IG waves and of the IG waves on sediment transport.

  - **Part 3c: Look for improvements in the performance of XBeach**
    With the results from the comparison between XBeach and the experiment data possible improvements to XBeach are suggested.

1.4 Report outline

Chapter 2 provides a detailed description of the flume experiments. It describes the setup of the flume, the scaling of relevant physical quantities, the different runs that were performed and the measurements that were done.

In Chapter 3 the hydrodynamic data collected during the experiments is analysed in order to identify the dominant hydrodynamic processes in a fringing reef environment, related to the water level on the reef, bed roughness and the steep forereef slope.

Chapter 4 describes and analyses the morphodynamic data obtained from sediment concentration and bed profile measurements and relates the measurements to the hydrodynamic processes discussed in Chapter 3.

The suitability, setup, calibration and results of the XBeach model of the flume experiments are treated in Chapter 5. It assesses the ability of XBeach to model the hydrodynamics and morphodynamics observed during the experiments and when possible, uses the results to better understand these processes. It also provides recommendations for improvement of the model XBeach.

The conclusions and recommendations that follow from this study are presented in Chapter 6.

2 Description of experimental set-up

2.1 Introduction

The experiments took place in the Scheldt Flume at Deltares in Delft in October-December 2012. The flume has a total length of 110 m and is equipped with wave generators on both sides so it can also be split into two flumes of 55 m each, which was the case for the experiments performed for this project. The part of the flume that was used is referred to as the Eastern Scheldt Flume. The flume has a width of 1 m and is 1.2 m high from the false bottom to the rim of the flume. The wave generator is equipped with second-order (Stokes) wave generation and active reflection compensation. This means that waves with the correct higher and lower bound harmonics can be generated and that the reflected waves propagating towards the wave board can be absorbed by the paddle motion. The wave generator can generate waves with periods ranging from 0.5 to 100 s and with a maximum significant wave height H_{m0} of 0.25 m (Deltares, 2012c).

In the flume the profile of a fringing reef was constructed which is shown schematically in Figure 2.1 with some terminology that will be used throughout this report. The first part of the study focussed on the hydrodynamics over the reef. For this part also the lagoon and beach were constructed out of smooth plywood. Identical test runs were performed with both a smooth bed and a bed with high roughness on the reef flat and forereef (described below).

For the second part of the study sediment was introduced into the flume in the lagoon and beach area behind the reef flat to look at sediment transport and morphological processes. This was also done for cases with a smooth and a rough bed.

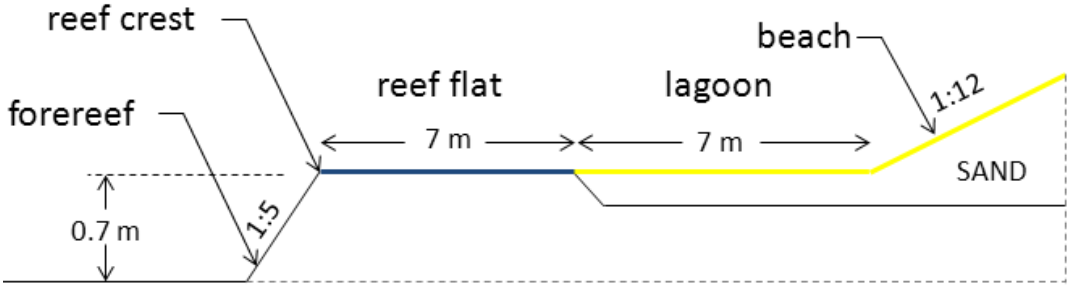

Figure 2.1 Schematic overview of the reef that was constructed in the flume with the terminology used for different sections of the reef

The topic of this thesis is sediment transport and therefore this report is focussed on the second part of the experiments, where the sediment has been introduced in the lagoon and beach area. For extensive treatment of the hydrodynamic experiments one is referred to Buckley (in prep). Some additional information about these runs can be found in appendix B of this report.

Below the setup of the flume and the reef will be described for the different stages of the experiment. Also the reasoning behind the scaling that was used is discussed. Subsequently the experimental program is presented with the runs that were performed during the entire study. Finally a description is given of all the measurements that were done and the devices and protocols that were used.

2.2 Flume setup

In the flume a generic model of a fringing coral reef, loosely based on Ningaloo Reef, West Australia, was constructed at a 1:15 scale. The structure is placed at one end of the flume and has a total length of 23.5 m and is constructed over the entire width of the flume. It consists of a horizontal approach (the false bottom), a 1:5 forereef slope from the bottom of the flume to a height of 0.7 m above the bottom, a horizontal reef flat of 7 m length, a lagoon with a sandy bed of 7 m length and a 1:12 sandy beach slope to the top of the flume at 1.2 m above the bottom.

The forereef slope and reef flat were constructed out of a plywood cover screwed on vertical plywood sheets placed along the glass walls of the flume. The cavity below the cover was filled with very coarse sand in order to provide stability of the structure and prevent return flow through the bed. Behind the reef flat a trench is left open and filled up with sand with a nominal diameter d_{50} of 115 mu creating a sandy bed lagoon. The result is the reef shape as shown in Figure 2.2.

The setup is different for simulation 1 and 2 than for simulation 3 and 4. For the first two simulations the smooth plywood covers were fitted with roughness elements consisting of concrete cubes of 1.8 cm spaced at 4 cm. In total approximately 8,000 concrete cubes were glued onto the covers by hand to achieve a hydraulic roughness comparable to real coral reefs, be it very schematised and regular. An impression of the reef sections with roughness elements is presented in Figure 2.3. For simulation 3 and 4 the covers with roughness elements are replaced by smooth covers to be able to compare sediment dynamics for a situation with a smooth and a rough bed on the forereef and reef flat.

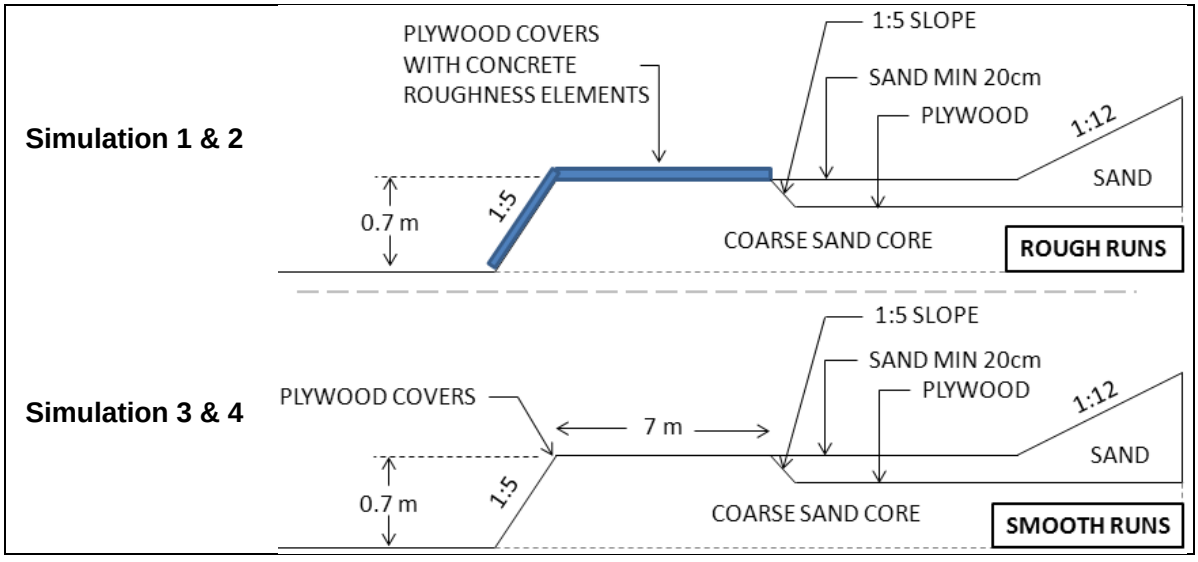

Figure 2.2 Schematic flume layout for the experiments

Figure 2.3 Impression of reef sections with concrete roughness elements

2.3 Scaling

In a flume study a scaled model of reality (or prototype) is used to collect data that is representative for the real situation. A flume offers a completely controlled environment, which enables one to focus on the phenomena of interest and keep other parameters constant at a desired level. A flume is also an ideal environment for detailed measurements at every location, while conditions in reality can be very energetic and make it very difficult to get good measurements, especially when looking at processes in the surf zone.

When scaling down a flow it is important to look at the dimensionless parameters that are most relevant for this type of flow, such as the Reynolds number and the Froude number. These numbers are important to scale down the hydrodynamics. To scale down sediment other parameters are important such as the grain size Reynolds number, the mobility number, the relative length criterion and the relative fall speed criterion (Hughes, 1993). In order to get a correct representation of the flow and morphodynamic processes, these parameter values should be kept constant as much as possible in the scaling process (the Reynolds number may be different as long as it remains in the turbulent regime). Since they often contain different physical quantities in nonlinear relations they can give rise to contradicting demands on the scaling of one quantity.

2.3.1 Scaling of hydrodynamics

When designing coastal scale models the Froude number is usually the most important criterion to be considered as inertial forces are primarily balanced by gravitational forces in these type of situations and the Froude number indicates the balance between these forces ($Fr = \frac{u}{\sqrt{gL}}$) Hughes (1993). Since we are dealing with a scale model of a coast Froude scaling was used for the hydrodynamics in this flume study.

Before looking at the scaling of different hydrodynamic quantities using the Froude number, first we define the scale ratio for a quantity x by: $N_x = \frac{x_p}{x_m}$ with x any physical quantity and subscript p and m indicating the prototype and the model value of x.

As mentioned above the Froude number in the model should be equal to the one in the model:

$$\left(\frac{u}{\sqrt{gL}}\right)_p = \left(\frac{u}{\sqrt{gL}}\right)_m \tag{2.1}$$

This can be rewritten to:

$$\frac{u_p}{u_m} = \sqrt{\left(\frac{g_p}{g_m}\right)\left(\frac{L_p}{L_m}\right)} \tag{2.2}$$

And then replaced by scale ratios:

$$N_u = \sqrt{N_g N_L} \tag{2.3}$$

By considering that the dimension of velocity is $\left[\frac{length}{time}\right]$, the scale ratio for velocity is N_L/N_t. This can be entered into the previous equation and rewritten, leading to:

$$N_t = \sqrt{\frac{N_L}{N_g}} \tag{2.4}$$

and $N_t = \sqrt{N_L}$ since g will be constant, stating that the scaling factor for time N_t is equal to the square root of the scaling factor for length N_L. The consequence is that the wave period with dimension of time has to be scaled by the square root of the length scale.

The selected length scale is 1:15 which was mainly determined based on the flume size, capabilities of the wave maker and the type of sediment to be used. For example the maximum was height that the wave maker can produce is 0.25 m so in order to maintain a realistic prototype wave height of several meters the scale factor cannot be much smaller. On the other hand, a larger scale factor would mean that the sediment scaling would be even harder, as discussed in the next section.

2.3.2 Scaling of sediment

According to Hughes (1993) for bed-load-dominated transport models the scale for the sediment grain size is equal to the length scale: $N_d = N_L$. In case of suspended load transport other processes become dominant and the correct scaling of the relative sediment fall speed and the mobility number of Shields become important. The relative fall speed is defined as $\omega = \frac{H}{w_s T}$ and indicates the relation between the particle fall velocity and the hydrodynamic conditions. The required scale relationships are as follows:

Mobility number criterion:

$$N_{mb} = \frac{N_\rho N_g N_L}{N_{\gamma_i} N_d} = 1 \tag{2.5}$$

Relative fall speed criterion:

$$\frac{N_\omega}{\sqrt{N_g N_L}} = 1 \tag{2.6}$$

The mobility number criterion reduces to $N_d = N_L = 15$ because all other ratios remain constant and the relative fall speed criterion reduces to $N_\omega = \sqrt{N_L} = 3.87$. It is clear that scaling the sediment (prototype d_{50} of 250-500 mu) by a factor 15 is impossible since that would lead to the use of cohesive sediment, which behaves completely different from non-cohesive sediment. It is even hard to achieve the 3.87 that follows from the fall speed criterion. Table 2.1 below shows that when using a d_{50} of 100 mu and assuming prototype d_{50} of 500 mu the relative fall speed criterion is only 0.885/0.371 = 2.38. Using a smaller d_{50} would mean that a fraction of the sediment is already in the cohesive regime.

Table 2.1 Rouse number and relative fall velocity for different sediment grain size diameter in prototype and model. The table on the right indicates which transport mode can be expected for different Rouse numbers

	Rouse Number	**Rel. fall velocity**
LWT Cases	**Rn = Ws / (k u*)**	**Vw**
Prototype (D50 = **500**)	2.21	0.885
Prototype (D50 = **250**)	1.11	0.442
Model (D50 = 100)	0.93	0.371
Model (D50 = 120)	1.09	0.436
Model (D50 = 150)	1.48	0.593
Model (D50 = 180)	1.91	0.762

Bed Load: >2.5
50% Susp: 1.2 - 2.5
100% Susp: 0.8 - 1.2
Wash Load: < 0.8

Above the classical scaling laws for suspended and bed-load dominated cases are described. An indication for the type of transport is given by the Rouse number which is a ratio between the sediment fall velocity w_s and an upwards velocity on the grain defined as the product of the von Karman constant κ and the shear velocity u_*: $R_n = \frac{w_s}{\kappa u_*}$ (Whipple, 2004). The right part of Table 2.1 shows which transport mode is dominant for different values of the Rouse Number. The prototype sediment grain size varies between 250 and 500 mu resulting in Rouse Numbers of 1.11 and 2.21 that fall in the range of 50-100% suspended transport so suspended transport is dominant in the prototype. The Rouse Number for different model values for the sediment grain size is calculated and falls within the same regime as the prototype values. It appears that in the prototype as well as in the model suspended transport is dominant.

It was already discussed above that the classical scaling laws for suspended load cannot be fully satisfied. It was therefore decided to go for a model d_{50} of 100-120 mu with a very narrow distribution in order to reduce the amount of fine and cohesive sediment as much as possible. Too much fine and cohesive sediment might cause high values of turbidity in the flume and make measurements with optical devices close to impossible. The table above shows that the Rouse Number for this type of sediment is about 1 and so the type of transport (mainly suspended) is conserved in the model, but since the prototype Rouse Number is between 1.11 and 2.21 it can be expected that the fraction of suspended transport in the model is higher than in prototype.

The sand for the flume experiments was obtained from the French supplier Sibelco and was of riverine origin with a d_{50} of 115 mu. The sieve curve is found in Figure 2.4 and shows that the sand has a very narrow distribution around the d_{50}.

2.3.3 Discussion

The classical model law for the relative fall speed velocity in combination with Froude scaling is the governing criterion for scale experiments reproducing surf zone profile response during erosive conditions according to Hughes (1993). The combination of this law with Froude

scaling preserves similarity in wave form, sediment fall path, wave-induced velocities, break point, breaker type and wave decay. However the bottom shear stress is not correctly scaled and this results in noticeable scale effects when wave breaking turbulence is **not** dominant in the domain being modelled.

In the area of interest, the lagoon and beach, it is indeed the case that wave breaking turbulence is not dominant and therefore scale effects are to be expected. These scale effects arise because the Shields parameter is not conserved and the turbulence is needed to bring sediment in suspension (Hughes, 1993). Without turbulence or with minimal turbulence the sediment suspension in the model will be much less than in prototype. Since the fall speed criterion was only partially fulfilled and the grain size in the model is larger than desired, the amount of suspension is in theory even more reduced in the model compared to the prototype, while according to the analysis of the Rouse number the fraction of suspended transport should be higher in the model than in prototype.

Besides this contradiction, there is some uncertainty regarding the differences between the type of sand that is used in the model and the type of sand present on a real reef. The sand that is used in the model is regular quartz sand whereas the sand of the reef will be made up of carbonate grains with a biogenic origin. Because of this biogenic origin the coral sand possibly consists of more irregular grains than the river sand, but this depends on the exact origin of the coral sand and the amount of weathering it has endured. The scale effects that might or might not arise are unclear, but it is important to keep in mind that they may be present.

This section about scaling of flow and sediment shows that with the contradicting parameters and the limitations of using a scaled research facility it is nearly impossible to get all the processes correctly scaled. In the experiments conducted for this research particularly the scaling of sediment was shown to lead to inevitable scale effects in the suspension of sediment particles. For the purpose of this thesis the scale effects are not insurmountable as no direct comparison is made to the prototype regarding the sediment measurements and the overall patterns that are observed are more relevant than the exact order of magnitude. The scale effects could become more obvious in the numerical modelling with XBeach.

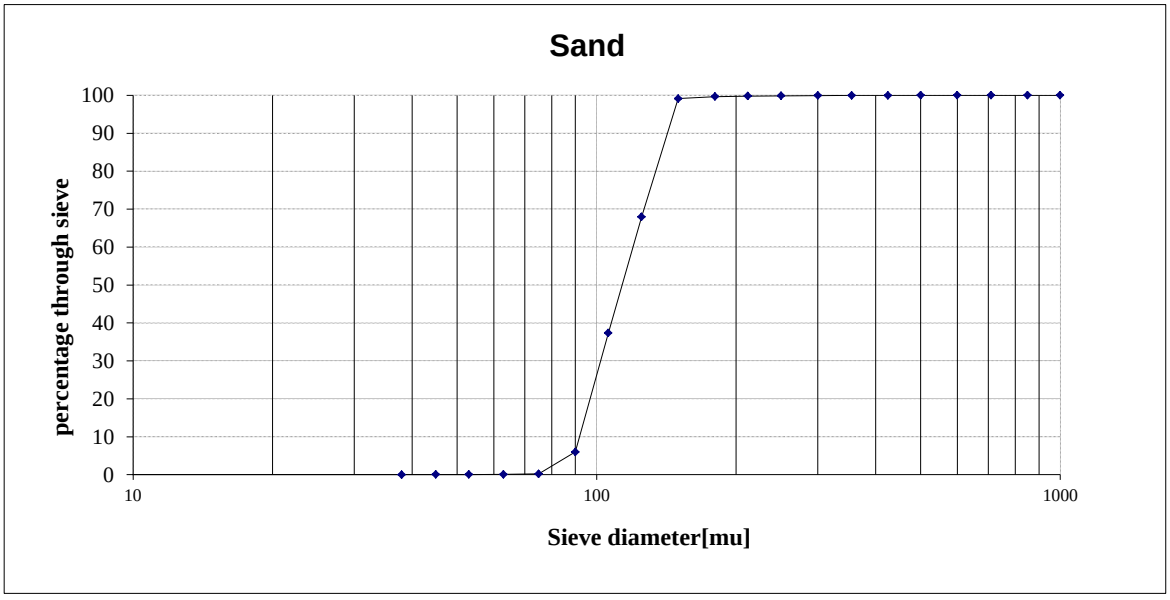

Figure 2.4 Sieve curve for the sand used in the flume experiments

2.4 Experimental program

The program of the morphological part of the experiments consisted of four simulations in total: for two different water depths on the reef (h_r); 0.05m and 0.1m (prototype 0.75 and 1.5 m), and for the rough and smooth reef flat topographies.

One wave condition was used with a significant wave height H_{m0} of 0.2 m (prototype 3 m) and a peak period T_p of 3.2 s (prototype 12.4 s). The wave generator was set such that it generated a ten-minute TMA-type wave spectra[1] and the total duration per condition was 7 hours to get significant morphological development. The ten-minute spectra enabled us to create vertical suspended sediment concentration distributions by moving the concentration measurement devices (FOSLIMs) up and down as explained further on. Each run was interrupted twice to let a profiler measure the cross-shore profile of the sandy part. Profile measurements were done before each run and after 1, 3, and 7 hours.

The schematic of Figure 2.5 and Table 2.2 show a summary of the conditions that were used. The green dashed line indicates the reef flat and forereef area that were fitted with roughness elements during simulation S01 and S02.

Because of the profiling interruptions each run consists of 3 parts. The first hour is referred to as part a, hour 2-3 is part b and hour 4-7 is part c (e.g. S01a, S03c). Simulation 3 had to be interrupted because the hard disk was full, hence an extra part d was used.

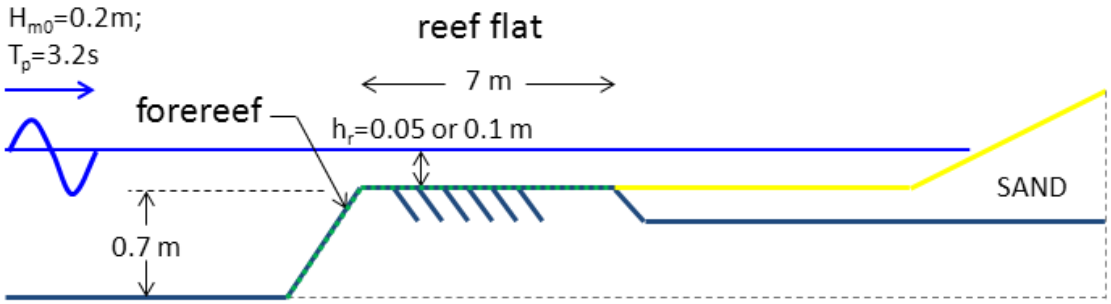

Figure 2.5 Schematic summary of different conditions during the experiments. The dotted green area indicates the reef flat and forereef where the roughness elements were applied in simulation S01 and S02.

Table 2.2 Overview of run ID's for the simulations. The conditions are target conditions and the actual, measured conditions may deviate.

Bed	**depth on reef(h_r): 0.1 m**	**depth on reef(h_r): 0.05 m**
rough	S01(a,b,c)	S02(a,b,c)
smooth	S03(a,b,c,d)	S04(a,b,c)
Target conditions for all runs: H_{m0}=0.2m; T_p=3.2s		

[1] *The TMA spectrum is a variation on the JONSWAP spectrum with a more generalised applicability from deep water to arbitrary-depth water as described in Holthuijsen (2007)*

2.5 Set-up of measurements

2.5.1 Introduction

The aim of the experiments is to obtain a very detailed dataset of waves propagating over a scaled coral reef to better understand hydrodynamics, morphodynamics and transport dynamics. In order to achieve this goal a large number of measuring instruments were positioned in and around the flume. Below, the type of instruments, the calibration, the placement and the measurement routines are treated. The instrumental setup to measure hydrodynamics such as waves and currents is discussed first. After that the measurements for the sediment concentrations are treated. Finally the measurement of the profile development of the sandy lagoon and beach will be described.

2.5.2 Hydrodynamics

To measure the hydrodynamics 18 wave height meters (WHM), 6 electromagnetic flow velocity meters (EMS) and a velocity profile meter (Vectrino II) were used. Below these instruments, the calibration and their positioning in the flume are described.

EMS flow velocity meters
An EMS flow meter uses the principle that a charge moving through an electromagnetic field causes a potential difference that is proportional to the velocity of that charge in the flow. The probe of an EMS is fitted with four electrodes to measure this voltage and the signal is converted to a flow velocity. The signal is obtained from the volume directly next to the probe and the electrodes, so the EMS measures the velocity at this one point. It measures both the velocity in cross-shore direction, u, and the alongshore velocity, v.

The EMS's are located at six locations along the flume and are centred. In Table 2.3 the exact position of each EMS is shown. x is the distance from the wave maker and y is the distance perpendicular to the centreline of the wave maker. Looking in positive x-direction y is positive to the left. z is the vertical position relative to the reef crest level.

Table 2.3 EMS positioning in the flume. x is the distance from the wave board, y is the distance perpendicular to the centreline of the wave board, z is the vertical distance relative to the reef crest and is positive upward.

EMS	x [m]	y [m]	z [m]	Direction of measurement
Shm11/12	16.28	0	-0.35	u,v
Shm21/22	29.54	0	-0.21	u,v
Shm23/24	32.34	0	0.01	u,v
Shm25/26	35.59	0	0.01	u,v
Shm27/28	40.14	0	0.04	u,v
Shm29/30	43.63	0	0.04	u,v

The flow velocity meters had already been calibrated by the manufacturer. The calibration was checked by Deltares personnel in a calibration flume and turned out to be correct and showed a linear relation between voltage and flow velocity in the range of interest. The two EMS's on the reef flat, Shm23/24 and Shm25/26, were attached to the bottom and therefore measuring in upward direction as opposed to the other EMS's that were hanging down into the water, measuring in downward direction, see Figure 2.6. After mounting the instruments in the flume the EMS measurements were compared with laser measurements which showed that there was no difference measuring in upward or downward direction.

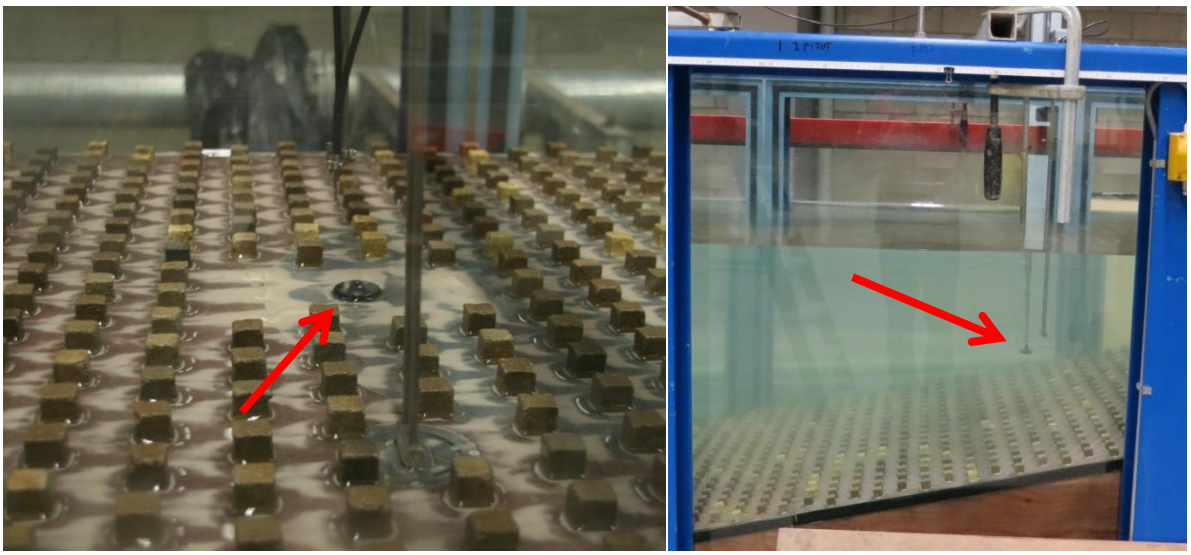

Figure 2.6 EMS flow velocity meter measuring in upward (left panel) and downward direction (right panel)

At the start of each run the voltage corresponding to zero flow velocity was checked and when necessary redefined in still water.

Wave height meters

To measure the waves and to be able to observe the spectral evolution of the waves over the reef eighteen wave gauges were used. The probe of the wave height meter consists of two parallel stainless steel rods mounted under a small box. The rods penetrate the water surface vertically and act as electrodes with the output voltage varying proportionally with the water level. The wave height meter is equipped with a reference electrode at the lower end of the rods which is used to compensate the measured water level for the effect of varying conductivity of the fluid (Deltares, 2012a).

The wave height meters (WHM) were placed in the flume at varying intervals. Two WHM's were placed offshore of the reef, while the other 16 were located above the reef slope or reef flat. Around the reef crest at x = 32.0 m the density of WHM's was highest to be able to observe the wave transformations in the surf zone in as great detail as possible. X is the distance from the wave maker and Y is the distance perpendicular to the centreline of the wave maker. Looking in positive x-direction y is positive to the left. In the table below the locations of the WHM's are given:

Table 2.4 Wave height meter positioning in the flume. X is the distance from the wave board, Y is the distance perpendicular to the centreline of the wave board.

WHM	X [m]	Y [m]		WHM	X [m]	Y [m]
Whm01	26.04	0		**Whm10**	32.94	0
Whm02	28.24	0		**Whm11**	34.24	0
Whm03	29.54	0		**Whm12**	35.59	-0.25
Whm04	30.24	0		**Whm13**	37.14	0
Whm05	30.84	0		**Whm14**	40.14	0.35
Whm06	31.11	0		**Whm15**	41.88	0.20
Whm07	31.30	0		**Whm16**	43.63	0.35
Whm08	31.69	0		**Whm17**	45.33	0.20
Whm09	32.34	-0.25		**Whm91**	16.28	0

To calibrate the wave height meters it was confirmed that each of them showed the same linear relation between the output voltage and actual wave height. Before each run the zero level was checked in still water and adjusted when necessary.

Velocity profile meter (acoustic Doppler velocimeter)
A Vectrino II was used to measure a velocity profile of the flow near the bed on the reef flat. The Vectrino II is an acoustic Doppler velocimeter (ADV) which uses ultrasound pulses to measure the flow velocity. The pulses are scattered by fine particles in the flow and four probes detect the Doppler shift in the signal which is proportional to the flow velocity (Uijttewaal, 2005). The Vectrino II is able to measure velocities in u, v and z direction over a vertical range of 3 cm with a resolution of 1 mm and a sampling rate of 100 Hz. It is equipped with software that also enables one to measure the distance to the bed (Nortek AS, 2012). This function was used in to look at vertical bed movement during the simulation.

The data collected with the Vectrino II was not used for this thesis.

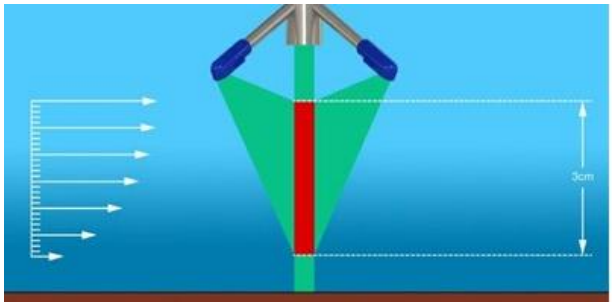

Figure 2.7 Vectrino II velocity profiling area (Nortek AS, 2012)

2.5.3 Sediment concentration measurements

The concentration of sediment in the flume is measured using multiple optical devices, called FOSLIMs, and using three sediment sampling devices.

FOSLIMs
The FOSLIM (Figure 2.8) is a device that measures concentrations of suspended matter at one point in the fluid using a near-infrared light beam. It measures the attenuation of this beam by reflection and absorption on the particles present in the fluid. After calibration it can determine concentrations of suspended sediment from the level of attenuation of the light beam.

Five FOSLIMs were placed on different cross-shore positions in the centre of the flume (Table 2.5). One was placed on the reef flat to measure the offshore transport of sediment. The remaining four devices were located above the sand bed in the lagoon. Since the FOSLIMs only measure the concentration at one location two of them were moved in the vertical direction at ten-minute intervals to get a vertical profile of the sediment distribution over the water column. Since a wave spectrum of ten-minutes is used the wave conditions determining the sediment concentrations will be exactly the same for each measurement period. Under the assumption that the effects of bed level changes on sediment concentrations can be neglected, a vertical sediment concentration profile can be created.

Figure 2.8 FOSLIM measuring probe (Deltares, 2012b)

Table 2.5 FOSLIM positioning in the flume. X is the distance from the wave board, Y is the distance perpendicular to the centreline of the wave board, Z is the vertical distance relative to the reef crest and is positive upward.

FOSLIM	X [m]	Y [m]	Z [m]
FOSLIM01	35.59	0.1	0.02
FOSLIM02	40.14	-0.2	0.02
FOSLIM03	41.88	-0.2	0.02
FOSLIM04	43.63	-0.2	0.02
FOSLIM05	45.33	-0.2	0.02

The FOSLIMs started measuring right before the first waves arrived at the start of a simulation and after interruptions to measure the cross-shore profile. At that moment the background turbidity that was still present in the water was measured. The FOSLIM devices are known to be sensitive to turbidity due to very fine particles and the measured concentration before the actual waves start, could be used in an analysis of the concentration signal as will be discussed further on in this report.

For each FOSLIM a voltage-concentration-curve was created in a calibration tank where the sediment concentration can be controlled very accurately. The curve was then used to convert the voltage signal measured during the experiments to a concentration signal.

Sediment sampling

Additional to the optical sediment concentration measurements water samples were taken from the flume during the experiments. The amount of sand in the samples was determined and converted to a concentration. The idea behind this manual sediment sampling was to have some values to compare the FOSLIM concentrations to and to make sure the order of magnitude of the FOSLIM concentrations is correct.

The samples were taken using a sediment sampling device consisting of multiple inlets aligned in vertical direction (Figure 2.9). The device will be referred to as multiple inlet suction sampler (or MISS) in this report. The multiple inlet suction sampler was positioned midway between FOSLIM03 and FOSLIM04 and the lowest inlet was positioned at 2 cm above the bed. A separate pump is connected to each inlet and by sucking in water through the inlets multiple samples of approximately one litre with a certain concentration of sediment are taken in at different levels in the water column. The filling takes approximately two minutes, so the sediment concentration is the averaged concentration over this period. The actual sediment concentration for each sample was determined by the following steps:

- Determine empty weight of the beakers
- Prepare Whatman ME27 membrane filters with 45 mu pores by placing them in aluminium trays
- Dry filters including tray for 1 hour at 105 °C and weigh afterwards
- Flush inlets by pumping out 500 ml of water before taking the actual sample

- Fill beaker up to 0.75 – 1 litre
- Weigh beaker with content and determine exact volume of water
- Lead beaker contents through the filters
- Flush beakers to make sure all the sediment is out
- Dry filters including sediment for 24 hours at 105 °C
- Weigh the samples to determine amount of sediment per sample
- Calculate the sediment concentration per sample

Apart from the multiple inlet suction sampler some single point samplers were used which use the same principle. The single point samples were taken at 2 cm above the bed at the location of WHM13 (x=37.14 m) and at x=33.26 m.

The tips of all inlet nozzles were directed horizontally and in the direction perpendicular to the plane of the wave orbital motion as described in Bosman et al. (1987). Investigating this transverse suction (TS) method, they found that it works well under two-dimensional wave conditions. They found that the measured concentrations should be corrected with a factor β depending on the sediment grain diameter d_{50} because the sediment trapping efficiency for this method is not 100%. Therefore the measured concentrations in our fringing reef experiments, using a d_{50} of 115 mu, were corrected by a factor of ~1.3 to obtain the actual concentration of sediment in the water.

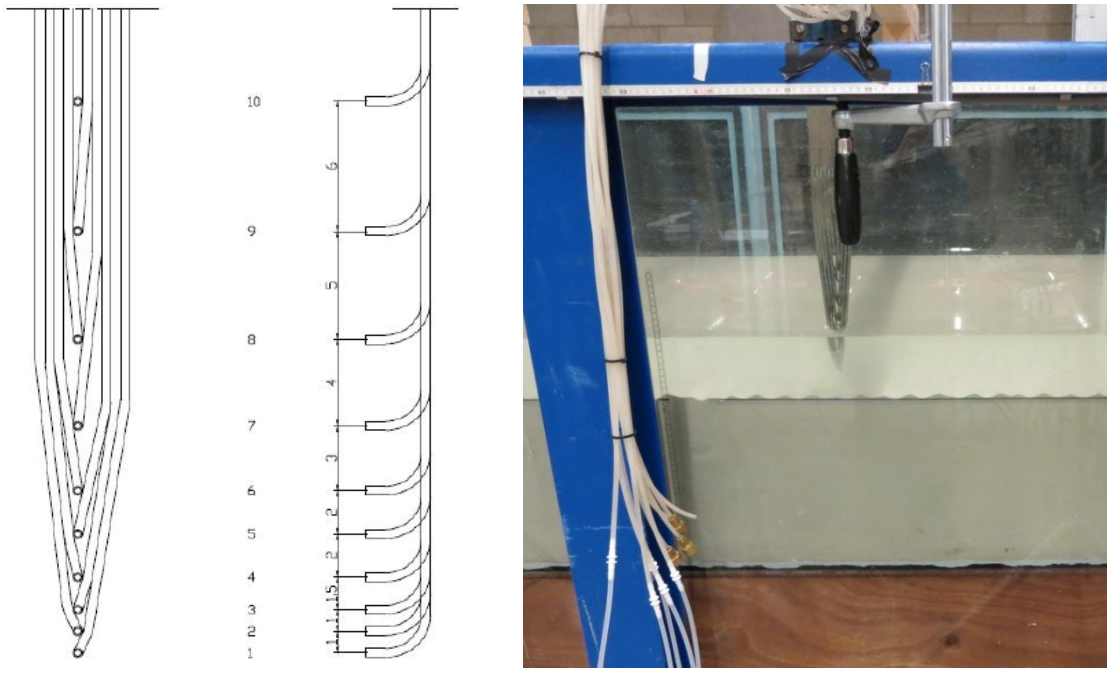

Figure 2.9 Left: Positioning and alignment of the inlets of the multiple inlet suction sampler (MISS). Right: photo of the MISS in the flume.

2.5.4 Bed profile measurements

During the tests the morphological developments in the lagoon and on the beach were monitored using several methods. The different methods are meant to complement one another, for cross-checking and to enable us to focus on specific locations or morphological phenomena (e.g. ripple formation).

Profiler

A custom made 3D profiler of Deltares was used to measure the cross-shore profile of the beach and the lagoon. The profiler moves step by step horizontally over rails on the edges of the flume using a stepper motor and measures the bottom level at each step. In this experiment it measured three profiles; one in the centre of the flume and two at a 0.3 m offset from the centre on both sides. The profile is measured using vertical rods that are lowered into the water until they feel the bottom. At the tip of the rods probes are attached that consist of a lightweight pin with a magnet on the tip. As the bottom is touched the pins are pressed in and the changing magnetic field is measured and amplified. When a certain threshold value is reached, so the pin is pressed in sufficiently, the motor moving the rod downward is stopped. The position of the motor is a measure for the position of vertical position of the rod. This position of the motor is read out by the measurement software controlling the profiler, returning the x-, y- and z-position of that point. Before each experiment a reference level is set by lowering the probes on a beam with a known height.

The advantage of measuring with a mechanical sensor is that it is possible to measure a profile below as well as above the water surface without any disturbance from reflections on the water surface or turbidity in the water.

Profile measurements were done before each run and at t = 1h, 3h and 7h. Before measuring the wave maker was stopped and the instruments above the lagoon were temporarily moved out of the flume in order for the profiler to move through. This took about 30 minutes each time after which the run would be continued. The strongest morphological developments were expected in the first hours, so the first profiles are taken at shorter time intervals.

Manual

Measurement strips were attached to the flume windows at 1 m intervals. Using these strips the height of the bed was measured manually which also enabled us the look at ripple formation. In case of ripple formation the height of the crest and trough of the ripple were written down. The height of the bed was determined every 10 minutes for the first hour, every 20 minutes for the two hours after that and every half hour for the last four hours. Here again the time interval between measurements increased during the run because less morphological change was expected at later stages.

Photo camera

Two cameras were placed next to the flume and set such that together they covered the entire beach slope and lagoon area. Every minute a photograph was taken of the level of the bed at the glass windows. The photographs were analysed with image processing software to enable us to follow the profile changes over time.

During each pause and at the end of each run pictures were taken manually of the profile of the lagoon and the beach from the side and top view. This was mainly to have images of the bed forms that were present.

Vectrino II

As mentioned before the Vectrino II is able to measure the vertical distance of the probe to the bed. This feature was used to collect data on the bed development around the transition from the lagoon to the beach slope.

2.5.5 Summary of instruments, positioning and measurements

Table 2.6 presents a summary of the positioning and type of the wave height meters, flow velocity meters and optical concentration meters in the flume. It shows which instruments are co-located and what their relative position is to different parts of the reef. The positioning of these instruments and their location numbers are visualised in Figure 2.10 by use of a colour coding which is explained in the caption. The position of the point samplers and MISS is also indicated.

Table 2.6 Grouping of different instruments in the flume per location

Location	X [m]	Wave height	Flow velocity	Sediment concentration	Position w.r.t. reef
1	16.28	whm91	shm11,shm12	-	Offshore
2	26.04	whm01	-	-	
3	28.24	whm02	-	-	Forereef slope at x=27.84-31.34
4	29.54	whm03	shm21,shm22	-	
5	30.24	whm04	-	-	
6	30.84	whm05	-	-	
7	31.11	whm06	-	-	
8	31.30	whm07	-	-	
9	31.69	whm08	-	-	Reef flat at x=31.34-38.34
10	32.34	whm09	shm23,shm24	-	
11	32.94	whm10	-	-	
12	34.24	whm11	-	-	
13	35.59	whm12	shm25,shm26	FOSLIM01	
14	37.14	whm13	-	-	
15	40.14	whm14	shm27,shm28	FOSLIM02	Lagoon with sandy bed at x=38.34-45.34
16	41.88	whm15	-	FOSLIM03	
17	43.63	whm16	shm29,shm30	FOSLIM04	
18	45.33	whm17	-	FOSLIM05	

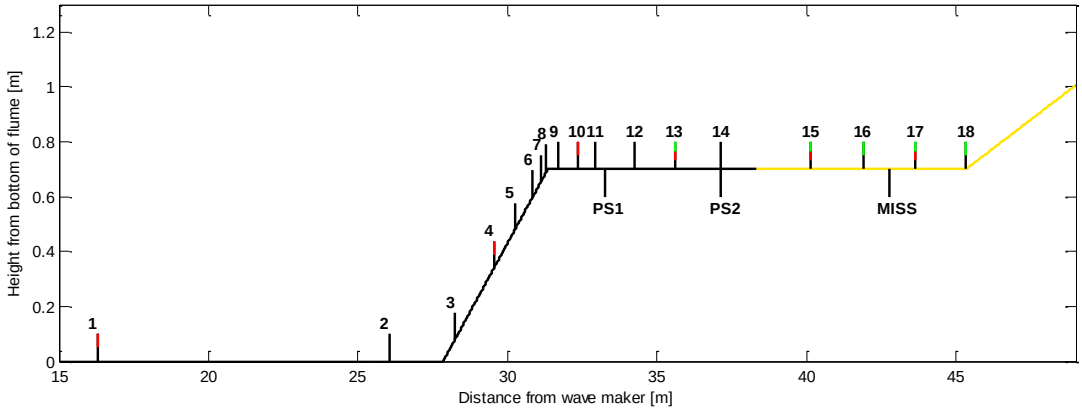

Figure 2.10 Overview of measurement locations. black line: WHM; red line: EMS; green line: FOSLIM; PS1 and PS2 indicate the location of point samplers 1 and 2 and MISS indicates the location of the multiple inlet suction sampler.

In Table 2.7 a summary of all measurement devices, required actions and the measurement frequency is shown.

Table 2.7 Summary of measurements and planning of actions

Instrument	Actions	Measurement frequency
FOSLIM	Move up/down FOSLIM02 and FOSLIM05	Continuous 40 Hz
Sediment sampler	t=0-1h: sample at t = 0.5 and 1 h t=1-3h: sample at t = 2 and 3 h t=3-7h: sample at t = 4.5, 6 and 7 h	Varies
Profiler	Profile at t = 0,1,3 and 7h	Varies
Measurement strips	t=0-1h: measure every 10min t=1-3h: measure every 20min t=3-7h: measure every 30min	Varies
Camera (automatic)	Photograph bed level	2 / minute
Camera (manual)	Photograph bed during interruptions of the runs and in the end	Varies
Vectrino II	Move device to different locations	Continuous 40 Hz
WHM	No actions	Continuous 40 Hz
EMS	No actions	Continuous 40 Hz

2.6 Data used in this thesis

Not all of the measurements described above were relevant for this thesis and its scope. The measurements that were used and will be treated below are the flow velocities, the wave heights and the concentration measurements, obtained by the FOSLIMs and the transverse suction samples. Also the ripple observations and the profile measurements are relevant for this thesis.

The remaining data did not fall within the scope of this thesis but could certainly be used to support and to further investigate part of its conclusions and to look into a range of different topics. Andrew Pomeroy and Mark Buckley are currently working on this as part of their PhD research at the University of Western Australia, so for further reading one is referred to their future publications.

3 Experiment data analysis: Hydrodynamics

3.1 Introduction

In this chapter analysis of the hydrodynamic data from the experiments is presented. The hydrodynamic data consists of surface elevation time series at 18 locations and flow velocity time series at 6 locations along the flume measured at 40 Hz. Using the time series the relevant hydrodynamic processes such as wave breaking, wave-induced set-up, short- and long-wave transformation, wave reflection and resonance are identified and analysed.

This chapter shows how the specific conditions in a fringing reef environment, i.e. high bed roughness and a steep forereef slope, affect these hydrodynamic processes by comparing the smooth and the rough cases and by using existing literature.

It is important to have a good understanding of the hydrodynamic processes that occur because it is these processes that will eventually cause the sediment to be stirred up and transported.

Section 3.2 starts with an explanation of the methodology used in this chapter to analyse the hydrodynamics. This section explains the concept of spectral analysis of waves and currents and separation of the signal into incoming and reflected and long and short wave time series.

Section 3.3 gives an overview of the data obtained from the measurements and some integral properties of the waves and currents that were derived from the data.

Subsequently section 3.4 uses the described methods to analyse the spectral evolution of total long and short wave height over the different reef sections and how this creates wave-induced set-up of the water level on the reef.

Next, section 3.5 categorises the long waves into infragravity (IG) and very low frequency (VLF) waves. The transformation of the IG waves is investigated focussing on reflection, dissipation, shoaling and breakpoint generation of these waves. For the VLF waves a relation is presented and described with a long period variation in the incoming short wave energy offshore.

Section 3.6 elaborates on reef flat seiching and shows that there is resonance on the reef flat at a frequency close to the eigen frequency of an idealised half-open basin. It also shows that there is a standing wave pattern in the entire flume.

Finally section 3.7 summarises the main findings and conclusions that can be drawn from this chapter.

3.2 Methodology

3.2.1 Spectral analysis

In order to analyse wave data and wave transformation variance density spectra are created from the time series. The variance density spectrum can be written as:

$$E(f) = \lim_{\Delta f \to 0} \frac{1}{\Delta f} E\left(\frac{1}{2} \underline{a_i}^2\right) \tag{3.1}$$

To obtain a correct variance density spectrum the surface elevation time series has to be stationary, meaning that the statistical properties of the signal such as the mean and standard deviation are constant for the selected time period. The first step in the analysis is therefore to find the period in which the surface elevation signal is stationary by determining the period in which the mean and standard deviation are constant. During the spin-up and spin-down the mean and standard deviation are varying and in between there is a long period with a stationary signal. For the following analysis only the stationary phase of the measurements is used.

To observe the evolution of waves over the reef use is made of the significant wave height H_{m0} and the root-mean-squared flow velocity u_{rms}. The significant wave height is found by looking at the variance of the energy density spectrum. The total variance of the spectrum is equal to the zeroth order moment of the spectrum m_0 expressed as $m_n = \int_0^\infty f^n E(f) df$. With m_0 the significant wave height H_{m0} can be found by $H_{m0} = 4 * \sqrt{m_0}$. The root-mean-squared wave height and velocity is found in a similar way: $H_{rms} = 2\sqrt{2} * \sqrt{m_0}$.

Spectral analysis is used throughout this chapter for example to create high or low pass filters that filter certain frequencies from the time signal in order to focus on processes that occur at these frequencies. It is also applied to separate incoming and reflected waves. Both applications will be explained in more detail in the sections to follow.

More details about the method of spectral analysis and the required Fourier transformations can be found in Appendix A.

3.2.2 Separation of incoming and reflected waves

The incoming waves will break on the forereef and on the beach behind the reef. At these locations not all wave energy is dissipated and part of the energy will reflect and propagate back towards the wave maker. The measured total surface elevation signals will therefore consist of incoming waves propagating shoreward and reflected waves propagating in offshore direction.

The total signal can be separated into its incoming and reflected component using co-located measurements of the surface elevation and the cross-shore velocity. The propagation velocity in the deeper parts of the flume is frequency-dependent via the dispersion relation (intermediate water depth: h/L>1/20). Therefore the separation of the signals for locations 1 and 4 is done in the frequency domain. On the reef the water is very shallow so all waves propagate with the same velocity. Then it is not necessary to go to the frequency domain, so for locations 10, 13, 15 and 17 on the reef the separation is done in the time domain (shallow

water depth: h/L<1/20 (Bosboom & Stive, 2011)). The methods are based on Guza et al. (1984) and will be discussed below.

3.2.2.1 *Separation incoming and reflecting waves in frequency domain*

For separation in the frequency domain the Fourier components, indicating the distribution of energy in the frequency domain, have to be obtained. The definition of the Fourier components of a time series is as follows:

$$F_n = \frac{1}{T}\int_0^T f(t)e^{-\frac{in2\pi t}{N\Delta t}}dt \tag{3.2}$$

Where N is the number of samples in the time series, $T = N\Delta t$ is the total length of the time series and Δt is the time interval between samples. The Fast Fourier Transform (FFT) takes advantage of several properties of the discrete time series when N is restricted to be a power of 2, i.e.: $N = 2^p$and p is an integer > 0 (Kirby, 1998). For details on the FFT algorithm the reader is referred to Cooley and Tukey (1965).

After performing the FFT on the wave gauge and EMS time series at one location the total value of each Fourier component F_n is the sum of the incoming and the reflected value:

Surface elevation: $F_\eta = F_{\eta,i} + F_{\eta,r}$ Flow velocity: $F_u = F_{u,i} + F_{u,r}$

Using the kinematic relations between wave height and flow velocity two extra equations are created: $F_{u,i} = \left(\frac{gk}{\omega}K_u\right)F_{\eta,i}$ and $F_{u,r} = -\left(\frac{gk}{\omega}K_u\right)F_{\eta,r}$ the four unknowns can be solved as follows:

Incoming surface elevation:

$$F_{\eta,i} = \frac{\frac{gk}{\omega}K_u F_\eta + F_u}{2K_u\frac{gk}{\omega}} \tag{3.3}$$

Reflected surface elevation:

$$F_{\eta,r} = \frac{\frac{gk}{\omega}K_u F_\eta - F_u}{2K_u\frac{gk}{\omega}} \tag{3.4}$$

Flow velocity under incoming wave:

$$F_{u,i} = \left(\frac{gk}{\omega}K_u\right)F_{\eta,i} \tag{3.5}$$

Flow velocity under reflected wave:

$$F_{u,r} = -\left(\frac{gk}{\omega}K_u\right)F_{\eta,r} \tag{3.6}$$

Where:

$K_u = \frac{cosh(k(h+zu))}{cosh(kh)}$	= velocity response factor
k	= wave number (2π/wave length L)
h	= local water depth
zu	= depth of velocity sensor below still water level (negative value)
F_η	= Fourier components of surface elevation; index i and r for incoming and reflected part
F_u	= Fourier components of flow velocity in u-direction; index i and r for incoming and reflecting part
g	= gravitational acceleration
ω	= cyclic frequency of the wave (2π/ wave period T)

K_u is a correction factor for the position of the velocity measurement in the water column as the wave induced flow velocity varies over the water depth, being highest near the surface and lowest near the bed.

Using the equations above the incoming and reflected frequency components of the velocity and surface elevation can be determined at the locations along the flume where an EMS is co-located with a wave height meter. By performing an inverse FFT on the incoming and reflecting components the incoming and reflected time series is obtained for the wave height and flow velocity.

3.2.2.2 Separation incoming and reflecting waves in time domain

Measurement locations 10, 13, 15 and 17 are in shallow water so the propagation velocity c no longer depends on the frequency and reduces to the shallow water asymptote: $c = \frac{\omega}{k} = \sqrt{gh}$. Also the velocity response factor is left out, because the flow velocity is assumed to be depth-uniform. The equations in the time domain are:

Surface elevation: $\eta = \eta_i + \eta_r$ Flow velocity: $u = u_i + u_r$
Again, using the constitutive relations this results in:

Incoming surface elevation:

$$\eta_i = \frac{\eta\sqrt{\frac{g}{h}} + u}{2\sqrt{\frac{g}{h}}} \tag{3.7}$$

Reflected surface elevation:

$$\eta_r = \frac{\eta\sqrt{\frac{g}{h}} - u}{2\sqrt{\frac{g}{h}}} \tag{3.8}$$

Flow velocity under incoming wave:

$$u_i = \sqrt{\frac{g}{h}}\eta_i \tag{3.9}$$

Flow velocity under reflected wave:

$$u_r = -\sqrt{\frac{g}{h}}\eta_r \tag{3.10}$$

Where:

η	= Surface elevation relative to mean total depth; index i and r for incoming and reflected part
u	= Flow velocity in u-direction; index i and r for incoming and reflecting part

Figure 3.1, upper panel shows the results of this separation method for measurement location 10. In this figure the total, incoming and reflected wave height is plotted in black, blue and red respectively. At some points the separation produces artefacts of which some are indicated in the figure with the green and black ellipsoids. At these peaks some of the total wave energy is allocated to the reflected wave, while it is very unlikely that these incoming and reflecting peaks would coincide in this way.
A possible explanation lies in the definition of the water depth h used in the above equation. The value of h used is constant at h_0 which is the water depth without any wave action. However, the waves generate a setup on the reef that increases the mean local water depth, which should be included in h.

Furthermore, on the reef flat the wave height is in the same order of magnitude as the water depth so under a wave crest the water depth can be double the value of the depth under a trough. Therefore the instantaneous value of h varies strongly and that will have an effect on the propagation velocity c (which is in the above equations via $\sqrt{\frac{g}{h}} = \frac{g}{\sqrt{gh}} = \frac{g}{c}$). Put differently: the waves will propagate in their own water depth. To account for these effects in shallow water Dingemans (1997) proposes the following formulation for the propagation velocity: $c = \sqrt{g(h+\zeta)}$ with $\zeta = H/2$.

This formulation can be implemented in the separation equations by defining the water depth as $h = h_0 + \eta$ where $\eta = \bar{\eta} + \tilde{\eta}$ so it consists of the mean set-up and an oscillating component by the waves. In the lower panel of Figure 3.1 the incoming and reflected waves are plotted as calculated with this adapted formulation. On the peaks indicated with the green ellipsoids the separation using $h = h_0 + \eta$ performs better than the one with $h = h_0$ as these peaks are now correctly allocated to the incoming wave. The improved performance also shows in the total variance of the incoming signal, contained in the parameter $H_{m0,i}$, as the value is increased. This means that over the entire time series a larger part of the total variance is allocated to the incoming signal. It is likely that this can be attributed to peaks in the surface elevation being correctly allocated to the incoming wave signal. The effect of including the instantaneous surface elevation is comparable on a different location on the reef, which is shown in Figure 3.2.

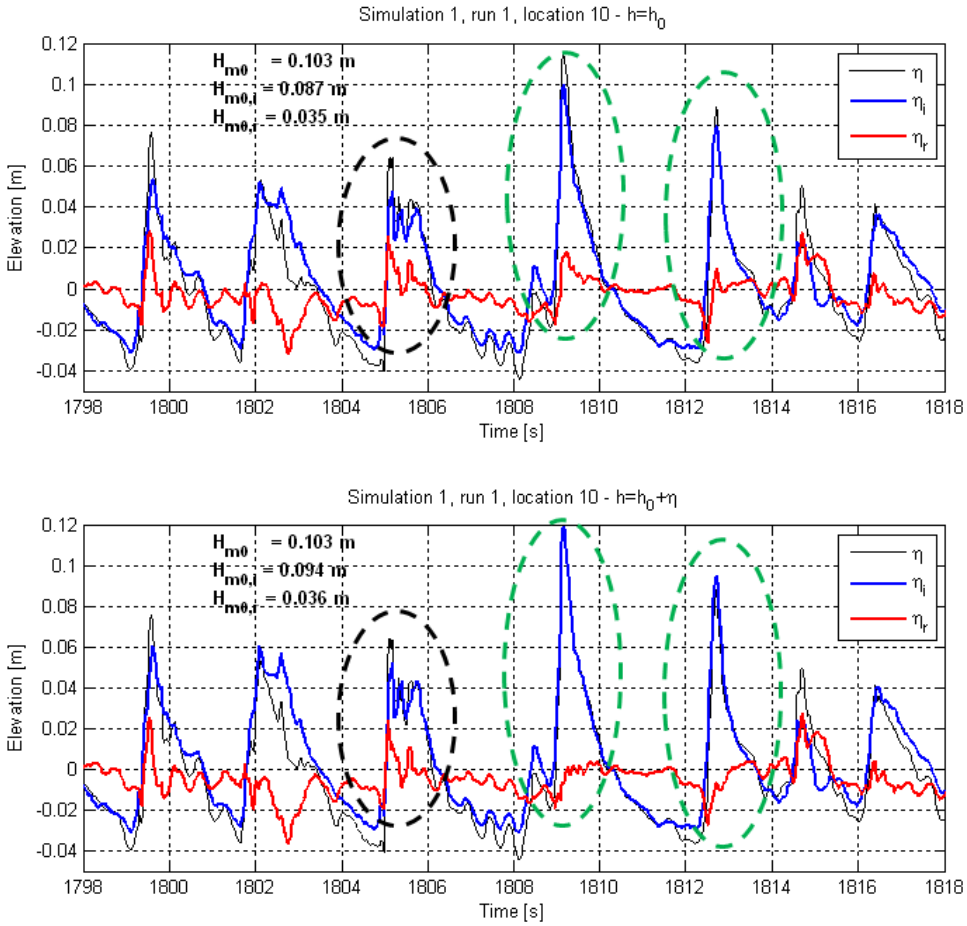

Figure 3.1 Separation of incoming and reflected surface elevation in the time domain; top figure is using a linear approach with $h=h_0$, the bottom figure uses $h=h_0+\eta_{tot}$ where η_{tot} includes the wave setup; location 10

Both figures also show that the separation including the instantaneous still creates artefacts at several peaks of which one is indicated with the black ellipsoid in Figure 3.1. In Figure 3.2 a more general pattern is visible of allocating part of the surface elevation to the reflected wave on most of the peaks. This is possibly due to the irregular shape of the waves. However, it is clear that defining the water depth as $h = h_0 + \eta$ improves the separation compared to using $h = h_0$; the peaks in the reflected surface elevation partly disappear or they become smaller.

The method used is based on the method of Guza et al. (1984) which is proposed for wave separation in shallow water. Therefore the results obtained with this method and by including the instantaneous surface elevation in the water depth, though not perfect, will be assumed to be sufficient for the purposes of this thesis. It is outside the scope of the thesis to look further into wave separation methods.

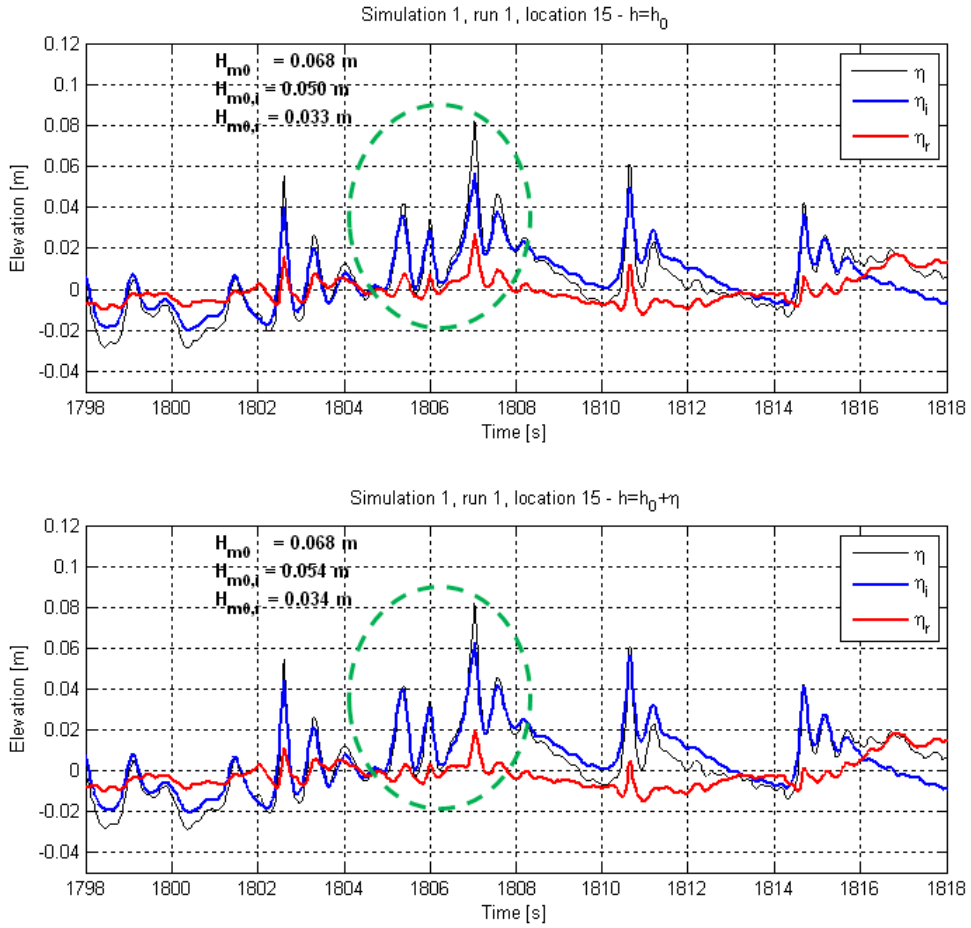

Figure 3.2 Separation of incoming and reflected surface elevation in the time domain; top figure is using a linear approach with $h=h_0$, the bottom figure uses $h=h_0+\eta_{tot}$ where η_{tot} includes the wave setup; location 15

3.2.3 Separation long and short waves

In the spectrum both long and short wave energy is represented. As part of the analysis of the wave activity and resulting sediment concentrations it is interesting to look at the dynamics of long or infragravity and short waves separately. Using the spectrum the low and high frequency motions can be separated. In order to do this first the offshore peak frequency f_p is determined, which is the frequency with the highest energy density. This peak frequency will be approximately equal to the target peak frequency that the wave maker is programmed to generate. Low frequency motions associated with infragravity waves are defined as motions with a frequency lower than the split frequency $f_{split}=f_p/2$ (Roelvink & Stive, 1989) above this value the motions are associated with short waves. This is visualised in Figure 3.3.

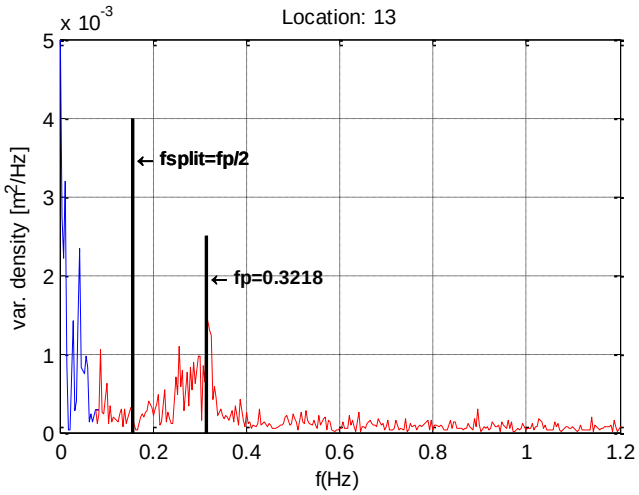

Figure 3.3 Variance density spectrum. The blue line represents long wave energy, the red line short wave energy. f_p is the offshore peak frequency.

The spectrum can be split up at this point and by performing an inverse FFT of the split spectrum we arrive back at a surface elevation signal with only long or short waves, see Figure 3.4.

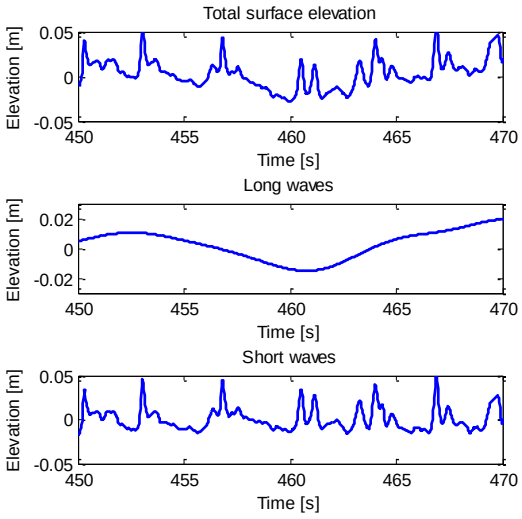

Figure 3.4 Total and long and short wave surface elevation

3.3 Data overview

3.3.1 General overview and information

Before analysing, the available raw data is inspected to assess the quality of the data, possible trends and deviations or errors. Figure 3.5 shows an example of the flow velocity and surface elevation measurements for the entire time series and for a period of 50 seconds for a close-up during run S01a at one location on the reef flat, and is representative of the entire dataset.

The measurements started just before the wave maker was turned on and the waves were gradually increased up to the intended significant wave height, so in all time series a spin-up can be observed. After stopping the wave maker the measurements continued for about 15 minutes to observe the spin-down, which is also visible in the time series. The stationary part of the time series shown is approximately 3600 seconds or 1 hour. All time series are measured at 40 Hz.

During the experiments instruments occasionally malfunctioned or were moved vertically for example because they were out of the water. This metadata was recorded in a log book. The data from those specific instruments is considered false and will not be used in the further analysis. This will be mentioned in the report when relevant.

It was found that the time series from the flow velocity meters is lagging behind the other measurements by 140ms. The velocity time series have been corrected for the time lag.

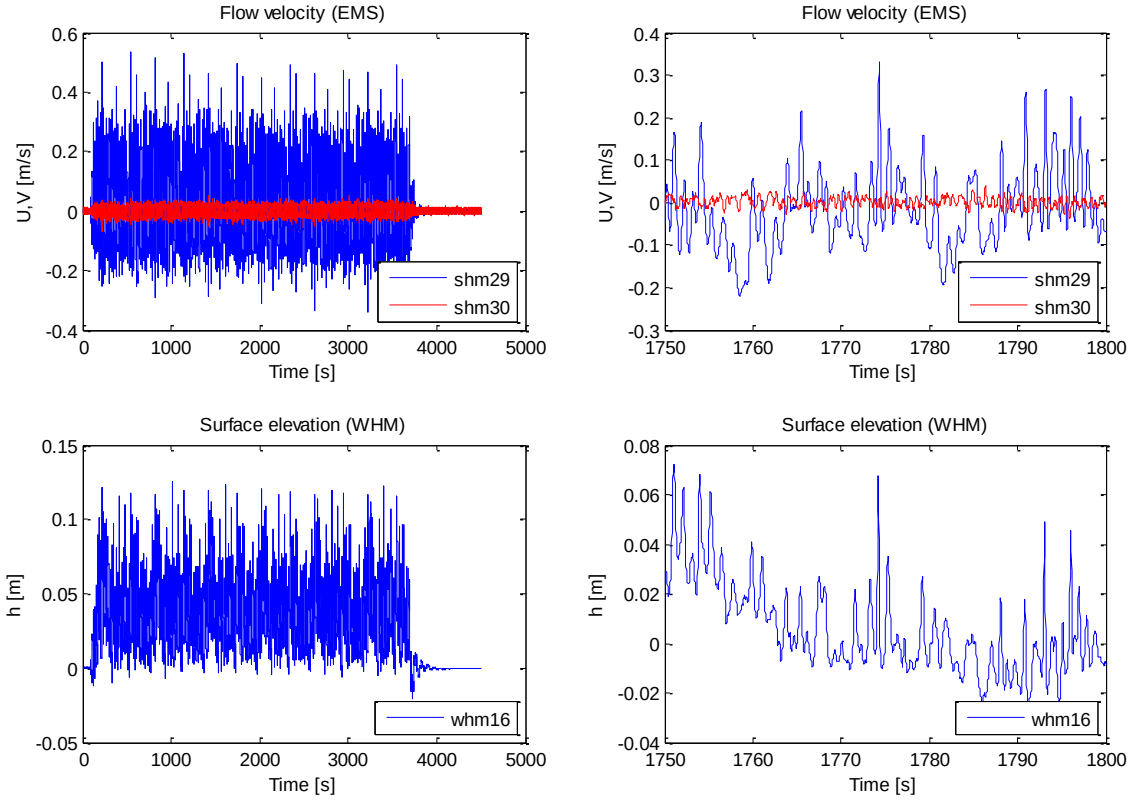

Figure 3.5 Overview of raw data available at measurement location 17. The blue line in the upper plots indicates the u-velocity, the red line indicates the v-velocity. Data is from run S01a.

3.3.2 Integral properties of surface elevation and flow

Hydrodynamic conditions are often represented in integral properties such as the significant wave height H_{m0}, peak period T_p, mean spectral period T_{m01} and root-mean-squared values of velocity or surface elevation. In Table 3.1 below some integral properties and target values are given for the experiments at the measurement location closest to the wave maker.

Table 3.1 Overview of wave parameters at location 1(offshore, closest to wave maker) for the first part of each run.

Location 1 (offshore)	S01a (rough,h_r=0.1)	S02a (rough,h_r=0.05)	S03a (smooth,h_r=0.1)	S04a (smooth,h_r=0.05)	Target value
$H_{m0,tot}$ [m]	0.215	0.217	0.216	0.218	-
$H_{m0,i}$ [m]	0.203	0.203	0.204	0.203	0.20
$H_{m0,r}$ [m]	0.048	0.055	0.054	0.062	-
f_p [Hz]	0.322	0.315	0.315	0.322	0.3125
Reflection coefficient: $H_{m0,r}$ / $H_{m0,i}$	0.236	0.271	0.265	0.305	-
T_p [s]	3.105	3.171	3.172	3.105	3.2
T_{m01} [s]	3.335	3.533	3.422	3.616	-
$u_{rms,total}$ [m/s]	0.147	0.154	0.148	0.157	-
$u_{rms,i}$ [m/s]	0.146	0.153	0.146	0.153	-
$u_{rms,r}$ [m/s]	0.041	0.047	0.044	0.052	-
$v_{rms,total}$ [m/s]	0.032	0.029	0.032	0.028	-

The target values of 3.2 s for the peak period and 0.20 m for the significant wave height are closely approached in the experiments. The reflection of wave energy on the reef appears to be significant varying between 23 and 31 per cent of the incoming wave energy. Reflection is slightly stronger for the smooth cases compared to the rough cases and for the cases with $h_r = 0.05\ m$ to the cases with $h_r = 0.1\ m$. The development of the reflection coefficient over the reef is visualised in Figure 3.6. On the reef flat the reflection is up to 80%, mainly because of long wave reflection and resonance on the reef flat. This will be explained further on section 3.5.1 on infragravity wave transformation and 3.6 on reef flat seiching.

The reflective wave height increases from the reef to offshore as 23 to 30% of the incoming short waves reflect on the reef edge. However, the reflection coefficient is lower, because the incoming short wave height is much higher offshore. The reflection coefficient shows that reflected waves are relatively more important on the reef flat.

The rms-values of the flow velocities in v-, or alongshore, direction are much smaller than those in u-, or cross-shore, direction. Since the velocity meters were located along the central axis of the flume the negligible cross-tank velocities indicate that there is no cross-tank standing modes present. The experiments will therefore be considered as a one-dimensional situation.

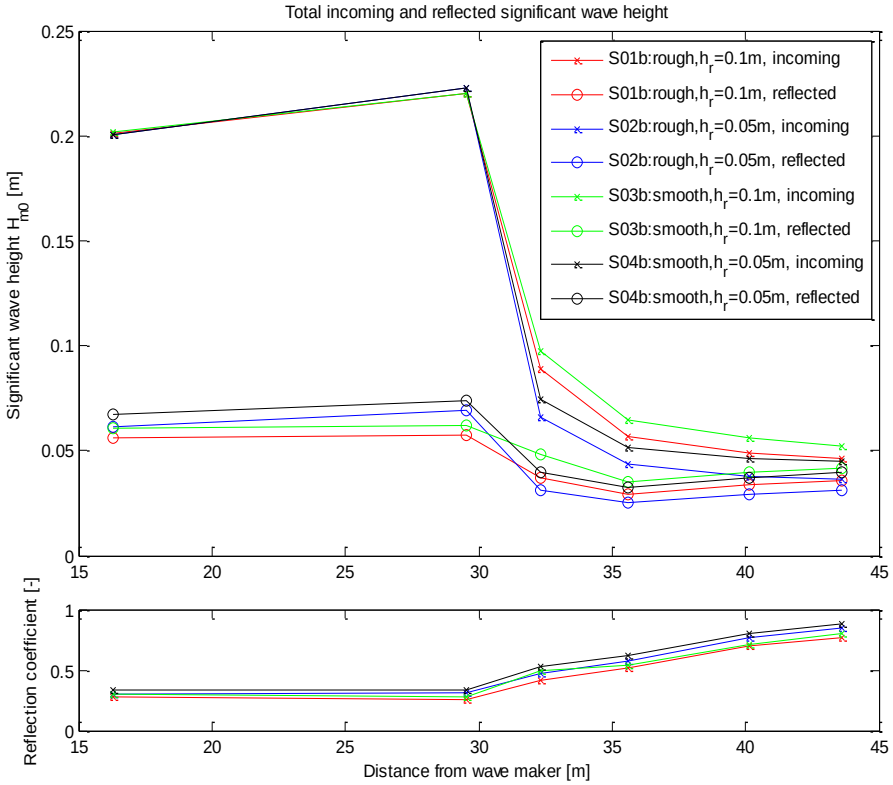

Figure 3.6 Incoming and reflected total wave height and reflection coefficient for all four simulations.

3.4 Total spectral evolution over the reef

The wave maker is programmed to generate waves with a peak period T_p of 3.2s and a significant wave height H_{m0} of 0.20m using a TMA-type wave spectrum that is repeated every 10 minutes. When the waves propagate towards and over the reef the spectrum will change its shape because of processes such as bottom friction, shoaling and wave breaking. In this section the effect of the reef on this spectral evolution is analysed by visualising the significant wave height, mean water level and flow velocity over the reef and by comparing the different cases.

3.4.1 Total long and short wave surface elevation

Figure 3.7 shows the variance density spectra of the total surface elevation for 8 locations in the flume for test S01a. The red part of the line indicates the short wave energy and the blue line indicates the long wave energy. Long waves are defined as motions with a frequency lower than half the peak frequency (Roelvink & Stive, 1989), above this value the motions are associated with short waves. These spectra give a first rough image of the processes that play a role in the spectral evolution over the reef:

- the effect of shoaling is evident at locations 4 and 6 on the reef slope, where the wave energy is increased
- the strong decrease in the energy closer to the crest of the reef, at locations 8 and 10, is indicative of wave breaking and possibly dissipation by bottom friction
- further up the reef the short wave energy continues to be dissipated, but the long wave energy is strongly increased when comparing location 8 to 16 near the end of the reef flat

Below the spectral evolution is analysed in more detail and the above observations are worked out.

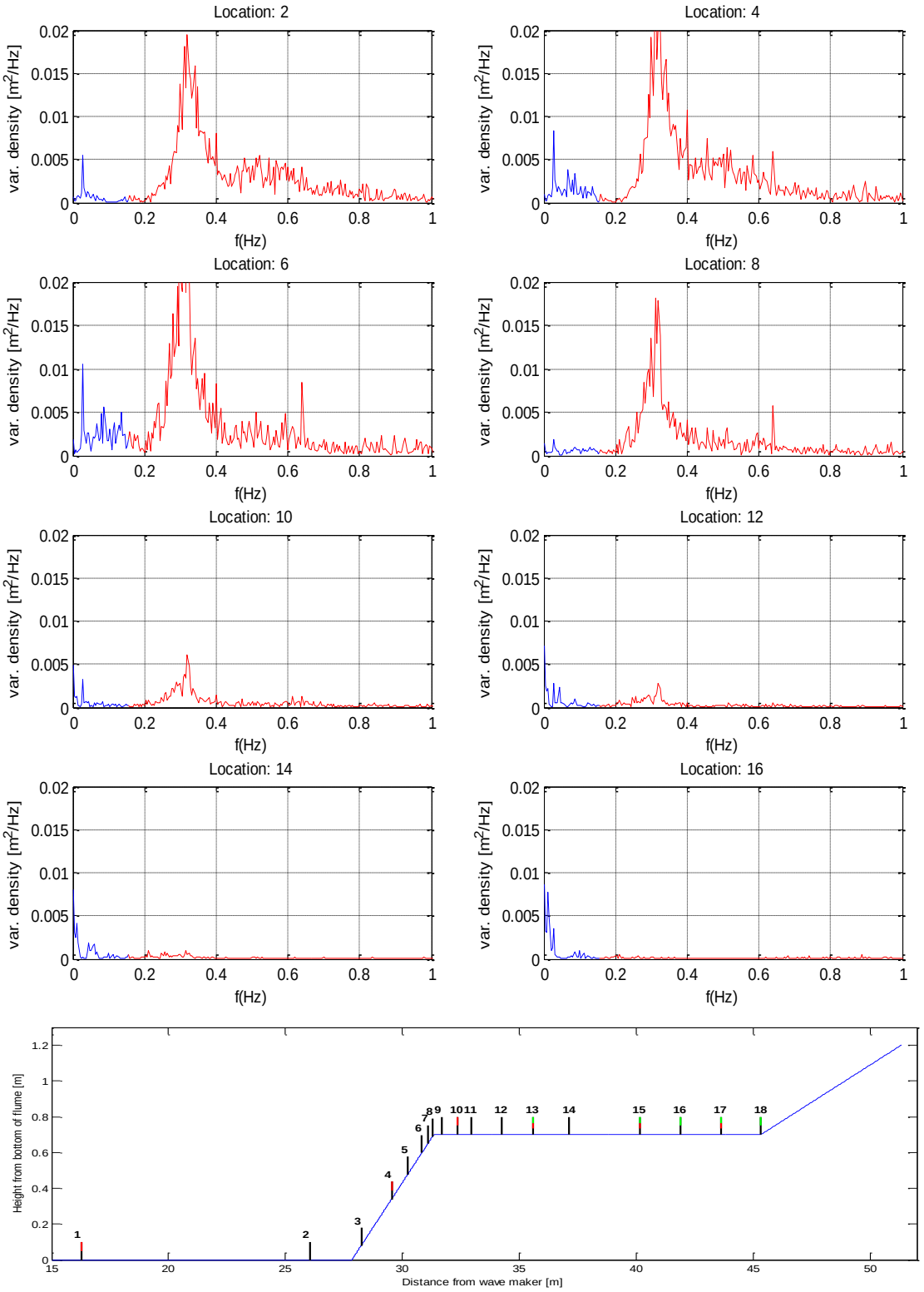

Figure 3.7 Instrument location and variance density spectra for simulation S01a. Long wave contribution to the spectrum is indicated in blue, short wave contribution in red.

By considering only the long or short wave part of the measured spectra the significant wave height H_{m0} can be determined for the long and the short waves at each of the measurement locations. To study the evolution of long and short waves the values of the significant wave

height per location are plotted versus the position in the flume in the upper panel of Figure 3.8. The reef shape is shown in the lower panel.

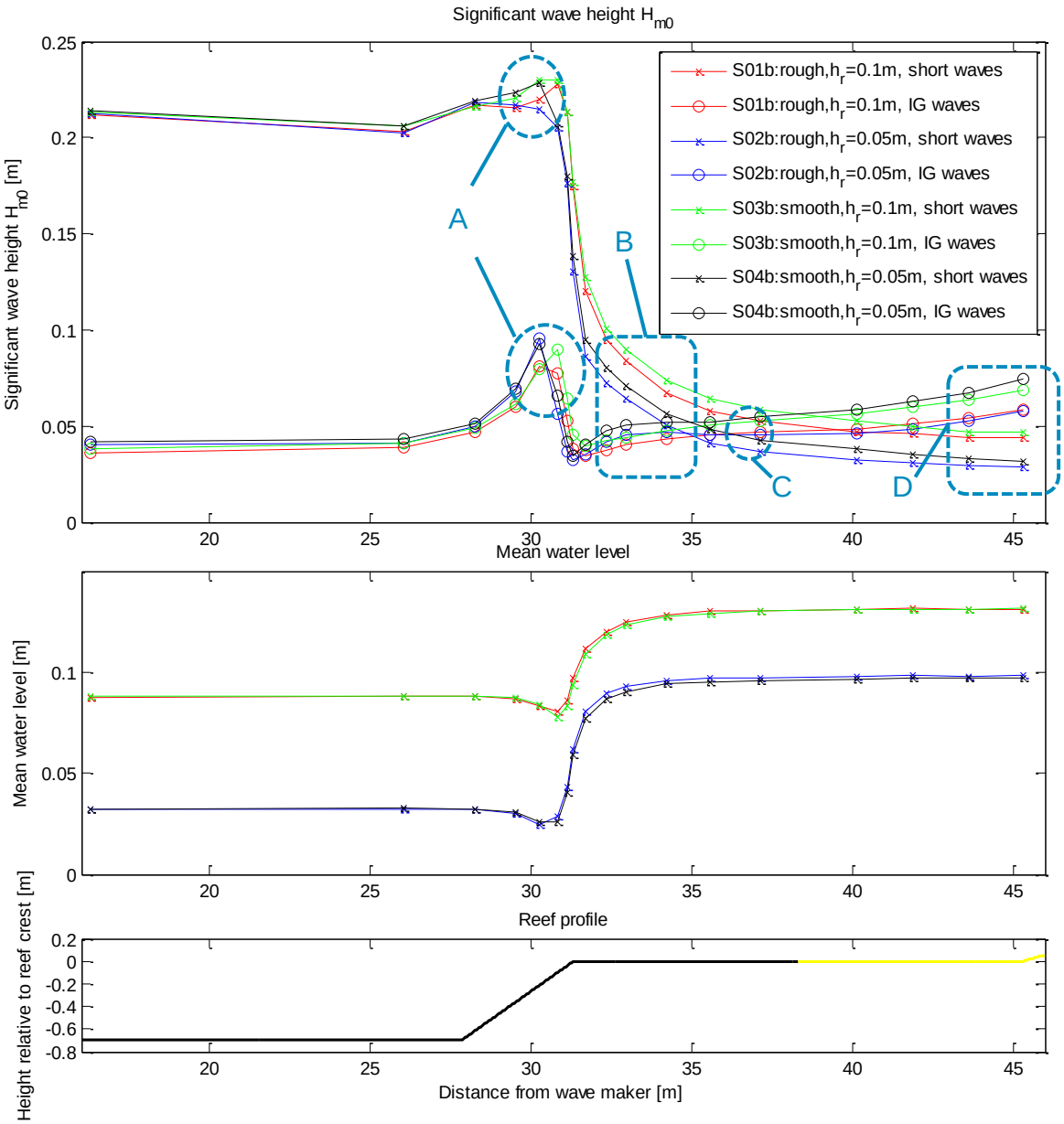

Figure 3.8 Upper panel: Evolution of total significant wave height H_{m0} for long and short waves. Compared for all four cases. Middle panel: Mean water levels relative to reef crest level. Lower panel: Reef profile; the black/yellow line indicates the position of the reef and the sand.

In this figure the total significant wave height H_{m0} of the long and short waves is shown for the measurement locations 2 to 18 and for all four cases. The bottom yellow/black line indicates the shape of the reef and the sandy bed. There are a number of phenomena and differences between the cases that can be observed which are indicated by the blue frames and referred to by A-D:

A. The black and blue lines indicate the two cases with a water depth on the reef (h_r) of 0.05 m, S02 and S04. The red and green lines indicate the two cases with h_r = 0.1m, S01 and S03. The long and short wave height for the cases S02 and S04 decreases

first, which means that the breakpoint is located further offshore. The long wave height decreases strongly around x=30-32 m which is likely to be caused by long wave breaking as discussed in Van Dongeren et al. (2013) for the Ningaloo Reef dataset. The long wave shoaling that is observed is treated in more detail in section 3.5.2.2.

B. The dissipation of the short waves is strongest for the cases S02 and S04 with shallower water on the reef. Also the increase of long wave energy after the reef crest is stronger for these cases. The increase of long wave energy after breaking suggests that the waves are generated by the breakpoint mechanism introduced by Symonds et al. (1982) which was discussed in the introduction of this report. The generation of long waves will be further elaborated in section 3.5.2.
C. Comparing the long waves for the rough cases S01 and S02 the long waves lose more energy in case S02. This suggests that the reduced water depth enhances the effect of bottom friction by the roughness elements. This is supported by the fact that the difference in dissipation is not as strong for the smooth cases S03 and S04, showing that it must indeed be the roughness elements causing the enhanced dissipation and not only the reduced water depth. The increased effect of friction for lower depths is in line with the findings of Hearn (1999).
D. At the end of the reef flat the long wave height is larger than the short wave height so the long waves dominate here. The long waves are grouped by roughness and the short waves are grouped by water depth.

The increase of the long wave energy towards the beach is quite remarkable as there must be a mechanism causing this increase. In order to analyse this energy increase Figure 3.9 shows the spectrum at location 17 on the reef for S01a. The green ellipsoids indicate three peaks at frequencies below 0.035 Hz, or wave periods larger than 50s. The peak at the lower frequency is related to a long period variation in the forcing as will be shown in section 3.5.2. The other peaks are related to resonance on the reef flat and in the entire flume(section 3.6). That explains part of the increasing wave height towards the beach and another part is explained by the reflection of progressive waves at the beach (section 3.5.1).

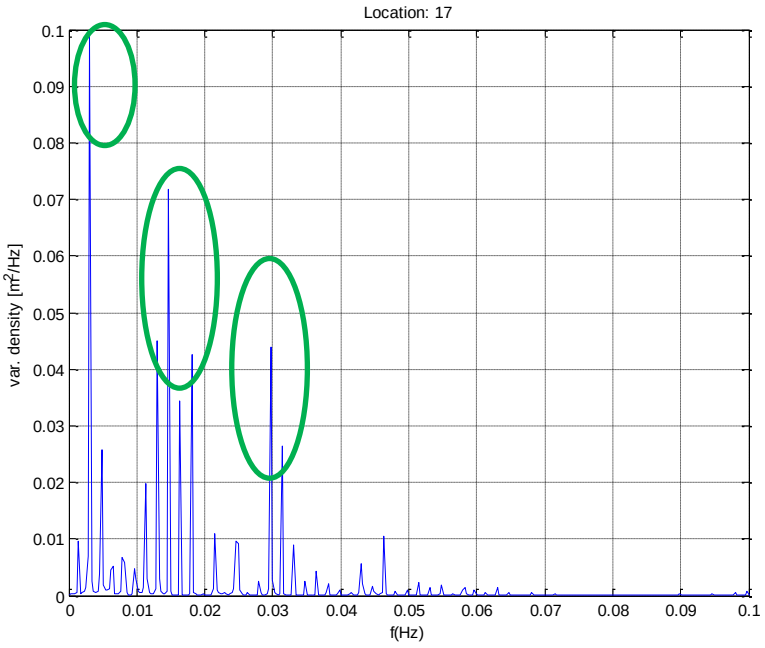

Figure 3.9 Surface elevation spectrum on the reef flat/lagoon at location 17 for simulation S01a

3.4.2 Wave-induced set-up of the water level

An interesting mean property is the mean value of the surface elevation for each measurement location. It shows the development of the wave-induced set-down and set-up of the water level from offshore to the beach at the back end of the reef. The variation in the mean water level is caused by the gradients in radiation stress as the waves shoal and break. The gradients results in a wave induced force that is balanced by a gradient in the water level as follows:

$$F_x = -\frac{dS_{xx}}{dx} = \rho g h \frac{d\bar{\eta}}{dx} + \tau_{bx}^E = \rho g (h_0 + \bar{\eta}) \frac{d\bar{\eta}}{dx} + \tau_{bx}^E \quad (3.11)$$

Where $\bar{\eta}$ is the mean water level, h_0 is the initial water level, $\frac{dS_{xx}}{dx}$ is the gradient in the wave radiation stress in x-direction and τ_{bx}^E is the bed friction using the Eulerian flow velocity. A decreasing value of S_{xx}, e.g. by wave breaking, will therefore result in a positive gradient in the mean water level, $\frac{d\bar{\eta}}{dx}$, and vice versa. The result is a set-down or set-up of the water level. The bed friction term is small compared to the wave forcing, but might have some effect because of the high bed roughness on the reef flat for simulation S01 and S02.

The mean value of the water level has been determined for the stationary part of the run, so excluding the spin-up and spin-down time, and has been plotted for each simulation in the middle panel of Figure 3.8.

The water level increase on the reef is quite large in all the simulations reaching almost 100% of the initial water level of 0.05 m for simulation s02 and s04. The water levels for s01 (rough bed) compared to s03 (smooth bed) are equal so for these simulations the increased bed roughness does not affect the setup. Simulation s02 does have a slightly stronger increase of the water level on the reef than s04 so it seems that the lower initial water level on the reef enhances the effect of the bed roughness on the set-up, though its contribution is still close to zero.
All four simulations show a small, local decrease in water level just before the reef crest. This is where the waves are shoaling so the radiation stress increases causing the observed set-down of the water level. In the offshore region between the wave maker and the reef crest the water level decreases overall because of mass conservation in the flume, since the total volume of water is constant.

Table 3.2 presents the mean water levels relative to the reef crest level that were measured offshore and on the reef. The difference between these values is Δh and should be balanced by the forcing by the breaking waves, neglecting the bed friction contribution. Since the water depth on the reef is lower in s02 and s04 the (depth-induced) wave breaking is stronger, leading to greater gradients in the radiation stress, a larger wave force and more set-up Δh. Also the water level gradient is multiplied by the water depth, $\rho g h \frac{d\bar{\eta}}{dx}$, so in the case of a smaller depth the gradient has to be larger to balance the wave forcing.

Table 3.2 Mean water levels during the experiments at different locations and the setup Δh. Water levels are in m and relative to reef crest level.

Simulation	Offshore	Location 15	Location 18	Δh
S01a	0.088	0.131	0.131	0.043
S02a	0.031	0.098	0.098	0.067
S03a	0.088	0.131	0.131	0.043
S04a	0.032	0.097	0.097	0.065

Since the reef is modeled in a flume and is more or less one-dimensional it is very different from the field where the reef will extend in alongshore direction. The fact that the experiments are one-dimensional leads to relatively high set-up compared to a real reef since the water cannot go anywhere while in reality the water will run off the reef through deeper channels that occur at more or less regular spatial intervals.

3.4.3 Flow velocity

The root-mean-squared flow velocity is a parameter indicating the magnitude of the velocity induced by the waves. The evolution of u_{rms} is plotted in Figure 3.10 together with the mean flow velocity, $\bar{u}$. In all cases and at all measurement locations u_{rms} is significantly larger than $\bar{u}$. Offshore, u_{rms} is highest for the low water depth cases (black and blue points), because the reflection on the reef is strongest for these cases. On the four locations on the reef the roughness reduces the RMS flow velocity so it is lower for the rough cases (red and blue points) than for the smooth cases (green and black lines). The same roughness-based grouping at the end of the reef as observed for the long wave height (Figure 3.8, area D) is observed for the RMS flow velocity.

The mean flow velocity is negative for all data points except the location closest to the beach for case S02. The mean value of the flow velocity strongly depends on the height of the measurement in the water column (see Table 3.3). The fact that the mean value is negative means that apparently the wave-induced mass flux mainly takes place at a level above that of the EMS and is compensated by an offshore-directed undertow at the level of the EMS, resulting in a negative mean value for the flow velocity.

Table 3.3 x and z position of EMS flow velocity meters

	shm11/12	shm21/22	shm23/24	shm25/26	shm27/28	shm29/30
x [m]	16.28	29.54	32.34	35.59	40.14	43.63
z [m]	-0.35	-0.21	0.01	0.01	0.04	0.04

The different vertical positioning of the EMS's and specific conditions at each of the locations explains most of the variation that is found in the mean of the velocity measurements over the reef, particularly in case S02, and makes it difficult to compare measurements at one location to another location.

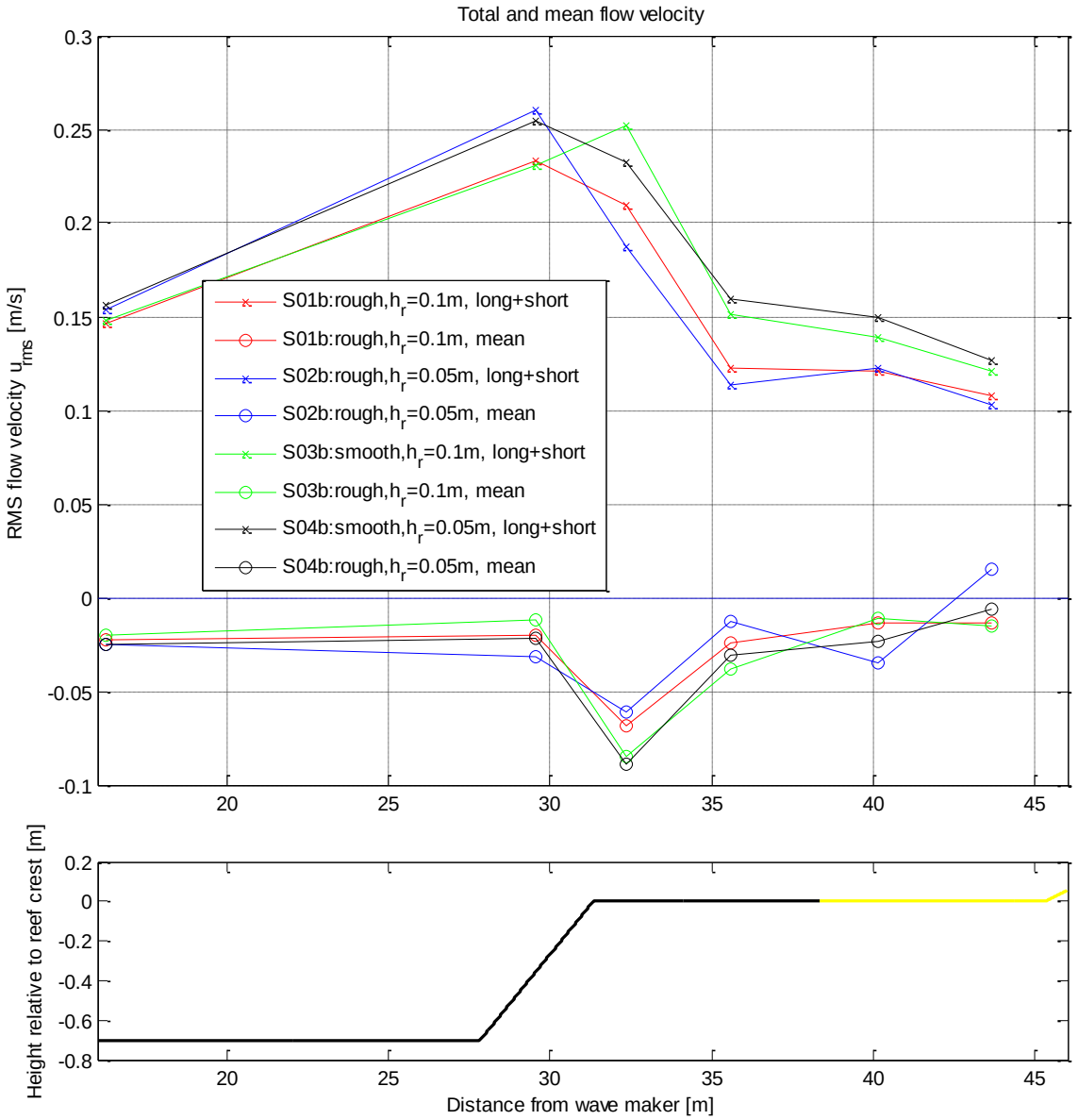

Figure 3.10 Evolution of the total RMS and mean flow velocity over the reef.

3.5 Long wave spectral evolution

Recent studies have emphasised the importance of long waves or infragravity (IG) waves on coral reefs, e.g. Pomeroy et al. (2012) and Van Dongeren et al. (2013). Both studies showed that waves in the IG band, in those cases defined as 0.004 – 0.04 Hz, start to dominate over short period wave motions (0.04 – 0.2 Hz) as the waves progress over the reef flat towards the lagoon and the beach. This phenomenon was also observed during the experiments (area D in Figure 3.8). Because of this long wave dominance on the reef flat and because many phenomena can be observed within the long wave frequency band this section will focus on the long waves.

As mentioned earlier, waves with a frequency smaller than half the peak frequency ($f_p/2$) will be considered as long waves. In turn these long waves consist of multiple contributions such as an oscillation at the eigen frequency of the reef flat and the flume and another motion at a lower frequency. Besides this there are also progressive, long waves propagating over the reef. In order to show these contributions and further analyse how different components of the long wave evolve, the long waves are split up into parts referred to as infragravity (IG) waves and very low frequency (VLF) waves. The separation is based on the observed frequencies on the reef flat (Figure 3.9):

- 0.035 Hz < f < $f_p/2$: infragravity waves (IG)
- 0 < f < 0.035 Hz : very low frequency waves (VLF)
    - Includes peaks at 0.016 Hz and 0.03(resonance) and 0.003 Hz

The separation in these categories is illustrated in Figure 3.11. Note that this spectrum is computed at location 5 and is not the same spectrum as the one in Figure 3.9. Using the separation as shown in the figure the transformation of the long wave components is analysed below.

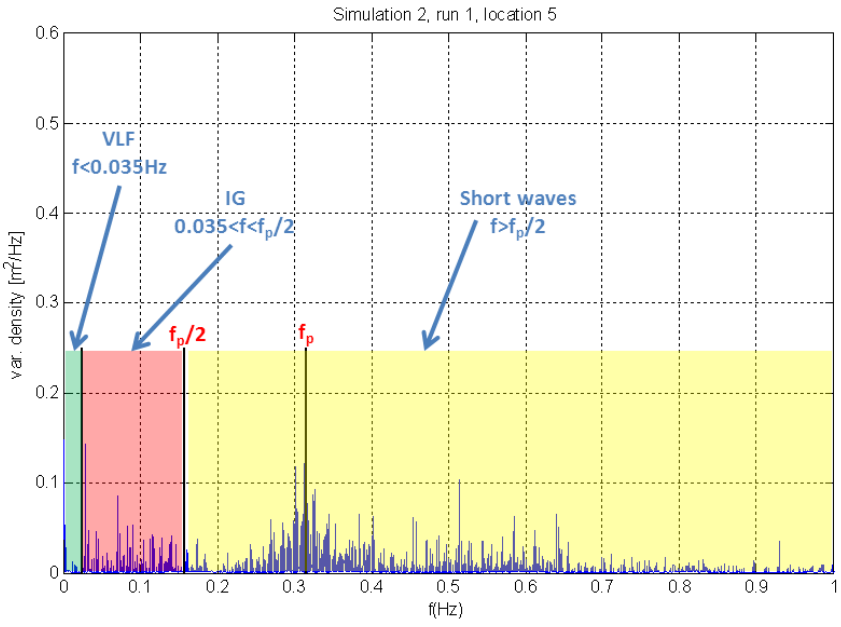

Figure 3.11 Definition of very low frequency waves (VLF), infragravity waves (IG) and short waves used in this report.

3.5.1 Infragravity waves (0.035 Hz < f < f_p/2)

In this section the infragravity part of the wave spectrum is considered together with the short waves. As explained, motions with a frequency below 0.035 Hz (VLF) are filtered out of the long wave surface elevation signal. The evolution of the total short and IG waves is shown in the upper panel of Figure 3.12. The VLF motion is presented in the middle panel of the figure.

The IG waves were separated in incoming and reflected components (Figure 3.13). In Figure 3.14, upper panel, the total flow velocity is plotted for the IG and short waves.

The following phenomena can be observed:

- From Figure 3.12 it is observed that on the reef flat and lagoon the significant wave height H_{m0} of the IG waves only is significantly smaller than for the total long waves for all four cases. The difference comes from removing the VLF motions as they apparently contain a large portion of the total energy on the reef flat.

- The shoaling of long waves before breaking (x=26-30 m) is quite strong and will be analysed in section 3.5.2.2.

- Dissipation of IG wave energy is visible in the reduction of H_{m0} at two locations:

    - at the short wave breakpoint around x=30 m; As already discussed in section 3.4.1 this could be because of depth-induced breaking of the long waves. It is however recommended to investigate this further.

    - as the waves progress over the reef flat between x=33 m and x=41 m; This dissipation is strongest for the two cases with bed roughness, S01 and S02.
        - Comparing S01(h_r=0.1m) and S02(h_r=0.05m) there is more dissipation for case S02. The lower water depth enhances the dissipation of long wave energy by the bed roughness.

- The increase of long wave energy (long wave generation) around the reef crest is slightly less for the rough cases, comparing S01 to S03 and S02 to S04. Long wave generation is treated in section 3.5.2.3.

- For all cases the long wave energy increases at the last two locations close to the beach. The increased wave energy is caused by reflection of the long waves on the beach. Figure 3.13 shows the incoming and reflected long waves where there is actually a slight decrease of the incoming wave height towards the beach. The increase in the total wave height is caused by the reflected part of the signal. The reflection of IG wave energy on the reef crest is also significant and at the offshore measurement location the reflected waves even dominate the incoming waves. Note that Figure 3.13 has less data points because signal separation can only be done at the locations with co-located flow velocity and wave height meters.

- Both the short and the IG wave flow velocity increase from offshore to the reef crest, which is caused by the shoaling of the waves. The short wave flow velocity decreases on the reef flat with decreasing short wave height. A clear effect of the bottom friction can be observed on the IG flow velocity with the velocity for the rough simulations being significantly smaller than that of their smooth counterparts. The difference

between rough and smooth is largest for the low water depth simulation which supports that the effect of bed friction on flow velocity is enhanced for lower water depths which is the same conclusion Hearn (1999) reached in his analysis of flow on coral reefs.

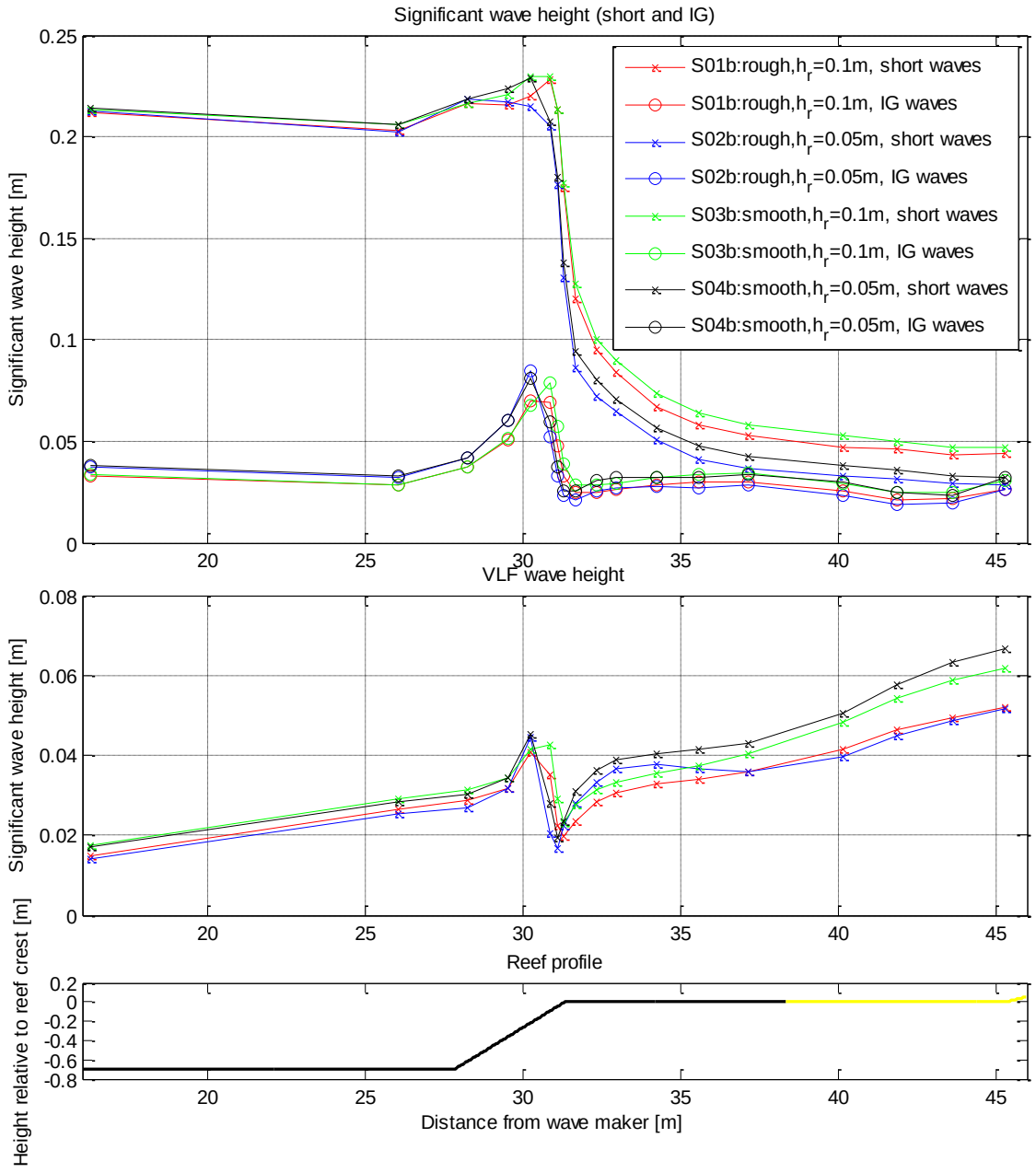

Figure 3.12 Upper panel: Evolution of total significant wave height H_{m0} for long(IG) and short waves. Middle panel: Evolution of total significant wave height for VLF waves. Lower panel: Reef profile

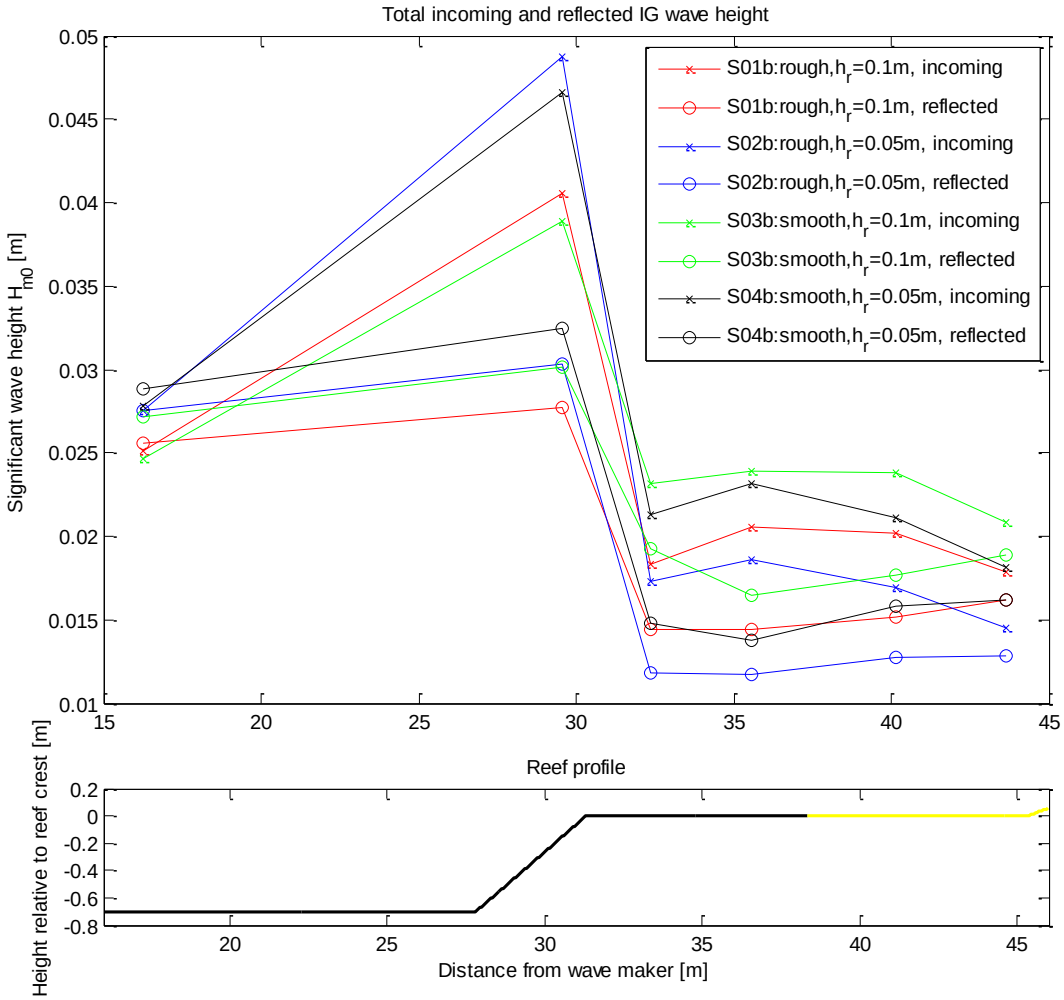

Figure 3.13 Evolution of incoming and reflected significant IG wave height H_{m0}.

To analyse the character of the waves in the IG range Figure 3.14 presents the evolution of the flow velocity belonging to the IG waves (upper panel) and the VLF waves (middle panel) and Figure 3.15 shows time series of the total long wave surface elevation and flow velocity on locations 10, 13, 15 and 17 on the reef.

Progressive waves would typically have a zero phase lag between flow velocity and surface elevation whereas standing waves are characterised by a 90° phase lag with the surface elevation lagging the flow velocity. Also the amplitude of a standing wave would increase towards the end of the reef and the velocity would decrease towards the end. The figures show that none of these typical characteristics of a standing wave are visible in the flow velocity transformation over the reef and in the time series.

Especially when comparing the time series and evolution to those of the waves in the VLF range (see Figure 3.20 for the time series) it is clear that the waves in the IG range must be mainly progressive waves. The evolution of the VLF flow velocity does strongly suggest the presence of a standing wave on the reef in the VLF frequency domain, see Figure 3.12, middle panel, and Figure 3.20. This is further analysed in section 3.5.3 about the analysis of the VLF motions and 3.6 about reef flat seiching.

Figure 3.12 also provides some insight regarding the grouping by bed roughness of the total long wave height that was observed in Figure 3.8 as it shows that the VLF wave height for the smooth cases is significantly larger than for the rough cases. Since the VLF wave height is shown in section 3.6 to consist of a standing wave for a large part, the grouping by bed roughness appears to be caused mainly by the effect of the bed roughness on the height of the standing wave.

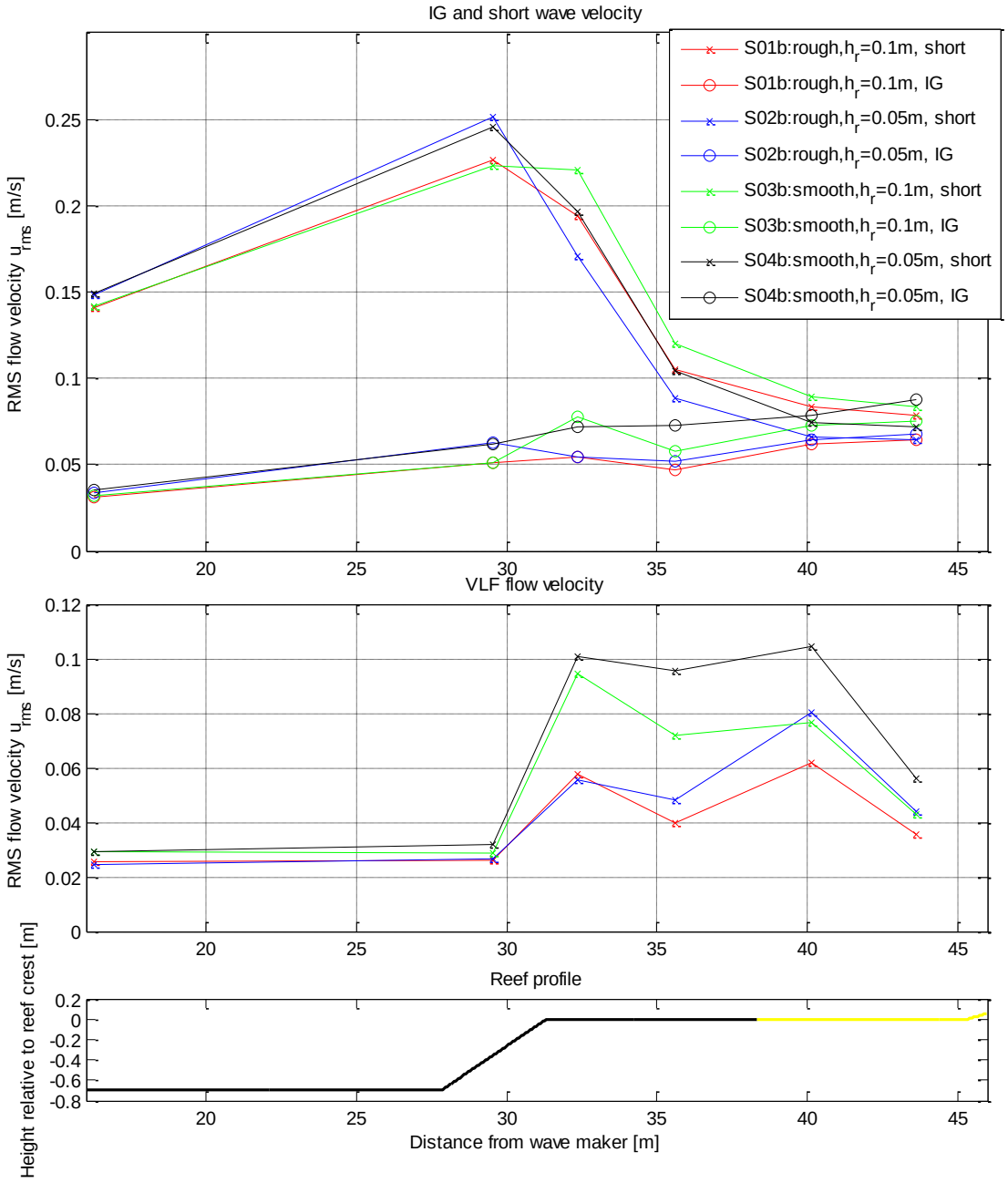

Figure 3.14 Evolution of total flow velocity u_{rms}; upper panel: long (IG) and short wave velocity; middle panel: VLF wave velocity

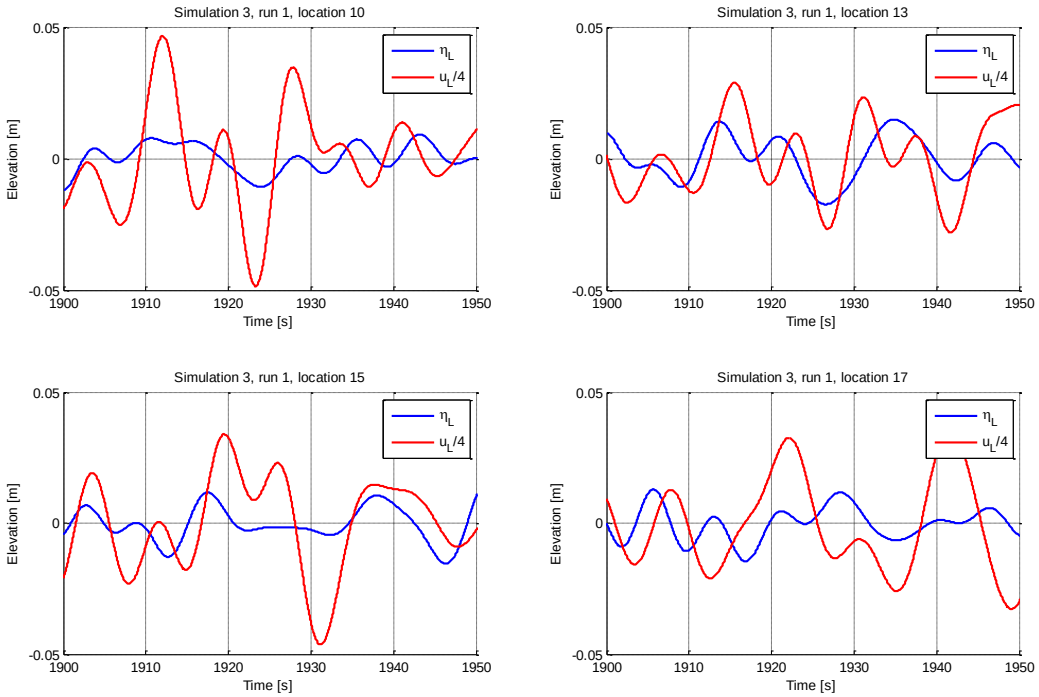

Figure 3.15 Total IG wave and flow velocity time series at 4 locations on the reef. For the purposes of this plot the flow velocity is divided by 4.

3.5.2 IG wave shoaling and generation around the short wave breakpoint

3.5.2.1 Introduction

The analysis of the spectral evolution over the reef showed that the long wave energy first increases and then strongly decreases as the long waves pass over the forereef slope. Subsequently the long wave energy increases on the reef crest and continues to increase on the reef. The above analysis of the long waves showed that the increase of long wave height on the reef, towards the beach is largely due to motions in the VLF domain (f<0.035Hz). Also in the IG domain a small increase in long wave height is observed due to reflection on the beach.

The presence of the IG waves offshore is explained using the well-known theory of Longuet-Higgins and Stewart (1962) about radiation stress, which explained the formation of *bound* long waves under wave groups. These waves are generated by the variation of wave height and therefore radiation stress under wave groups with waves of different frequencies. This variation causes a small set down of the water level under the higher waves in the group and a small setup under lower waves. This creates a long wave that travels with, and is bound to, the wave group. These long waves are in general thought to be released from the wave group at the short wave breakpoint and propagate towards the beach as free long waves where they reflect and propagate back in a seaward direction.

Besides this generation mechanism of freely propagating IG waves in the nearshore there is the theory proposed by Symonds et al. (1982) that IG waves are generated by the moving short wave breakpoint, referred to as the breakpoint mechanism. According to this theory long waves are generated by the temporal variation in breakpoint location of the short waves that travel in groups. The breakpoint moves up and down in onshore and offshore direction because the higher waves break farther offshore than the lower waves in a group. The moving breakpoint causes a varying forcing on the water column, which behaves comparable to a wave maker and will generate waves at the group period and its harmonics.

The normalised **surf zone width parameter** by Symonds et al. (1982) can be used to indicate the relative importance of breakpoint forcing for the IG waves:

$$\chi \stackrel{\text{def}}{=} \frac{4\pi^2 h_b}{g T_{IG}^2 h_x^2} \tag{3.12}$$

It depends on the depth of breaking h_b, a representative long wave period T_{IG} and the steepness of the bed slope h_x. Closely related to the surf zone width parameter is the **normalised bed slope parameter** proposed by Battjes et al. (2004):

$$\beta \stackrel{\text{def}}{=} \frac{h_x}{\omega}\sqrt{\frac{g}{h}} \tag{3.13}$$

With h the representative depth on the slope and ω the angular frequency. β is related to χ via $\chi = \beta_b^{-2}$ where the subscript b on β indicates that h_b was substituted for h. The normalised bed slope parameter was suggested by Battjes et al. (2004) as an indicator for the type of long wave shoaling present at different frequencies distinguishing between a steep slope regime and a mild slope regime. On mild slopes energy is transferred from the short waves to the long waves and the long waves are released after breaking of the short waves.

On steep slopes there is insufficient time for the progressive release of the long forced waves. In that case IG waves can be generated by a breakpoint mechanism.

Baldock (2012) also looked into the different theories for long wave generation and found that the generation mechanism of freely propagating IG waves in the nearshore by release of the bound long wave is shown to be particularly strong for beaches with a mild slope regime and mild wave conditions (low short wave steepness). While for the steep slope regime and steep waves it is the breakpoint mechanism causing the generation of IG waves.

Baldock (2012) proposed a **surf beat similarity parameter** to indicate the type of surf beat that is likely to dominate in different conditions. This parameter depends on the relative beach slope parameter χ and the wave steepness of the offshore short waves, $\frac{H_{o,sw}}{L_{o,sw}}$:

$$\xi = \chi^{-\frac{1}{2}} \left(\frac{H_{o,sw}}{L_{o,sw}} \right)^{\frac{1}{2}} \tag{3.14}$$

Below these parameters are used to look into the long wave shoaling and the generation of IG waves in the surf zone.

3.5.2.2 *Long wave shoaling*

The value of Battjes' bed slope parameter β is used in this section to analyse the shoaling of the IG waves and compare this to the theory of Battjes et al. (2004). The value of β found for the experiments is at least 0.7 using a frequency of 0.16 Hz and a representative depth at the start of the slope of 0.8 m. These values are selected such that the value of β represents a minimum value. 0.7 is already a lot higher than the highest value found by Battjes et al. (2004), which is 0.3. In their situation a bed slope parameter value exceeding this upper limit was shown to be sufficiently large for the shoaling to follow Green's law where free long waves shoal by $h^{-\frac{1}{4}}$.

This is explained by the fact that on steep slopes, indicated with a high β, there is insufficient time for energy transfer between short waves and long waves, so the long waves behave as free long waves, which theoretically shoal according to Green's law.

The shoaling regime observed in the experiments was investigated by plotting curves following different shoaling rates together with the measured incoming long wave height, see Figure 3.16. Unfortunately only one data point is available in the shoaling region. This point is on the curve of a shoaling regime following according to $h^{-\frac{3}{4}}$. To get some more confirmation the same plot is also created for the total long waves so that more data points are available in Figure 3.17. Here too the shoaling of the long waves appears to follow approximately the same shoaling regime of $h^{-\frac{3}{4}}$.

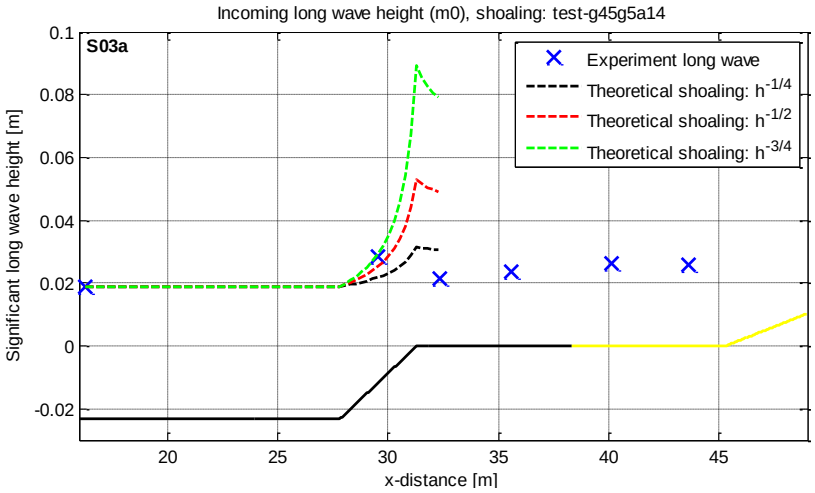

Figure 3.16 H_{m0} values for incoming long waves indicated with blue crosses. Dashed curves indicate theoretical shoaling of the long waves by different powers of h. Curves are initiated with the incoming long wave height at x=16.28 m (location 1).

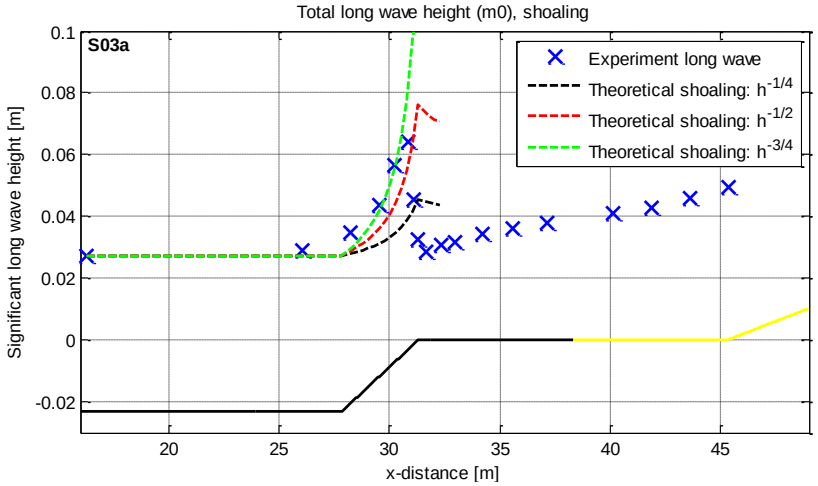

Figure 3.17 H_{m0} values for total long waves indicated with blue crosses. Dashed curves indicate theoretical shoaling of the long waves by different powers of h. Curves are initiated with the total long wave height at x=16.28 m (location 1).

The shoaling apparently does not follow the conservative Green shoaling law and therefore there must be some transfer of energy towards the long waves. This finding is consistent with Pomeroy et al. (2012) where the same increase of IG energy in the shoaling zone was found for Ningaloo Reef.

Using a field study performed on the Ningaloo Reef in Western Australia, they looked into the generation of free IG waves on the reef. The steep forereef slope of 1:20 resulted in a high value for the surf beat similarity parameter indicating that the breakpoint mechanism should be dominant for this situation. The presence of the breakpoint mechanism was confirmed with numerical modelling so the results are consistent with the research done by Baldock (2012). Because coral reefs in general have very steep forereef slopes it would be likely that the breakpoint mechanism is generating IG wave energy in the experiments as well.

3.5.2.3 *Analysis of long wave generation during experiments*

The surf beat similarity parameter ξ of Baldock (2012) indicating the type of surf beat to be expected is related to the normalised bed slope parameter β_b via the normalised surf zone width parameter χ. The value of the surf beat similarity parameter ξ for the experiments is about 0.55 using $h_b = 0.2$, $T_{IG} = 16$, and $h_x = 1{:}5$. This value is much higher than the value of 0.2 found by Baldock (2012) for steep beaches and is in the same order of the 0.8 that was found by Pomeroy et al. (2012). This suggests that IG waves are dominantly generated by the breakpoint forcing mechanism in the experiments.

Another characteristic of the breakpoint mechanism is a change of correlation between the short wave envelope and the IG wave as it progresses over the reef slope and reef flat. The correlation is negative offshore corresponding to a bound long wave under the short wave group. In the surf zone the correlation changes sign and becomes positive. To test if this was also the case in the experiments a similar plot to the one in Pomeroy et al. (2012) was created to follow the development of the correlation between the short wave envelope and the bound long wave. Both plots are shown in Figure 3.18. The correlation between the short wave envelope at offshore location 1 and the IG wave at the measurement locations is plotted in time and space. The blue line indicates the theoretical wave propagation speed integrated over the depth. The figure was created for simulation S01a, but was similar for all simulations.

The plot for the experiments show a similar pattern as the plot from Ningaloo reef. Offshore the correlation is negative (blue) and around the breakpoint it switches to positive (red) and continues to propagate on the reef flat.

The results from the experiments are very consistent with the results obtained from the Ningaloo field data, strongly suggesting that the breakpoint mechanism of IG waves is dominant in both cases. The results also appear to show that the long waves dissipate together with the short waves in the surf zone. Though in agreement with Pomeroy et al. (2012) it should be noted that it remains unclear what happens exactly to the long bound wave in the surf zone. Whether the bound long waves are, partially or completely, released, (re-)generated or dissipated together with the short waves remains subject of debate.

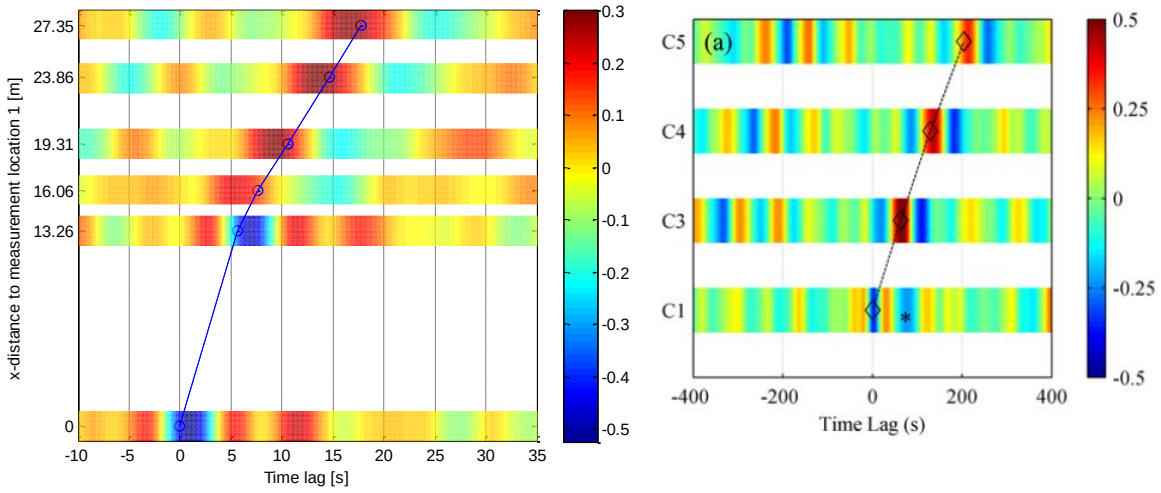

Figure 3.18 Left figure from s01a: Cross correlation averaged over the simulation period of short wave envelope at x=0 with the long wave time series at location 4, 10, 13, 15 and 17. The blue line indicates the theoretical propagation speed trajectory obtained from integration of the bathymetry. Right figure from Pomeroy et al. (2012): comparable plot for field experiments on Ningaloo Reef.

3.5.3 Very low frequency waves (f<0.035Hz)

As observed from Figure 3.9 quite some energy is present at the very low frequencies where f<0.035Hz. The VLF part of the spectrum shows three distinct peaks; one around 0.016 or 0.012 Hz, one around 0.03 Hz and one around 0.003 Hz. In section 3.6 it will be discussed that two of these peaks are likely to be related to oscillations at the Eigen frequency of the reef flat. Besides that there is another energy peak in the observed spectrum at a frequency below the Eigen frequency. This peak is possibly related to some variation in the offshore forcing by the short waves as will be explained below. In this section this last peak is analysed further.

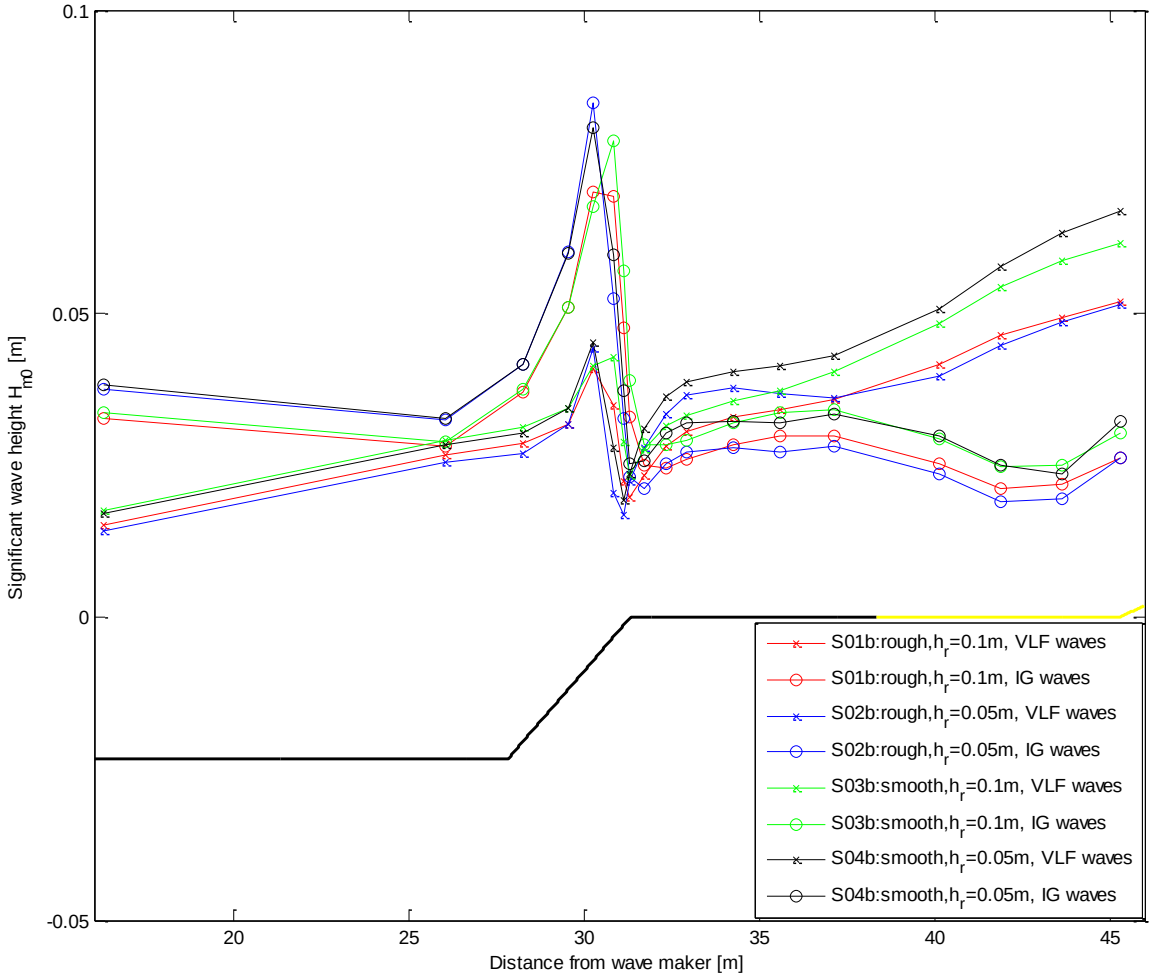

Figure 3.19 Wave height evolution of long waves (IG range) and waves in the VLF domain.

Figure 3.19 shows the VLF wave height compared to the infragravity wave height. The IG wave height for the low water depth cases S02 and S04 shows a small increase in magnitude just after the reef crest, which does not occur for the deep water cases S01 and S03. This increase is not understood, but could be related to unreliable measurements or separation methods in the area right after the breakpoint e.g. due to presence of bubbles or very irregular waves.

The VLF wave height increases very strongly over the reef flat for all four cases. The continuously increasing VLF wave height towards the beach at the back of the reef flat is

clearly different than the development of the infragravity wave height and is one of the characteristics of a standing wave.

Another characteristic of a standing wave is a 90-degree phase difference between flow velocity and surface elevation. In Figure 3.20 a time series for the surface elevation and the flow velocity is plotted for the VLF motions at four locations on the reef flat. The presence of a standing wave is unmistakable considering the fact that the surface elevation and the flow velocity are 90 degrees out of phase and the amplitude of the surface elevation more than doubles from the reef crest towards the beach. The flow velocity is highest near the reef crest at the node of the standing wave, the amplitude is highest near the beach at the antinode of the wave, recall also Figure 3.14, middle panel.

Also the last criterion for a standing wave is fulfilled as the surface elevation at all four locations on the reef flat is more or less in phase.

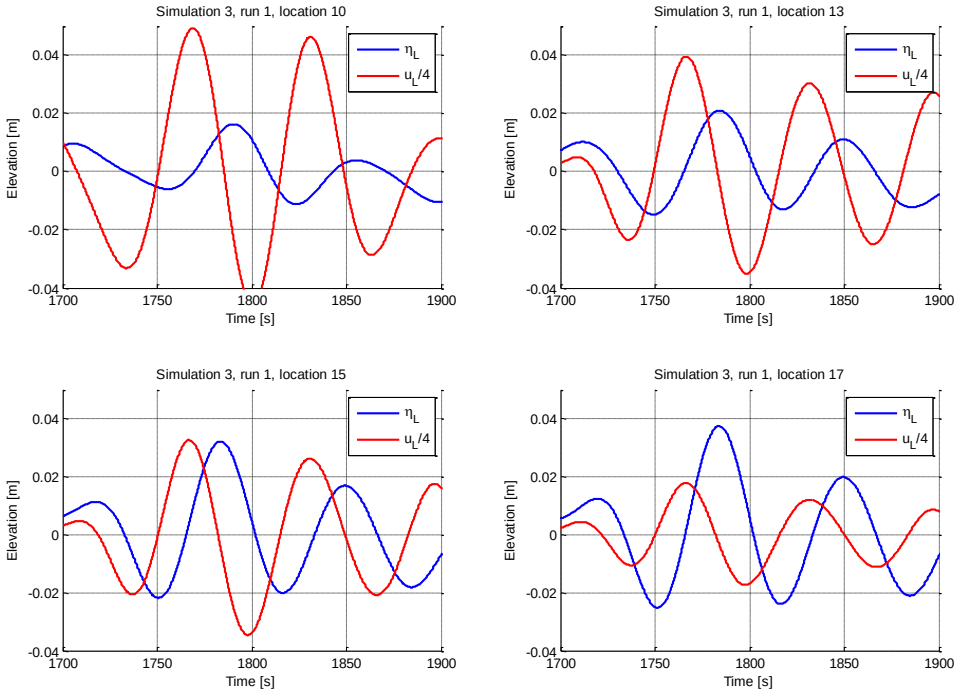

Figure 3.20 Total VLF wave and flow velocity time series at 4 locations on the reef. For the purposes of this plot the flow velocity is divided by 4.

Next the peak in the spectrum around 0.003 Hz is considered (Figure 3.21). It is hypothesized that this motion with a period of about 300 seconds is forced directly by the waves offshore of the reef by a variation of the short wave height on the time scale of multiple wave groups. This hypothesis is partly based on observations during the experiments where it appeared as if water was pushed onto the reef by short wave action until a certain point when a strong return current occurred and a large amount of water flowed back off the reef. This filling and flushing of the reef flat appeared to have a period in the order of minutes.

If the short waves are actually forcing this phenomenon, it should stop as soon as the wave forcing is stopped, as opposed to the resonance, which will dampen out more gradually (see further ahead in Figure 3.26). This is investigated below by analysing the spectrum after the wave forcing has stopped.

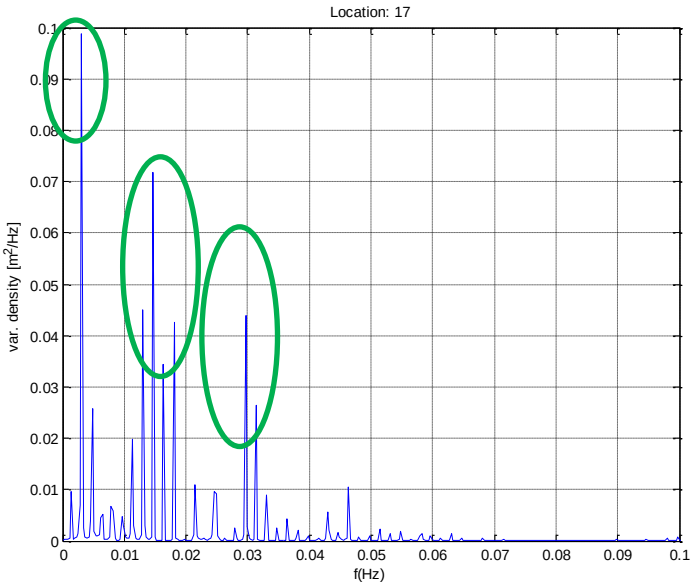

Figure 3.21 Identical to Figure 3.9; Surface elevation spectrum on the reef flat/lagoon at location 17. During waves.

Figure 3.22 shows the spectrum of the surface elevation after the wave forcing has stopped for part a of all four simulations. A peak at the resonance frequency and a very small peak at a lower frequency is clearly visible in all simulations, except simulation 2, which is the simulation where the resonant oscillations died out the fastest. Because the period over which the spectrum is created is relatively short, approximately 15 minutes, and because the signal is not stationary during this period, the resulting spectra should be treated with care. Still there is a general trend that the very long period motion around 0.003 Hz seems to die out faster than the resonance motion and the peak is much less pronounced than during waves. This gives some support to the hypothesis that the very low frequency motion is directly related to a forcing offshore of the reef.

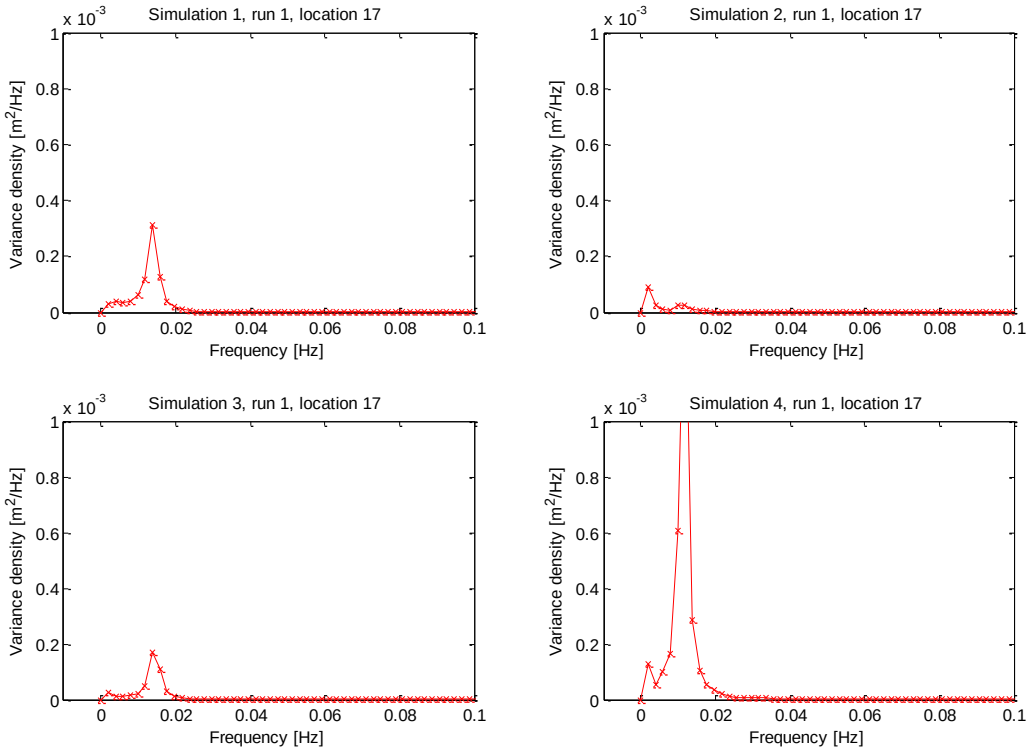

Figure 3.22 Variance density spectra of spin-down part of the time series for all four runs

Next it is investigated how the offshore forcing is causing the long period motion on the reef. The surface elevation signal at location 17 near the back of the reef is low pass filtered to obtain only the signal with frequencies below 0.01 Hz or periods larger than 100s. This low frequency signal is shown as the blue line in Figure 3.23. There is a clearly an oscillation with a period of about 300s visible in the signal and the amplitude appears to be modulated to some degree by oscillations at lower and higher frequencies. The oscillation is observed in all four simulations.

Since observations during the experiments suggested that the short waves play a role, the surface elevation signal offshore of the reef at location 4 is filtered to contain only short waves. A running mean of 50s of the envelope of this short wave signal is obtained to look for some periodicity in the short wave energy, shown as the red line in the figure. The result is still a rather spikey line when compared to the long waves with f<0.01 Hz on the reef, but there does seem to be some long period oscillations in the 50s average of the short wave envelope, which are repeated every 600 seconds by the wave maker.

The long period oscillation in the running mean of the short wave envelope is made more clear by applying a low pass filter to the running mean at 0.01 Hz (green line). The result is quite remarkable as it closely resembles the very long wave motion on the reef. It is important to notice that the green line does not simply represent the same long wave motion as on the reef, because the long wave motion offshore and on the reef should be in anti-phase. That the offshore motion and the motion on the reef are in anti-phase follows from a short movie that was created of the very low frequency surface elevation and the very low frequency wave time series offshore in the figure (black dashed line). Two screenshots of the movie are shown in Figure 3.24. The reef crest is at x=31.34m and the reef flat is on the right of this point. The left panel shows a lowered water level offshore and a raised water level on the reef at t=2516s. The right panel is created at t=2596s and shows a raised water level offshore and

a lowered water level on the reef flat; the oscillations offshore and on the reef are in anti-phase. The very long wave offshore is indeed in anti-phase with the very long wave on the reef (black dashed line).

The resemblance between the low pass filtered short wave envelope offshore and the long wave motion on the reef strongly suggests that the latter is forced by the former. So it appears that the very long wave motion on the reef is forced by a long period variation in the short wave height. This is in line with visual observations during the experiments of the water stored on the reef periodically draining off the beach.

The fact that the period of the observed VLF motions is related to the repeated forcing signal by the wave maker does not mean that the motions are artificial in the sense that they would not occur in nature. Of course, in nature wave conditions are constantly changing and conditions are never repeated as in the experiments, but still the mechanism of a long period variation of short waves forcing VLF motions on reefs or beaches can exist, only the period of these motions might vary with the wave conditions in time.

The above analysis suggests a possible relation between a variation in the short wave energy and very low frequency motions. This could for example be relevant for explaining the occurrence and periodicity in transient rip currents on beaches. Further research is recommended to look into the process more closely and possibly extend these findings for a two-dimensional domain and for field data but that is beyond the scope of this report.

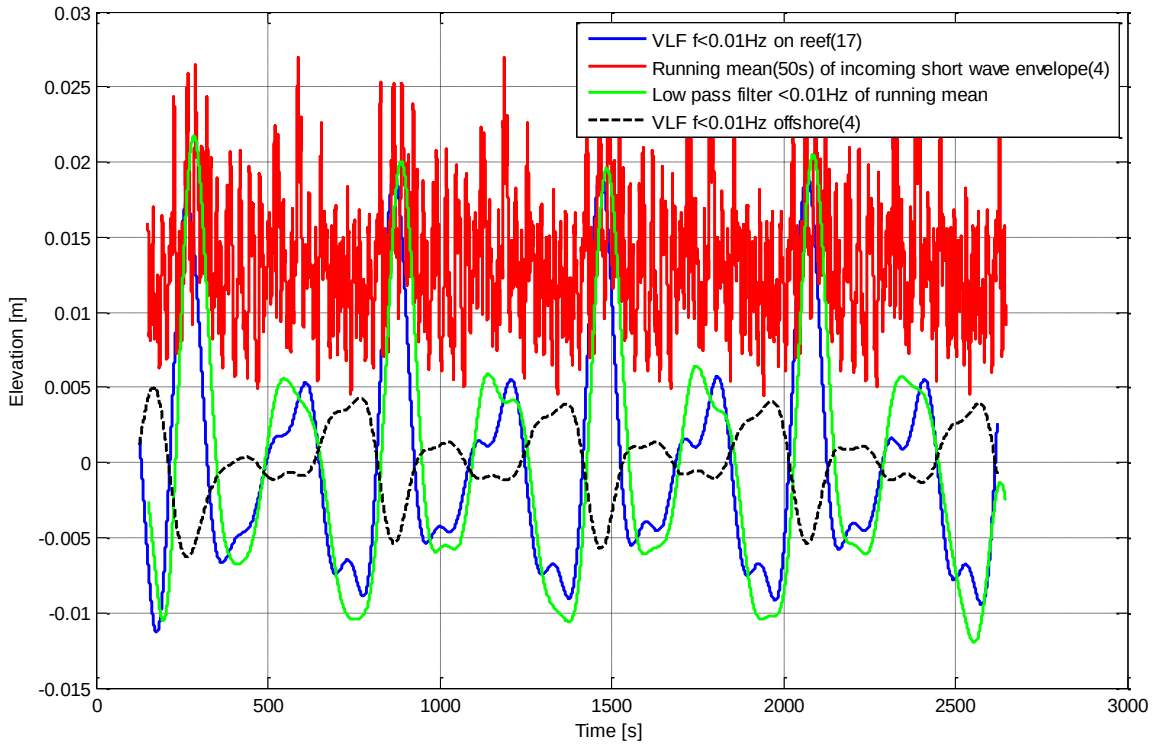

Figure 3.23 Forcing of a very long period motion (f<0.01 Hz) on the reef at location 17(blue) by a long period variation(green) in a 50s running mean of the offshore short wave envelope at location 4(red). The black dashed line is the very long wave offshore at location 4.

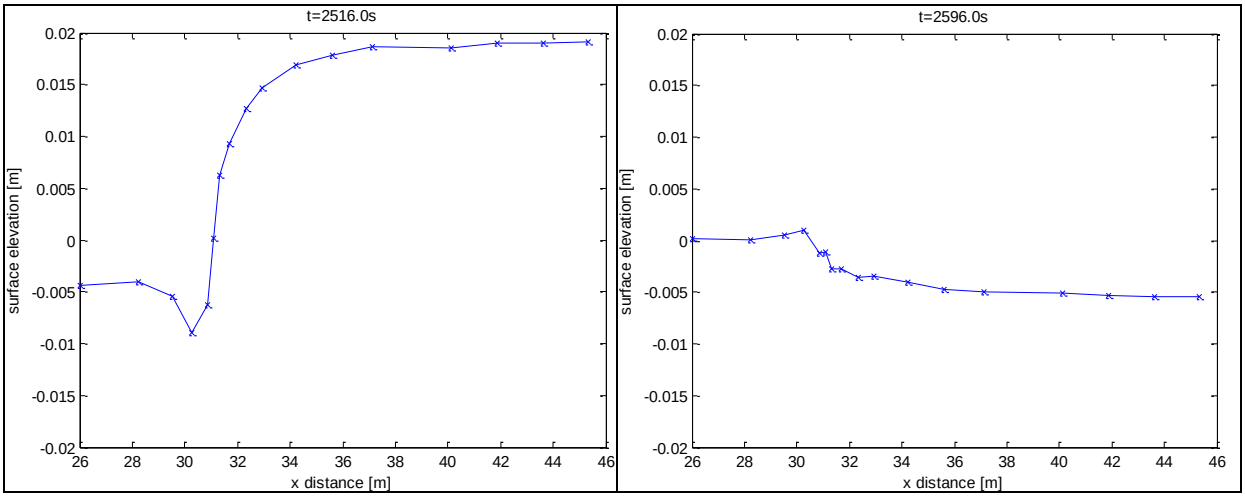

Figure 3.24 Screenshots of a movie showing the very long wave height in the flume develop in time.

3.6 Reef flat seiching

As discussed above there are three large peaks in the spectrum indicated by green ellipsoids in Figure 3.25. One peak is around a frequency of 0.016 Hz or a wave period of 60s, another one at 0.03 Hz or a wave period of 33s, the last peak is around 0.003 Hz or a wave period of 330s. The peak around 330s has already been discussed above. Regarding the other peaks it was observed from time series that a standing wave is present on the reef with a frequency in the same range as the peak at 0.016 Hz. The mechanisms causing the peaks are different as the 330s peak is related to filling and flushing directly forced by the offshore waves whereas the 60s peak is caused by the fact that the eigen frequency of the reef flat is matched by some part of the forcing offshore. This leads to resonance on the reef flat enhancing the motions at the eigen frequency and hence the high peak in the spectrum on the reef at this particular frequency. Below the reef flat seiching is analysed in more detail using the measurements that were done after the wave maker was stopped. The 0.03 Hz peak is related to a standing wave in the entire flume and is also discussed below.

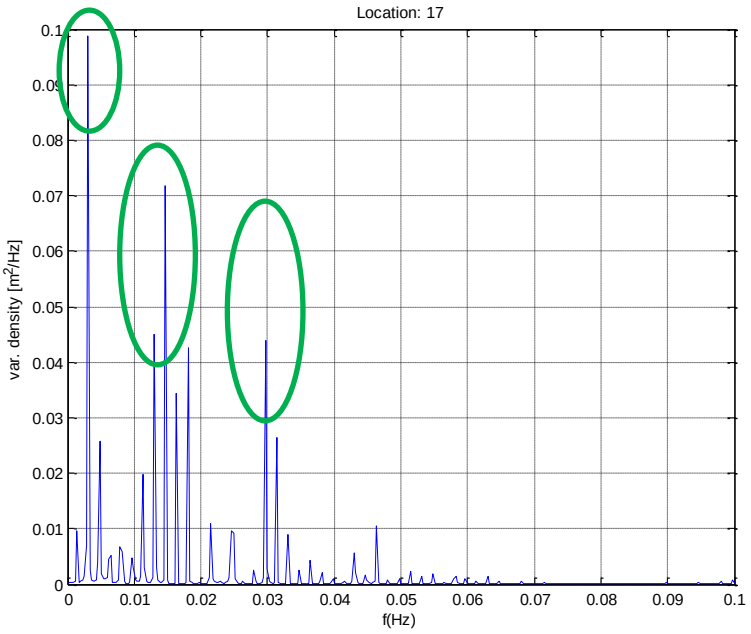

Figure 3.25 Variance density spectrum of surface elevation at location 17 for simulation S01a

This measured period of spin down can be used to explain the peak of energy around 0.016 Hz. As the forcing is turned off, the oscillations of the surface elevation that remain are caused by resonance at the Eigen frequency of the reef flat. In Figure 3.26 these oscillations can be observed for each of the four simulations that were done (S01a-S04a). Per simulation the top figure shows the time series of the surface elevation for the total time that was measured. The bottom figure is a close-up of the low frequency oscillations at the end of each run. Comparing simulations with a rough bed, S01a and S02a, the oscillations are damped much stronger for S02a. Again the reduced water depth appears to enhance the friction by the roughness elements. The damping is not only because of the reduced depth, because in simulation S04a the damping is much weaker.

A visual estimate is made of the period and corresponding frequency of the observed oscillations, summarised in Table 3.4. The observed period and frequency for case S01a agrees reasonably with the peak in the spectrum at 0.016 Hz. The observed period appears

to depend on the water depth on the reef h_r as it is equal for S01a and S03a and for S02a and S04a.

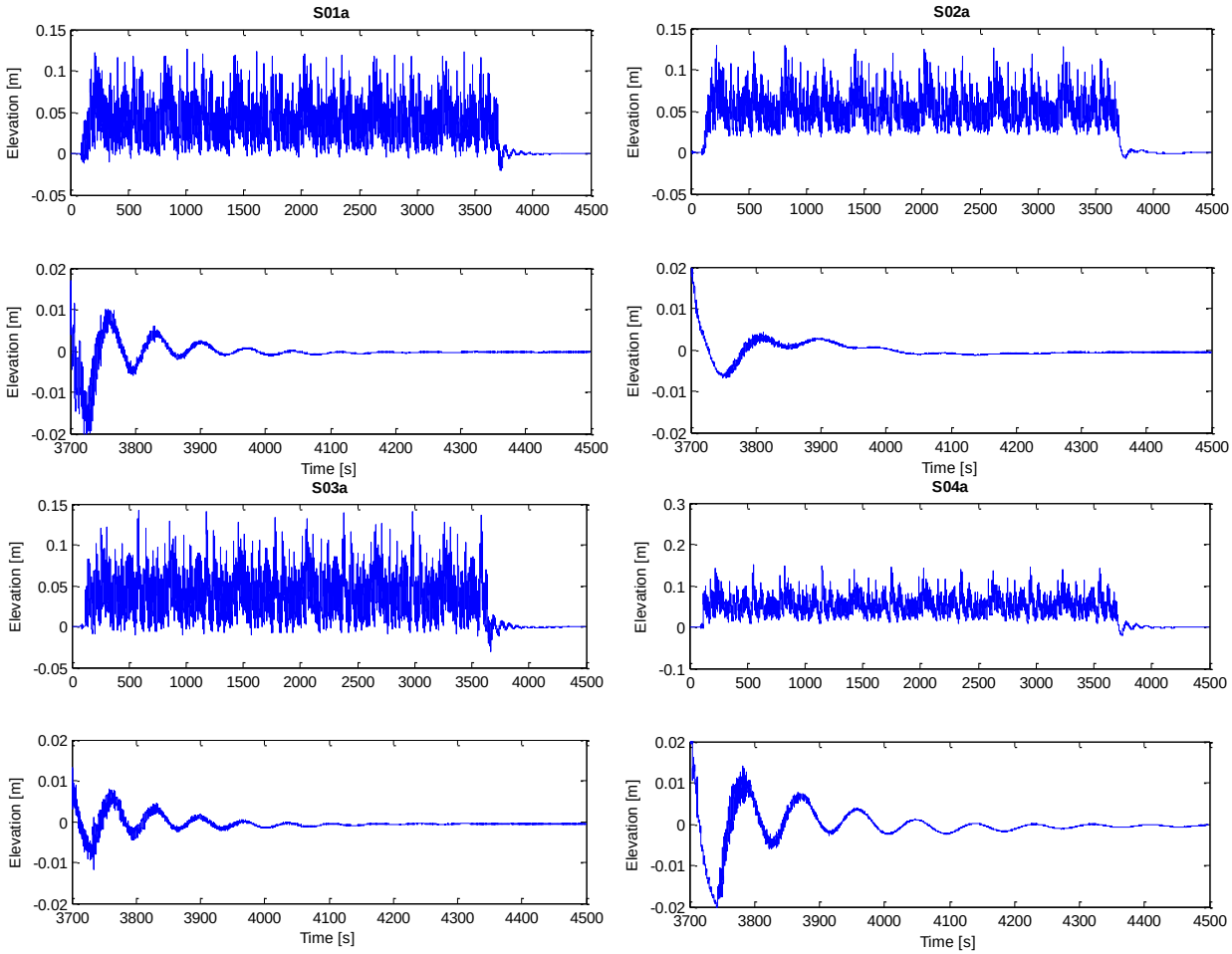

Figure 3.26 Time series of surface elevation at location 17 for S01a-S04a. Top figure is the total time series, bottom figure is a close-up of the period when the wave maker has stopped.

To compare the observed period with the theoretical eigen period of a basin, the eigen period is calculated by the approximation of Dean and Dalrymple (1991). The reef flat is schematised as a basin with one closed end and one open end. The lowest order oscillation that can exist in that case is a wave with a node on the open end, at the reef crest, and an antinode on the closed end, at the beach. The period of this oscillation can be calculated by using the fact that the distance between the node and antinode is a quarter of the wave length and using that the period $T = \frac{L}{c}$. The expression obtained for the eigen period of the reef flat becomes:

$$T = \frac{4 * L_f}{\sqrt{gh}} \tag{3.15}$$

The calculated values of the eigen period are included in the table and they compare quite well with the visually observed period of the oscillations after the forcing is stopped, considering that the schematisation is quite rough. The peak that was observed in the

spectrum at location 17 is therefore likely to be caused by resonance at the eigen frequency of the reef flat, also called seiching.

Table 3.4 Overview of observed and calculated resonance period/frequency for all simulations

Simulation	Visually observed period of oscillation [s]	Frequency [Hz]	Calculated eigen period reef flat [s]
S01a h_r=0.1m rough bed	65	0.015	56.5
S02a h_r=0.05m rough bed	83	0.012	80
S03a h_r=0.1m smooth bed	65	0.015	56.5
S04a h_r=0.05m smooth bed	83	0.012	80

Theoretically the wave propagation velocity can be influenced by the bottom friction and can in turn result in a different eigen period of a basin. According to Roelvink and Reniers (2012) the wave propagation velocity is affected by the bottom friction in the rough cases as follows:

$$c = \sqrt{gh}\frac{1}{\sqrt{1+\varphi^2}} \tag{3.16}$$

Where φ is a dimensionless friction coefficient:

$$\varphi = \frac{\lambda}{\omega h} \approx \frac{\pi/4 c_f \hat{u}}{2\pi h/T} = \frac{c_f \hat{u} T}{8h} \tag{3.17}$$

Where c_f is the bottom friction coefficient, $\hat{u}$ is the amplitude of the orbital velocity, T is the wave period and h is the water depth. Using $c_f = 0.1$, $\hat{u} = \sqrt{\frac{g}{h}} * \frac{H}{2}$, $h = 0.1\,m$, $H = 0.04\,m$ and $T = 65s\ or\ 83$s it is found that the theoretical propagation velocity c is reduced with about 40%. Filling this new propagation in equation (3.15) results in an almost doubled value of the eigen period of the basin, so theoretically there should be a difference between the eigen period of the smooth and of the rough cases. This difference, however, is not observed in the measurements.

The eigen period of the flume as a whole is found with the formula for a coupled basin which is identical to the one for the reef flat only using the length and depth of the offshore part (Dean & Dalrymple, 1991):

$$T = \frac{2.73 L_2}{\sqrt{g h_2}} \tag{3.18}$$

The first harmonic component of the eigen frequency of the flume is computed to be 0.03 Hz which agrees very well to the frequency of the peak observed in the variance density spectrum. The surface elevation at all time steps at the measurement locations along the flume is plotted in Figure 3.27. The standing wave pattern is unmistakable and from right to

left it shows an antinode at the beach, a node on the reef flat and an antinode at the reef crest. Extrapolating the plot to x=0 would result in a node at the wave maker. The wave maker is not a solid wall, so the virtual length of the flume is extended behind the wave maker with the distance from the reef crest to the wave maker. At the end of this virtual part there would be an antinode in the surface elevation and a node in the velocity (u=0).

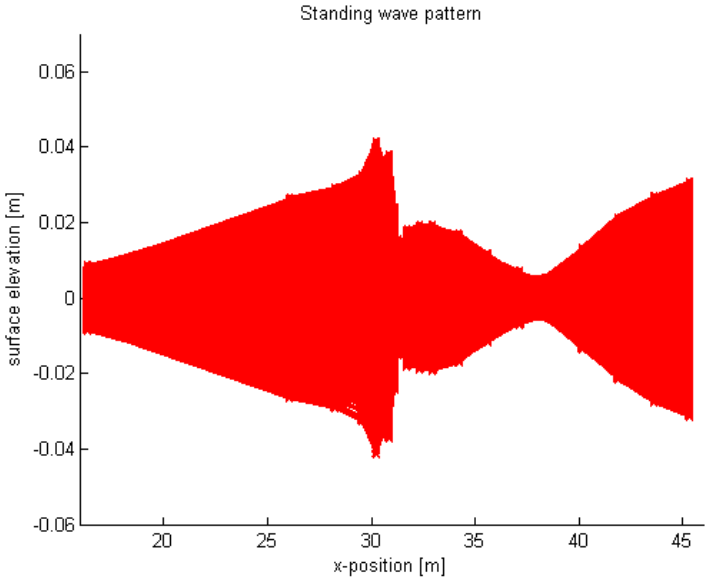

Figure 3.27 Standing wave pattern in the flume at 0.03 Hz

3.7 Summary and conclusions

In this chapter the hydrodynamic data obtained from the experiments was analysed and the important processes were identified in order to provide an answer to the research question:

How do waves transform over a smooth and rough fringing reef?

The specific conditions in a fringing reef environment were shown to have influence on many processes such as infragravity (IG) wave generation, IG wave transformation, seiching, wave-induced setup and wave reflection. In general the findings in this chapter agree well with existing literature about long waves and hydrodynamics on reefs.

Below the main conclusions and some recommendations that were established are summarised.

3.7.1 Conclusions

Analysis of the integral parameters provided an overview of the experiments and provided an insight in some of the hydrodynamic processes that were present. It was found that there is a rather strong reflection of wave energy on the reef crest of 23 to 30% of the incoming wave energy. The reflection of wave energy on the beach is around 80% and is mainly attributed to long waves that are dominant on the reef flat area. The reflection is strongest for the cases S02 and S04 with a lower water depth $h_r = 0.05\,m$. Root-mean-squared values for the velocity in alongshore direction were found to be much smaller than those in cross-shore direction so the experiments will be considered one-dimensional.

The mean water levels were used to determine the wave-induced set-up and set-down. In the shoaling zone a small set-down was found. It was also found that the overall water level offshore was lowered because the water level on the reef was raised and water in the flume is conserved. The water level on the reef was raised significantly to almost double the initial water level h_r for simulation S02 and S04. The set-up was largest for these simulations because of stronger wave forcing and a smaller water column on which the forcing was active. The effect of bed friction on the set-up was negligible comparing S01 and S03, and gave a very minor contribution to the set-up for case S02.

The results of the spectral evolution analysis of the total long wave height ($f<f_p/2$) confirmed the importance of long waves on a fringing coral reef as it showed that they become dominant towards the lagoon and beach. Consistent with Hearn (1999) it was found that a lower water depth enhances the effect of bed friction on waves and flow velocity. Near the beach it was found that the short waves are grouped by water depth, because of depth-induced breaking, and the total long wave height is grouped by bed roughness, mainly by the effect of bed roughness on the seiching motion.

It was observed that the total long wave energy increases towards the beach caused by resonance at the Eigen frequency of the reef flat and the flume and reflection of progressive waves on the beach slope. The long waves were separated into an IG ($0.035<f<f_p/2$ Hz) and a very low frequency, or VLF, range ($0<f<0.035$ Hz) for further analysis.

The IG wave shoaling and generation around the short wave breakpoint was analysed using the normalised bed slope parameter by Battjes et al. (2004) and the surf zone similarity parameter from Baldock (2012). The long waves were observed to shoal according to $h^{-\frac{3}{4}}$

which is not in agreement with the value of -1/4 from Green's law which should be the shoaling regime according to Battjes et al. (2004) for the bed slope parameter of 0.7 that was found. The fact that the IG waves shoal according to $h^{-\frac{3}{4}}$ indicates that there is transfer of energy to the long waves. This could be attributed to the breakpoint mechanism of Symonds et al. (1982) since the results showed that waves were breaking in a steep slope regime and the breakpoint mechanism is supposed to be dominant in that case. The results are in agreement with results from Pomeroy et al. (2012) who showed that long waves are generated at the breakpoint in Ningaloo Reef field data. The reflection of IG wave energy on the reef crest is significant and at the offshore measurement location the reflected waves even dominate the incoming waves.

The VLF range included three peaks in the spectrum which were analysed in detail: a standing wave with a period in the order of 60-80 seconds and one at about 33 seconds and a long period motion of 330 seconds. Analysis of the short wave variation offshore indicated that the 330s motion might be forced by a long period variation in the short wave energy offshore from the reef.

The presence of a standing wave was supported by a decrease of the flow velocity and an increase of wave height at VLF frequencies towards the beach and a clear standing wave pattern observed in time series of waves and flow velocities on the reef. A plot of surface elevation at all time steps showed a standing wave pattern in the entire flume. The observed frequencies of the standing waves showed to agree quite well with theoretical values of the Eigen frequency of the reef and the flume and varied with depth.

3.7.2 Recommendations

It was discussed that the separation of incoming and reflected waves and flow velocity gave rise to some artefacts where the wave height was attributed incorrectly to the reflected wave. It is recommended to look into improving this method by taking into account the nonlinearities and the irregular wave shape as observed on the reef flat.

The observed motion at a period around 330s on the reef was shown to possibly be related to a long period variation in the short wave energy offshore. I recommend to look into this phenomenon further in a more detailed analysis of the data. Relating this long period motion to variation in the short wave forcing can prove to be practically relevant to get a better understanding and prediction of rip currents for example.

The long wave evolution in the shoaling and surf zone was analysed in this report and the breaking of short waves on the steep slope was found to cause generation of long waves by the breakpoint mechanism. It was observed that the long waves shoal on the reef slope and then dissipate a significant portion of their energy possibly due to breaking. The exact processes that play a role in long wave evolution through the surf zone are still under debate and would be an interesting topic for further research.

All processes described are observed in the quasi-1D environment of the Scheldt Flume at Deltares. One-dimensional modelling is a good start to get an understanding of all the processes that are relevant for a certain situation. Now that some of these processes have been established, it would be possible to compare observations with data from a two-dimensional experiment. For example the wave-induced set-up and the resonance might be strongly affected by two-dimensional processes.

4 Morphological experiment data analysis: Sediment concentration and bed profile measurements

4.1 Introduction

This chapter presents the analysis of the data obtained from sediment concentration measurements using the FOSLIMs and multiple suction samplers described in section 2.5.3. It describes how the sediment suspension and transport and bed profile developments are related to the hydrodynamic processes identified in chapter 3.

Figure 4.1 gives an overview of the measurements and their location in the flume. The green lines indicate the locations of the FOSLIMs of which one was located on the hard reef flat and four above the sandy bed of the lagoon, coinciding with measurement stations 13, 15, 16, 17 and 18. The suction samplers, indicated with PS1, PS2 and MISS, were intended to verify the FOSLIM measurements and to observe the amount of offshore transport. The concentrations obtained with these sampling devices proved to be quite useful as explained in the following sections.

Before each run and after one, three and seven hours the bed profile of sandy area was measured. These measurements are also discussed and compared to the concentration measurements in this chapter.

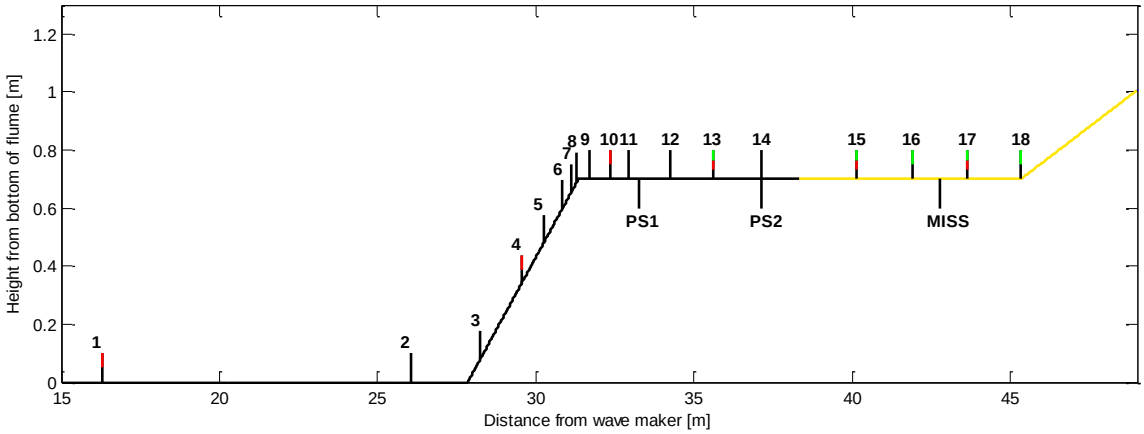

Figure 4.1 Overview of measurement locations; FOSLIM concentration meters are indicated with green, the two point samplers are indicated with PS1/2, the multiple inlet suction sampler with MISS.

Section 4.2 starts with a general overview of the concentration measurements during the entire experiment. The mean FOSLIM and sampling concentrations are determined, analysed and compared. Depth-averaging of the sampling and FOSLIM concentrations by curve-fitting is discussed. For the FOSLIMs this is possible at location 15 and 18 since these FOSLIMs were moved vertically during the runs to measure the concentration at 2, 4 and 6 cm above the bed. 10-minute spectra were generated by the wave maker so the hydrodynamic conditions in the flume were repeated every 10 minutes. Combined with the vertical movement of the FOSLIM this fact was used to create vertical sediment concentration profiles. In order to do this the total FOSLIM time series was cut up into multiple intervals coinciding with a vertical position change. These intervals were synchronised and truncated using the hydrodynamics in such a way that each interval is forced by identical

hydrodynamics. This will be referred to as ‘FOSLIM stacking’. With the mean at each vertical position three data points are obtained and these are used to create a vertical concentration profile that can be depth-integrated. In the overview also the observations of ripples in the bed is discussed.

Section 4.3 assesses both long and short wave velocity contributions to bed-load transport using the third order flow velocity moment as introduced by Roelvink and Stive (1989). Their definition is extended to include higher-order long wave moments and subsequently the development of the different components of the velocity moment over the reef flat is determined and analysed.

Next, section 4.4 focuses on the correlation between measured hydrodynamics and suspended sediment concentrations. The process of sediment suspension is of a stochastic nature in the sense that it can be hard to attribute suspension events directly to a particular hydrodynamic process. Therefore use is made of averaging and low-pass filtering to obtain correlation between long and short wave flow velocity and sediment concentrations.

As the last part of the analysis section 4.5 presents the profile development of the bed level in the lagoon and beach area. The profile development is used to verify the findings of the earlier sections.

Finally, section 4.6 summarises the most important findings and conclusions of the sediment data analysis and how they can be compared to the numerical model XBeach.

4.2 Overview of measurements

This section starts with an overview of the averaged, measured concentrations with the FOSLIMs and the different suction samplers, points out some general trends in these concentrations and assesses the quality of the measurements. Next, to be able to compare XBeach with the experiments, it is required to obtain depth averaged concentrations from the experiment, because XBeach only outputs depth averaged values. The computation of the depth averaged concentrations is discussed further below in this section as well as observations of the bed ripple height.

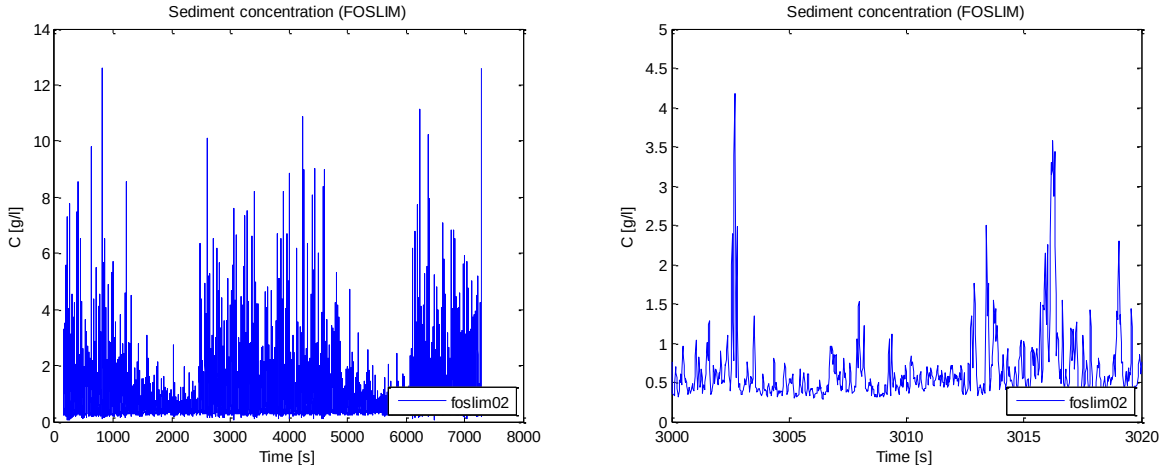

Figure 4.2 Example of concentration signal in g/l measured at location 15; left panel: entire time series, right panel: close-up of 20 seconds.

4.2.1 Mean concentrations on reef

Suspended sediment concentrations were measured on the reef by means of five FOSLIMs, one multiple inlet suction sampler (MISS) with five suction tubes, and two suction samplers with a single suction tube.

The single point samplers and the FOSLIM at location 13 were located seaward of the sandy lagoon to observe the amount of offshore transport of sediment. The remaining four FOSLIMs and the MISS were located above the sandy lagoon (Figure 4.1). An example of the FOSLIM signal for simulation S01b is found in Figure 4.2. This is one of the 'stacked' FOSLIMs and the effect of moving the FOSLIM vertically is visible in the signal for example in the discontinuities around 1300, 1900 and 2500 seconds where the concentration suddenly drops as the FOSLIM is moved from 2 to 4 to 6 cm above the bed and increases as it is moved back to 2 cm.

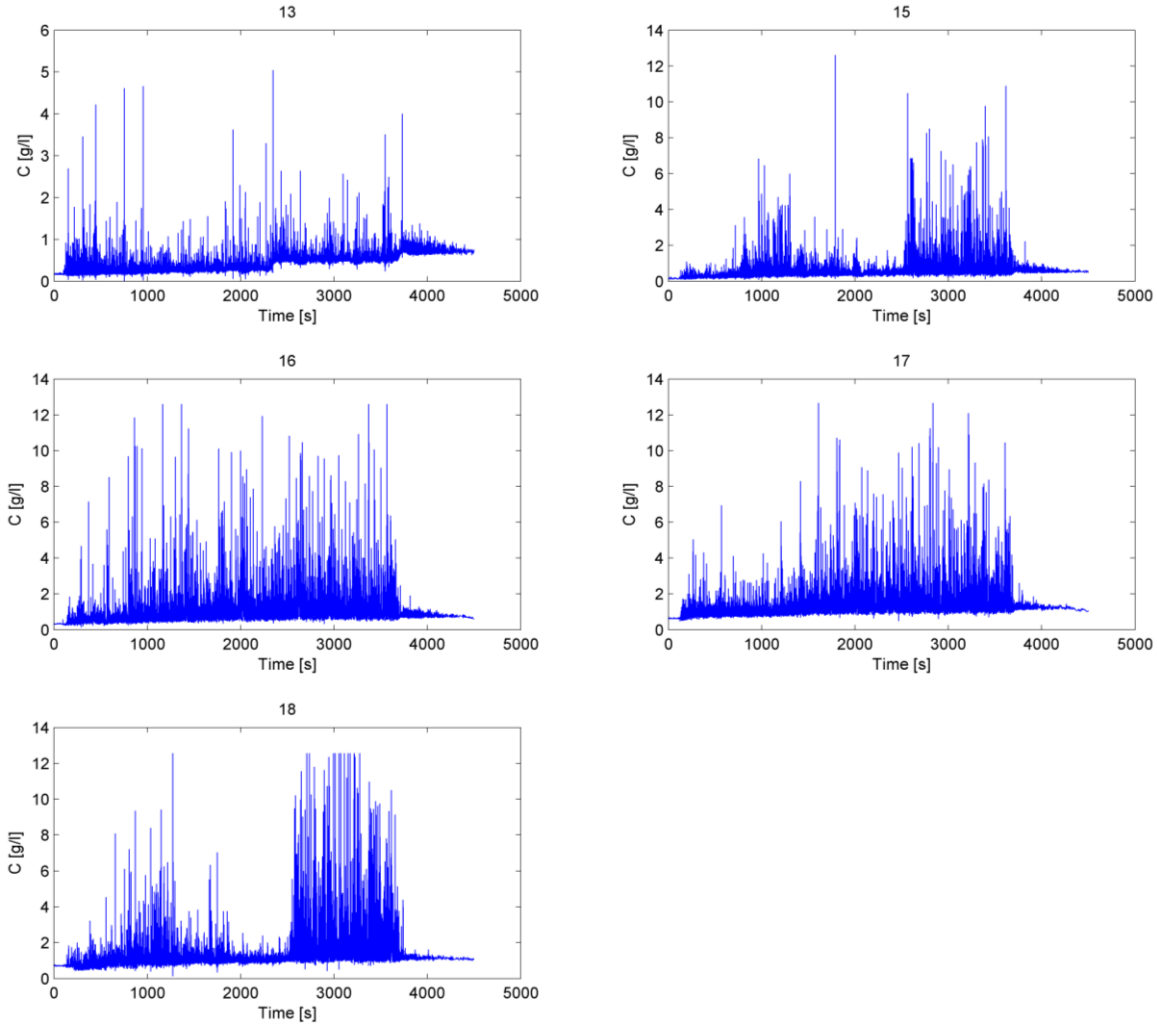

Figure 4.3 Overview of sediment concentration time series measured by the FOSLIMs at different locations using S02a as an example. The measurement station belonging to the signal is shown above each panel. Concentration in g/l.

Figure 4.3 presents an overview of the concentration time series that were measured with the FOSLIMs at all measurement locations in the flume during simulation S02a. The time series

suggest that the FOSLIMs measure a certain background concentration as the measured concentration is not zero at t=0 and remains more or less constant after the waves have stopped approximately 900 seconds before the end of the measurement time series. Similar figures for other simulations can be found in Appendix C and show the same tendency. The start and end concentrations were not constant for the different parts and simulations, varying between 0 and >1 g/l. These values are caused by the fact that at the end of a run, and sometimes also at the start, the water was still turbid because the fine particles were not yet settled. Even though the sediment used was supposed to be very narrow graded with a very small fraction of fines the turbidity was quite significant, see for example Figure 4.4. The figure shows a section of the flume with a rippled bed and a very turbid and non-transparent water column during one of the breaks so there was no wave activity.

Figure 4.4 Turbidity in the water and ripple formation during simulation S01

The optical measurement by the FOSLIMs turned out to be very sensitive to this turbidity. It was therefore decided to subtract the observed background concentration from the total signal measured by the FOSLIMs.

After subtracting the background concentration, the averaged, measured concentration at 2 cm above the bed by the FOSLIMs was calculated over the entire time series for each part of each simulation. The level of 2 cm was used because the three FOSLIMs at location 13, 16 and 17 remained at 2 cm above the bed for the entire experiment. The result is presented in Table 4.1.

The same table for the mean concentrations without subtracting the background concentrations can be found in the appendix for comparison.

Table 4.1 Mean measured concentrations with FOSLIMs per part of each simulation at 2 cm above the bed. ***Mean of start and end concentration is subtracted from the values of Table 7.3 (appendix).*** *Concentrations in g/l. (*FOSLIM malfunctioned during run;**Run interrupted)*

S01	Location						S02	Location				
Part	13	15	16	17	18		**Part**	13	15	16	17	18
a	-0.03	*	0.40	0.54	0.66		**a**	-0.03	0.21	0.47	0.41	0.30
b	0.04	0.43	0.85	0.82	1.07		**b**	-0.08	0.15	0.45	0.52	0.43
c	0.06	0.56	0.52	0.98	0.74		**c**	0.01	0.24	0.41	0.36	0.44
Mean	**0.02**	**0.49**	**0.59**	**0.78**	**0.82**		**Mean**	**-0.04**	**0.20**	**0.44**	**0.43**	**0.39**
Mean concentrations in g/l												
S03	Location						S04	Location				
Part	13	15	16	17	18		**Part**	13	15	16	17	18
a	-0.17	0.56	0.86	0.57	0.72		**a**	-0.01	0.33	0.42	0.42	0.51
b	0.03	0.78	1.11	1.03	1.11		**b**	0.06	0.50	0.57	0.80	0.59
c	**	**	**	**	**		**c**	0.03	0.37	0.53	0.78	0.57
d	0.08	0.74	0.84	1.21	0.96							
Mean	**-0.02**	**0.69**	**0.93**	**0.94**	**0.93**		**Mean**	**0.03**	**0.40**	**0.50**	**0.67**	**0.56**

In all four simulations the concentration at location 15 is lower than the other locations on the sandy part (16, 17 and 18). The concentrations at the other locations on the sand do not show a clear trend and the variation in the values appears to fall within the scatter that can be expected when doing concentration measurements.

The concentration at location 13 is very low for all simulations and sometimes goes below zero because of subtraction of the background concentration, so the measured concentration at location 13 is considered to be <0.1 g/l.

Comparing the simulations S01 and S03 with h_r=0.1m to S02 and S04 with h_r=0.05m shows that the measured concentrations over the sandy bed are higher for S01 and S03. An explanation could be in the short wave flow velocity which is higher for S01 and S03 (Figure 3.14) as the short wave height is mainly depth-dependent (area D in Figure 3.8).

The differences between different parts of simulations are possibly explained by the influence of the background turbidity itself on the concentrations measured by the FOSLIMs, effectively 'blocking' the actual measurement, and by the subtraction of different background concentration values.

The suction samplers measure by a different principle than the FOSLIMs and can be used for comparison and verification. Table 4.2 shows the concentrations that were measured 2 cm above the bed with the MISS. In case there were multiple samples taken during one part of a simulation, the average value is used. The values in the table have been corrected with a factor of 1.3 following Bosman et al. (1987) to compensate the fact that the sediment particle trapping is not 100% efficient when sucking in transverse direction.

The MISS was located between location 16 and 17 so the concentration should be compared to the FOSLIMs at these locations. For the comparison between FOSLIMs and MISS the FOSLIM concentrations *with* and *without* background concentrations are considered. Without subtracting the background concentration the difference between MISS and FOSLIMs is varying over the simulations between -40.1% and +21.5%. The subtraction of the background concentration leads to more consistent results as the FOSLIM concentrations are

approximately half the value of the MISS concentrations for all simulations (44.3% - 56.9%), which suggests that the subtraction of the background concentration is a good choice.

The fact that the FOSLIM concentrations are consistently about 50% lower than the sample concentrations could be related to the turbidity 'blocking' the measurement of larger grains, so removing the turbidity-related background concentrations results in low values for the FOSLIM concentrations.

The use of averaging over the complete simulation in this case has the effect of cancelling out some of the errors in the concentration measurements for both the FOSLIMs and the MISS. For the FOSLIMs these errors are likely to be caused by the influence of the turbidity of the water from fine sediment particles and other possible errors related to measuring concentrations optically at a high frequency.

The samples were taken by pumping water from the flume during a two minute period, so the resulting concentration is an average over just that period, and not over the entire run so the measured concentration depends on the moment the sample was taken. Furthermore the entire process from taking the sample to finding the dry weight of sediment to calculate the concentration is quite sensitive to human errors, such as spilling during transportation and filtering of the samples. Finally the correction factor of 1.3 has an uncertainty of about 3%. An advantage of the sampling method is that it is insensitive to possible background turbidity in the water as these fine particles hardly contribute to the total weight of the sample.

Table 4.2 Concentrations measured with the MISS at 2 cm above the bed per part of each simulation and the mean of these concentrations compared to the mean value of FOSLIM 16 and 17 over the entire simulation and to the mean of these FOSLIMs with the background concentration subtracted. Concentrations in g/l

part of simulation	S01	S02	S03	S04
a	1.41	0.75	2.06	1.88
b	1.03	0.97	1.49	1.05
c	1.27	0.67	1.89	1.19
d	-	-	1.71	-
mean MISS	1.24	0.79	1.79	1.37
mean FOSLIM 16/17 ***background C included***	1.27	0.96	1.13	0.82
difference [%]	**+2.4**	**+21.5**	**-36.9**	**-40.1**
mean FOSLIM 16/17 ***background C subtracted***	0.69	0.44	0.93	0.59
difference [%]	**-44.4**	**-44.3**	**-48**	**-56.9**

Table 4.3 Concentrations measured with the point suction sampler at 2 cm above the bed. PS1 was placed at x=33.26 m, PS2 at location 14 (x=37.14 m). Concentrations in g/l. The values for FOSLIM 13 are considered to be close to zero since some negative concentrations are found. (see Table 4.1)*

	S01		S02		S03		S04	
part of simulation	PS1	PS2	PS1	PS2	PS1	PS2	PS1	PS2
a	0.01	0.02	0.02	0.04	0.01	0.05	0.00	0.05
b	0.03	0.07	0.01	0.09	0.02	0.09	0.03	0.04
c	0.3	-	0.01	0.06	0.06	0.18	0.02	0.12
d					0.07	0.20		
mean point samplers	**0.11**	**0.05**	**0.01**	**0.06**	**0.04**	**0.13**	**0.02**	**0.08**

The point samples that were taken on the reef flat are presented in Table 4.3 and show that there was very little offshore transport over the reef flat. The concentrations measured by PS1 and PS2 are close to zero which is in agreement with the FOSLIM signal at location 13.

Considering the abovementioned uncertainties in both concentration measurement methods, the deviations between the two were to be expected and the results should be treated with care and consideration. However, for the purposes of comparing the experiment with a depth averaged model like XBeach the results are quite usable, since an order of magnitude agreement with XBeach would already be very satisfactory regarding sediment concentrations. Also for comparing general trends between the experiments and XBeach the measurements suffice.

4.2.2 Depth averaged concentrations

As mentioned above, depth averaged concentrations were obtained to compare the experiments to XBeach. This was done using a standard Rouse concentration profile which is fitted through the data points for the FOSLIMs at location 15 and 18 at 2, 4 and 6 cm above the bed and for the MISS at 2, 3, 4, 5.5 and 7.5 cm above the bed. The formulation for this standard Rouse concentration profile is the following (Van Rijn, 1993):

$$\frac{c}{c_a} = \left(\frac{a}{h-a}\frac{h-z}{z}\right)^{\frac{w_s}{\kappa u_{*,w}}} \tag{4.1}$$

Where:

c = concentration [kg/m^3]
c_a = reference concentration [kg/m^3]
a = thickness of bed load layer (reference level) [m]
h = water depth [m]
z = height above bed [m]
w_s = particle fall velocity for suspended sediment [m/s]
κ = Von Karman constant (0.4) [-]
$u_{*,w}$ = time-averaged bed-shear velocity [m/s]

The concentration profile is fitted through the measured data points using the reference concentration c_a and the exponent $\frac{w_s}{\kappa u_{*,w}} = Z$ as free parameters. The fit is made based on a least-square-error curve-fitting method. For the thickness of the bed load layer a a typical value of a half ripple height is selected, $\frac{1}{2}\Delta_r$ (Van Rijn, 1993), which is determined at 5 mm from observations, see Figure 4.4. The water depth h is selected as the mean water level over the entire time series, so it includes the wave setup. The Rouse profile assumes that c=0 at the water surface. The actual curve fitting shows at least for the sampled concentrations that this is a good assumption.

The concentration profile is fitted through the five data points for each sampling event separately. The FOSLIM concentrations at different levels are also measured at multiple instants but appear more scattered than the sampling concentrations. In order to correct this to some extent the fit is made through the average of the FOSLIM concentrations at each height above the bed. See the examples in Figure 4.5 below where the concentration profiles for the simulations S02c, S03b and S04a are shown for both the sampled concentrations and the FOSLIM concentrations.

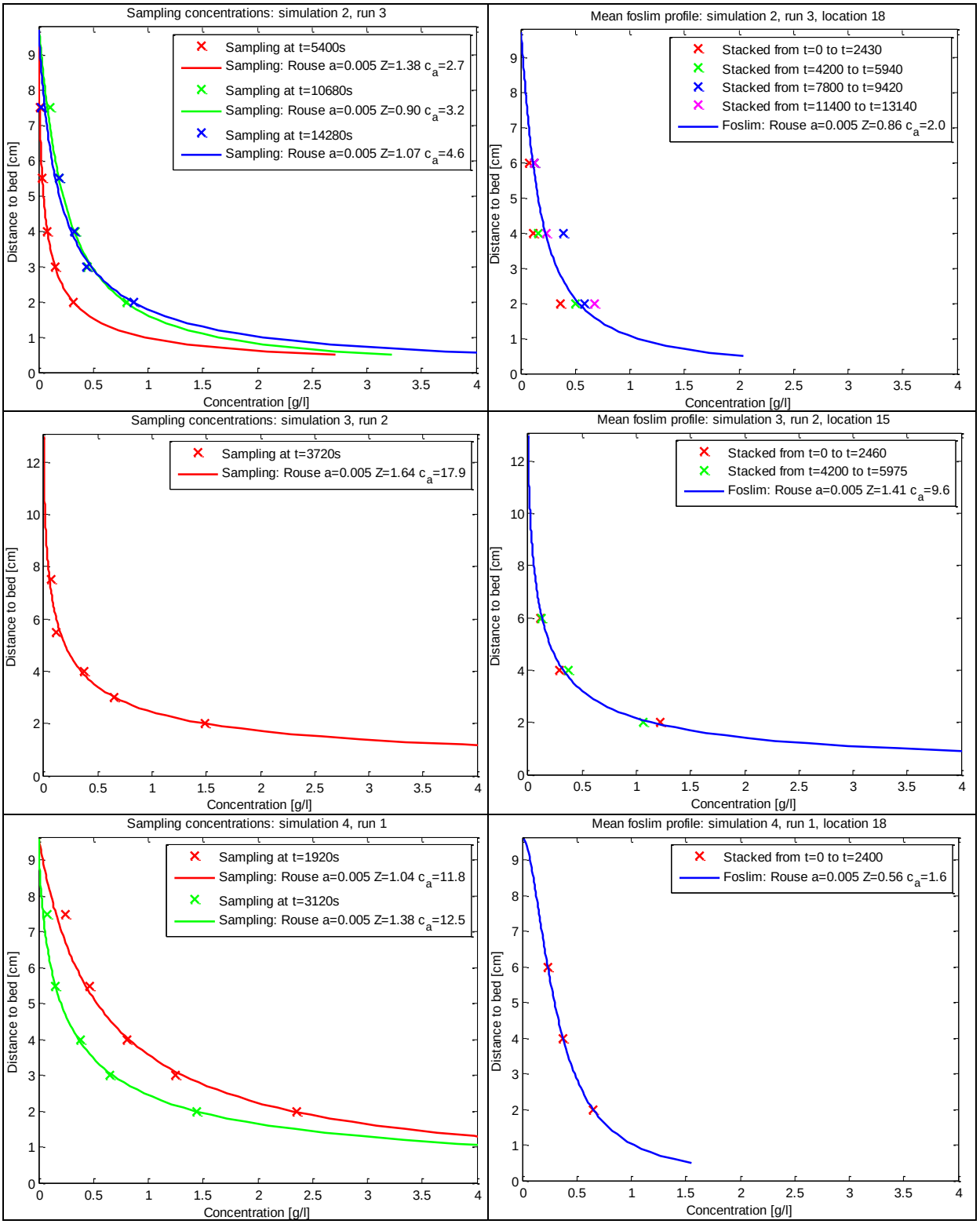

Figure 4.5 Examples of Rouse profile fitting on sediment sample concentrations (left) and FOSLIM concentrations (right)

The shape of the profile based on the sampling appears more consistent comparing the different simulations and samples and in general shows a stronger decrease in concentration when moving up the water column than the FOSLIM concentration profile. The difference in

behaviour of the concentration over the vertical could be explained by a relative sensitivity of the FOSLIMs for turbidity by fine particles. Fine particles have a lower fall velocity than coarse particles so that they are more easily moved up the water column and they take longer to settle. Therefore the FOSLIMs measure a higher concentration higher in the water column. The sampling concentrations measured at z = 2cm are much higher than the FOSLIM concentrations at that level. Together with the larger vertical concentration gradient the result is that the sampling concentration profile gives rather high concentrations near the bed.

*Table 4.4 Depth averaged concentrations per part of a simulation for each sample taken (S1, S2 and S3) and for the stacked FOSLIM concentrations at location 15 and 18 (F15 and F18), including the mean over the entire simulation. Concentrations are in g/l. Note that the number of samples taken varied per simulation explaining the 'missing' values in the table. * FOSLIM malfunctioned; **error in depth-averaging*

S01	**Measurement**					**S02**	**Measurement**				
Part	S 1	S 2	F 15	F 18		**Part**	S 1	S 2	S 3	F 15	F 18
a		0.65	*	**		**a**	0.64	0.24		0.12	**
b	0.45	0.47	**	0.56		**b**	0.44	0.78		**	**
c			0.35	0.50		**c**	0.2	0.43	0.48	0.17	0.29
Mean	**0.52**		**0.35**	**0.53**			**0.46**			**0.15**	**0.29**
Depth averaged concentrations in g/l											
S03	**Measurement**					**S04**	**Measurement**				
Part	S 1	S 2	F 15	F 18		**Part**	S 1	S 2	S 3	F 15	F 18
a	1		0.41	0.44		**a**	1.3	0.91		0.29	0.38
b	0.78		0.53	0.82		**b**	0.66	0.53		0.28	0.39
c	0.63	1.10	**	**		**c**	0.48	0.76	1.13	0.25	**
d	0.65	0.85	0.46	0.69							
Mean	**0.84**		**0.47**	**0.65**			**0.82**			**0.27**	**0.39**

The concentration profiles are integrated over the water column and divided by the water depth to get the depth averaged concentrations as shown in Table 4.4. The hydrodynamic conditions during each part of a simulation are constant, so it is possible to take a mean over all depth averaged concentrations for all the samples and for each of the FOSLIMs in one simulation. The resulting mean values of the depth averaged concentrations are also presented in the table. The number of samples taken varied per simulation explaining the empty spaces in the table.

The MISS is located approximately in the middle between the FOSLIM locations 15 and 18. In all simulations there is an increase in the depth-averaged concentration from location 15 to 18. In simulations S01 the value of the mean depth-averaged concentration obtained by sampling is between those of FOSLIM location 15 and 18 whereas in the other simulations the value found by sampling is higher than both FOSLIM concentrations. Comparing deep to shallow cases, S01 to S02 and S03 to S04, the concentrations found for the deep cases are slightly higher for the sampling measurement method and for the FOSLIM measurements the difference between deep and shallow is larger.

An explanation for these differences could be in the fact that in general a high scatter is observed in sediment concentration measurements and in some cases only one depth-averaged concentration is available which creates a very high uncertainty about the value. The difference between deep and shallow cases for the FOSLIM concentrations could be explained by the depth-averaging method since the FOSLIMs measure relatively high concentrations higher in the water column. This affects the shape of the concentration profile

leading to differences when the profile is integrated over depth, compare for example Figure 4.5 middle right panel to the bottom right panel.

The curve-fitting function returns a value for the reference concentration c_a and the Rouse number ($Z = \frac{w_s}{\kappa u_{*,w}}$). Particularly the value of the Rouse number that is obtained for each fit gives some useful information regarding the concentration data, because it can relate the type of profile obtained to a dominant mode of transport, see Table 4.5.

Table 4.5 Transport modes as a function of the Rouse number categorisation (repeated from Table 2.1)

Bed Load: >2.5	**bed**
50% Suspended load: 1.2 - 2.5	**s50**
100% Suspended load: 0.8 - 1.2	**s100**
Wash Load: < 0.8	**wash**

The computed values of the Rouse numbers obtained by fitting are summarised in Table 4.6 for all simulations. The mean of all Rouse numbers is calculated by averaging over an entire simulation and matched to one of the transport modes of Table 4.5. The mean values for the sampling concentration profiles range from 1.14 to 1.33, which would indicate mainly suspended transport, with a small contribution of bed load transport. The mean values for the FOSLIM concentration profiles range from 0.69 to 1.38, indicating a wash load regime for the shallow water cases and a suspended regime for the deep water cases.

The relatively low Rouse numbers for the shallow water cases are mainly related to the shape of the profile being different for a larger water depth, compare again the middle right panel and the bottom right panel of Figure 4.5, where the top part of the curve is shaped differently to achieve c=0 at the water surface. This effect, combined with in general a smaller vertical gradient in the data points compared to the sampling measurements, leads to a lower Rouse number for the shallow water cases.

The less steep vertical gradient observed in the FOSLIM measurements supports previous remarks that the FOSLIMs are sensitive to the turbidity that was present in the water column (Figure 4.4). As the figure shows, the turbidity was uniform over the water column and so the FOSLIMs measured a relatively high concentration at each vertical position, whereas the sampling method performed better in measuring the vertical gradient in sediment concentrations because it is insensitive to the turbidity.

Without removing the background concentration the Rouse numbers belonging to the FOSLIM concentrations were all in or very close to the wash load regime (appendix C), whereas they are in or closer to the suspended load regime when the background concentration is removed. As discussed in section 2.3 about scaling it is desirable to maintain the transport regime between the prototype and the model.

This is achieved quite well in the experiments as the sampling Rouse numbers are in the suspended load regime for all simulations and the FOSLIM Rouse numbers are in the suspended regime for simulation S01 and S03.

Table 4.6 Rouse numbers $Z = \frac{w_s}{\kappa u_{*,w}}$ from sample concentration profiles (s1, s2, s3) and for FOSLIM concentration profiles (f15, f18). The bottom row of each simulation indicates the type of transport related to the Rouse number.

s01	S1	S2	F15	F18		s02	S1	S2	S3	F15	F18
a	1.37		*	**		a	1.26	1.27		0.49	**
b	0.93	1.12	**	1.14		b	1.39	1.39		**	**
c			1.2	1.28		c	1.38	0.9	1.07	1.08	0.86
mean	1.14		1.2	1.21		mean	1.24			0.79	0.86
cat.	s100		s100	s50		cat.	s50			wash	s100
Rouse numbers											
s03	S1	S2	F15	F18		s04	S1	S2	S3	F15	F18
a	1.48		1.1	1.1		a	1.04	1.38		0.62	0.56
b	1.64		1.41	1.49		b	1.07	0.91		0.63	0.73
c	0.98	1.44	**	**		c	1.03	2.13	1.11	0.82	**
d	1.13	1.31	1.18	1.54							
mean	1.33		1.23	1.38		mean	1.24			0.69	0.65
cat.	s50		s50	s50		cat.	s50			wash	wash

4.2.3 Ripples

During the experiments the development of bed forms was manually registered by means of measurement tapes that were attached to the outside of the flume at 1m intervals (Figure 4.6). The tapes were used to measure the height of the ripples that were developing at the sandy part of the reef flat, or the lagoon. It was observed that ripples started forming within minutes after the start of the experiment and that they were fully developed after about 10 minutes. The ripple height varied from a few millimetres to 18 mm. An average value of 10 mm was assumed for the calculation of depth averaged concentrations. After formation the ripples were slowly moving in onshore direction.

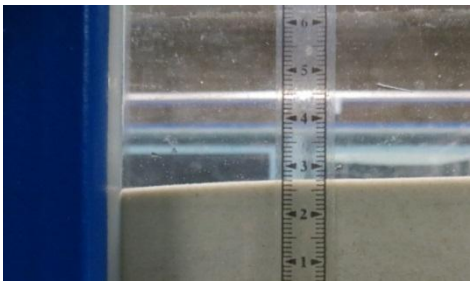

Figure 4.6 Measurement tape for measuring ripple height

The presence of ripples can affect the sediment concentration measurements in two ways. The first one is that as the flow passes over the ripple crest vortices are shed on the leeside of the ripple. These vortices suspend a small ‘cloud’ of sediment locally, see Figure 4.7, which is then partially advected and partially settles down to the bed again. This phenomenon may lead to peaks in the measured concentration signal. The presence of ripples also influences the height of the measurement devices above the bed so it will vary with +/- 0.5 ripple height. Since the sediment concentration in general is depth dependent with higher concentrations closer to the bed, the varying distance to the bed can have an effect on the measured concentrations over time.

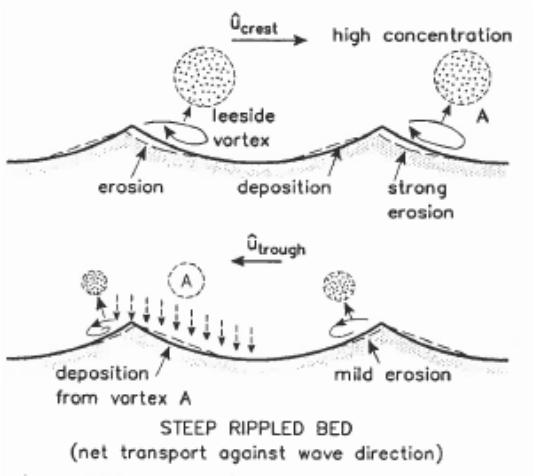

Figure 4.7 Effect of ripples on sediment suspension (figure from: Van Rijn (1993))

The possible role of ripples that is described above falls outside the scope of this thesis but should be further investigated to understand their role in the flume experiments.

4.2.4 Discussion

Table 4.4 shows that the depth-averaged concentrations for the FOSLIMs are lower than those of the sampling method, except for simulation S01. The difference per simulation is more likely to be caused by the measurements methods as such than by some physical phenomenon, particularly since the methods are very different and the shortcomings were already explained above. It was also found that in general the FOSLIM concentrations are consistently lower than the sampling concentrations by about 50% (Table 4.2).

One-on-one comparison of these measured depth-averaged concentrations with XBeach would therefore be unrealistic and the aim should be to get the order of magnitude of the concentrations right. The analysis in this section shows that the measurements by sampling are less sensitive to turbidity and were more consistent than the FOSLIM measurements, so they can be considered more reliable.

It was found that the sediment concentration increased from the seaward side of the lagoon towards the beach, so we could look for that trend in XBeach as well.

4.3 Flow velocity moments

4.3.1 Introduction

This section uses an approach of Roelvink and Stive (1989) to investigate the role of long and short waves in sediment transport. In their approach the flow velocity is subdivided into a wave group mean and a time-varying component as follows:

$$u(t) = \bar{u} + \tilde{u}(t) \tag{4.2}$$

The time-varying component $\tilde{u}(t)$ contains both the variation on the time scale of wave groups and on that of individual waves:

$$\tilde{u} = u_s + u_L \tag{4.3}$$

The third order velocity moment, $\langle u|u|^2 \rangle$, is a measure of wave skewness, which is an asymmetry about the horizontal axis with shallower troughs and larger peaks. A positive skewness indicates a landward sediment transport and vice versa for a negative skewness. The third order velocity moment can therefore be used to predict morphological developments and to assess the contribution of long and short waves. It is decomposed using a Taylor series expansion and assuming $|\bar{u}| < |\tilde{u}|$ (which is correct, see Figure 3.10) as follows:

$$\langle u|u|^2 \rangle = \langle \tilde{u}|\tilde{u}|^2 \rangle + 3\bar{u}\langle |\tilde{u}|^2 \rangle + \bar{u}^3 \tag{4.4}$$

Where < > denotes time averaging. The terms $3\bar{u}\langle |\tilde{u}|^2 \rangle$ and $\bar{u}^3$ are the contributions of the mean flow and the term $\langle \tilde{u}|\tilde{u}|^2 \rangle$ is the contribution of the time-varying component at the time scale ranging from that of wave groups to the individual waves. This time-varying component can be decomposed as follows, using equation (4.3):

$$\langle \tilde{u}|\tilde{u}|^2 \rangle = \langle u_s|u_s|^2 \rangle + 3\langle u_L|u_s|^2 \rangle \tag{4.5}$$

Where in Roelvink and Stive (1989) it is assumed that $u_L \ll u_s$ and u_s to be uncorrelated to $|u_L|^2$ and $|u_L|^3$. The two terms on the right-hand side are the short and the long wave contribution to the third order velocity moment and are referred to by Van Dongeren et al. (2007) as:

- $\boldsymbol{guss} = \langle u_s|u_s|^2 \rangle$ (**short** wave transport and stirring)
- $\boldsymbol{guls} = 3\langle u_l|u_s|^2 \rangle$ (**long** wave transport, short wave stirring)

By calculating the so-called guss and guls the contributions of short and long waves to on- or offshore suspended and bed load transport can be assessed.

This section will look into the development of the third order velocity moment over the reef flat and extend the decomposition of the time-varying component, $\langle \tilde{u}|\tilde{u}|^2 \rangle$, into guss and guls because the assumption that $u_L \ll u_s$ has already been shown to be no longer valid on the reef flat.

Also the contribution of the time-varying component is compared to the contribution of the mean flow components, $3\bar{u}\langle|\tilde{u}|^2\rangle$ and $\bar{u}^3$. This mean flow is usually referred to as undertow and is mainly directed in offshore direction.

4.3.2 Development of velocity moments over the reef flat

4.3.2.1 Time-varying contribution

Without the assumption that the short wave velocity is much larger than the long wave the decomposition of the time-varying part third order velocity moment contains two extra terms with $|u_L|^2$. The quadratic terms $|u_s|^2$ and $|u_L|^2$ can be interpreted as stirring of sediment by the short and long wave velocity respectively. The total decomposition including long wave stirring becomes:

$$\langle\tilde{u}|\tilde{u}|^2\rangle = \langle u_s|u_s|^2\rangle + 3\langle u_L|u_s|^2\rangle + 3\langle u_s|u_L|^2\rangle + \langle u_L|u_L|^2\rangle \quad (4.6)$$

Besides the guss and guls two new terms appear which are named in the same manner which was also described by Rocha et al. (2013) for a different case:

- $\boldsymbol{gusl} = 3\langle u_s|u_L|^2\rangle$ (short wave transport, long wave stirring)
- $\boldsymbol{gull} = \langle u_L|u_L|^2\rangle$ (long wave transport and stirring)

First the development of the time-varying components of the total third order velocity moment over the reef is considered in Table 4.7. Particularly the values at location 15 and 17 are interesting, because these are on the sandy bed of the lagoon. The values are all positive so that would indicate a trend of landward transport by the time-varying components in the velocity moment. The values decrease strongly from location 10 at the reef crest to location 13, 15 and 17 close to and on the sandy lagoon. The values decrease slightly from 13 to 15 and remain more or less constant from 15 to 17, except for case S04b.

Table 4.7 Total third order velocity moment at the four reef locations and for all four simulations.

$\boldsymbol{total} = \langle\tilde{\boldsymbol{u}}|\tilde{\boldsymbol{u}}|^2\rangle * \boldsymbol{10^{-2}}$	**10**	**13**	**15**	**17**
S01b	0.85	0.114	0.078	0.077
S02b	0.75	0.099	0.093	0.10
S03b	1.67	0.14	0.10	0.11
S04b	1.39	0.20	0.145	0.18

Next the relative contributions by the guss, guls, gusl and gull and their development over the reef is determined for all the simulations. The results are presented in Figure 4.8. The contributions are relative to the total time-varying part of the third order velocity moment and add up to 1 at each location.

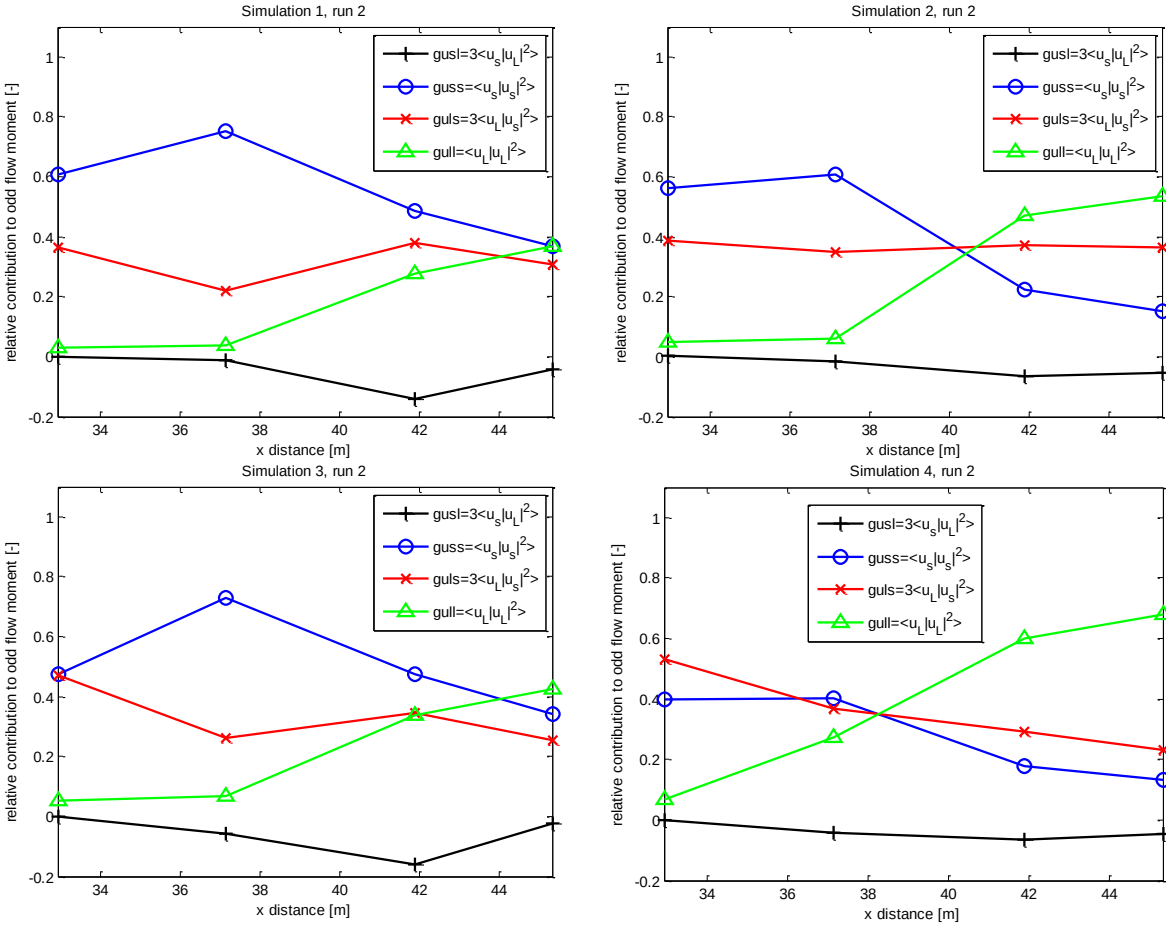

Figure 4.8 Relative contribution as fraction of the total of each of the four components (guss, guls, gusl, gull) to the total third order velocity moment and the evolution over the reef.

It is clear that for the experiments the assumption of $u_L \ll u_s$ is no longer valid since in all simulations the green line of the *gull* becomes the dominant contributing component for the third order velocity moment. It can therefore be expected that the sediment transport in the lagoon is mainly caused by the long waves through long wave stirring and advection. The relative contribution of the *gull* is largest for the cases with a low water depth (2 and 4) since the remaining short wave velocity in those cases is relatively small because of depth-induced breaking of the short waves. Also in the deeper water cases (1 and 3) the contribution of the *gull* is dominant at the end of the lagoon, but in those cases the transport related to the short wave stirring, which is the sum of the *guss* and *guls,* remains more important as these terms together (red and blue line) are the largest contribution to the velocity moment.

Comparing the cases with bed roughness to the cases without roughness, so S01 to S03 and S02 to S04, the effect of the roughness is that it reduces the relative contribution of the *gull* to the total velocity moment. The effect is particularly strong comparing the low water depth cases S02 and S04 and is in agreement with the long wave height and flow velocity evolution found in chapter 3 (Figure 3.8 and Figure 3.14).

The black line indicates the *gusl* which is related to long wave stirring and short wave transport. This term is small and negative for all simulations, indicating a small fraction of offshore transport by the short wave velocity.

As discussed in the previous chapter, the VLF motions of seiching and a short wave related motion contribute significantly to the long wave energy on the reef. This contribution is included in the long wave flow velocity in the above analysis and particularly makes up a large part of the *gull* component. The above plots with the motions at the VLF frequencies filtered out of the long wave flow velocity signal are found in appendix D.

4.3.2.2 *Mean flow contribution*

Besides the time-varying contribution to the third order velocity moment, there is also a contribution by the mean flow, as discussed above. The mean flow contribution to the third order velocity moment is expressed in the terms $3\bar{u}\langle|\tilde{u}|^2\rangle$ and $\bar{u}^3$. Since $\bar{u} < \tilde{u}$ the term $\bar{u}^3$ was found to be negligible. The other term is decomposed using (4.3):

$$\mathbf{3\bar{u}\langle|\tilde{u}|^2\rangle = 3\langle u_s^2\rangle\bar{u} + 3\langle u_L^2\rangle\bar{u}} + 6\langle u_s u_L\rangle\bar{u} + 3\langle u_s^2\rangle\bar{u}^2 + 3\langle u_L^2\rangle\bar{u}^2 \qquad (4.7)$$

The three last terms on the right hand side were checked and found to be negligible compared to the first two terms and are therefore not considered. The first two terms on the right hand side are interpreted according to Rocha et al. (2013):

- $3\langle u_s^2\rangle\bar{u}$ (**short** wave stirring, transport by mean flow)
- $3\langle u_L^2\rangle\bar{u}$ (**long** wave stirring, transport by mean flow)

In the plots in Figure 4.9 the development over the reef of time-varying contribution, $\langle\tilde{u}|\tilde{u}|^2\rangle$, is compared to the total mean flow contribution, $3\bar{u}\langle|\tilde{u}|^2\rangle$, for all four simulations. The short and long part of the mean flow contribution, $3\langle u_s^2\rangle\bar{u}$ and $3\langle u_L^2\rangle\bar{u}$, are also plotted separately. The contributions are computed as fraction of the total third order flow velocity moment to indicate the relative importance of each term. The total third order flow velocity moment is also plotted and is equal to the sum of the mean and the time-varying fraction. The long and short wave contribution (blue and red line), add up to the mean fraction (green line).

The mean flow is negative in all cases (except for the point closest to the beach in simulation S02b) and therefore leads to a negative contribution to the third order flow velocity moment. The magnitude of the mean flow contribution and the time-varying contribution is not far apart, with the time-varying contribution being slightly larger in general, leading to a mostly positive value of the total third order velocity moment.

On the sandy lagoon area, the last two data-points, the total third order moment is positive except for the data-point around x=42 m in the two shallow water cases, S02 and S04. This is caused by a relatively high, negative value of the mean flow, $\bar{u}$, and a high value of the long wave height at this location. Except for these two points the long and short wave stirring term are about the same magnitude.

The graphs show that the mean flow contribution, consisting of long and short wave stirring, is quite significant. The contribution is related to an offshore directed undertow and is therefore always negative. The positive value close to the beach in simulation S02 could be related to the vertical position of the EMS in relation to the flow velocity profile. The total third order velocity moment shows an increasing trend towards the beach and is mostly positive on the sandy area, still indicating onshore directed transport at most locations.

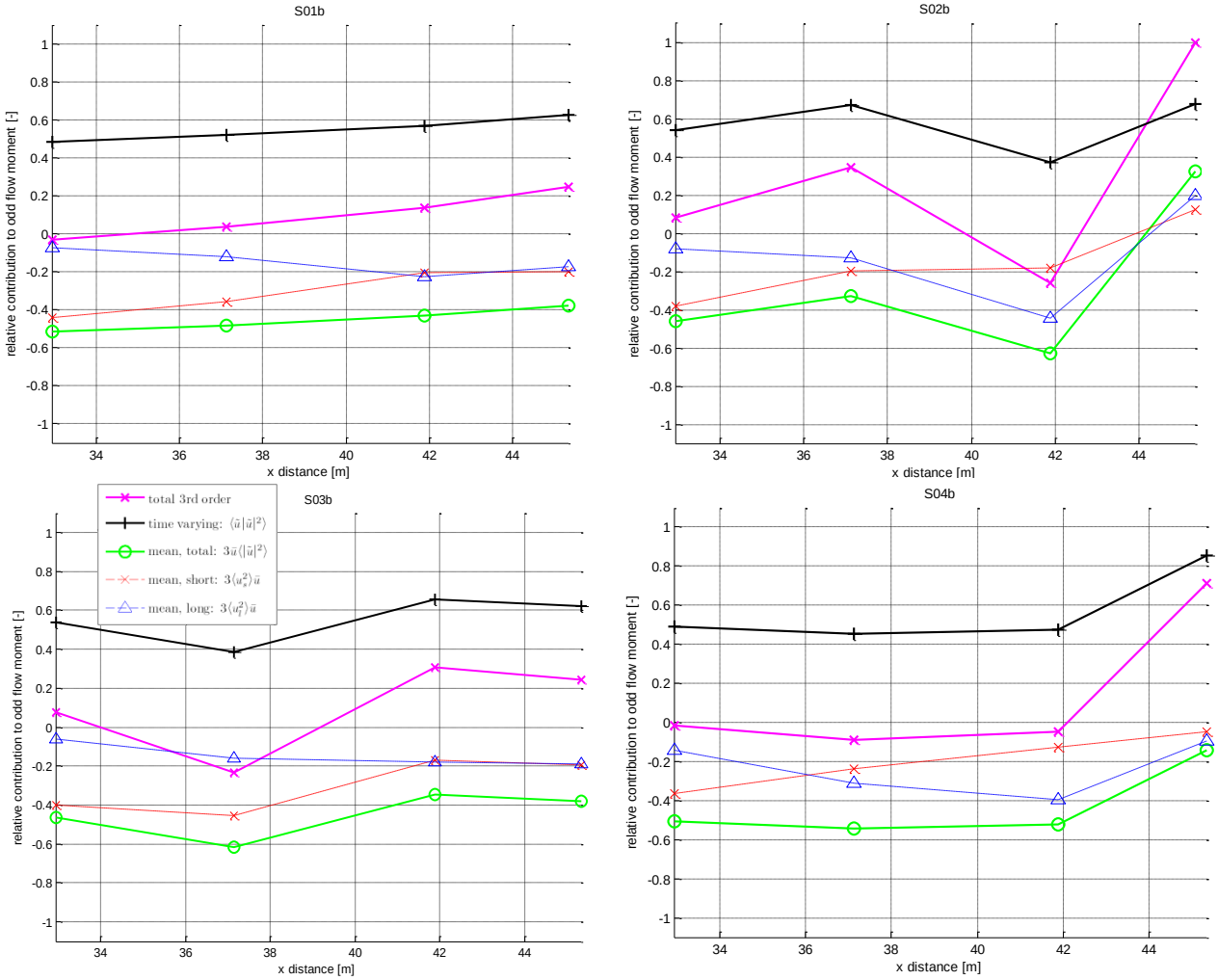

Figure 4.9 Relative contribution as fraction of the total of the time-varying component, $\langle \tilde{u}|\tilde{u}|^2 \rangle$, and the mean flow component, $3\bar{u}\langle|\tilde{u}|^2\rangle$, to the total third order velocity moment and the evolution over the reef. The long and short wave part of the mean flow component are also indicated separately.

4.3.3 Conclusions

In this section the method described by Roelvink and Stive (1989) to find long and short wave flow velocity contribution to the third order flow velocity moment was used. The third order velocity moment is a measure for the skewness of the waves and is related to sediment transport. The assumption that $u_L \ll u_s$ is no longer valid for the experiments so the original expansion of Roelvink and Stive (1989) was extended with two terms related to long wave stirring, see equation (4.6). The two terms are referred to as *gull* and *gusl*.

The evolution of the different components over the reef flat was computed and presented in Figure 4.8. The results show that the contribution related to long wave stirring and transport or advection indeed cannot be neglected in the experiments and even becomes the dominant contribution close to the beach. The results are consistent with the analysis of chapter 3 where it was shown that long waves are dominant in the lagoon. Also the effect of the bed roughness shows in the results, reducing the contribution of the *gull*, and is in agreement with observations described in the previous chapter.

The contribution of the time-varying part, $\langle\tilde{u}|\tilde{u}|^2\rangle$, to the total third order velocity moment is positive, indicating onshore directed transport. There is also a contribution by the mean flow, or undertow, $3\bar{u}\langle|\tilde{u}|^2\rangle$, which results in a negative contribution to the third order moment. The magnitude of this contribution is significant and about the same magnitude of the time-varying part. Still, the total third order velocity moment in general shows an increasing trend towards the beach and is mostly positive on the sandy area, indicating onshore directed transport at most locations.

4.4 Correlation measured sediment concentrations and hydrodynamics

4.4.1 Introduction

The previous paragraph suggests that both long and short waves contribute to sediment transport and suspension. This paragraph attempts to quantify these contribution by looking at the correlation between the concentration and velocity signals. As mentioned in the introduction of this chapter it is hard to correlate sediment suspension directly to a particular hydrodynamic process because of the stochastic nature of sediment suspension. The FOSLIMs, wave gauges and flow velocity meters all measured instantaneous values at 40 Hz, but it turns out that little research is available on methods to directly correlate these signals.

Figure 4.10 illustrates the situation showing the surface elevation, flow velocity and sediment concentration time series at location 17 at some time interval. Visually the suspension events at 1794, 1810 and 1818 seconds appear to be related to the hydrodynamics. The largest suspension event around 1810s coincides with a peak in the flow velocity while the concentration peak around 1818 is even higher but it seems to be related to the peak in the surface elevation. However the two peaks in the surface elevation at 1813-1814s do not cause as much suspension. This shows that due to the spikey nature and stochastic behaviour of the concentration time series the exact correlation to the hydrodynamics is hard to quantify.

Below one method is used which was described by Alsina and Cáceres (2011) to find a correlation between the concentration signal and the short wave flow velocity. For the long waves use is made of low-pass filtering of the sediment concentration signal, where the distinction between long waves and short waves is still made based on a division at half the peak frequency.

The correlation function of Alsina and Cáceres (2011) takes two vectors as input and returns a value between -1 and 1 to indicate how strong the signals are correlated, with 1 meaning that there is a direct linear relation between the two signals and -1 indicating that the signals are inversely correlated. A value of 0 means that the signals have no relation at all.

For the analysis in the following two sections FOSLIM04 at measurement location 17 is used because it is close to the back end of the reef and was not shifted in vertical direction, though similar correlations were found for other measurement locations.

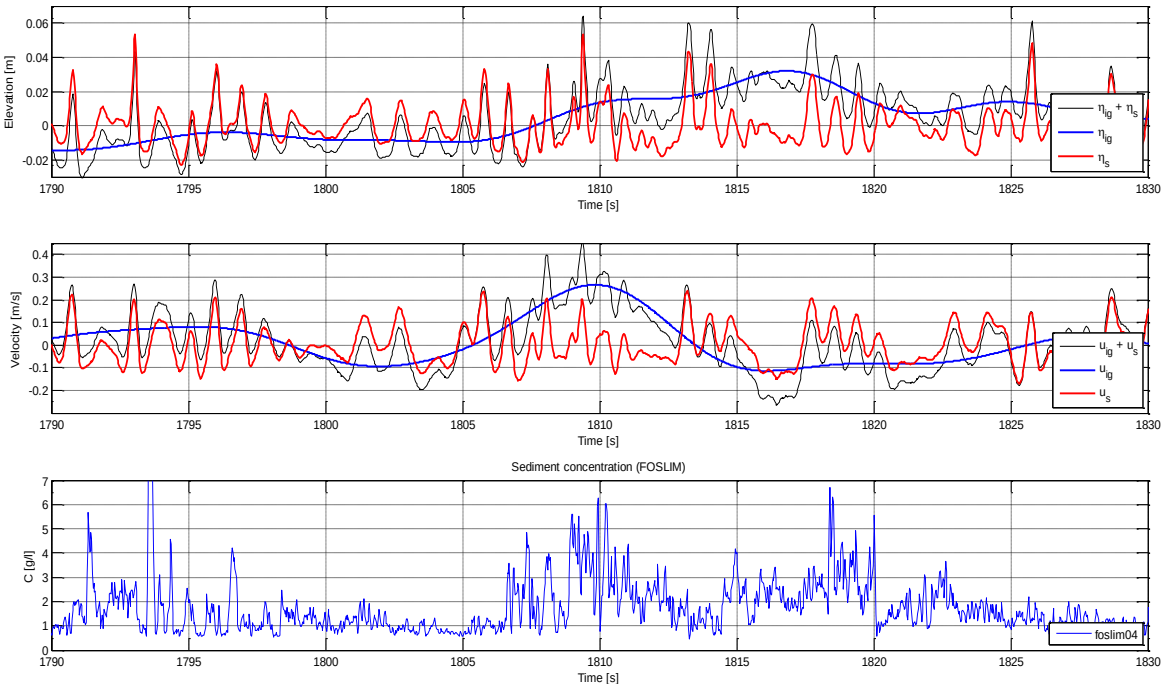

Figure 4.10 Example of time series of surface elevation (top panel), flow velocity (middle panel) and sediment concentration (bottom panel). The total surface elevation and flow velocity is shown and the IG and short waves separately.

4.4.2 Correlation sediment concentration and short waves

As mentioned in the introduction sediment suspension is largely a stochastic process, which is difficult to correlate directly to the instantaneous flow velocity. For the short waves it was attempted to correlate the instantaneous sediment concentration to different variations of the short wave velocity: u_s, $|u_s|$, and u_s^2. None of these attempts resulted in a significant correlation above 0.1.

Alsina and Cáceres (2011) looked at the correlation between hydrodynamics and suspended sediment concentrations in the inner surf zone. Their method uses a running average of the sediment concentration and the short wave flow velocity squared: u_s^2. A running average removes some of the variance from the signal and makes it more smooth taking out some of the random effects. The described method produced good correlations for their data on a steep beach in the order of 0.3-0.4.

The method of Alsina and Cáceres (2011) was applied to the data from the flume experiments, creating a 4s running mean of u_s^2 and the suspended sediment concentration. An example of the resulting time series is presented in Figure 4.11; the top panel for the short wave velocity squared and the bottom panel for the sediment concentration.

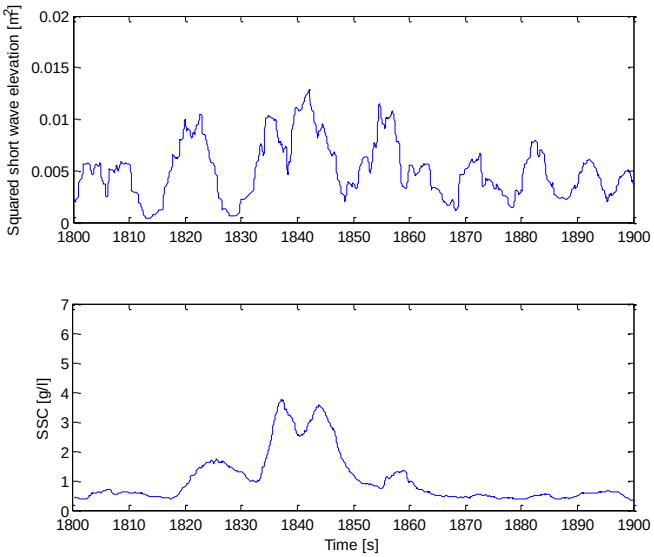

Figure 4.11 Time series of running mean of squared short wave flow velocity (top) and of suspended sediment concentration(bottom)

Next the correlation is calculated between the two time series for different time lags and presented in Table 4.8. Significant correlations are found varying between 0.28 and 0.37 with a maximum time lag of 2 seconds. The correlations indicate that at least part of the suspension of sediment can be attributed the short wave flow velocity. The values for the correlations are consistent with those found by Alsina and Cáceres (2011).

Table 4.8 Correlation and time lag between the a running mean of the short wave flow velocity squared and sediment concentration signal

	S01b (loc. 17)		**S02b (loc. 17)**		**S03b (loc. 17)**		**S04b (loc. 17)**	
	max corr.	time lag[s]	max corr.	time lag[s]	max corr.	time lag[s]	max corr.	time lag[s]
$\langle u_s^2 c \rangle$	0.28	1.3	0.37	1.1	0.35	1.8	0.3	2

4.4.3 Correlation sediment concentration and long waves

To assess a possible role of the long wave flow velocity in stirring up the sediment also the correlation between the long wave flow velocity and the suspended sediment concentration is investigated. The long wave flow velocity u_L remains defined as the velocity signal with a frequency below $f_p/2$. Again, a direct correlation between u_L and the raw concentration signal is not found. If u_L would have influence on the sediment concentration it seems reasonable that this influence can be found in a long period oscillation in the concentration signal.

So in order to find a possible correlation the sediment concentration signal was filtered at different frequencies, leaving only the signal below that frequency. An example of the result of filtering is shown in Figure 4.12 where the concentration signal is filtered below 0.08 Hz.

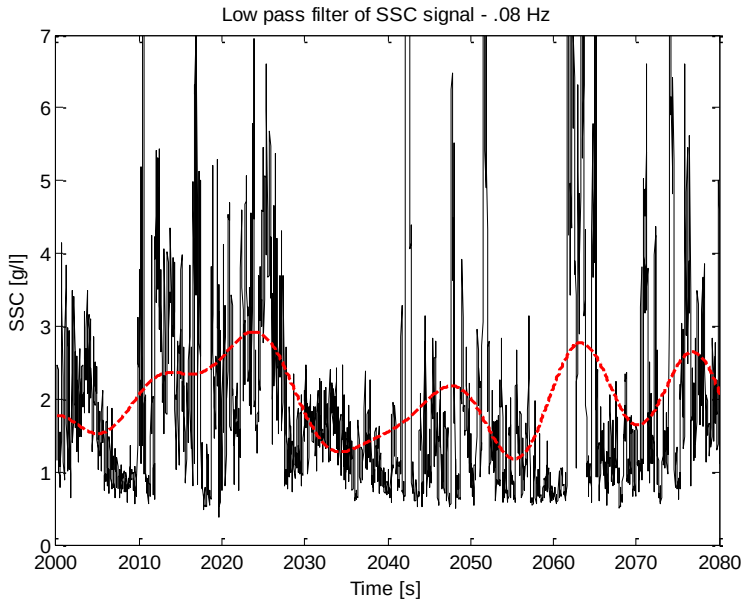

Figure 4.12 Effect of low-pass filtering at 0.08 Hz (red line) of the raw sediment concentration signal(black).

Of all frequencies that were attempted for filtering the sediment concentration signal by far the best results were obtained by filtering at 0.08 Hz, leaving the signal in the range 0<f<0.08 Hz. The values for the correlation were found using similar plots to the one shown in Figure 4.13. The physical meaning of this plot is that it shows how strong the filtered sediment concentration signal and the long wave flow velocity are related at a varying time lag. In this case the time lag indicates the time between the actual stirring or advection by the flow velocity and the measurement of the sediment concentration related to the stirring or advection. The sediment may not be stirred instantaneously and it needs some time to move up the water column to the height of the FOSLIM. Also when sediment is advected by the flow velocity this may lead to a time lag. However, the lag should be small compared to the wave period. The maximum correlation in the plot and the corresponding time lag were determined and the results for all simulations are presented in Table 4.9.

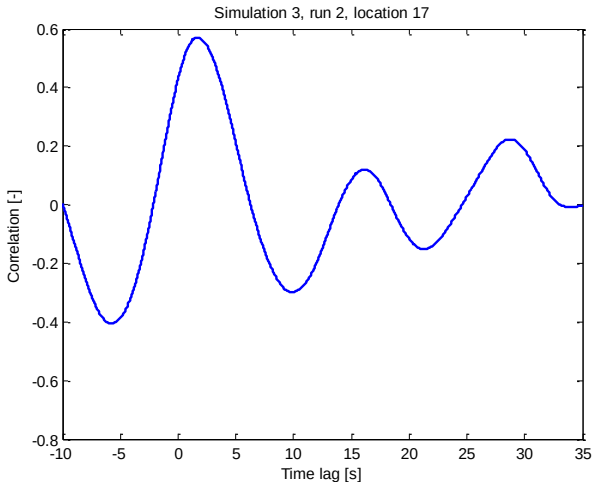

Figure 4.13 Resulting correlation and time lag from the correlation analysis.

Table 4.9 Correlation and time lag between long wave flow velocity u_L and low pass filtered (0.08 Hz) sediment concentration signal $c_{0.08}$.

	S01b (loc. 17)		S02b (loc. 17)		S03b (loc. 17)		S04b (loc. 17)	
	max corr.	time lag[s]	max corr.	time lag[s]	max corr.	time lag[s]	max corr.	time lag[s]
$\langle \boldsymbol{u_L c_{0.08}} \rangle$	0.5	2.2	0.48	1.2	0.57	1.7	0.35	3.5

The correlations are quite large and suggest that there is a relation between the long waves and the measured suspended sediment concentration. The time lag varies between 1.2 and 3.5s, which is relatively small compared to the long wave period, which is in the order of 5-7 times the peak frequency, so 15-20s. The long waves appear to cause a long period variation in the sediment signal at location 17.

The physical meaning of this correlation is a bit unclear since a correlation between the sediment concentration and u_L would suggest that a high concentration is mainly related to positive flow velocities. Physically a correlation with u_L^2 would be more meaningful and in agreement with the *gull* contribution from the previous paragraph, but as Table 4.10 shows, the use of u_L^2 produces only low correlations at relatively high time lags.

Table 4.10 Correlation and time lag between long wave flow velocity squared u_L^2 and low pass filtered (0.08 Hz) sediment concentration signal $c_{0.08}$.

	S01b (loc. 17)		S02b (loc. 17)		S03b (loc. 17)		S04b (loc. 17)	
	max corr.	time lag[s]	max corr.	time lag[s]	max corr.	time lag[s]	max corr.	time lag[s]
$\langle \boldsymbol{u_L^2 c_{0.08}} \rangle$	0.18	7.5	0.13	0.5	0.23	5.5	0.29	6

4.4.4 Discussion

The above sections have shown that it is hard to correlate the measured sediment concentrations directly to the hydrodynamics. Visually some relation between episodes of high sediment suspension and the wave height or flow velocity can be observed (Figure 4.10), but it remains a challenge to quantify the exact relation.

By means of averaging and low-pass-filtering the stochastic variability in the concentration signal was reduced and a correlation was found with both the long and the short wave flow velocity. The correlations indicate that both long and short wave influence the measured sediment concentration but the exact processes underlying these correlations remain unclear. Though it is likely that the short waves stir up the sediment and the long waves contribute by stirring up and advecting the sediment.

The role of long waves in sediment dynamics is a specific feature for a fringing reef lagoon environment as it was already shown that long wave height is equal to or dominates the short wave height in the lagoon.

4.5 Bed profile development in lagoon and beach area

Bed profile measurements were performed before each simulation and after one, three and seven hours. The measurements are summarised in Figure 4.14 for all simulations. The profile developments look similar for all the simulations with a lowering of the bed level at the start of the lagoon (x=38-40 m) and an increase of the bed level in the remaining part of the lagoon (x=40-45 m). Also a steepening of the beach slope is observed and the formation of a swash bar at a height of about 0.20-0.25 m. The swash bar is logically located at a lower level for simulation 2 and 4.

There are two clearly observable differences between the rough (1 and 2) and the smooth (3 and 4) cases. The first one is in the shape of the swash bar which seems to be more pronounced and located higher up the slope for the smooth cases and secondly the lowering of the bed level at the start of the lagoon appears to be slightly stronger in the smooth cases.

Both differences are likely to be an effect of the larger long wave height and corresponding flow velocity in the lagoon for the smooth cases. The flow velocity at the onset of the lagoon is higher in the smooth cases causing more clear-water scour at the transition from hard reef to the sandy lagoon. At the beach the long waves are higher for case 3 and 4 increasing the intensity with which the swash bar is developed.

It is suggested to relate these observations to the run-up measurements that were done during the hydrodynamic part of the experiments (Buckley (in prep)).

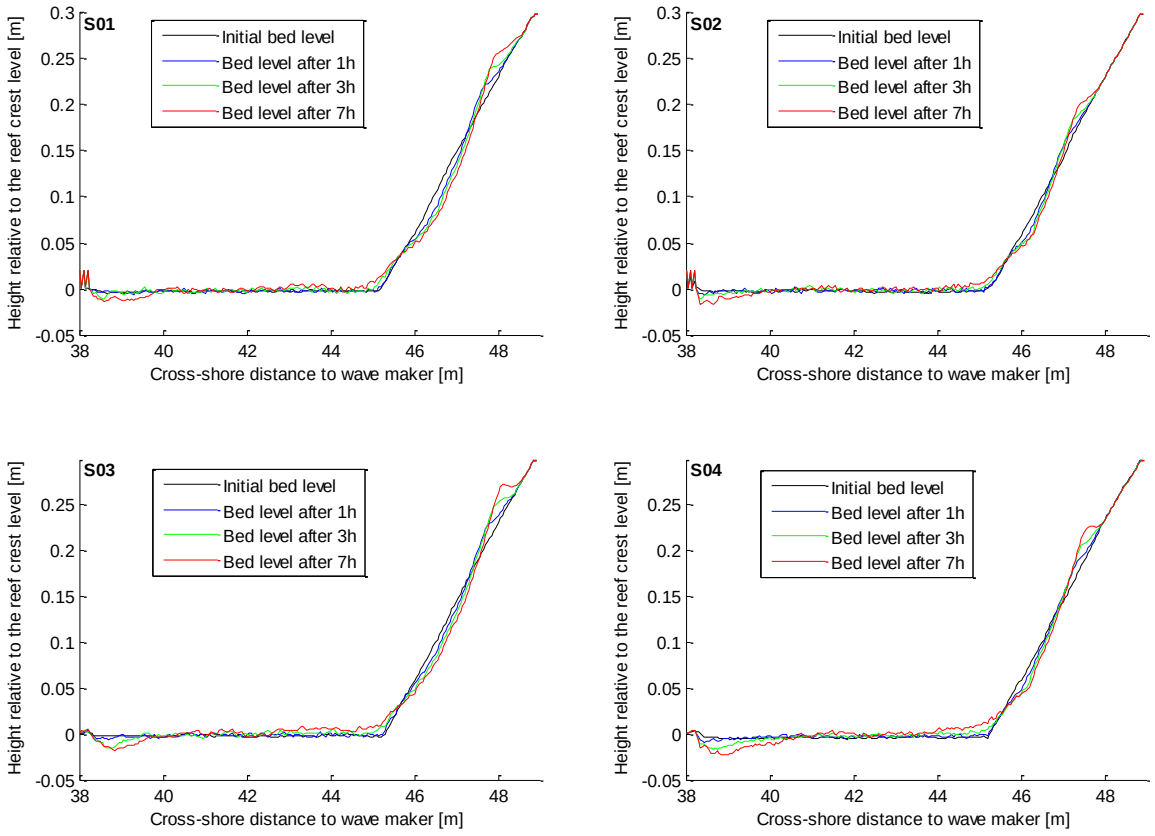

Figure 4.14 Profile development for all four simulations

Relating the observed profile development to the previous sections the role of the long waves is indeed visible in the profile development. Also the suggested onshore directed transport appears in the profile measurements as sand is transported from the seaward side of the lagoon towards the beach.

Figure 4.12 shows the local and cumulative bed level change for each simulation. The local bed level change is computed as the difference between the measured bed level at the start and at the end, after 7 hours, of the experiment. The cumulative bed level change indicates the areas where there is erosion and deposition of sediment; a decreasing trend means erosion and an increasing trend means deposition of sediment.

The erosion and deposition areas are more or less equal for all simulations, starting with erosion at the onset of the lagoon at x=38.34 m until about x=40 m. From x=40-45.5 m there is deposition of sediment, of which the origin is partially the first erosion region (38.34-40 m) and partially the second erosion region at about x=45.5-47.5 m (x=45.5.-46.5 m for shallow cases). This can be concluded because at some point the cumulative bed level change becomes positive, which means that the erosion of the first area equals the deposition up to that point. Additional deposition of sand can only occur if sand is supplied from further shoreward in the lagoon. The second area of deposition is at x=47.5-48.5 m (x=46.8.-47.7 m for shallow cases) and this sediment originates from the erosion area just next to it.

As already described above there are some differences between the simulations which slightly change in which area there is deposition or erosion. In the shallow cases for example the swash bar is positioned more offshore, which is reflected in Figure 4.12 where the deposition area starts more offshore than in the deep water cases at x=47 m. Furthermore, in the smooth, shallow case S04 the erosion at the onset of the sandy lagoon is much stronger than in all other cases. Another difference is observed when comparing the deep to the shallow cases; the total amount of erosion around x=46 m is much stronger for the deep cases and is therefore likely to be related to the short waves being higher in these cases.

The cumulative bed level change was expected to be about zero or less at the beach side of the lagoon since a small amount was lost offshore. However, in three of the four cases the final value of the cumulative bed level change is above zero, in theory suggesting an increase of the total amount of sand. The largest increase amounting to an average overall rise of the bed level of 1.3 mm. There are many possible causes for this increase, such as measurement inaccuracies, ripples in the bed and a change in the packing of the sand. Particularly the last one seems plausible since the upper layer of the sand has been stirred up and moved a lot, so the packing might have become less dense, slightly increasing the total volume of the sand. Still, the final error in the cumulative bed level change is thought to be small enough for the above conclusions to remain valid.

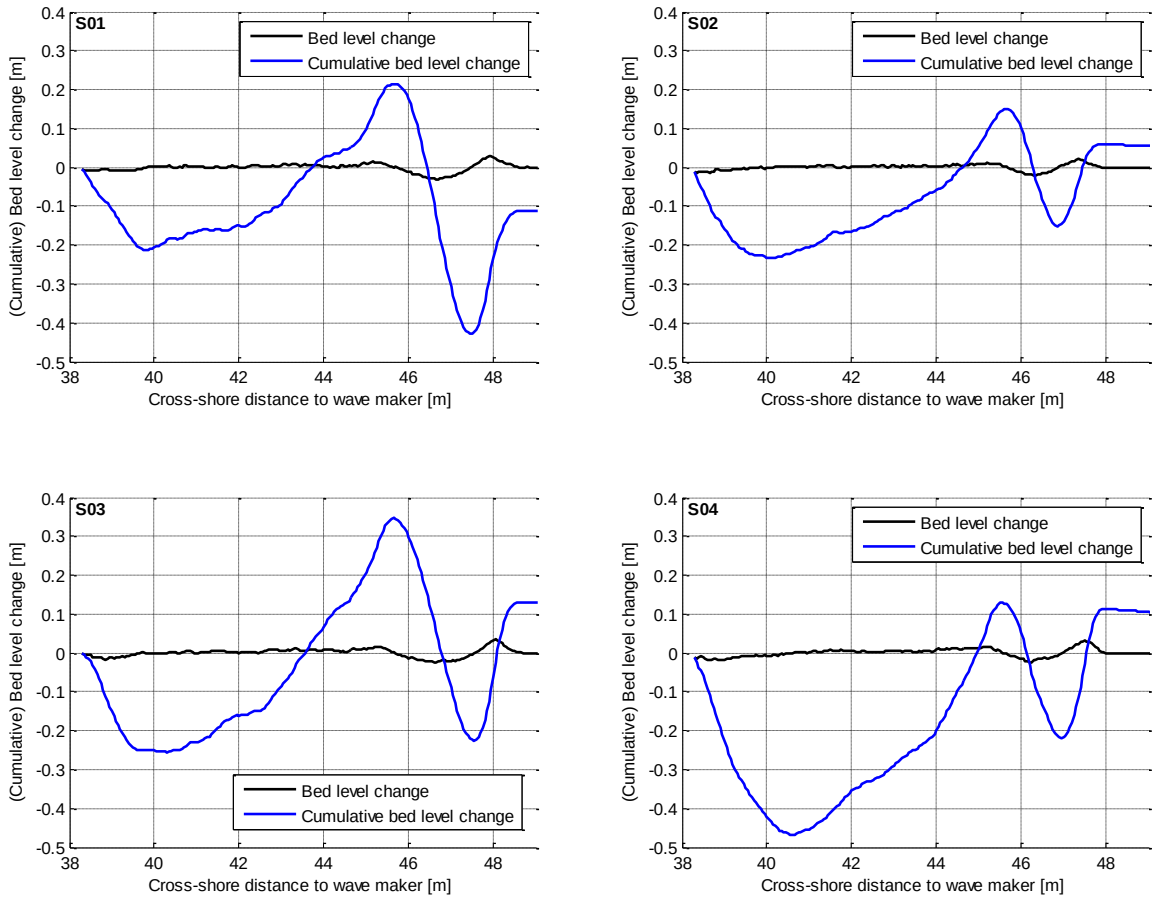

Figure 4.15 Local and cumulative bed level change

4.6 Conclusions and recommendations

In this chapter the concentration and profile measurements have been analysed and combined with the hydrodynamic data to supply an answer to the research question:

How do the measured sediment concentrations and bed-profile developments relate to the hydrodynamics?

It was found that the specific hydrodynamics of a fringing reef environment are reflected in the sediment transport and suspension and in the bed profile development. The effect of bed friction on long waves and of long waves themselves was shown in the various analyses in this chapter of which the most important conclusions and recommendations are discussed below.

4.6.1 Conclusions

Analysis of the depth-averaged concentrations measured with the sampling devices and those with the FOSLIMs did not produce very consistent results and showed that there is a large scatter and uncertainty in the data, indicating that an order of magnitude agreement with XBeach regarding sediment concentrations should be the objective rather than an exact match of the concentrations. An increase in the sediment concentrations from the seaward side of the lagoon towards the beach could also be reproduced in XBeach.

This analysis also showed that the FOSLIMs are rather sensitive to a background turbidity by fine particles in the water which reduces the quality and reliability of the measurements.

The analysis of the third order velocity moment shows that the contribution related to long wave stirring and transport or advection becomes the dominant contribution close to the beach. The results are consistent with the analysis of chapter 3 where it was shown that long waves are dominant in the lagoon. Also the effect of the bed roughness shows in the results, reducing the contribution of the *gull*, and is in agreement with observations described in the previous chapter. In the deep water cases (1 and 3) the contribution of the *gull* is dominant at the end of the lagoon, but in those cases the transport related to the short wave stirring, which is the sum of the *guss* and *guls,* remains more important as these terms together are the largest contribution to the velocity moment.

The contribution of the time-varying part, $\langle\tilde{u}|\tilde{u}|^2\rangle$, to the total third order velocity moment is positive, indicating onshore directed transport. There is also a contribution by the mean flow, or undertow, $3\bar{u}\langle|\tilde{u}|^2\rangle$, which results in a negative contribution to the third order moment. The magnitude of this contribution is significant and about the same magnitude of the time-varying part. Still, the total third order velocity moment in general shows an increasing trend towards the beach and is mostly positive on the sandy area, indicating onshore directed transport at most locations.

Combined with the correlation analysis and the bed profile developments this paints a very consistent picture in which both the short and the long waves play a role, but the long waves appear to be the dominant factor in sediment transport and bed profile development especially close to the beach. Also the effect of the roughness elements becomes visible, mainly in the shape of the swash bar, which is different for rough and smooth cases. This shows that the dominance of long waves in a fringing reef lagoon indeed results in different sediment dynamics than for example on a regular sandy beach. The long wave dominance

should theoretically mean that the wave-group averaged model XBeach is very suitable for modelling this type of reefs including the sediment dynamics.

The depth-averaged concentrations that were determined for the sampling measurements (Table 4.4) are lower for the rough cases 1 and 2 than for the smooth cases 3 and 4. This is consistent with the results discussed above showing that long waves play an important role in the sediment dynamics since the long wave heights for these rough cases were lower than for the smooth cases as discussed in chapter 3.

4.6.2 Recommendations

The ripple observations and the possible role of ripples has been discussed briefly in this chapter. It is recommended to look further into their role and how they affect the measured concentrations, the hydrodynamics and the bed profile development.

It has become clear that the FOSLIM measurements have a shortcoming in the sense that they are sensitive to turbidity in the water column. However, the instantaneous concentrations and spikes that they measure still offer very valuable information and therefore we recommend this to be studied in detail in order to gain more insight in what is causing the peaks in the measured concentrations. Also the ‘stacked’ FOSLIM signal can provide useful information to further analyse sediment suspension and advection processes.

It would be interesting to relate the position of the swash bar (Figure 4.14) to the run-up measurements that were done during the hydrodynamic part of the experiments. This would allow one to quantify the role of long waves in swash bar dynamics.

5 Comparison of XBeach and experiment results

5.1 Introduction

An XBeach model was set up to simulate the flume experiments and to assess the capability of XBeach to model sediment transport in a fringing reef environment. This chapter presents a comparison between the XBeach model results and the experiment data and assesses the performance of XBeach using its default sediment transport formulation. It analyses the suitability of XBeach to model the experiments and presents recommendations to improve this.

In order to model sediment transport, the hydrodynamics have to be reproduced rather accurately and therefore this chapter also analyses the performance of XBeach to model the hydrodynamic conditions of the flume experiments.

Section 5.2 starts with a description of the model XBeach and its most important features. It explains the theoretical suitability of XBeach to model the experiments and it explains how the model of the flume was set up and calibrated.

Next, section 5.3 compares the performance in reproducing the hydrodynamics of the experiments. It compares the wave-induced set-up, the short and long wave transformation, the flow velocity, the reef flat seiching and the generation of long waves.

Section 5.4 compares the sediment concentrations and bed profile development computed by the model to the data. The ability of XBeach to correctly reproduce these sediment processes, is analysed and recommendations are provided to improve the performance of the model.

Finally, section 5.5 summarises the most important conclusions and recommendations that were established in this chapter and relates them to the research questions.

5.2 XBeach

5.2.1 Description and suitability of the model

For the description of the XBeach model the manual by Roelvink et al. (2010) and the article by Roelvink et al. (2009) are used as a reference. In this section a brief description of the model is presented. This section also discusses the suitability of XBeach to model the flume experiments. For more details about XBeach and its equations one is referred to appendix E.

XBeach is a 2D horizontal model solving the equations for wave propagation, flow, sediment transport and bottom changes for various boundary conditions. The model is wave-group averaged, taking into account the variation of short wave energy in time to obtain the long wave motions forced by this variation. This is referred to as ‘surf beat’ as it was already long known by surfers. The surf beat is thought to be one of the dominant factors causing dune erosion, overtopping and overwash as it is responsible for most of the swash waves that hit the dunes. The desire to model these processes correctly is what led to the development of the XBeach model.

The model is based on two equations: the wave action equation and the shallow water equation. The wave action equation is used to compute the variation of the short wave energy, for example by short wave groupiness. This variation in short wave energy creates gradients in radiation stress generating a wave force F_x, which is used as input for the shallow water equation, where it can generate a long wave (surf beat), but also for example a set-up of the water level.

Besides short wave groupiness, other processes such as wave breaking and bed friction also play a role in the computation of the short wave energy. The wave energy due to breaking, D_w, is by default modelled according to Roelvink (1993) as cited in the XBeach manual (Roelvink et al., 2010) as follows:

$$D_w = \frac{2\alpha}{T_{rep}} Q_b E_w \frac{H_{rms}}{h} \tag{5.1}$$

Where Q_b is a probability function, α is a calibration factor of O(1), T_{rep} is a representative wave period e.g. the peak period, E_w is the total wave energy, n is a shape parameter, γ the breaker index and h the local water depth. The term $\frac{H_{rms}}{h}$ is a slight adaptation of the original formulation to apply the original energy dissipation formulation that follows from bore analogy (Van Thiel de Vries, 2009).

The wave action balance is coupled to a roller energy balance where dissipation of wave energy D_w serves as a source term for the roller energy balance. This balance captures the process of roller formation and propagation and contributes to the wave force F_x via the radiation stress induced by the roller.
For bed friction related dissipation of short wave energy a term D_f is included in the wave action balance. This term is calculated as:

$$D_f = \frac{2}{3}\rho\pi f_w \left(\frac{\pi H}{T_{rep}\sinh kh}\right)^3 \tag{5.2}$$

Where f_w is the wave friction factor which should be selected according to the bed roughness. Typical values for the wave friction factor are 0.03 for a sandy bed and 0.3-0.6 for a rough coral reef bed (Pomeroy, 2011; Pomeroy et al., 2012; Van Dongeren et al., 2013).

Besides the friction on waves, equation (5.2), XBeach also includes bottom friction on the flow through the bed shear stress, τ_{bx}^E, in the shallow water equation. The value of τ is computed according to the approach of Ruessink et al. (2001):

$$\tau = C_f \rho u_E \sqrt{(1.16 u_{rms})^2 + \bar{\nu}^2} \tag{5.3}$$

Where C_f is the flow friction factor, u_E is the local Eulerian velocity, u_{rms} is the local orbital velocity and $\bar{\nu}$ is viscosity. A typical value for coral reefs would be approximately 0.1, whereas for a smoother, sandy bed it would be 0.003.

The sediment transport in XBeach is modelled with a depth-averaged advection diffusion equation by Galappatti (1983). The entrainment of sediment is determined by the mismatch between the actual concentration C and the equilibrium concentration c_{eq}. The equilibrium

concentration is calculated with the transport formulation of Van Rijn (2007) which has been extended with near-bed turbulence, resulting in (Van Thiel de Vries, 2009):

$$c_{eq} = \frac{A_{sb}}{h}\left(\sqrt{(u^E)^2 + 0.64u_{rms,2}^2} - u_{cr}\right)^{1.5} + \frac{A_{ss}}{h}\left(\sqrt{(u^E)^2 + 0.64u_{rms,2}^2} - u_{cr}\right)^{2.4} \quad (5.4)$$

Where A_{sb} and A_{ss} are a bed load and a suspended load coefficient respectively, u^E is the Eulerian flow velocity, $u_{rms,2}$ is the near-bed wave orbital flow velocity including turbulence and u_{cr} is the critical flow velocity defined as $u_{cr} = \alpha u_{cr,c} + (1-\alpha)u_{cr,w}$, where $u_{cr,c}$ is the critical flow velocity for steady flows based on Shields and $u_{cr,w}$ is the critical flow velocity for waves following Komar and Miller (1975). α is a weighting coefficient defined as: $u^E/(u^E + u_{rms,2})$.

On a coral reef there are a number of key processes that need to be modelled in order to get a correct representation of reality. They follow from literature and from the results of the experiments (compare Pomeroy (2011)):

- Long wave generation and transformation;
- Wave induced set-up on the reef;
- Intense wave breaking on the reef crest;
- Bed friction
- Sediment suspension and transport

The first two processes are included through the coupling of the short wave action balance to the shallow water equation in such a way that the variations in the short wave energy lead to a wave force in the shallow water equation, which can for example generate long waves and set-up of the water level. The wave breaking process is also modelled in XBeach and can be calibrated to meet the requirements of a coral reef environment. Bed friction is included by a separate wave and flow friction factor. It was already shown that XBeach gives rather good results on the first four, hydrodynamic processes for example by Pomeroy (2011), Pomeroy et al. (2012) and Van Dongeren et al. (2013).

Although XBeach was created to model dune erosion by storm events, the equations described above are able to capture the key, hydrodynamic processes on a coral reef and therefore XBeach should be a suitable tool to model the experiments as well.

Sediment transport during extreme storm events is quite different from the situation in the sandy lagoon. During a storm event $u >> u_{cr}$ and there is high turbulence in the water column, while in the sandy lagoon turbulence is not as high and the actual flow velocity is close to the critical flow velocity. XBeach has not been used to date to model sediment suspension and transport on a coral reef and it is one of the objectives of this thesis to assess the performance of XBeach to model the sediment concentrations and the profile development observed in the experiments.

5.2.2 Model set-up

The XBeach model of the flume was set up as a one-dimensional model with the offshore boundary close to the position of the most offshore measurement location at x=16.28m. The boundary in XBeach was located at x=16.34 in order to get the reef structure correctly on the

model grid. The location of the boundary in XBeach near a measurement location was mainly determined by the fact that time series of measured wave conditions from the experiments were used as boundary conditions for the XBeach model. The grid cell size dx was chosen at 0.25 m. Results were compared with a higher resolution model but the comparison did not show significant differences, so a value of 0.25 m was found to be sufficient. In the model the reef flat level was defined as h=0.

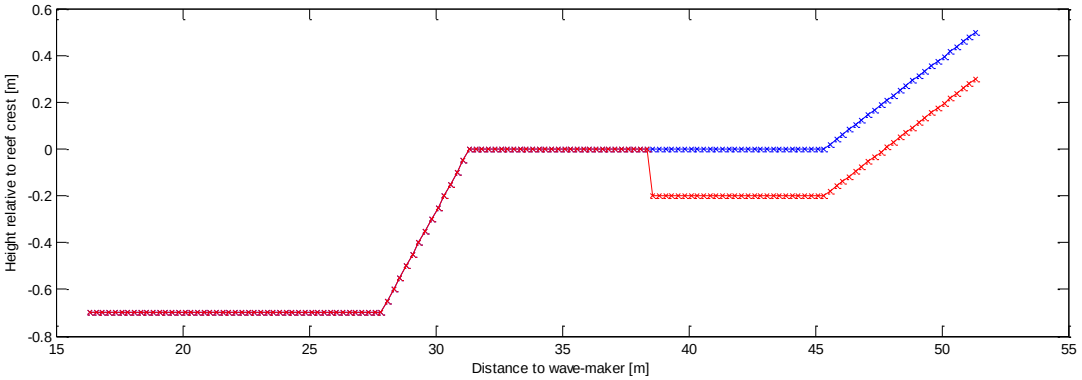

Figure 5.1 XBeach grid; Grid points are indicated with an x, red indicates a non-erodible layer, blue indicates an erodible layer of sediment in the grid.

At the offshore boundary a weakly-reflective boundary condition is applied which allows waves and currents to pass through the boundary to the deep sea with minimal reflection. At the back of the beach a no flux boundary condition is applied, but it has no real meaning since the water will never reach this boundary. For the lateral boundaries a Neumann boundary condition is used which implies that there are no gradients in surface elevation and velocities in alongshore direction. Since the model is 1D and the waves have normal incidence the type of lateral boundary should not influence the results. As mentioned above measured time series from the experiment were imposed as wave boundary condition. A boundary condition file was created with incoming long wave height and short wave energy time series from the experiment data. The XBeach results show a small mismatch at the boundary between the long wave height from the model and the experiments for cases S01 and S04. The reason for this was not identified, but could be related to some error in the separation of the model results into incoming and reflected waves.

The first XBeach model runs were done with mainly default parameter settings. The results were analysed and parameters adjusted when necessary. Relevant parameter settings that were used and adjusted will be discussed in the next section about calibration of the model.

5.2.3 Calibration

5.2.3.1 Short wave height

Before any sediment was introduced in the XBeach model, the hydrodynamics had to be calibrated. The rough cases would introduce an extra complicating parameter so calibration was done using simulation S03a with the smooth reef flat and forereef.

The short wave energy, modelled in the wave action balance, forces the long waves and setup through the shallow water equations. So the first step in the calibration was to get the short wave evolution and breaking correctly represented in XBeach. To get a good comparison with the experiment data the incoming short wave height was used. Separation

into incoming and reflected waves could only be done for the six measurement locations with a co-located flow velocity meter. These six locations were then used to calibrate the short wave height in XBeach

Using the default breaking formulation of Roelvink (1993) with the adaptation described above, option break=3 in XBeach, the dissipation of short wave energy in the breaking process is not as strong as during the experiments. The breaking process on the reef is very energetic and the breakers are of the plunging type. The experiment data shows that the waves break very hard in the sense that they lose a large part of their energy and this is not modelled correctly with the break=3 option in XBeach. This is illustrated in Figure 5.2. The point where the waves start to break is modelled by the breaker index $\gamma = \frac{H_{rms}}{h}$ and this is modelled correctly, only the waves appear to stop breaking in XBeach at greater depth than in the experiments. Daly et al. (2012) adjusted the breaker model to include a second breaker index, γ_r which is actually a reformation index and it sets the depth where the waves stop breaking. With this breaker model it is possible to force the waves to keep breaking to smaller depths. The breaking process using this breaking model (break = 4) is also shown in the figure.

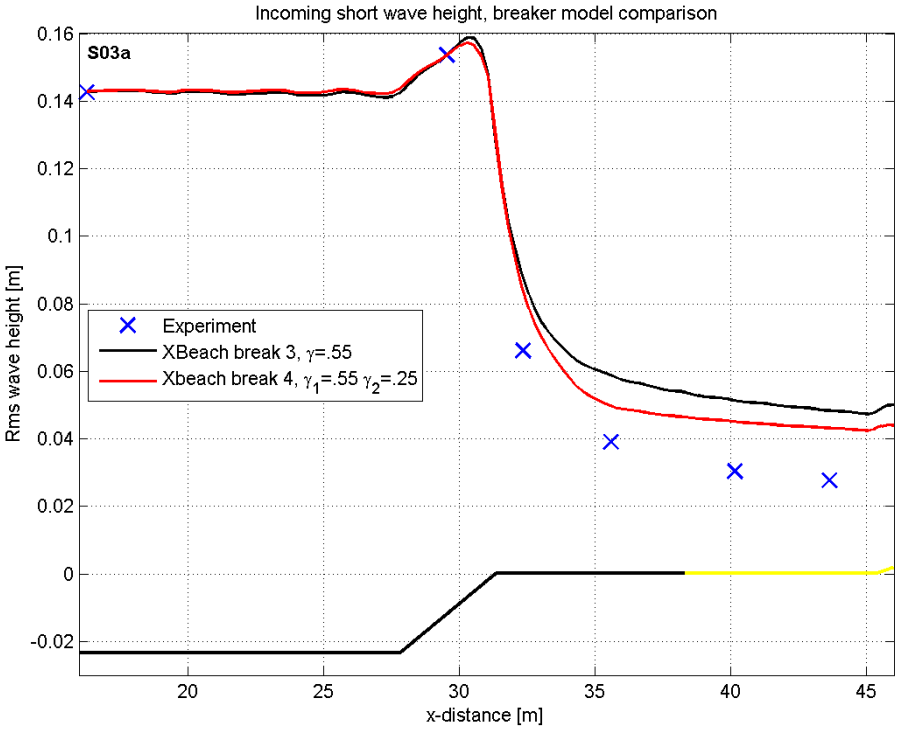

Figure 5.2 Short wave height in XBeach (black and red line) for the standard Roelvink breaker model (break 3) and the Roelvink and Daly breaker model (break 4), and the experiments (blue crosses)

It is clear that it is necessary to have more control over the breaking process in XBeach so the breaking model of Daly et al. (2012) is preferred. The breaker formulation is as follows:

$$D_w = \frac{2\alpha}{T_{rep}} Q_b E_w \frac{H_{rms}}{h} \tag{5.5}$$

The parameter α is factor which generally represents the intensity of wave dissipation and should be $O(1)$. It can be used to increase or decrease the amount of energy that is lost in

the process of breaking. Together with γ_1, which determines the depth where the waves start breaking, and γ_2, which determines the depth where they start reforming, α is used to calibrate the short wave evolution.

To find the best combination of these parameters a sensitivity analysis was done using the RMS-error based on the six data-points as an indicator of the performance. The results are presented in Table 5.1.

First different combinations of the two breaker parameters γ_1 and γ_2 are tested and the RMS-errors are shown in the upper part of the table. The values of $\gamma_1 = 0.45$ and $\gamma_2 = 0.05$ give the smallest RMS-error. These values are used to determine the value of the wave dissipation intensity parameter α with the smallest RMS-error, which is 1.4 as shown in the last row of the table. The resulting short wave evolution is plotted in the right panel of Figure 5.3.

Table 5.1 RMS-errors for XBeach H_{rms} compared to the experiment H_{rms} for different combinations of the breaker parameters γ_1 and γ_2 and α

RMS-error α=1		γ_2 0.05	0.15	0.25
γ_1	0.45	0.0104	0.0112	0.0138
	0.55	0.0119	0.0142	0.0174
	0.65	0.0131	0.0163	0.0200
RMS-error γ_1/γ_2		α 0.8	1.2	1.4
0.45/0.05		0.0152	0.0071	0.0052

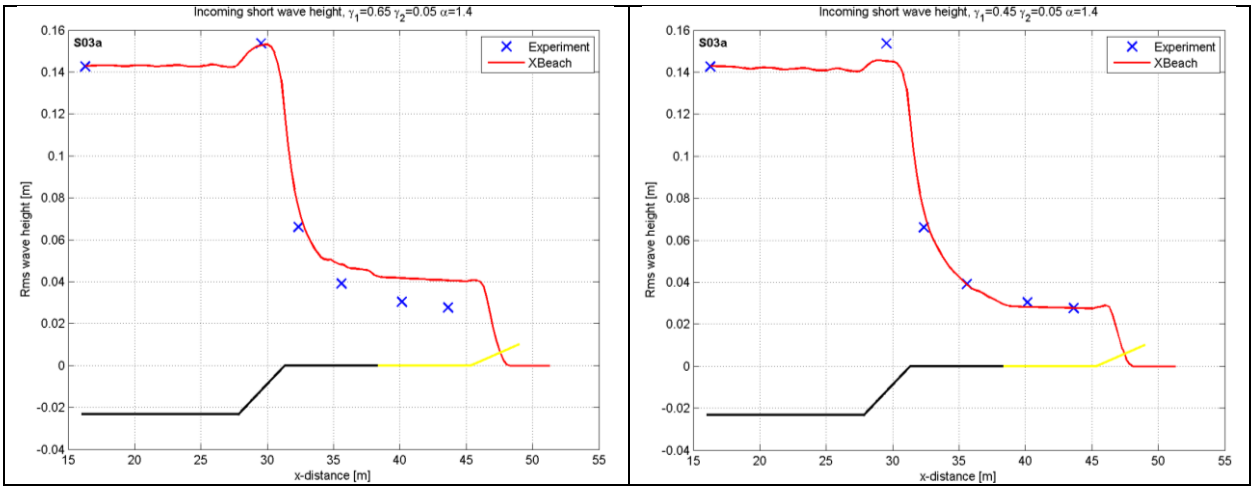

Figure 5.3 H_{rms} evolution over the reef, XBeach compared to experiments. Left panel: $\gamma_1 = 0.65, \gamma_2 = 0.05, \alpha = 1.4$. Right panel: $\gamma_1 = 0.45, \gamma_2 = 0.05, \alpha = 1.4$

The model represents the experiment data quite well, except for the data-point on the reef crest, which is a consequence of using a low value for γ_1 as the waves start breaking before they have shoaled to the level observed in the experiments. This can be corrected using a higher value of $\gamma_1 = 0.65$ as shown in the left panel of the figure but comes at the expense of the short wave height on the reef. This is quite surprising as the γ_2 parameter indicating the water depth where waves should stop breaking is equal in both cases.

A completely correct representation of the hydrodynamics is preferred, but since the ultimate goal is to model sediment concentrations a correct representation of the hydrodynamics on the sandy lagoon part is the most important goal and is achieved using the values of $\gamma_1 = 0.45, \gamma_2 = 0.05, \alpha = 1.4$ with a small RMS-error.

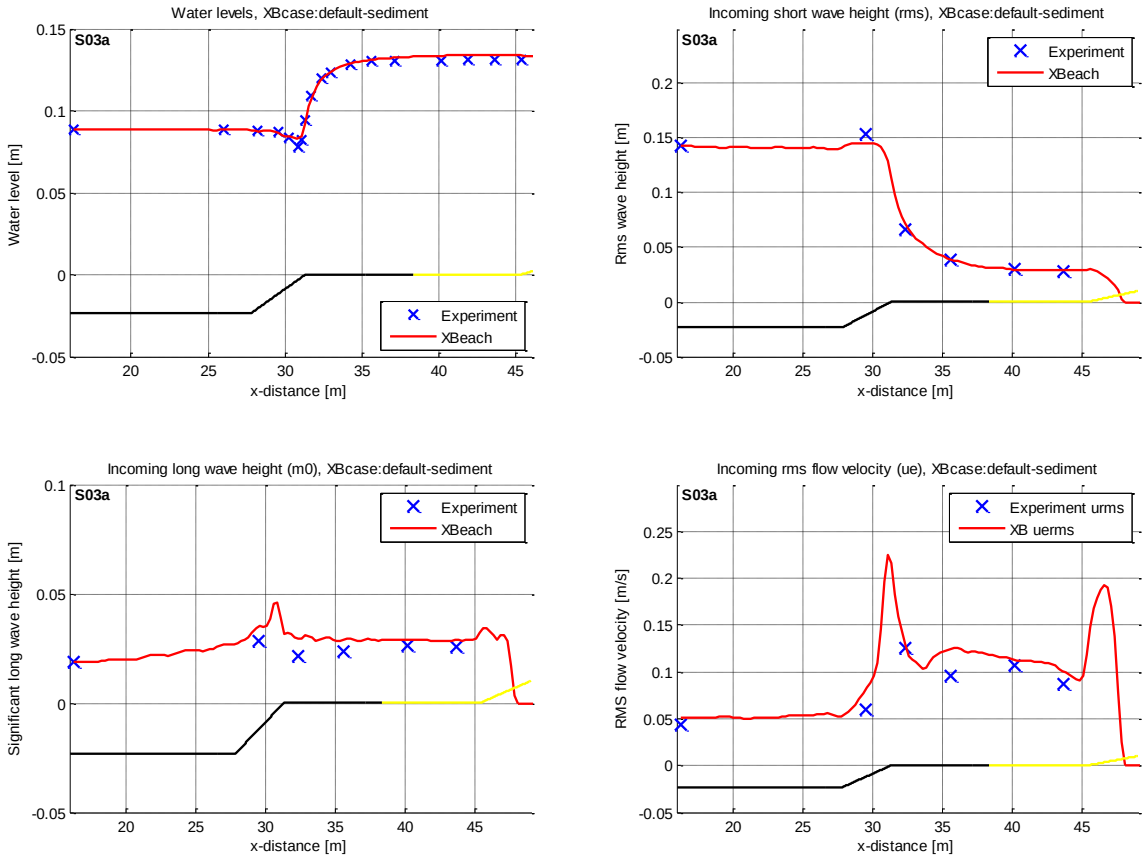

Figure 5.4 Results for S03a after calibration; top left: water levels; top right: RMS short wave height $H_{rms,s}$; bottom left: RMS long wave height $H_{rms,IG}$; bottom right: RMS long wave flow velocity $u_{rms,IG}$.

Figure 5.4 shows the results of the XBeach simulation after calibration of the short wave height for the mean water levels, long wave height, flow velocity (and short wave height).

The mean water levels (top left panel) that are mainly determined by the wave induced setup agree well with the experiment data. The setdown around the reef crest (x=31 m) is slightly under predicted and the water level on the four measurement locations closest to the beach is slightly over predicted.

The long wave height (bottom left panel) is somewhat higher in XBeach than in the experiments. Particularly on the sandy lagoon area (x=38-45 m) however, the agreement with the experiments is good.

The root-mean-squared flow velocity, u_{rms} (bottom right panel), agrees very reasonably with the data. Regarding sediment modelling the two data-points on the sandy area are important and are predicted rather well in XBeach.

5.2.3.2 *Bed friction calibration (S01 and S02)*

For the simulations with a rough reef flat, S01 and S02, the bed friction in XBeach has to be calibrated. As mentioned above there is a wave friction factor, f_w, which works on the short wave energy, and a flow friction factor, c_f, which works on the mean and long wave flow velocity through the shallow water equation. Typical values for f_w on coral reefs are 0.2 – 0.6 and the value for c_f should be around 0.1.

The calibration shows that for the case of the experiments $f_w = 0.3$ and $c_f = 0.1$ give good results. In Figure 5.5 below, this is shown and compared to a simulation with a standard, low friction to observe the effect of the bed friction on the mean water levels, short wave height, long wave height and flow velocity. In the two bottom panels a clear effect of the bottom friction is observed on the long wave height and the flow velocity. The model agrees rather well with the experiment data.

There is also a clear effect on the wave-induced set-up of the water level on the reef, which is shown in the top left panel. By adding friction in XBeach the set-up is strongly increased and the offshore water level had to be lowered in order to reach the correct water level on the reef, since the objective of this thesis is to model sediment transport on the reef flat area. The effect of bed friction on the set-up is discussed further in the next paragraph about the comparison of the XBeach results with the experiment data (5.3.1).

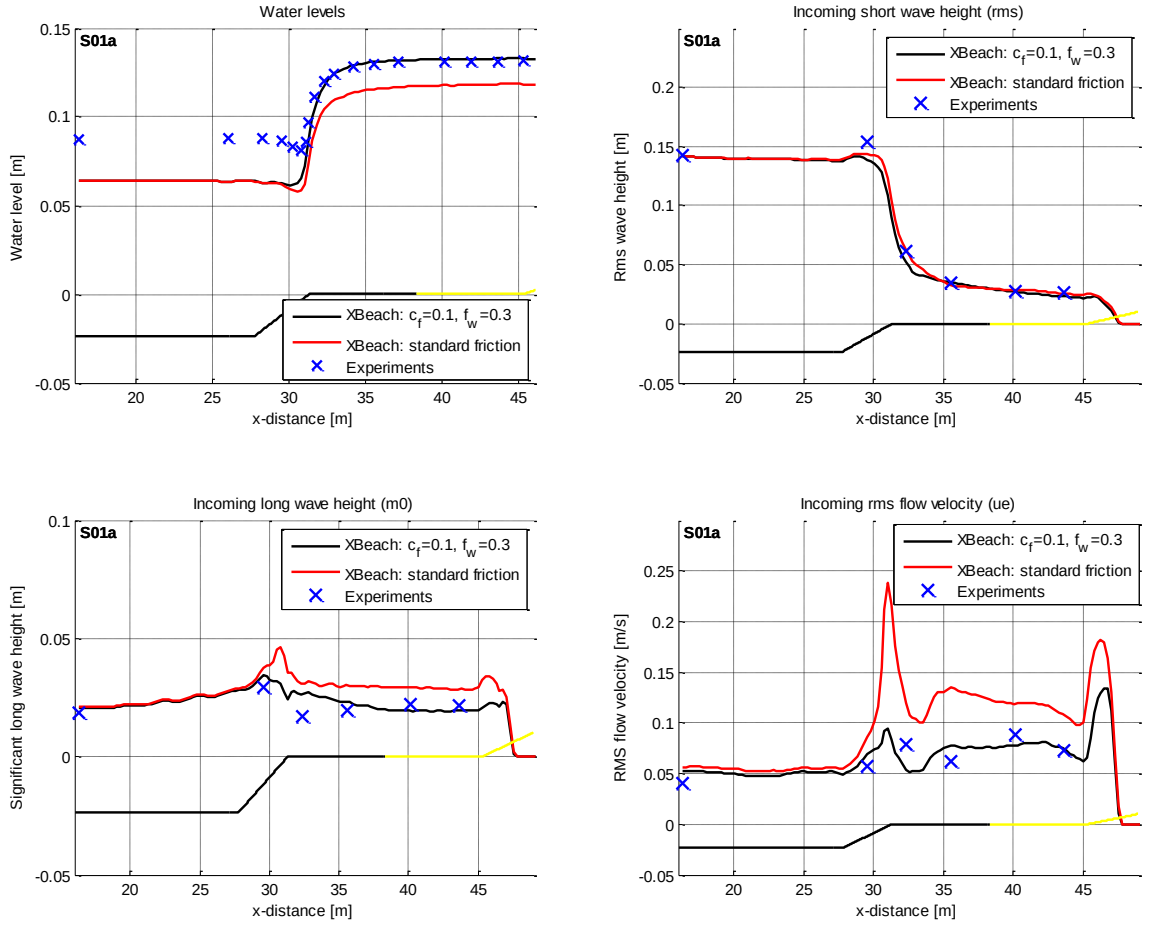

Figure 5.5 Calibration of friction coefficient for flow, c_f, and for waves, f_w. Standard friction refers to the friction used in the smooth cases, so c_f=0.003 and f_w=0.03.

5.2.3.3 Discussion

XBeach was calibrated for the smooth bed simulation S03 by adjusting the parameters related to the wave breaking process to reproduce the short wave transformation from the experiment data. The results were compared for the mean water levels, short wave height, long wave height and flow velocities and agreed quite well with the experiment data.

The same settings were used to calibrate the bed friction for simulation S01. The bed friction is represented in two parameters, f_w and c_f, related to short waves and currents respectively. It was found that the best result is achieved using f_w=0.3 and c_f=0.1, which is in line with available literature on modelling coral reef environments.

The wave breaking process was modelled using the breaker model of Daly et al. (2012) which allows one to set the water depth where the waves stop breaking by a parameter γ_2, which proved to be a necessary option to reproduced the short wave height transformation from the experiments. It was found that the influence of parameter γ_2 is unclear, because it gives different results for different values for the parameter γ_1, which was shown in Figure 5.3. However, that did not lead to any problems for the calibration of the model in this case.

The simulations with high bed friction showed an increased set-up of the water level on the reef compared to the cases with standard bed friction. In order to model the processes on the reef correctly the offshore water level was lowered such that the water level on the reef is equal to that of the experiments. The effect of bed friction on the set-up is discussed further in the next paragraph about the comparison of the XBeach results with the experiment data (5.3.1).

5.3 Comparison hydrodynamics between XBeach and experiments

5.3.1 Set-up

Wave-induced set-up of the water level on the reef is caused by the a negative gradient in the cross-shore radiation stress as the waves break on the reef crest. The resulting wave force, F_x, is balanced by a water level gradient, $\frac{d\bar{\eta}}{dx}$, and a bed shear stress, τ_{bx}^E, as it follows from the (reduced) momentum balance:

$$F_x = -\frac{dS_{xx}}{dx} = \rho g h \frac{d\bar{\eta}}{dx} + \tau_{bx}^E = \rho g (h_0 + \bar{\eta}) \frac{d\bar{\eta}}{dx} + \tau_{bx}^E \tag{5.6}$$

The results of the XBeach simulations are compared with the experiment data in Figure 5.6. What stands out is the fact that there is no difference in water levels between the rough and smooth cases in the laboratory data, but there is significant difference between rough and smooth in the XBeach simulations. The set-up of the smooth cases is reproduced correctly, but the set-up of the rough cases is overestimated compared to the experiment data.

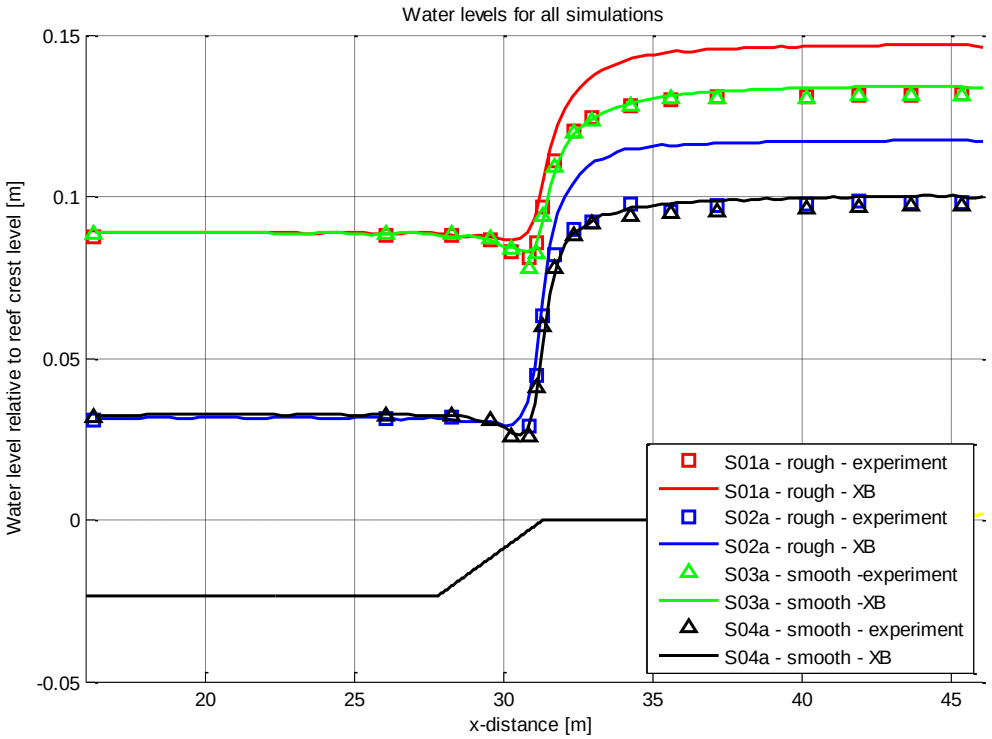

Figure 5.6 XBeach mean water levels compared to the mean water levels from the experiments

In Figure 5.7, upper panel, the momentum balance (shallow water equation) for the XBeach simulations of the rough case S01 (left panel) and the smooth case S03 (right panel) is presented. The terms are averaged over the entire simulation time. For the sake of completion advection and viscosity are included in the plot, but it is mainly a balance between the wave force F_x on the one hand and the water level gradient $\frac{d\bar{\eta}}{dx}$ and the bed shear stress τ_{bx}^{E} on the other hand. The momentum balance shows that the bed shear stress due to bottom roughness (black line) is much larger for the rough case than for the smooth case and that it is compensated by an increase in the water level gradient and with that an increased set-up of the water level.

The middle panel shows the effect of the bed friction on the dissipation of wave energy for S01 and S03. The shape of the total dissipation is very similar to the shape of the wave force F_x in the upper panel for both cases. The effect of the wave friction factor on the dissipation is clearly observed for case S01 where almost half of the total dissipation is related to dissipation by friction, D_f, whereas in case S03 nearly all dissipation is due to wave breaking, D_b. It can be concluded that the effect of bed friction on wave dissipation is significant.

The increased set-up for the rough cases observed in the model is not in agreement with the measured set-up during the experiments. This is related to how the effect of the bed roughness is modelled in XBeach which uses the Eulerian flow velocity to calculate the bed shear stress. The mean Eulerian flow velocity is offshore-directed due to the undertow and leads to a bed shear stress in opposite, i.e. onshore, direction. This shear stress acts as an extra force on the water column, creating extra set-up in the model. However, in the reality of the experiments the interaction between hydrodynamics and bed roughness is different in such a way that no additional set-up is generated.

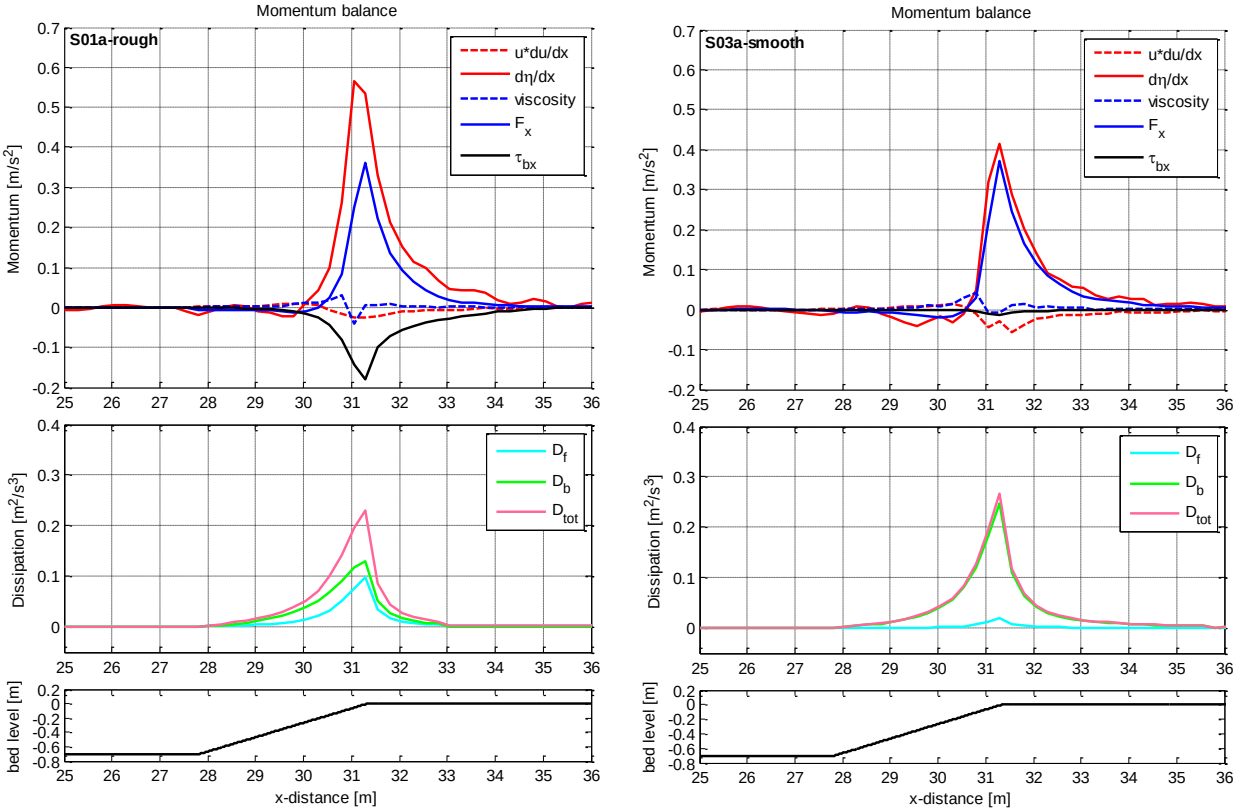

Figure 5.7 Upper panel: Mean value of the terms of the momentum balance for the XBeach simulation of rough case, S01 (left) and smooth case, S03 (right); Middle panel: Dissipation by wave friction, D_f, wave breaking, D_b and the sum of those two, D_{tot}; Bottom panel: bathymetry

It could be argued that the dissipation of wave energy by friction rather than breaking should not be contributing to the radiation stress gradient. That would reduce the wave force term in the momentum balance, F_x, and would compensate the increase of set-up by the bed shear stress, τ_{bx}^{E}.

Dean and Bender (2006) suggest that an extra force should be included in the momentum equation which results from the effect of the bed roughness on near-bed orbital velocities. They argue that for nonlinear waves, as is the case in the experiments, the mean bed shear stress induced by the near-bed particle velocity becomes non-zero and can exert a force on the water column counter to the direction of wave propagation. This net force is caused by the asymmetry of the near-bed flow velocity and, as it is directed counter to wave propagation, would lead to a set-down of the water level.

This effect is not included in XBeach as it assumes linear waves. From the results of the experiments it would appear that it is the set-down by this force that exactly compensates the extra set-up by the bed shear stress term, τ_{bx}^{E}, in the momentum equation so that there is no net effect of the bed roughness on the set-up of the water level on the reef.

This would be a rather big coincidence so whether this theory actually holds is subject of debate and should be further investigated. What the comparison between model and data does show is that the effect of bed roughness on wave-induced set-up is rather complex and that its implementation in XBeach is not yet completely correct, at least not for the case of a scaled fringing coral reef.

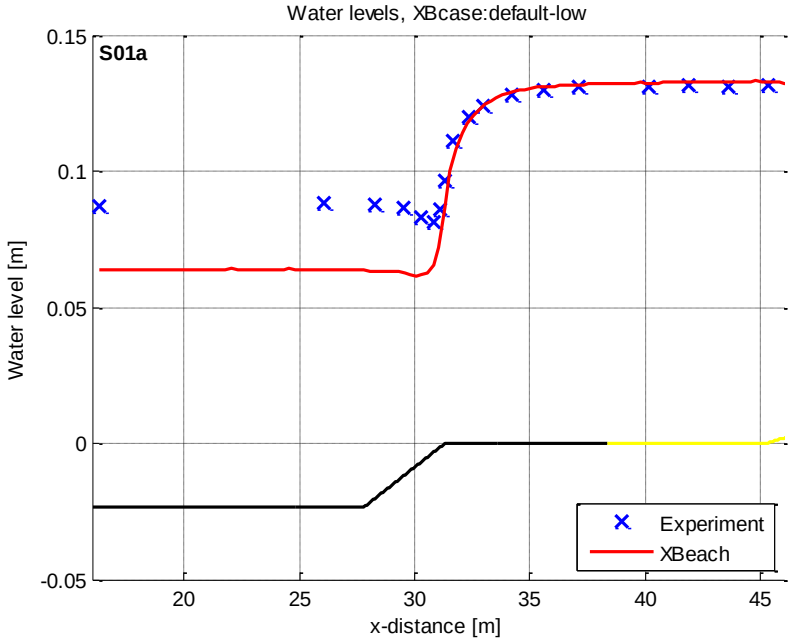

Figure 5.8 Mean water levels XBeach and experiments: the offshore water level is lowered in XBeach in order to get the correct water level on the reef

Figure 5.8 shows the correction that was made to the water level offshore in order to reach the correct water level on the reef flat. It was found that the correction can only be applied for simulation S01, because for S02 it causes the water levels over the reef to become unrealistically low. This would no longer give a correct representation of the physical processes, but also causes instability of the model XBeach.

5.3.2 Long and short wave height transformation

The calibration of the XBeach model was based on simulation S03 and used mainly the short wave height. The results for simulation S03 and the other simulations, S01 and S04, are summarised in Figure 5.9 for the incoming short wave height. The short wave height from the experiments is reproduced very well, particularly on the reef flat area, which is the area of interest for modelling sediment concentrations and transport. The depth-dependency of the short wave height, as opposed to the roughness-dependency of the long wave height, observed in the experiments is also found in the model results.

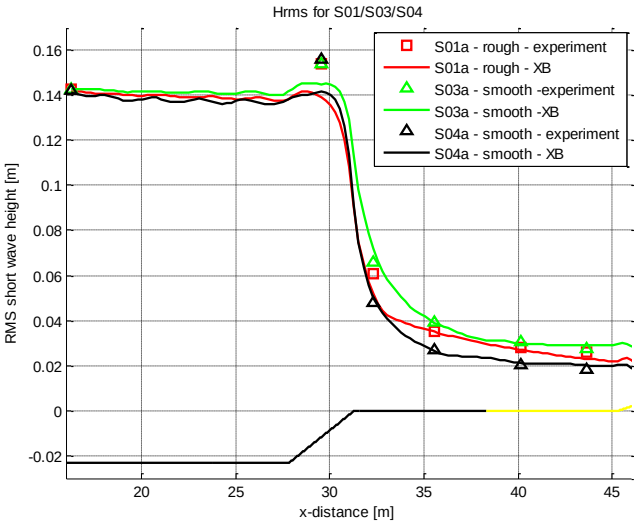

Figure 5.9 Root mean squared short wave for XBeach and the experiments (incoming only)

The XBeach simulation of the rough case S01 undershoots the data point closest to the beach (x=43.63 m) as a consequence of the wave related friction factor f_w. In XBeach this factor does not vary in space while the friction on the sandy lagoon should be lower than the value on the reef flat part where the roughness elements were placed. The error is small in an absolute and a relative sense, e.g. compared to the long waves, so it was considered negligible.

In the shoaling region on the reef slope, around x=30 m, the short wave height is increased in the experiments, but not in the XBeach simulation. This is a consequence of the breaker model that was used in XBeach which is set in such a way that the waves start breaking earlier than in the experiments, reducing the increase of the wave height during the shoaling process.

The short waves in XBeach force the long waves through the shallow water equation. The resulting, incoming long wave height for the three simulations is presented in Figure 5.10 and reflected long wave height in Figure 5.11. In the offshore region the long wave height in XBeach is increasing rather strongly before the reef slope and the increase starts already at the offshore boundary. This does not happen in the experiments, recall Figure 3.17, where the wave height starts to increase just before the reef slope.

The increase of the long wave height in XBeach before the reef slope is possibly related to the use of measured long wave height and short wave energy time series as a boundary condition. In XBeach the propagation of these two parameters is computed in two different equations, which could lead to a small mismatch between the two in such a way that the resulting phase difference induces transfer of energy from the short waves to the long waves.

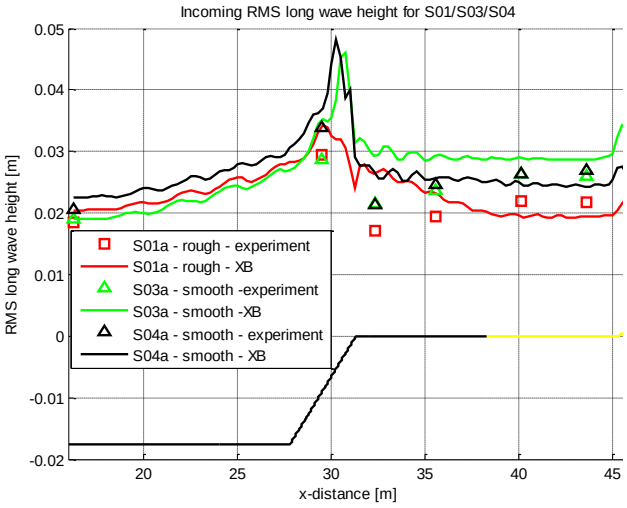

Figure 5.10 Root mean squared long wave for XBeach and the experiments (incoming only)

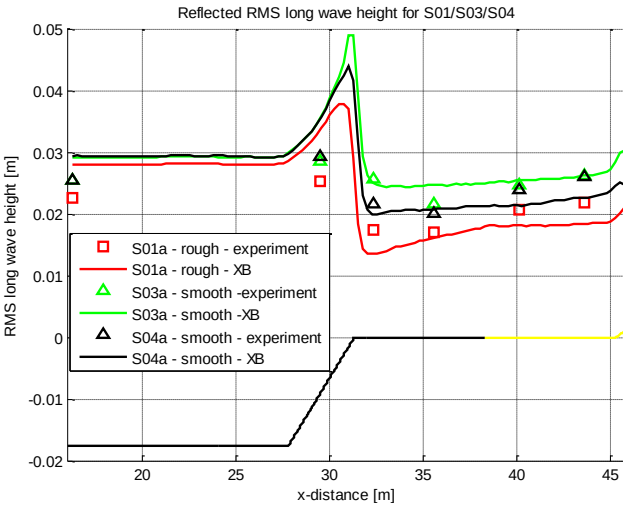

Figure 5.11 Root mean squared long wave for XBeach and the experiments (reflected only)

The reflection of long waves in XBeach on the reef crest is stronger than observed in the experiments. The reflection on the beach is close to 100%, which is in agreement with the data from the experiment.

After the breakpoint the simulated, incoming wave height (Figure 5.10) is clearly largest for the smooth and deep water case S03, while in the experiments the long wave height is equal for S03 and S04. In all cases the long wave height after the breakpoint is overestimated in XBeach as too much energy is apparently conserved or generated at the breakpoint in the model. The results show that the long wave height after the breakpoint in XBeach depends on the water depth and on roughness as for both the low water depth case S04 and the rough case S01 it is lower than for S03.

In the smooth cases the incoming wave height in the model remains more or less constant over the reef flat and the sandy lagoon area, while it increases towards the beach in the experiments, which was found to be related to reef flat seiching. Comparison of XBeach and the data suggests that XBeach does not (fully) reproduce the reef flat seiching. The transformation of the long wave height is different for the rough case S01 as the long wave height decreases over the rough reef flat area (x=32-38 m) and also remains more or less constant over the sand bed (x=38-45 m).

The strong shoaling of the long waves is observed in the XBeach results as well as in the experimental data. For a better comparison the total long wave height is used to increase the number of available data points, see Figure 5.12. The figure shows that the offshore wave height in XBeach is too high, but at the point of maximum shoaling around x=30 m the model results are quite close to the experiment data. Also the fact that shoaling is strongest for S04 is reproduced by XBeach.

The plots of the total long wave height show that XBeach does capture the increase of the long wave height over the reef towards the beach, particularly in the smooth cases. The increase is reproduced rather well for simulation S03, but for S01 and S04 the increase is not as strong as in the experiments. In case S01 the roughness causes a decrease of the wave height and as section 5.3.4 shows, the energy at the seiching frequency is much lower for S01 than for the other two cases. This can explain why the wave height on the sandy lagoon

is much lower in the XBeach simulation than in the experiments, where the effect of roughness on seiching was not as strong.

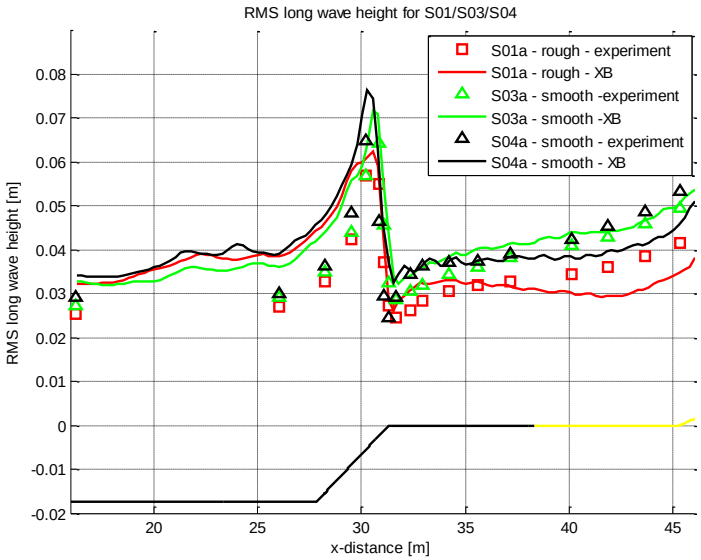

Figure 5.12 Root mean squared long wave for XBeach and the experiments (incoming+reflected)

In summary, the short wave transformation is reproduced very well by XBeach, particularly on the reef flat area, which is the area of interest for modelling sediment concentrations and transport. The depth-dependency of the short wave height, as opposed to the roughness-dependency of the long wave height, observed in the experiments is also found in the model results.

The long wave height is reproduced reasonably by the model. The important processes of shoaling and dissipation are modelled well and the increase of the total wave height over the reef flat is well reproduced for the cases S03 and S04.

At some points the long wave transformation deviates:

- The reflection at the reef crest is too high in XBeach, the reflection at the beach is similar to what was observed in the experiments.
- In the offshore region there is a constant transfer of energy to the long waves, which was not found in the experiments. This is possibly related to the way XBeach computes the propagation of short wave energy and long waves in combination with the specification of measured time series as a boundary condition.
- The generation or conservation of long wave energy is too high, particularly for case S03.
- The increase of long wave energy is correctly reproduced for S03, reasonably for S04 and is less or absent in S01. This suggests that the seiching in XBeach is not as strong as in the experiments.

5.3.3 Flow velocity

It is important that the model reproduces the flow velocities on the reef flat and sandy lagoon correctly as sediment suspension and transport is mainly related to the flow velocity. Figure 5.13 shows the model results and the experiment data for the root mean squared, long wave flow velocity. The model results approach the measured flow velocity quite well. The deviations on the sandy lagoon area between model and data are small so the prerequisites

to model sediment suspension and transport and achieve an order of magnitude agreement are present.

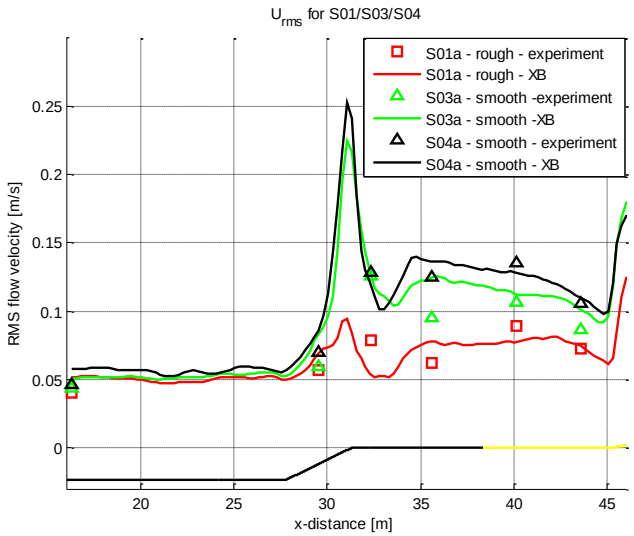

Figure 5.13 Root mean squared long wave flow velocity for XBeach and the experiments

5.3.4 Resonance

It was demonstrated in chapter 3 about the hydrodynamic data analysis that reef flat seiching was an important phenomenon during the experiments that contributed significantly to the long wave height on the reef flat and sandy lagoon. This section analyses the model results to assess how well XBeach reproduces the reef flat seiching. Section 5.3.2 showed that the increasing long wave height on the reef flat is not reproduced correctly for case S01 (rough, deep) and S04(smooth, shallow), but it is reproduced in case S03(smooth, deep). To investigate how well the seiching is reproduced in XBeach the water level time series and spectra are analysed. The top panels in Figure 5.14 show the water level time series from XBeach for all three cases, including the part after the waves at the boundary had stopped. The bottom and middle panels compare the measured and modelled spectra at x=43 m on the reef flat.

Starting with the time series, the model results show that there are oscillations after the waves are stopped at approximately t=3500-3700s for all cases. These oscillations are not forced and must therefore be related to the eigen frequency of the reef flat. The motions dampen out most rapidly in the rough case S01, whereas in both smooth cases more and stronger oscillations are observed. Particularly the oscillations for case S04 are strong and long-lasting. A possible explanation for this is that the water level drops significantly at t=3550s for S04, creating a strong initial oscillation which is larger and takes longer to dampen out than the oscillation observed in S03.

The spectra from XBeach (bottom panels) confirm the abovementioned observations from section 5.3.2 as the energy at the seiching frequencies (deep~0.016 Hz, shallow~0.012 Hz) is highest for case S03, slightly lower for S04 and very low for S01. Comparing S01 and S03, the energy at the seiching frequency is reduced more strongly by the bed roughness in XBeach than in the experiments. This is also in agreement with the described long wave transformation in XBeach.

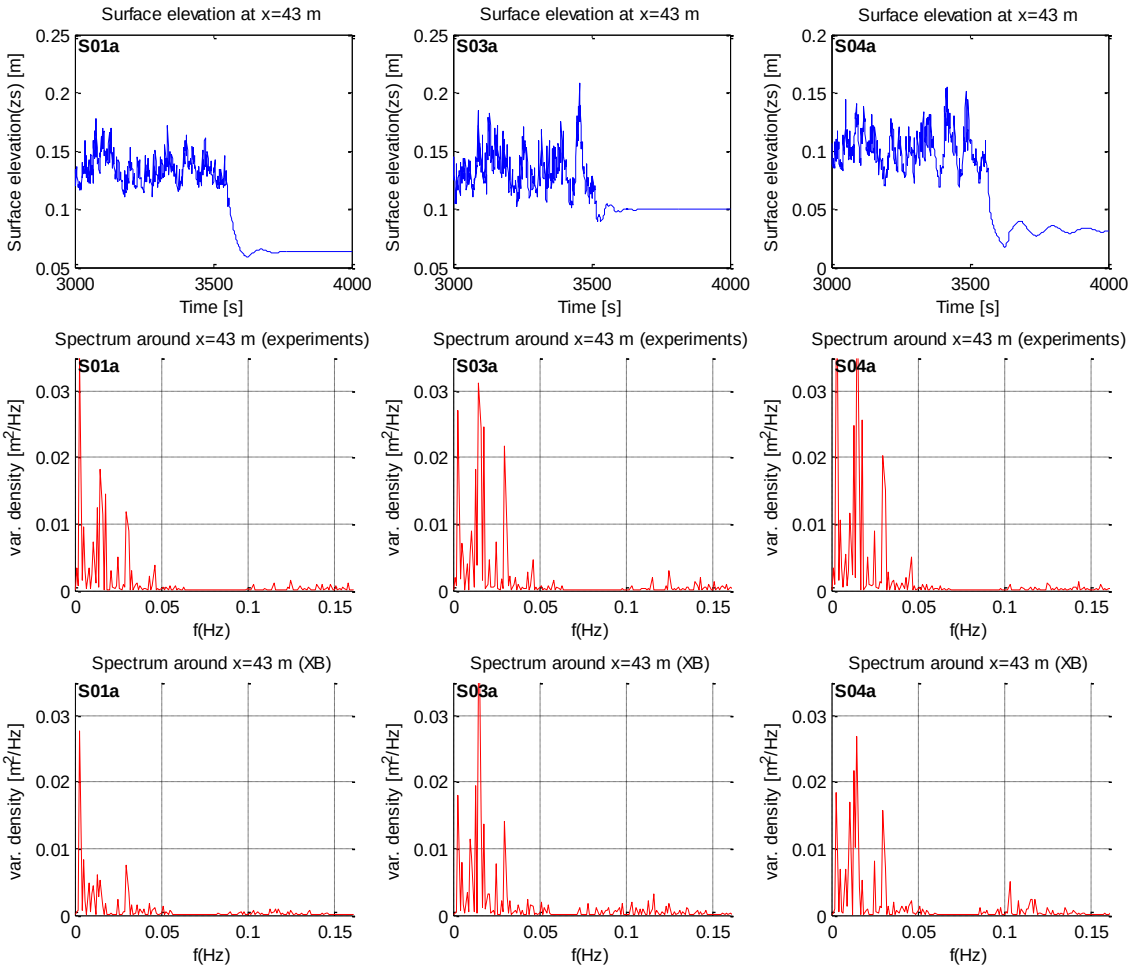

Figure 5.14 Top panels: water level time series including the part after the waves from the boundary condition had stopped at about 3550s for S01, S03 and S04 from XBeach; middle panels: spectrum of the measured surface elevation at x=43 m for simulation S01, S03 and S04; bottom panels: spectrum of the simulated surface elevation in XBeach at x=43 m for S01, S03 and S04.

In general the spectra computed from XBeach and from the experiments are very similar. The reef flat seiching is reproduced and also the peak at 0.003 Hz appears in the XBeach spectra. However, the magnitude of the seiching is not modelled correctly in case S01 and S04 and is affected by bed roughness and water depth. The influence of these parameters is stronger in XBeach than in the experiments and comparing S03 and S04 the effect of decreasing the water depth on the seiching intensity is opposite in XBeach compared to the experiments.

5.3.5 Long wave generation

Another phenomenon which was shown to be present in the experiments is the generation of free long waves by the breakpoint mechanism of Symonds et al. (1982). This was shown by plotting the cross correlation averaged over a run of the short wave envelope at one location with the long wave time series along the flume. A characteristic of the breakpoint mechanism is a shift of this correlation from negative to positive at the short wave breakpoint. Figure 5.15 shows the plots of this correlation in time and space for the experiments and the model. The agreement between the model and the experiments is very well as both show the reversal of the correlation around the short wave breakpoint. This provides support for the presence of the breakpoint mechanism for generation of free long waves on the reef flat.

These results are in agreement with the analysis and modelling work done by Pomeroy et al. (2012).

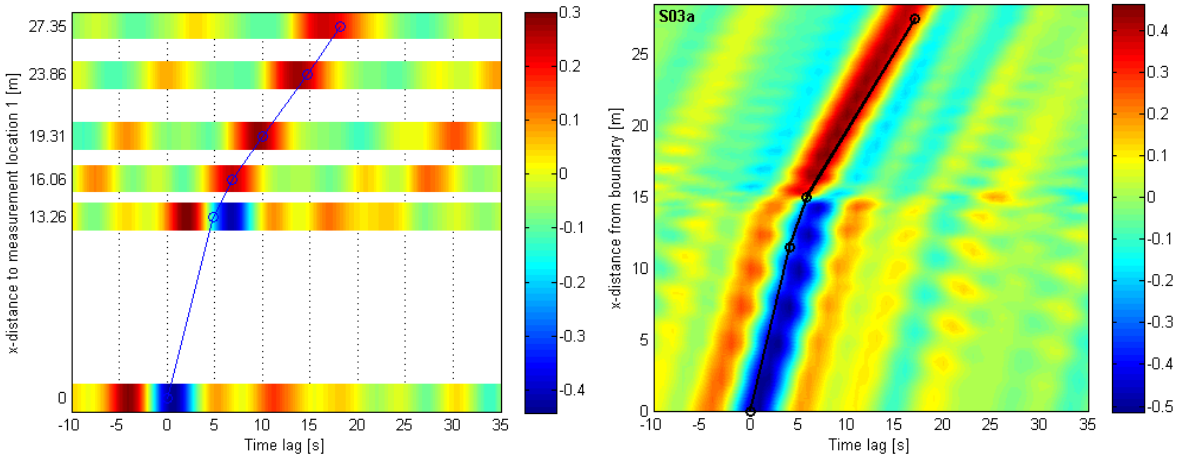

Figure 5.15 Left figure from s03a: Cross correlation averaged over the simulation period of short wave envelope at x=0 with the long wave time series at location 4, 10, 13, 15 and 17. The blue line indicates the theoretical propagation speed trajectory obtained from integration of the bathymetry. Right figure is the same plot based on the results of the XBeach simulation of S03a.

5.4 Comparison sediment concentrations between XBeach and experiments

5.4.1 Results from XBeach and experiments

One of the objectives of this thesis is to assess the ability of XBeach to model the suspended sediment concentrations observed during the experiments using its default sediment transport formulation (equation (5.4)). It was already concluded in chapter 4 that an order of magnitude agreement between the model and the data would be a good result. The modelled concentrations obtained from XBeach did not show significant differences between the cases so it is sufficient to analyse only one case. Therefore this section focuses on analysis of case S03.

To compare the experiments to the model, the depth-averaged concentrations of Table 4.4 are considered. The average over the entire case S03 is computed for the FOSLIMs at location 15 and 18 and for the multiple inlet suction sampler (MISS). These values are plotted in Figure 5.16 together with the average suspended sediment concentration from XBeach (parameter *ccg*).

The figure shows that the modelled sediment concentrations above the flat area of the sandy lagoon are much lower than the measured concentrations. There is hardly any suspension in XBeach in this area, while significant suspension was measured and visually observed in the experiments above the entire sandy lagoon area. In section 5.4.2 the large difference between the model and the experiments is analysed in more detail.

No measurements were done on the beach slope, where the sediment concentration values in the model show a high peak. This is caused mainly by the breaking of the remaining short waves but it cannot be compared to any concentration measurements. Analysis of the bed profile development below shows that the model concentrations in the beach area are probably too high.

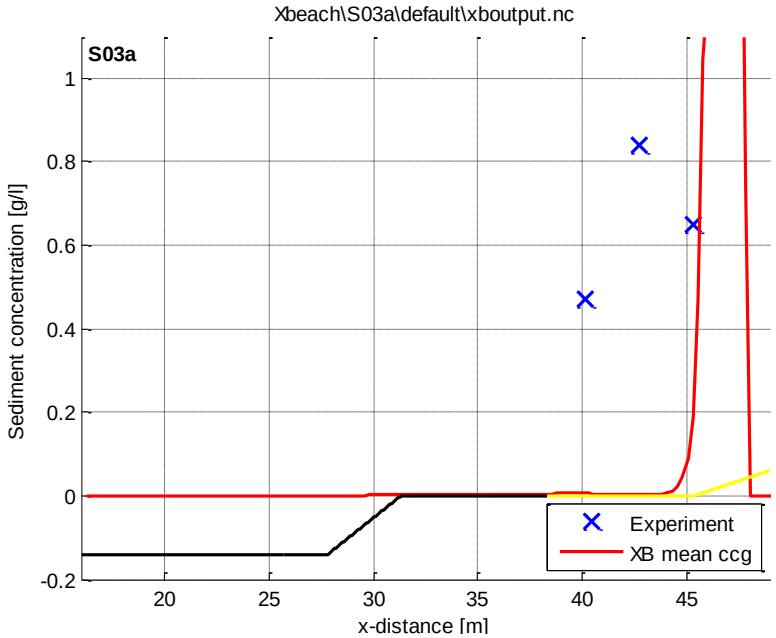

Figure 5.16 Depth-averaged suspended sediment concentration for XBeach and experiments, averaged over the entire simulation. The experiment data points from left to right: FOSLIM at location 15, MISS, FOSLIM at location 18.

The difference in suspended sediment concentrations between model and data also results in a different profile development. Figure 5.17 presents the development of the bed profile after 1 hour of simulation in XBeach together with the measured, final bed level after running the experiment for 7 hours.

Although the simulation times are not equal, it is clear that the measured bed profile development is not reproduced in XBeach and that this would not improve by using equal simulation times. One hour of XBeach simulation shows a development of the beach slope which is already more pronounced than the development after seven hours in the experiments. The sediment eroded from the beach is transported downslope in the model whereas in the experiments a large portion was transported upslope to form a swash bar. This suggests that there are different physical processes active in the model and in the experiments.

As opposed to the strong bed level changes in the beach area, there are hardly any changes in the bed level of the sandy lagoon in XBeach. This agrees with the sediment concentration data from XBeach, which showed that there is very little suspension in the sandy lagoon area in the model. The sediment suspension in XBeach is analysed in further detail in the next section.

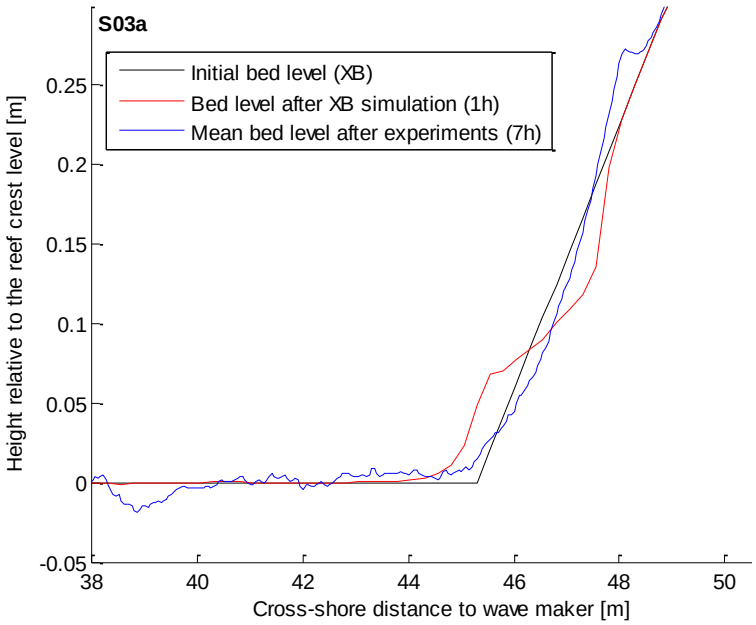

Figure 5.17 Bed profile evolution after 1 hour of simulation by XBeach compared to 7 hours during the experiments.

5.4.2 Analysis of XBeach performance

The previous section showed that the suspension of sediment in the model is much smaller than the observed and measured suspension during the experiments. In this section the Van Thiel/Van Rijn sediment transport formulation, which is implemented in XBeach, is analysed to understand why the suspension of sediment is not correctly reproduced. The formulation reads:

$$c_{eq} = \frac{A_{sb}}{h}\left(\sqrt{(u^E)^2 + 0.64u_{rms,2}^2} - u_{cr}\right)^{1.5} + \frac{A_{ss}}{h}\left(\sqrt{(u^E)^2 + 0.64u_{rms,2}^2} - u_{cr}\right)^{2.4} \quad (5.7)$$

The formulation computes the instantaneous equilibrium sediment concentration as a function of an instantaneous velocity minus a critical velocity, $c_{eq} = f(u - u_{cr})$, and determines the contribution of bed-load and suspended load separately. The equilibrium concentration then serves as input for an advection-diffusion equation from which the transport and instantaneous concentration can be computed. Since the model results show that there is hardly any suspension of sediment, the functioning of the formulation is assessed by emulating it in MATLAB, using the hydrodynamic output of the XBeach model as input for the formulation.

The result is a time series of the instantaneous equilibrium concentration based on the hydrodynamics that were computed by the XBeach model and is plotted in the upper left panel of Figure 5.18. This equilibrium concentration c_{eq} is considered as a measure for the suspended sediment concentration at a particular time during the simulation. The time series shows that the suspended concentration remains below 1 g/l and is zero a large part of the time. The averaged concentration is close to zero. These low or zero concentrations do not agree with observations and measurements that showed that sediment was constantly present in the water column and that the mean concentrations were in the order of 0.5-1 g/l.

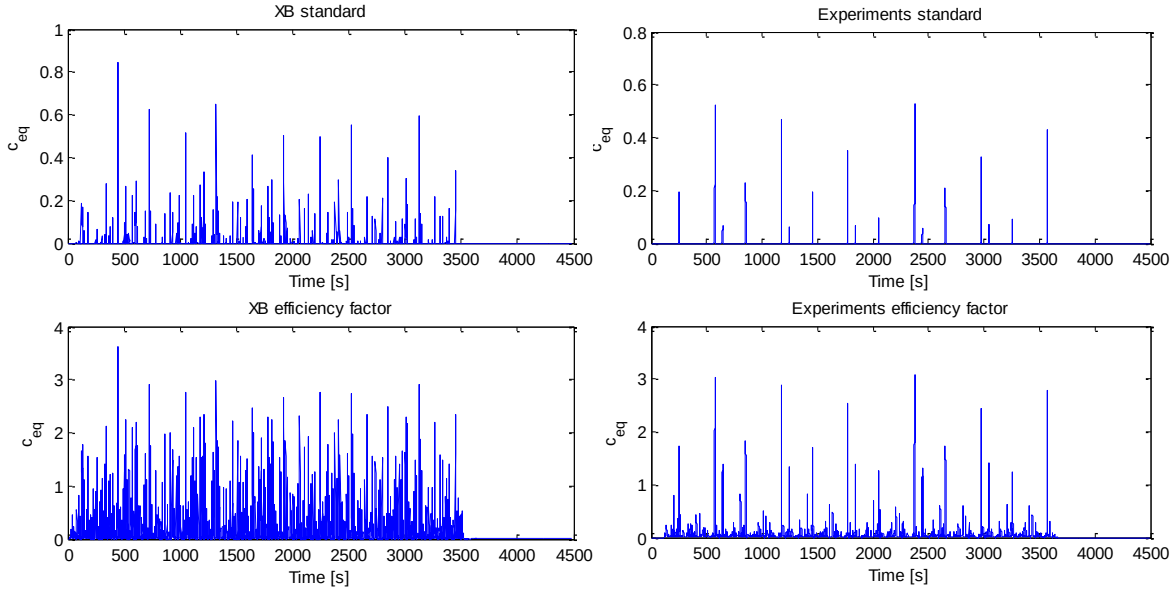

Figure 5.18 Equilibrium sediment concentration c_{eq} computed using the default XBeach sediment transport formulation and based on modelled and measured hydrodynamics. Left panels: based on XBeach hydro; Right panels: based on measured hydro. Top panels: default; Bottom panels: using current-related efficiency factor.

To investigate what causes the lack of sediment suspension the instantaneous concentration is also computed using the measured data from the experiments as input for the sediment transport formulation. The resulting time series is plotted in the upper right graph of Figure 5.18 and it shows that according to the sediment transport formulation there should be hardly any suspension of sediment during the experiments, based on the measured hydrodynamics. The modeled suspension in XBeach is even slightly higher, which is a result of the higher flow velocities in XBeach(Figure 5.13).

Since the experiments already showed that under the hydrodynamic conditions that were present there was significant suspension, it can be concluded that the current implementation of this sediment transport formulation is not suitable to model the sediment concentrations of the experiments correctly. The above analysis shows that the error is not caused by incorrect modelling of the hydrodynamics as the flow velocities are even slightly overestimated in XBeach. The concentration measurements show that there is significant suspension of sediment even when $u<u_{cr}$.

The initial area of application of XBeach was the modelling of dune erosion during storm events and some assumptions in the model and the transport formulation are based on this type of situations. During a storm event for example, one can safely assume that $u>>u_{cr}$ so that the threshold of motion is exceeded by far, whereas in scale experiments the actual flow velocities are in the same order of magnitude as the critical velocity. In that case inaccuracies in either the critical velocity or the actual velocity can have a significant effect on the amount of sediment suspension.

Another assumption underlying XBeach and its transport formulation is that the height of the bed-forms can be neglected when compared to the water depth, so the model assumes no bed-forms. In the experiments ripples up to 2 cm in height were observed, which is a significant portion of the total mean water depth of 13 cm. In the computation of the critical velocity the grain size bed roughness night is used, $k_s = 3d_{90}$. The bed roughness height can also be related to the ripple height in the order of the ripple height, $k_{s,c} = \Delta_r$, which is referred to as the current related bed roughness height. Based on these two roughness heights Van Rijn (1993) defined a current efficiency factor:

$$\mu_c = \frac{f`_c}{f_c} = \log^{-2}\frac{12h}{3d_{90}} \Big/ \log^{-2}\frac{12h}{k_{s,c}} \tag{5.8}$$

This current efficiency factor was implemented in the transport formulation, multiplying it to the critical velocity, u_{cr}. The resulting suspended sediment concentration time series are shown in the bottom panels of Figure 5.18 again for both the modeled and the measured hydrodynamics. The theoretical suspended sediment concentrations are strongly increased in both plots and particularly the concentrations based on the XBeach hydrodynamics compare reasonably with the measured time series (e.g. Figure 4.3).

Using this efficiency factor does appear to provide a solution for the lack of sediment suspension, however, the physical meaning of this efficiency factor in the application described above is unclear. The next section discusses this and discusses the issues that were encountered modeling sediment transport and concentrations in XBeach in general.

5.4.3 Discussion and recommendations

The average suspended sediment concentration and the bed profile development that were obtained from the model XBeach were compared to the measured concentrations and bed profile development. The comparison shows that the suspension of sediment on the reef flat, which was observed in the experiments, is not reproduced in XBeach using the default sediment transport formulation of Van Thiel/Van Rijn. As a result the bed profile development in this area in XBeach is close to zero. Also the development of the beach profile and the swash bar was not correctly reproduced in XBeach. This section discusses the lack of sediment suspension and the analysis described in the previous section and provides recommendations for improvements of XBeach.

The concentration measurements show that there is significant suspension of sediment even when $u<u_{cr}$ according to the transport formulation. Based on this observation there are at least three hypotheses that might explain the under-prediction of sediment suspension by this formulation:

- the forcing related to the velocity is somehow underestimated and should be increased by some factor, for example because the effect of turbulence is not sufficiently accounted for.
- the resistance of the grains, represented in the critical velocity should be lower for example by using the current related bed roughness height instead of the grain size related bed roughness height as was shown in the previous section. Another reason for lowering the critical velocity could be to account for the fact that the also the long wave velocity, u^E, is oscillating and more effective in stirring up sediment than a steady current.
- the concept of a transport formulation using a critical velocity is not the most suitable solution for this specific case and another approach should be used, for example the energetics approach of Bailard (1981), which couples the dissipation of energy by the flow directly to sediment suspension and transport. Dissipation by for example the bed ripples will increase sediment suspension in this approach.

It was shown that the current efficiency factor (equation 5.8) can be used to reduce the critical velocity and increase the amount of suspension of sediment. The physical reasoning behind this is that the ripples influence the flow by increasing the bed shear stress and lowering the actual velocity that is used as input for the formulation. The result is that the amount of suspension is reduced, while it can be argued that it should increase, because the bed shear stress is increased. The current efficiency factor might account for this.

Of course, it is rather obvious that suspension increases when the critical velocity is lowered and therefore it should be further investigated whether it is physically correct to use this current efficiency factor. Also the other hypotheses potentially offer a solution to eventually be able to model sediment transport in a scaled fringing reef environment.

Besides the lack of suspension, the second issue that was found is that XBeach does not reproduce the formation of the swash bar. The swash bar is formed as waves run up the beach and carry sediment upslope. The experiment data shows that during run down not all of this sediment is moved down again and a bar is formed. Apparently XBeach is not capable of modelling this process as in the model sand is only eroded from the beach and a typical dune erosion slope is created. If the application of XBeach is to be extended to a wider range

of application areas it is recommended to include the processes underlying swash bar formation in the model.

5.5 Conclusions and recommendations

In this chapter the results of modelling the flume experiments with XBeach were discussed. Both the hydrodynamics and the morphodynamics computed by the model were compared to the experiment data in order to answer the following research questions:

How does the model XBeach with its default sediment transport formulas compare to the data?

What improvements should be made to XBeach to improve the suitability to model cases comparable to the experiments?

Regarding the first question it was shown that although the hydrodynamics on the reef such as wave-induced set-up (smooth cases), wave transformation, flow velocity, seiching and the breakpoint mechanism were modelled rather well in general, XBeach does not reproduce sediment concentrations and bed profile development correctly. Analysis of the transport formulation showed that there is hardly any suspension in the model, because the velocity remains below the critical velocity a large part of the time. To answer the second question the processes that were not modelled correctly were identified and suggestions were provided to improve modelling of these processes.

The most important conclusions and recommendations are presented below.

5.5.1 Conclusions

The model was set up using the measured time series as boundary conditions and was calibrated based on the short wave height. To model the short wave breaking the breaker model of Daly et al. (2012) was applied and the parameters γ_1, γ_2 and α were used to calibrate the breaker model to the data, giving good results. The rough cases were calibrated using the current friction factor $c_f = 0.1$ and wave friction factor $f_w = 0.3$, which is approximately in agreement with literature about modelling a fringing reef environment.

Regarding the hydrodynamics, the processes that were reproduced very well, were the short wave height, flow velocity and the breakpoint mechanism. The plot of the correlation of the short wave envelope with the long wave height agreed very well with the plot based on the experimental data. Both plots showed the same change of sign of the correlation at the breakpoint as the plot by Pomeroy et al. (2012), which was based on the field data from Ningaloo Reef (Figure 3.18 in this report). The spectra on the reef flat were very similar in shape for all cases comparing model to data (Figure 5.14) showing that for example the reef flat seiching is also reproduced by XBeach.

The long wave height agreed reasonably with the data, but offshore there was too much reflection in the model and there was a transfer of energy to the long wave before the reef slope, which was not observed in the data. After the breakpoint the conservation or generation of long waves was too high in XBeach and it was affected by bed roughness and water depth. The increase of long wave energy over the reef flat was well reproduced in the model for S03, but not for S01 and S04. It was shown that this is related to the reef flat seiching which is not as strong in the model as in the experiments for the cases S01 and S04.

The wave-induced set-up was analysed in detail and it was shown that the set-up in XBeach increased due to bed friction, while in the experiments the set-up was not affected at all by the bed roughness. The set-up was reproduced very well for the smooth cases, but was overestimated significantly in the rough cases. The model results also showed that for case S01 almost half of the wave dissipation is due to bed friction. In the next section some recommendations are presented regarding wave-induced set-up in XBeach.

The morphodynamics in XBeach were compared to the data by the measured suspended sediment concentrations and bed profile development. XBeach did not reproduce the sediment concentrations and the bed profile development in the sandy lagoon area. Also the beach profile development was incorrectly predicted by XBeach as sediment was only transported downslope, whereas in the experiments a swash bar was formed at the point of maximum run-up.

The suspended sediment concentrations in the model were close to zero. Analysis of the sediment transport formulation showed that the actual velocity only rarely exceeded the critical velocity in the sandy lagoon and therefore no suspension or transport of sediment could occur.

5.5.2 Recommendations

The effect of bed roughness on wave-induced set-up was found to be rather complex. In the experiments the bed roughness had no influence on the set-up while in XBeach the set-up increased significantly when a high bed roughness value was used. According to Dean and Bender (2006) an extra force should be introduced that accounts for a shear stress exerted by the roughness elements on the water column counter to the direction of wave propagation. This force is caused by nonlinearity of the near-bed particle velocities. It is recommended to study this theory to implement it in XBeach. Their theory also included effects of vegetation on set-up, so this could increase the suitability of XBeach to model different cases.

The use of XBeach and its default sediment transport formulation resulted in very little sediment suspension in the sandy lagoon, which was in total disagreement with the data. Three solutions were proposed of which application of a current efficiency factor to account for the effect of bed ripples was shown to be effective in increasing sediment suspension. The physical reasoning behind this is that the ripples influence the flow by increasing the bed shear stress and lowering the actual velocity that is used as input for the formulation. The result is that the amount of suspension is reduced, while it can be argued that it should increase, because the bed shear stress is increased. The current efficiency factor might account for this.

Further research is needed to investigate whether it is physically correct to use such a factor, since it is rather obvious that reducing the critical velocity by any factor would increase sediment suspension. It is also recommended to look into other approaches to model sediment transport, such as the energetics approach, and to check whether the oscillation of the velocity is sufficiently accounted for.

Besides the lack of suspension, the second issue that was found is that XBeach does not reproduce the formation of the swash bar. The swash bar is formed as waves run up the beach and carry sediment upslope. The experiment data shows that during run down not all of this sediment is moved down again and a bar is formed. Apparently XBeach is not capable

of modelling this process as in the model sand is only eroded from the beach and a typical dune erosion slope is created. If the application of XBeach is to be extended to a wider range of application areas it is recommended to include the processes underlying swash bar formation in the model.

6 Conclusions and recommendations

6.1 Introduction

This study investigated wave and sediment dynamics over a fringing reef by analysing laboratory data and by numerical modelling. The hydrodynamic data obtained from the experiments was analysed and the important processes were identified in order to provide an answer to the research question:

How do waves transform over a smooth and rough fringing reef?

The specific conditions in a fringing reef environment were shown to have influence on many processes such as infragravity(IG) wave generation, IG wave transformation, seiching, wave-induced setup and wave reflection. In general the findings from the data analysis agree well with existing literature about long waves and hydrodynamics on reefs.

Also the concentration and profile measurements have been analysed and combined with the hydrodynamic data to supply an answer to the research question:

How do the measured sediment concentrations and bed-profile developments relate to the hydrodynamics?

It was found that the specific hydrodynamics of a fringing reef environment are reflected in the sediment transport and suspension and in the bed profile development. The effect of bed friction on long waves and of long waves themselves was shown in the various analyses in this report.

The flume experiments were modelled using XBeach to improve understanding of the relevant processes and to assess the ability of XBeach to model the hydrodynamics and morphodynamics. Both the hydrodynamics and the morphodynamics computed by the model were compared to the experiment data in order to answer the following research questions:

How does the model XBeach with its default sediment transport formulas compare to the data?

What improvements should be made to XBeach to improve the suitability to model cases comparable to the experiments?

Regarding the first question it was shown that although the hydrodynamics on the reef such as wave-induced set-up(smooth cases), wave transformation, flow velocity, seiching and the breakpoint mechanism were modelled rather well in general, XBeach does not reproduce sediment concentrations and bed profile development correctly. Analysis of the transport formulation showed that there is hardly any suspension in the model, because the velocity remains below the critical velocity a large part of the time. To answer the second question the processes that were not modelled correctly were identified and suggestions were provided to improve modelling of these processes.

The main conclusions and recommendations that were established in this report, are summarised below.

6.2 Conclusions

6.2.1 Hydrodynamics

Analysis of the integral parameters provided an overview of the experiments and provided an insight in some of the hydrodynamic processes that were present. It was found that there is a rather strong reflection of wave energy on the reef crest of 23 to 30% of the incoming wave energy. The reflection of wave energy on the beach is around 80% and is mainly attributed to long waves that are dominant on the reef flat area. The reflection is strongest for the cases S02 and S04 with a lower water depth $h_r = 0.05\,m$. Root-mean-squared values for the velocity in alongshore direction were found to be much smaller than those in cross-shore direction so the experiments will be considered one-dimensional.

The mean water levels were used to determine the wave-induced set-up and set-down. In the shoaling zone a small set-down was found. It was also found that the overall water level offshore was lowered because the water level on the reef was raised and water in the flume is conserved. The water level on the reef was raised significantly to almost double the initial water level h_r for simulation S02 and S04. The set-up was largest for these simulations because of stronger wave forcing and a smaller water column on which the forcing was active. The effect of bed friction on the set-up was negligible comparing S01 and S03, and gave a very minor contribution to the set-up for case S02.

The results of the spectral evolution analysis of the total long wave height ($f<f_p/2$) confirmed the importance of long waves on a fringing coral reef as it showed that they become dominant towards the lagoon and beach. Consistent with Hearn (1999) it was found that a lower water depth enhances the effect of bed friction on waves and flow velocity. Near the beach it was found that the short waves are grouped by water depth, because of depth-induced breaking, and the total long wave height is grouped by bed roughness, mainly by the effect of bed roughness on the seiching motion.

It was observed that the total long wave energy increases towards the beach caused by resonance at the Eigen frequency of the reef flat and the flume and reflection of progressive waves on the beach slope. The long waves were separated into an IG ($0.035<f<f_p/2$ Hz) and a very low frequency, or VLF, range ($0<f<0.035$ Hz) for further analysis.

The IG wave shoaling and generation around the short wave breakpoint was analysed using the normalised bed slope parameter by Battjes et al. (2004) and the surf zone similarity parameter from Baldock (2012). The long waves were observed to shoal according to $h^{-\frac{3}{4}}$ which is not in agreement with the value of -1/4 from Green's law which should be the shoaling regime according to Battjes et al. (2004) for the bed slope parameter of 0.7 that was found. The fact that the IG waves shoal according to $h^{-\frac{3}{4}}$ indicates that there is transfer of energy to the long waves. This could be attributed to the breakpoint mechanism of Symonds et al. (1982) since the results showed that waves were breaking in a steep slope regime and the breakpoint mechanism is supposed to be dominant in that case. The results are in agreement with results from Pomeroy et al. (2012) who showed that long waves are generated at the breakpoint in Ningaloo Reef field data. The reflection of IG wave energy on the reef crest is significant and at the offshore measurement location the reflected waves even dominate the incoming waves.

The VLF range included three peaks in the spectrum which were analysed in detail: a standing wave with a period in the order of 60-80 seconds and one at about 33 seconds and

a long period motion of 330 seconds. Analysis of the short wave variation offshore indicated that the 330s motion might be forced by a long period variation in the short wave energy offshore from the reef.

The presence of a standing wave was supported by a decrease of the flow velocity and an increase of wave height at VLF frequencies towards the beach and a clear standing wave pattern observed in time series of waves and flow velocities on the reef. A plot of surface elevation at all time steps showed a standing wave pattern in the entire flume. The observed frequencies of the standing waves showed to agree quite well with theoretical values of the Eigen frequency of the reef and the flume and varied with depth.

6.2.2 Sediment dynamics

Analysis of the depth-averaged concentrations measured with the sampling devices and those with the FOSLIMs did not produce very consistent results and showed that there is a large scatter and uncertainty in the data, indicating that an order of magnitude agreement with XBeach regarding sediment concentrations should be the objective rather than an exact match of the concentrations. An increase in the sediment concentrations from the seaward side of the lagoon towards the beach could also be reproduced in XBeach.

This analysis also showed that the FOSLIMs are rather sensitive to a background turbidity by fine particles in the water which reduces the quality and reliability of the measurements.

The analysis of the third order velocity moment shows that the contribution related to long wave stirring and transport or advection becomes the dominant contribution close to the beach. The results are consistent with the analysis of chapter 3 where it was shown that long waves are dominant in the lagoon. Also the effect of the bed roughness shows in the results, reducing the contribution of the *gull*, and is in agreement with observations described in the previous chapter. In the deep water cases (1 and 3) the contribution of the *gull* is dominant at the end of the lagoon, but in those cases the transport related to the short wave stirring, which is the sum of the *guss* and *guls,* remains more important as these terms together are the largest contribution to the velocity moment.

The contribution of the time-varying part, $\langle \tilde{u}|\tilde{u}|^2 \rangle$, to the total third order velocity moment is positive, indicating onshore directed transport. There is also a contribution by the mean flow, or undertow, $3\bar{u}\langle|\tilde{u}|^2\rangle$, which results in a negative contribution to the third order moment. The magnitude of this contribution is significant and about the same magnitude of the time-varying part. Still, the total third order velocity moment in general shows an increasing trend towards the beach and is mostly positive on the sandy area, indicating onshore directed transport at most locations.

Combined with the correlation analysis and the bed profile developments this paints a very consistent picture in which both the short and the long waves play a role, but the long waves appear to be the dominant factor in sediment transport and bed profile development especially close to the beach. Also the effect of the roughness elements becomes visible, mainly in the shape of the swash bar, which is different for rough and smooth cases. This shows that the dominance of long waves in a fringing reef lagoon indeed results in different sediment dynamics than for example on a regular sandy beach. The long wave dominance should theoretically mean that the wave-group averaged model XBeach is very suitable for modelling this type of reefs including the sediment dynamics.

The depth-averaged concentrations that were determined for the sampling measurements (Table 4.4) are lower for the rough cases 1 and 2 than for the smooth cases 3 and 4. This is consistent with the results discussed above showing that long waves play an important role in the sediment dynamics since the long wave heights for these rough cases were lower than for the smooth cases as discussed in chapter 3.

6.2.3 XBeach modelling

The model was set up using the measured time series as boundary conditions and was calibrated based on the short wave height. To model the short wave breaking the breaker model of Daly et al. (2012) was applied and the parameters γ_1, γ_2 and α were used to calibrate the breaker model to the data, giving good results. The rough cases were calibrated using the current friction factor $c_f = 0.1$ and wave friction factor $f_w = 0.3$, which is approximately in agreement with literature about modelling a fringing reef environment.

Regarding the hydrodynamics, the processes that were reproduced very well, were the short wave height, flow velocity and the breakpoint mechanism. The plot of the correlation of the short wave envelope with the long wave height agreed very well with the plot based on the experimental data. Both plots showed the same change of sign of the correlation at the breakpoint as the plot by Pomeroy et al. (2012), which was based on the field data from Ningaloo Reef (Figure 3.18 in this report). The spectra on the reef flat were very similar in shape for all cases comparing model to data (Figure 5.14) showing that for example the reef flat seiching is also reproduced by XBeach.

The long wave height agreed reasonably with the data, but offshore there was too much reflection in the model and there was a transfer of energy to the long wave before the reef slope, which was not observed in the data. After the breakpoint the conservation or generation of long waves was too high in XBeach and it was affected by bed roughness and water depth. The increase of long wave energy over the reef flat was well reproduced in the model for S03, but not for S01 and S04. It was shown that this is related to the reef flat seiching which is not as strong in the model as in the experiments for the cases S01 and S04.

The wave-induced set-up was analysed in detail and it was shown that the set-up in XBeach increased due to bed friction, while in the experiments the set-up was not affected at all by the bed roughness. The set-up was reproduced very well for the smooth cases, but was overestimated significantly in the rough cases. The model results also showed that for case S01 almost half of the wave dissipation is due to bed friction. In the next section some recommendations are presented regarding wave-induced set-up in XBeach.

The morphodynamics in XBeach were compared to the data by the measured suspended sediment concentrations and bed profile development. XBeach did not reproduce the sediment concentrations and the bed profile development in the sandy lagoon area. Also the beach profile development was incorrectly predicted by XBeach as sediment was only transported downslope, whereas in the experiments a swash bar was formed at the point of maximum run-up.

The suspended sediment concentrations in the model were close to zero. Analysis of the sediment transport formulation showed that the actual velocity only rarely exceeded the critical velocity in the sandy lagoon and therefore no suspension or transport of sediment could occur.

6.3 Recommendations

6.3.1 Hydrodynamics

It was discussed that the separation of incoming and reflected waves and flow velocity gave rise to some artefacts where the wave height was attributed incorrectly to the reflected wave. It is recommended to look into improving this method by taking into account the nonlinearities and the irregular wave shape as observed on the reef flat.

The observed motion at a period around 330s on the reef was shown to possibly be related to a long period variation in the short wave energy offshore. It is recommended to look into this phenomenon further in a more detailed analysis of the data. Relating this long period motion to variation in the short wave forcing can prove to be practically relevant to get a better understanding and prediction of rip currents for example.

The long wave evolution in the shoaling and surf zone was analysed in this report and the breaking of short waves on the steep slope was found to cause generation of long waves by the breakpoint mechanism. It was observed that the long waves shoal on the reef slope and then dissipate a significant portion of their energy possibly due to breaking. The exact processes that play a role in long wave evolution through the surf zone are still under debate and would be an interesting topic for further research.

All processes described are observed in the quasi-1D environment of the Scheldt Flume at Deltares. One-dimensional modelling is a good start to get an understanding of all the processes that are relevant for a certain situation. Now that some of these processes have been established, it would be possible to compare observations with data from a two-dimensional experiment. For example the wave-induced set-up and the resonance might be strongly affected by two-dimensional processes.

6.3.2 Sediment dynamics

The ripple observations and the possible role of ripples has been discussed briefly in this chapter. It is recommended to look further into their role and how they affect the measured concentrations, the hydrodynamics and the bed profile development.

It has become clear that the FOSLIM measurements have a shortcoming in the sense that they are sensitive to turbidity in the water column. However, the instantaneous concentrations and spikes that they measure still offer very valuable information and therefore we recommend this to be studied in detail in order to gain more insight in what is causing the peaks in the measured concentrations. Also the ‘stacked’ FOSLIM signal can provide useful information to further analyse sediment suspension and advection processes.

It would be interesting to relate the position of the swash bar (Figure 4.14) to the run-up measurements that were done during the hydrodynamic part of the experiments. This would allow one to quantify the role of long waves in swash bar dynamics.

6.3.3 XBeach modelling

The effect of bed roughness on wave-induced set-up was found to be rather complex. In the experiments the bed roughness had no influence on the set-up while in XBeach the set-up increased significantly when a high bed roughness value was used. According to Dean and

Bender (2006) an extra force should be introduced that accounts for a shear stress exerted by the roughness elements on the water column counter to the direction of wave propagation. This force is caused by nonlinearity of the near-bed particle velocities. It is recommended to study this theory to implement it in XBeach. Their theory also included effects of vegetation on set-up, so this could increase the suitability of XBeach to model different cases.

The use of XBeach and its default sediment transport formulation resulted in very little sediment suspension in the sandy lagoon, which was in total disagreement with the data. Three solutions were proposed of which application of a current efficiency factor to account for the effect of bed ripples was shown to be effective in increasing sediment suspension. The physical reasoning behind this is that the ripples influence the flow by increasing the bed shear stress and lowering the actual velocity that is used as input for the formulation. The result is that the amount of suspension is reduced, while it can be argued that it should increase, because the bed shear stress is increased. The current efficiency factor might account for this.

Further research is needed to investigate whether it is physically correct to use such a factor, since it is rather obvious that reducing the critical velocity by any factor would increase sediment suspension. It is also recommended to look into other approaches to model sediment transport, such as the energetics approach, and to check whether the oscillation of the velocity is sufficiently accounted for.

Besides the lack of suspension, the second issue that was found is that XBeach does not reproduce the formation of the swash bar. The swash bar is formed as waves run up the beach and carry sediment upslope. The experiment data shows that during run down not all of this sediment is moved down again and a bar is formed. Apparently XBeach is not capable of modelling this process as in the model sand is only eroded from the beach and a typical dune erosion slope is created. If the application of XBeach is to be extended to a wider range of application areas it is recommended to include the processes underlying swash bar formation in the model.

These and some additional issues regarding the XBeach model are summarised in appendix F.

7 References

Alsina, J.M., & Cáceres, I. (2011). Sediment suspension events in the inner surf and swash zone. Measurements in large-scale and high-energy wave conditions. *Coastal Engineering, 58*(8), 657-670.

Bailard, J.A. (1981). An energetics total load sediment transport model for a plane sloping beach. *Journal of Geophysical Research: Oceans (1978–2012), 86*(C11), 10938-10954.

Baldock, T.E. (2012). Dissipation of incident forced long waves in the surf zone—Implications for the concept of “bound” wave release at short wave breaking. *Coastal Engineering, 60*(0), 276-285. doi: 10.1016/j.coastaleng.2011.11.002

Battjes, J., Bakkenes, H., Janssen, T., & Van Dongeren, A. (2004). Shoaling of subharmonic gravity waves. *Journal of Geophysical Research: Oceans (1978–2012), 109*(C2).

Bosboom, J., & Stive, M.J.F. (2011). *Coastal Dynamics I: Lecture Notes CT4305*: VSSD.

Bosman, J.J., Van Der Velden, E.T.J.M., & Hulsbergen, C.H. (1987). Sediment concentration measurement by transverse suction. *Coastal Engineering, 11*(4), 353-370.

Cooley, J.W., & Tukey, J.W. (1965). An algorithm for the machine calculation of complex Fourier series. *Mathematics of computation, 19*(90), 297-301.

Daly, C., Roelvink, D., Van Dongeren, A., Van Thiel De Vries, J., & Mccall, R. (2012). Validation of an advective-deterministic approach to short wave breaking in a surf-beat model. *Coastal Engineering, 60*, 69-83.

Darwin, C. (1842). *On the Structure and Distribution of Coral Reefs. Being the First Part of the Geology of the Voyage of the Beagle Under the Command of Capt. Fitzroy, R. N. During the Years 1832 to 1836.* : Smith Elder and Co., London.

Dean, R., & Bender, C.J. (2006). Static wave setup with emphasis on damping effects by vegetation and bottom friction. *Coastal Engineering, 53*(2), 149-156.

Dean, R., & Dalrymple, R. (1991). Water wave mechanics for scientists and engineers. *World Sci entific, Advanced Series on Ocean Eng, 2*.

Deltares. (2012a). GHM - Deltares. Retrieved 05-12, 2012, from http://www.deltares.nl/en/facilities/instrumentation/ghm

Deltares. (2012b). OSLIM/FOSLIM - Deltares. Retrieved 05-12, 2012, from http://www.deltares.nl/en/facilities/instrumentation/oslim-foslim

Deltares. (2012c). Scheldt Flume - Deltares. Retrieved 05-12, 2012, from http://www.deltares.nl/en/facility/107930/scheldt-flume/869853

Deltares. (2012d). User Manual Delft3D-FLOW: Simulation of multi-dimensional hydrodynamic flows and transport phenomena, including sediments. *Deltares, Delft, Netherlands*.

Dingemans, M.W. (1997). *Water wave propagation over uneven bottoms: Linear wave propagation* (Vol. 13): World Scientific.

Galappatti, R. (1983). A depth integrated model for suspended transport.

Guza, R., Thornton, E., & Holman, R. (1984). Swash on steep and shallow beaches. *Coastal Engineering Proceedings, 1*(19).

Hearn, C.J. (1999). Wave-breaking hydrodynamics within coral reef systems and the effect of changing relative sea level. *Journal of Geophysical Research, 104*(C12), 30007-30019.

Holthuijsen, L.H. (2007). *Waves in oceanic and coastal waters*: Cambridge University Press.

Hughes, S.A. (1993). *Physical models and laboratory techniques in coastal engineering* (Vol. 7): World Scientific Publishing Company Incorporated.

Kirby, J.T. (1998). Analysis of regular and random ocean waves. *Course notes for University of Delaware course# CIEG681*.

Komar, P. (1998). *Beach Processes and Sedimentation* (2nd ed.). Upper Saddle River, N.J.: Prentice-Hall.

Komar, P., & Miller, M.C. (1975). On the comparison between the threshold of sediment motion under waves and unidirectional currents with a discussion of the practical evaluation of the threshold; reply. *Journal of Sedimentary Research, 45*(1), 362-367.

Lee, T.T., & Black, K.P. (1978). *The energy spectra of surf waves on a coral reef.* Paper presented at the Proceedings of the International Conference on Coastal Engineering.

Lowe, R.J., Falter, J.L., Bandet, M.D., Pawlak, G., Atkinson, M.J., Monismith, S.G., & Koseff, J.R. (2005). Spectral wave dissipation over a barrier reef. *Journal of Geophysical Research, 110*(C4), C04001.

Lowe, R.J., Falter, J.L., Koseff, J.R., Monismith, S.G., & Atkinson, M.J. (2007). Spectral wave flow attenuation within submerged canopies: Implications for wave energy dissipation. *Journal of geophysical research, 112*(C5), C05018.

Lugo-Fernandez, A., Roberts, H., Wiseman Jr, W., & Carter, B. (1998). Water level and currents of tidal and infragravity periods at Tague Reef, St. Croix (USVI). *Coral Reefs, 17*(4), 343-349.

Munk, W.H. (1949). Surf beats. *Eos Trans. AGU, 30*, 849-854.

Munk, W.H., & Sargent, M.C. (1948). Adjustment of Bikini Atoll to ocean waves. *Trans. Am. Geophys. Union, 29*, 855-860.

Nortek As. (2012). Vectrino II - Nortek International. Retrieved 05-12, 2012, from http://www.nortek-as.com/en/products/velocimeters/vectrino-ii

Pomeroy, A. (2011). *Low frequency wave resonance on fringing reefs.* (MSc Thesis), TU Delft, Delft.

Pomeroy, A., Lowe, R., Symonds, G., Van Dongeren, A., & Moore, C. (2012). The dynamics of infragravity wave transformation over a fringing reef. *Journal of Geophysical Research: Oceans (1978–2012), 117*(C11).

Rocha, M.V., Michallet, H., Silva, P.A., Abreu, T., & Barthélemy, E. (2013). Nonlinearities of short and long waves across the shoaling, surf and swash zones: Physical model results. *Proceedings Coastal Dynamics 2013*.

Roelvink, D. (1993). Dissipation in random wave groups incident on a beach. *Coastal Engineering, 19*(1), 127-150.

Roelvink, D., & Reniers, A. (2012). *A guide to modeling coastal morphology* (Vol. 12): World Scientific.

Roelvink, D., Reniers, A., Van Dongeren, A., Van Thiel De Vries, J., Lescinski, J., & Mccall, R. (2010). XBeach model description and manual: UNESCO-IHE Institute for Water Education.

Roelvink, D., Reniers, A., Van Dongeren, A., Van Thiel De Vries, J., Mccall, R., & Lescinski, J. (2009). Modelling storm impacts on beaches, dunes and barrier islands. *Coastal Engineering, 56*(11), 1133-1152.

Roelvink, D., & Stive, M. (1989). Bar-generating cross-shore flow mechanisms on a beach. *J. Geophys. Res, 94*(C4), 4785-4800.

Ruessink, B., Miles, J., Feddersen, F., Guza, R., & Elgar, S. (2001). Modeling the alongshore current on barred beaches. *Journal of Geophysical Research: Oceans (1978–2012), 106*(C10), 22451-22463.

Soulsby, R. (1997). *Dynamics of marine sands: a manual for practical applications*: Thomas Telford.

Storlazzi, C.D., Elias, E., Field, M., & Presto, M. (2011). Numerical modeling of the impact of sea-level rise on fringing coral reef hydrodynamics and sediment transport. *Coral Reefs, 30*, 83-96.

Storlazzi, C.D., Field, M.E., Bothner, M.H., Presto, M., & Draut, A.E. (2009). Sedimentation processes in a coral reef embayment: Hanalei Bay, Kauai. *Marine Geology, 264*(3), 140-151.

Symonds, G., Huntley, D.A., & Bowen, A.J. (1982). Two-Dimensional Surf Beat: Long Wave Generation by a Time-Varying Breakpoint. *Journal of Geophysical Research, 87*(C1), 492-498.

Uijttewaal, W. (2005). Turbulence in hydraulics. *Delft University of Technology. Lecture Notes*.

Van Dongeren, A., Lowe, R., Pomeroy, A., Trang, D.M., Roelvink, D., Symonds, G., & Ranasinghe, R. (2013). Numerical modeling of low-frequency wave dynamics over a fringing coral reef. *Coastal Engineering, 73*, 178-190. doi: 10.1016/j.coastaleng.2012.11.004

Van Dongeren, A., Wenneker, I., Roelvink, D., & Rusdin, A. (2007). A Boussinesq-type wave driver for a morphodynamical model. *Proceedings of the Coastal Engineering Conference*, 3129-3141.

Van Rijn, L.C. (1993). *Principles of sediment transport in rivers, estuaries and coastal seas* (Vol. 1006): Aqua publications Amsterdam.

Van Rijn, L.C. (2007). Unified view of sediment transport by currents and waves, part I, II, III and IV. *Journal of Hydraulic Engineering, 133*(6 and 7).

Van Thiel De Vries, J. (2009). Dune erosion during storm surges. PhD Thesis, Delft University of Technology, Delft, The Netherlands.

Whipple, K. (2004). 12.163 Course Notes: MIT Open Courseware.

Young, I.R. (1989). Wave transformation over coral reefs. *Journal of Geophysical Research, 94*(C7), 9779-9789.

A Data processing

This appendix describes some general observations from the experiment logbook which were relevant for processing of the data. It also explains the principles of spectral analysis for time series of surface elevation and flow velocity.

General
Before starting the actual analysis of the data the experiment logbook and notes are checked for any relevant information for processing the data. Important and relevant findings are summed up below.

- General:
  - Velocity signal is delayed 140 ms
- Run S01 – rough
  - Data of FOSLIM02 is incorrect due to malfunctioning of the device during part a. After part a the device was repaired and functioning properly again.
  - FOSLIM05 was raised 2cm during part b of the run after 42 minutes.
- Run S02 – rough
  - Whm03 and whm04 were lowered 5cm during part a, because they were out of the water part of the time.
  - Shm 27/28, 29/30 moved 'up' during test part b(not visible in time series).
  - FOSLIM05 moved a bit down after 2 hours and 40 minutes during part c, because it was out of the water now and then.
- Run S03 – smooth
  - During part c possible offset noticed of FOSLIM01.
  - During part c measurement stopped after 7430s because the disk space was full. Part d is a continuation of part c.

Spectral analysis
In order to analyse wave data variance density spectra are created from the time series. The idea behind spectral analysis is that the time series from the wave gauges, and wave time series in general, can be represented by a superposition of an infinite number of cosine waves with a random phase and amplitude. With a Fourier analysis the values of the amplitude and phase for each frequency can be determined so that the original time series is reproduced.

The result of the Fourier analysis is a spectrum which shows the distribution of the wave energy over different frequencies. A wave spectrum is usually created as a variance density spectrum (instead of wave amplitude) for two reasons: the first one is that the variance of the amplitude ($\frac{1}{2}a^2$) is a more relevant statistical quantity than the amplitude itself as the sum of the variances of the wave components is equal to the variance of the sum of the wave components. That is not the case for the amplitude variance. The second reason is that the variance is proportional to physical properties such as the wave energy according to linear wave theory by multiplying by the density and the gravitational acceleration ($E = \frac{1}{2}\rho g a^2$) (Holthuijsen, 2007).

The variance density spectrum can be written as:

$$E(f) = \lim_{\Delta f \to 0} \frac{1}{\Delta f} E\left(\frac{1}{2} \underline{a_i}^2\right)$$

To obtain a correct variance density spectrum the surface elevation time series has to be stationary, meaning that the statistical properties of the signal such as the mean and standard deviation are constant for the selected time period. The first step in the analysis is therefore to find the period in which the surface elevation signal is stationary by determining the period in which the mean and standard deviation are constant. An example of the procedure for one time series is shown in Figure 7.1. During the spin-up and spin-down the mean and standard deviation are varying and in between there is a long period with a stationary signal. For the following analysis only the stationary phase of the measurements is used also for the sediment concentration and velocity.

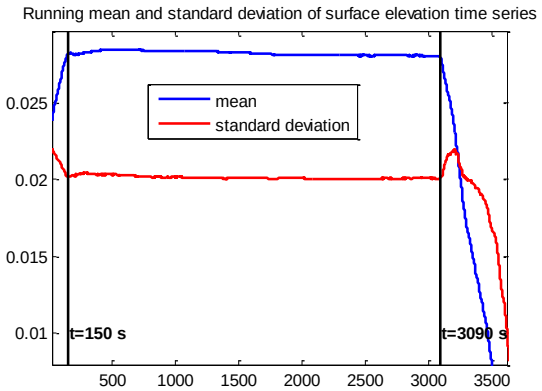

Figure 7.1 Finding the stationary part of a time series by finding period of constant mean and standard deviation

The non-stationary parts of the time series are cut off and the remaining signal is detrended. Detrending removes the mean and any linear trend from the signal for example created by setup, see Figure 7.2.

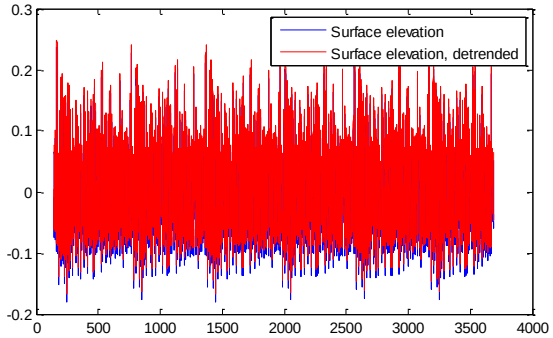

Figure 7.2 Detrending the surface elevation signal

Next the discrete spectrum can be calculated by Fourier transforming the surface elevation time series using the Fast Fourier Transform (FFT) algorithm.

- Determine the Fourier transform of the time series of η consisting of N elements: $F_{N,\eta} = fft(\eta)/N$. The Fourier transform variable F_N is a vector consisting of N elements with (N-2)/2 complex conjugate pairs. When plotted this looks like a spectrum which is mirrored at N/2. To create a real spectrum as we are used to see it, the complex conjugates for n>N/2 have to be folded back into the first part of the

spectrum. After dividing by $\frac{1}{T} = \Delta f$ and taking the absolute values a very grassy amplitude spectrum is obtained.

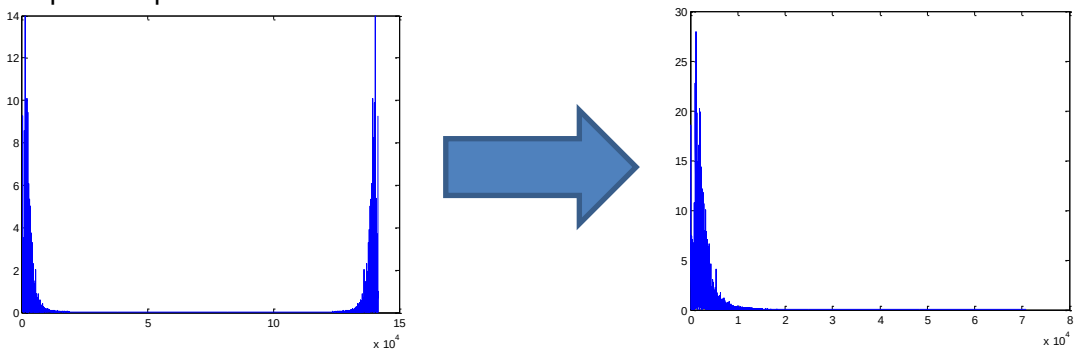

Figure 7.3 Folding the spectrum at N/2

- To get the variance density distribution the elements of the Fourier vector F_N are squared, folded at N/2 and divided by Δf. Plotting these values against the frequency f results in the variance density spectrum:

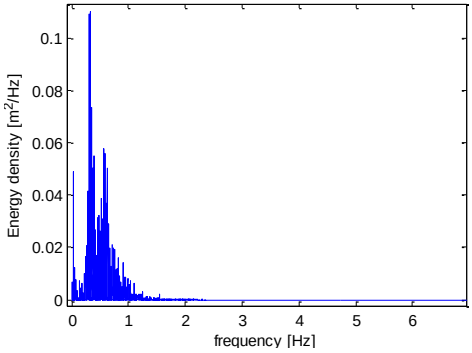

Figure 7.4 The (very grassy) energy density spectrum

- To check if the transformation was successful the total variance of the signal can be found by simply integrating the spectrum over the frequency axis. The resulting total variance should be equal to the variance of the original surface elevation time series. Also, using the inverse Fast Fourier Transform should result in the same signal again. The total variance of the spectrum is equal to the zeroth order moment of the spectrum m_0 expressed as $m_n = \int_0^\infty f^n E(f) df$. The significant wave height H_{m0} can be found by $H_{m0} = 4 * \sqrt{m_0}$.
- Because the surface elevation is a discrete signal, the spectrum also appears in a discrete and therefore grassy form. This is the case, because in practice it is not possible to take the limit of Δf→0 since Δf is determined by the length of the time series by Δf=1/T. In order to get a smoother spectrum several techniques are available. The first one is bin-averaging which means that the spectrum is averaged over larger frequency bins of n*Δf. The second method is an ensemble-averaging method in which the time series is split up into multiple parts and a spectrum is calculated for each of the separate parts. Then the ensemble-average of all of the spectra is taken, giving a much smoother spectrum. The figure below shows the result of both methods. The total number of elements in the time series was about 140,000, so for the ensemble averaging about 70 samples were used, because the samples were allowed to overlap 50%. Both methods for smoothing give similar results and have the disadvantage that the frequency resolution becomes lower.

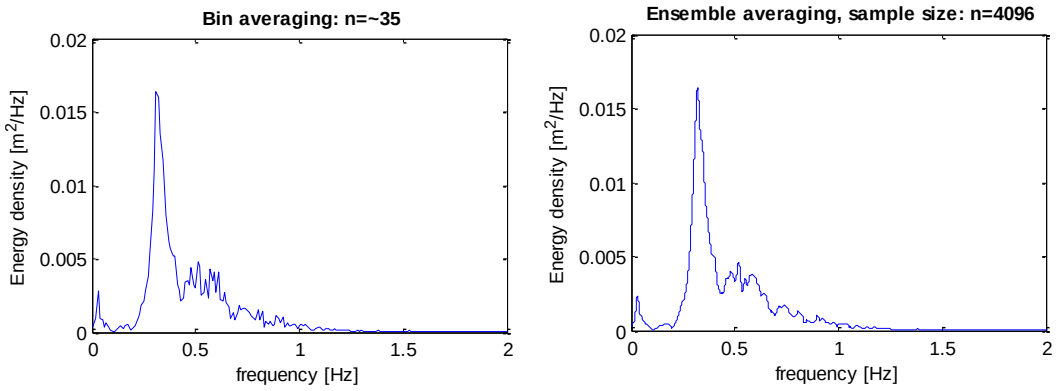

Figure 7.5 Bin averaging and ensemble averaging compared

In the spectrum both long and short wave energy is represented. As part of the analysis of the wave activity and resulting sediment concentrations it is interesting to look at the role of long or infragravity and short waves separately. With the spectrum the low and high frequency motions can be separated. In order to do this first the offshore peak frequency f_p is determined, which is the frequency with the highest energy density. This peak frequency will be approximately equal to the target peak frequency that the wave maker is programmed to generate. Low frequency motions associated with infragravity waves are defined as motions with a frequency lower than the split frequency $f_{split}=f_p/2$ (Roelvink & Stive, 1989),

B Information about hydrodynamic experiments

This section provides information about the hydrodynamic part of the experiments, as this was not included in the main report. It describes the setup of the flume for this part of the experiments and presents the runs that were performed.

Stage 1: Hydrodynamics, smooth bed
In the flume a generic model of a fringing coral reef, loosely based on Ningaloo Reef, West Australia, was constructed at a 1:36 scale. The structure was placed at one end of the flume and has a total length of 23.5 m. It consisted of a 1:5 forereef slope from the bottom of the flume to a height of 0.7 m above the bottom, a horizontal reef flat of 14 m length and a 1:12 beach slope to the top of the flume at 1.2m above the bottom.

The smooth slopes and reef flat were constructed out of a plywood cover screwed on vertical plywood sheets placed along the glass walls of the flume. The cavity below the cover was filled with very coarse sand. A sketch of the layout of the flume for all stages can also be found in Figure 7.6.

Stage 2: Hydrodynamics, rough bed
The setup for stage 2 was the same as for stage 1 and the same test runs will be performed, the only difference being that we created a bed with a high roughness value on the reef slope and reef flat. The smooth plywood covers were replaced by similar covers that have roughness elements placed on them consisting of concrete cubes of 1.8 cm spaced at 4 cm. In total approximately 8,000 concrete cubes were glued onto the covers by hand to achieve a hydraulic roughness comparable to real coral reefs, be it very schematised and regular.

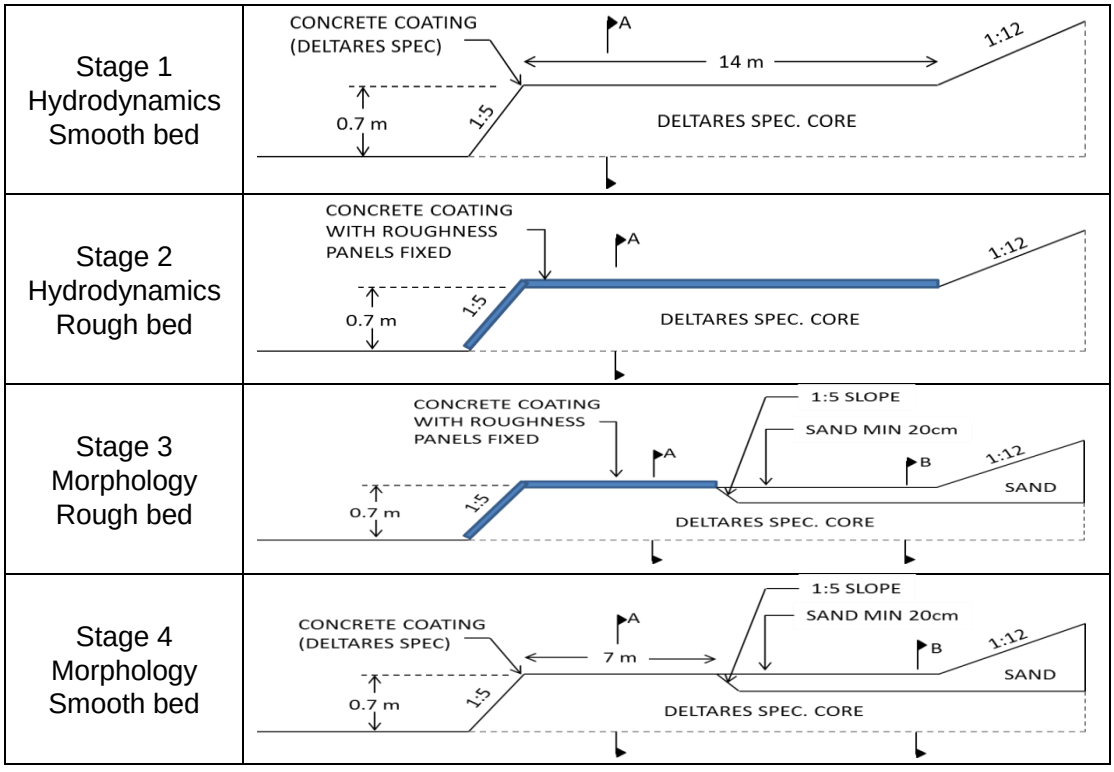

Figure 7.6 Flume layout for all stages

Stage 3: Morphology, rough bed
For the test runs to measure sediment concentrations and transport the setup of the flume was changed. 7 meters of timber representing the back of the reef flat and the timber representing the beach slope was removed. This created a trench behind the remaining part of the reef flat. The trench was filled up with sand of 120 mu and a new sandy beach slope was be created at the end of the flume. The forereef and reef flat were still covered with the concrete roughness elements. The length scale was changed to 1:15 in order to get a better representation of the sediment transport as was explained in the section on scaling in Chapter 2.

Stage 4: Morphology, smooth bed
For the final stage of the study the covers with roughness elements were replaced by smooth plywood covers to be able to compare sediment transport for a situation with a smooth and a rough bed on the forereef and reef flat.

See Figure 7.6 or a summary of the setup for different stages of the experiment.

Experimental program
For the hydrodynamic part of the project 16 runs were conducted for both the smooth situation and the situation with high roughness. The simulations were performed with irregular waves with a significant wave height H_{m0} ranging from 0.04 to 0.24 m (prototype 1.4 to 8.6 m) and with peak periods T_p from 1.3 to 3.2 s (prototype 7.9 to 19.2 s). Five different water levels h_r were used with h_r defined relative to the level of the reef crest (at 0.7 m above the flume bottom). One run lasted one hour in which a 30 minute TMA type wave spectrum (gamma=3.3) was sent out by the wave generator. The rest of the time was for spin up of the flume and to let all the waves dampen out in the end.

In the table below the complete program for the runs for the hydrodynamic part of the project is shown. All runs will be performed with and without bottom roughness, so there are 32 runs in total. The conditions are target conditions and the actual, measured conditions may deviate.

Table 7.1 Overview of runs for the hydrodynamic part of the experiments. All runs are performed with smooth and rough bottom.

Run	h_r [m]	H_{m0} [m]	T_p [s]	Info
1	0.04	0.04	2.26	6 runs with varying offshore significant wave height H_{m0}
2	0.04	0.08	2.26	
3	0.04	0.12	2.26	
4	0.04	0.16	2.26	
5	0.04	0.20	2.26	
6	0.04	0.24	2.26	
7	0.04	0.08	1.31	2 runs with varying peak period T_p
8	0.04	0.08	3.20	
9	0.00	0.08	2.26	4 runs with varying water depth h_r and H_{m0}=0.08 m
10	0.02	0.08	2.26	
11	0.06	0.08	2.26	
12	0.09	0.08	2.26	
13	0.00	0.16	2.26	4 runs with varying water depth h_r and H_{m0}=0.16 m
14	0.02	0.16	2.26	
15	0.06	0.16	2.26	
16	0.09	0.16	2.26	

The second part of the project focused on sediment transport. Tests were performed with the same wave conditions and two different water depths on the reef; 0.05m and 0.1m (prototype 0.75 and 1.5 m). One wave condition was used with a significant wave height H_{m0} of 0.2 m (prototype 3 m) and a peak period T_p of 3.2 s (prototype 12.4 s). The wave generator was set such that it generated ten minute wave spectra and the total duration per condition was 7 hours to get significant morphological development. The ten minute spectra enabled us to create vertical suspended sediment concentration distributions by moving the measurement devices up and down as explained further below. Each run was interrupted twice to let the profiler measure the profile of the sandy part. Profiling was done before each run and after 1, 3, and 7 hours. Both wave conditions were applied for a rough and a smooth bed, so 4 runs in total. The conditions for the runs with sediment are summarised in the table below.

Table 7.2 Overview of run ID's for sediment transport part of experiment

Bed	**depth on reef(h_r): 0.1 m**	**depth on reef(h_r): 0.05 m**
rough	S01	S02
smooth	S03	S04
Target condition for all runs: H_{m0}=0.2m; T_p=3.2s		

Because of the profiling interruptions each run consists of 3 parts. The first hour is referred to as part **a**, hour 2-3 is part **b** and hour 4-7 is part **c** (e.g. S01a, S03c).

C Concentration measurements

Below an overview is presented of the concentration time series measured by the FOSLIMs to investigate the background concentration in the signals. This background concentration has been subtracted for the analyses in the main report (section 4.2) and for comparison the mean concentrations and Rouse number are presented without subtraction of the background concentration.

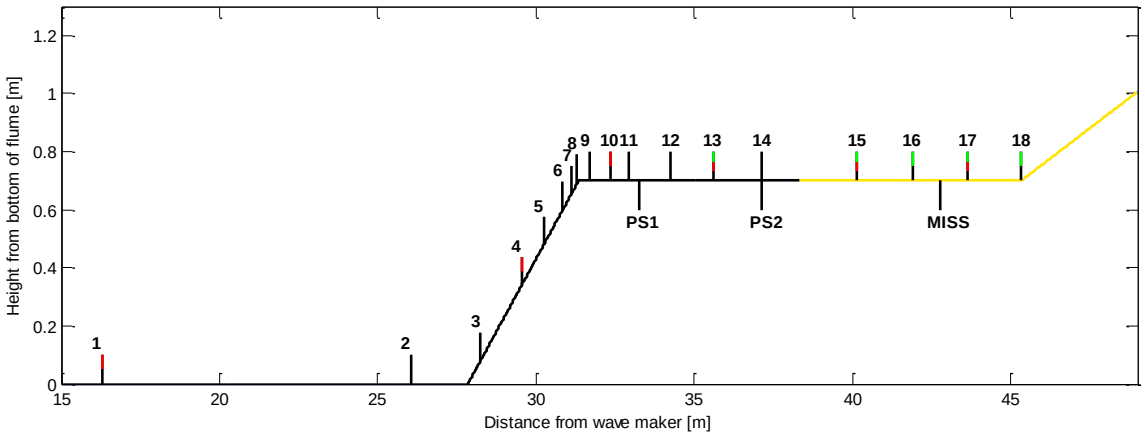

Figure 7.7 Overview of measurement locations. black line: WHM; red line: EMS; green line: FOSLIM; PS1 and PS2 indicate the location of point samplers 1 and 2 and MISS indicates the location of the multiple inlet suction sampler.

Overview of FOSLIM concentration time series per simulation:

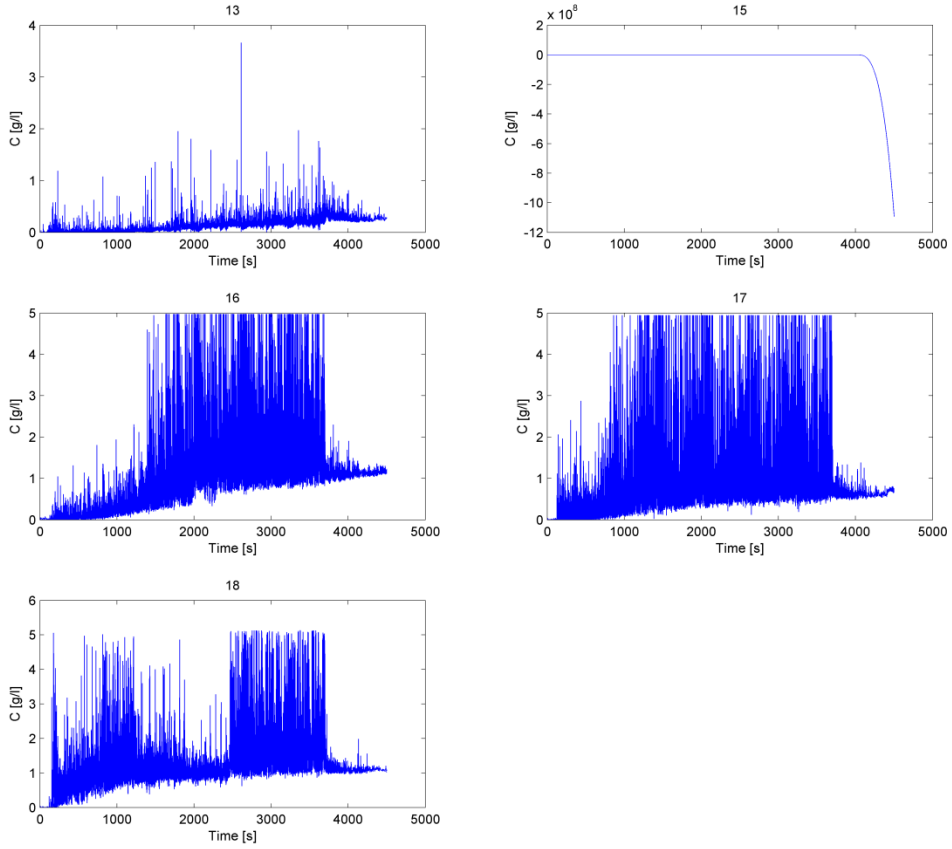

Figure 7.8 Time series of FOSLIM concentration measurements at all locations for simulation S01a

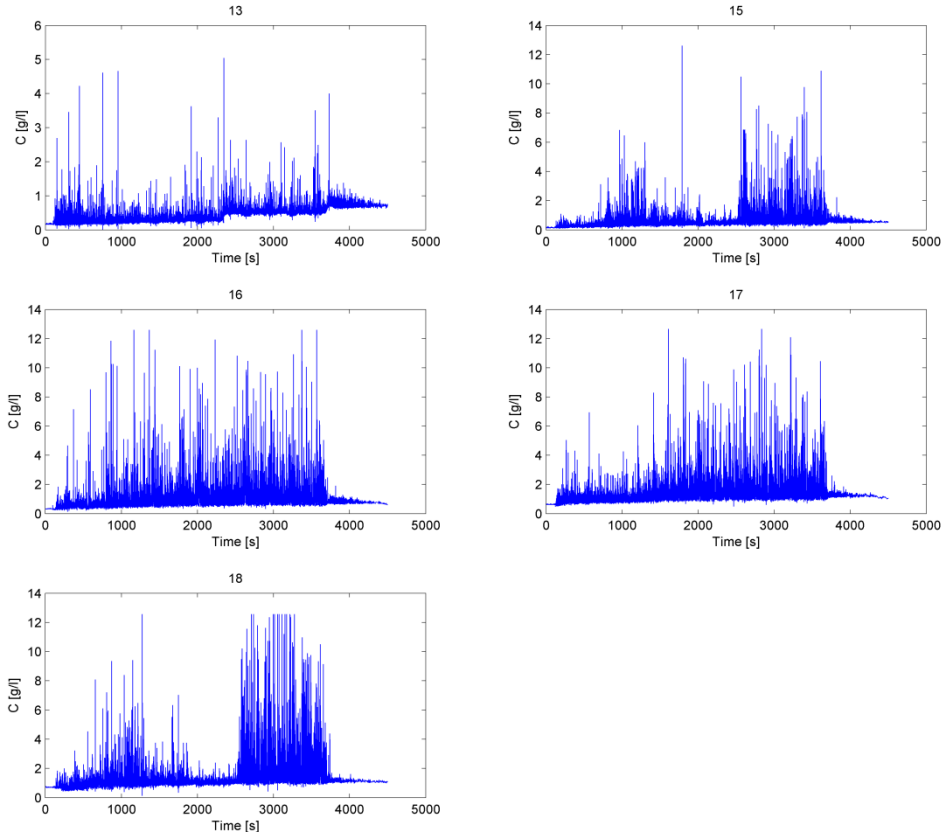

Figure 7.9 Time series of FOSLIM concentration measurements at all locations for simulation S02a

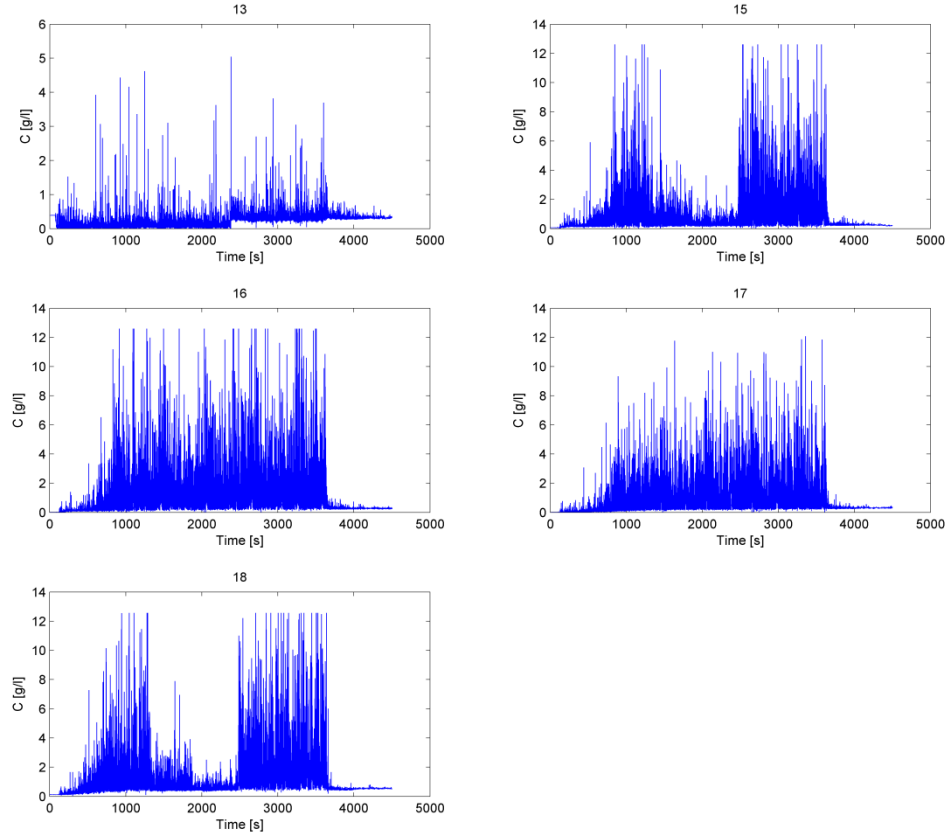

Figure 7.10 Time series of FOSLIM concentration measurements at all locations for simulation S03a

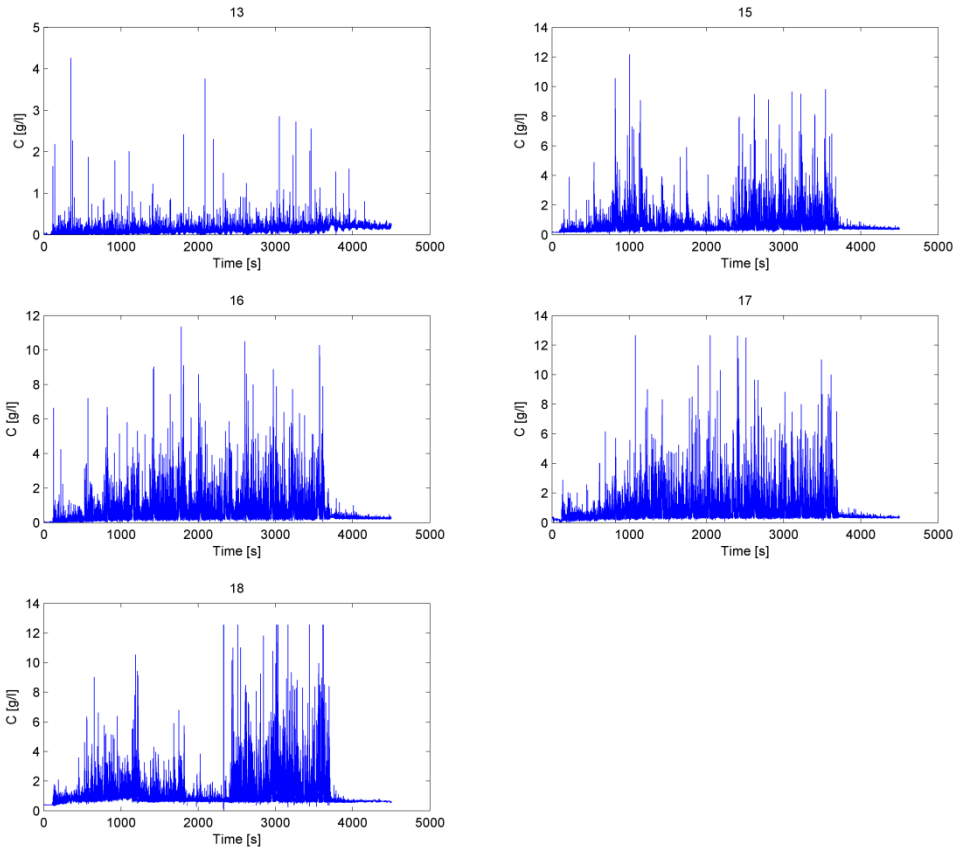

Figure 7.11 Time series of FOSLIM concentration measurements at all locations for simulation S04a

Mean FOSLIM concentrations without compensation for the background concentration:

Table 7.3 Mean measured concentrations with FOSLIMs per part of each simulation at 2 cm above the bed. ***With background concentration included.*** *Concentrations in g/l. (* FOSLIM malfunctioned during run)*

S01	**Location**						**S02**	**Location**				
Part	13	15	16	17	18		**Part**	13	15	16	17	18
a	0.11	*	1.03	0.89	1.14		**a**	0.41	0.54	0.93	1.27	1.02
b	0.31	1.24	1.52	1.4	1.94		**b**	0.61	0.69	0.98	1.25	1.37
c	0.31	1.29	1.21	1.54	1.88		**c**	0.08	0.51	0.63	0.65	0.7
Mean	**0.24**	**1.27**	**1.25**	**1.28**	**1.65**		**Mean**	**0.37**	**0.58**	**0.85**	**1.06**	**1.03**
Mean concentrations in g/l												
S03	**Location**						**S04**	**Location**				
Part	13	15	16	17	18		**Part**	13	15	16	17	18
a	0.18	1.08	0.99	0.76	1.35		**a**	0.1	0.77	0.55	0.74	1.16
b	0.39	1.34	1.37	1.22	2.18		**b**	0.52	0.75	0.8	0.96	0.99
c	0.81	1.33	1.13	1.18	1.61		**c**	1.35	0.75	0.91	0.96	1.36
d	1.19	1.30	1	1.41	1.74							
Mean	**0.64**	**1.26**	**1.12**	**1.14**	**1.72**		**Mean**	**0.66**	**0.76**	**0.75**	**0.89**	**1.17**

Table 7.4 Concentrations measured with the point suction sampler at 2 cm above the bed. PS1 was placed at x=33.26 m, PS2 at location 14 (x=37.14 m) and FOSLIM 13 at x=35.59 m. Concentrations in g/l.

	S01		**S02**		**S03**		**S04**	
part of simulation	PS1	PS2	PS1	PS2	PS1	PS2	PS1	PS2
a	0.01	0.02	0.02	0.04	0.01	0.05	0.00	0.05
b	0.03	0.07	0.01	0.09	0.02	0.09	0.03	0.04
c	0.3	-	0.01	0.06	0.06	0.18	0.02	0.12
d					0.07	0.20		
mean point samplers	**0.11**	**0.05**	**0.01**	**0.06**	**0.04**	**0.13**	**0.02**	**0.08**
mean FOSLIM 13	**0.24**		**0.37**		**0.64**		**0.66**	

Rouse numbers without compensation for background concentration:

Table 7.5 Rouse numbers $Z = \frac{w_s}{\kappa u_{*,w}}$ from sample concentration profiles (s1, s2, s3) and for FOSLIM concentration profiles (f15, f18). The bottom row of each simulation indicates the type of transport related to the Rouse number.

s01	**S1**	**S2**	**F15**	**F18**		**s02**	**S1**	**S2**	**S3**	**F15**	**F18**
a	1.37		0.87	0.11		**a**	1.26	1.27		0.14	0
b	0.93	1.12	0.56	0.55		**b**	1.39	1.39		0.33	0.43
c			0.53	0.52		**c**	1.38	0.9	1.07	0.45	0.53
mean	1.14		0.65	0.39		**mean**	1.24			0.31	0.32
cat.	**s100**		**wash**	**wash**		**cat.**	**s50**			**wash**	**wash**
s03	**S1**	**S2**	**F15**	**F18**		**s04**	**S1**	**S2**	**S3**	**F15**	**F18**
a	1.48		0.84	0.65		**a**	1.04	1.38		0.32	0.25
b	1.64		0.99	0.87		**b**	1.07	0.91		0.34	0.41
c	0.98	1.44	0.91	1.03		**c**	1.03	2.13	1.11	0.36	0.52
d	1.13	1.31	0.75	0.89							
mean	1.33		0.87	0.86		**mean**	1.24			0.34	0.39
cat.	**s50**		**s100**	**s100**		**cat.**	**s50**			**wash**	**wash**

D Flow velocity moments without VLF motions

The plots below show the development of the components of the time-varying part of the third order velocity moment where the VLF motions(0<f<0.035 Hz) were filtered out of the velocity signal. The VLF motions include seiching and a short wave forcing related motion.

These plots were compared to Figure 4.8 and show that without the VLF motions the gull contribution becomes smaller, particularly at the data points at x=37.14 and x=41.88. Also the guls contribution decreases slightly.

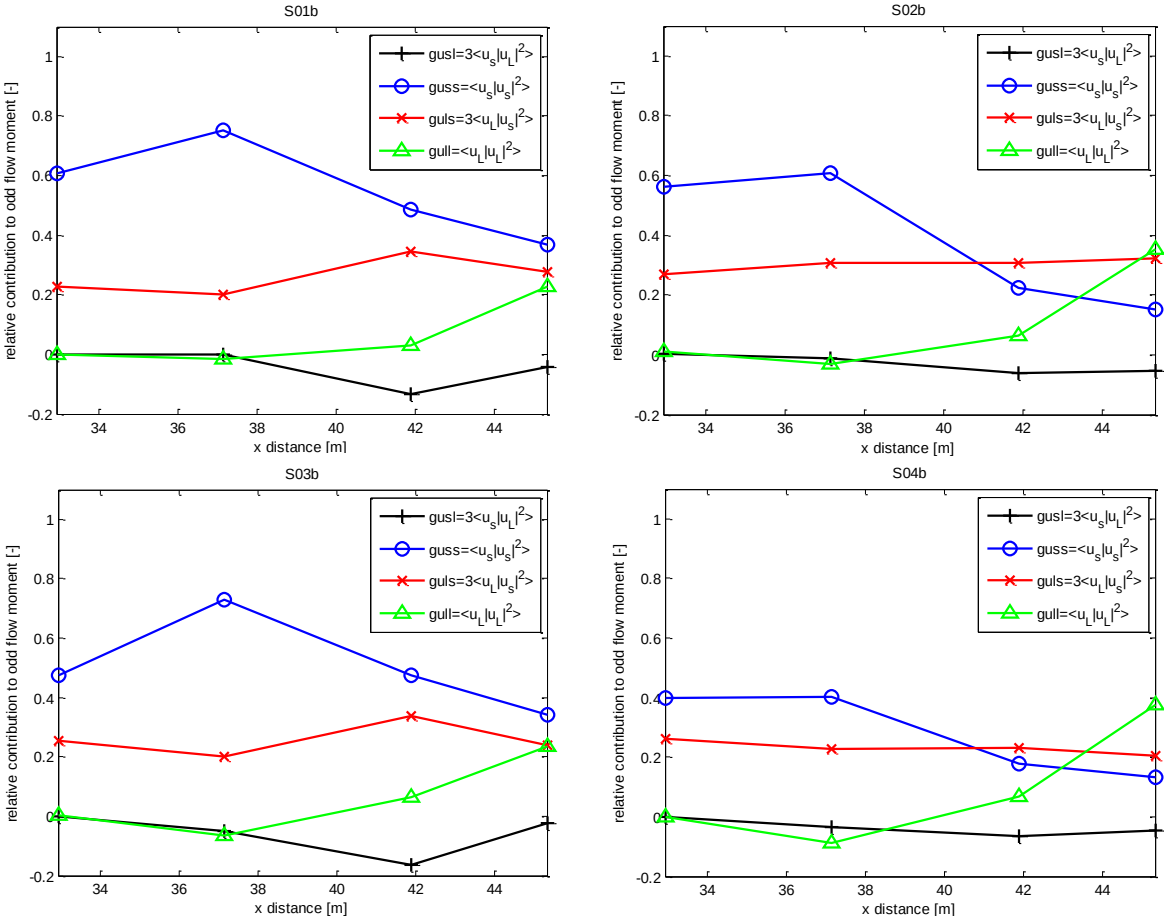

Figure 7.12 Relative contribution as fraction of the total of each of the four components (guss, guls, gusl, gull) to the total third order velocity moment and the evolution over the reef. The VLF motions as described in the report(seiching and short wave forced motion) are filtered out of the velocity signal.

E XBeach model description

For the description of the XBeach model the manual by Roelvink et al. (2010) and the article by Roelvink et al. (2009) are used as a reference. For a more detailed description of the model one is referred to these publications.

General
XBeach is a 2D horizontal model solving the equations for wave propagation, flow, sediment transport and bottom changes for various boundary conditions. The model is wave-group averaged taking into account the variation of short wave energy in time to obtained the long wave motions forced by this variation. This is referred to as 'surf beat' as it was already long know by surfers. The surf beat is thought to be one of the dominant factors causing dune erosion, overtopping and overwash as it is responsible for most of the swash waves that hit the dunes. The desire to model these processes correctly is what lead to the development of the XBeach model.

Coordinate system and grid setup
In the XBeach coordinate system the computational x-axis is always perpendicular to the coast and the y-axis is in alongshore direction. It is possible to relate the grid to real world coordinates by defining the position and the orientation of the origin. The grid size in both directions may vary but the grid has to be rectilinear.

XBeach uses a staggered grid with the bed levels, water levels, water depths and concentrations defined in the cell centres, and the velocities and transports defined at the cell interfaces.

Short wave action balance
The short wave forcing in the shallow water momentum equation is calculated from a time dependent version of the wave action balance equation:

$$\frac{\partial A}{\partial t}+\frac{\partial c_x A}{\partial x}+\frac{\partial c_y A}{\partial y}+\frac{\partial c_\theta A}{\partial \theta}=-\frac{D_w}{\sigma}$$

With the wave action:

$$A(x,y,t,\theta)=\frac{S_w(x,y,t,\theta)}{\sigma(x,y,t,\theta)}$$

Where S_w represents the wave energy density, σ the intrinsic wave frequency, D_w is the wave energy dissipation due to wave breaking and c_x, c_y and c_θ the wave group velocity in x-, y- and θ-direction.

The group velocity in x- and y-direction is defined as $c_x = c_g \cos(\theta) + u_L$ and $c_y = c_g \sin(\theta) + v_L$ where u_L and v_L are the cross-shore and alongshore depth-averaged Lagrangian velocities respectively and the wave group velocity is calculated according to linear wave theory.

The wave energy due to breaking, D_w, is by default modelled according to Roelvink (1993) as cited in the XBeach manual (Roelvink et al., 2010) as follows:

$$D_w = \frac{2\alpha}{T_{rep}} Q_b E_w \frac{H_{rms}}{h}$$

Where Q_b is the fraction of breaking wave, defined as:

$$Q_b = 1 - \exp\left(-\left(\frac{H_{rms}}{H_{max}}\right)^n\right), H = \sqrt{\frac{8E_w}{\rho g}}, H_{max} = \frac{\gamma \tanh kh}{k}$$

And α is O(1), T_{rep} is a representative wave period e.g. the peak period, E_w is the total wave energy, n is a shape parameter, γ the breaker index and h the local water depth. The term $\frac{H_{rms}}{h}$ is a slight adaptation of the original formulation to apply the original energy dissipation formulation that follows from bore analogy (Van Thiel de Vries, 2009).

In the wave action balance a term D_f for bed friction related dissipation of short wave energy can be included. This term is calculated as:

$$D_f = \frac{2}{3}\rho\pi f_w \left(\frac{\pi H}{T_{rep} \sinh kh}\right)^3$$

Where f_w is the wave friction factor which should be selected according to the bed roughness. Typical values for the wave friction factor are 0.03 for a sandy bed and 0.3-0.6 for a rough coral reef bed.

Roller energy balance

The wave action balance is coupled to a roller energy balance where dissipation of wave energy D_w serves as a source term for the roller energy balance. The balance for the roller energy E_r is given by:

$$\frac{\partial S_r}{\partial t} + \frac{c_x S_r}{\partial x} + \frac{c_y S_r}{\partial y} + \frac{c_\theta S_r}{\partial \theta} = -D_r + D_w$$

D_r is the total roller energy dissipation modelled as:

$$\overline{D}_r = 2g\beta_r E_r / c$$

The total roller energy is distributed over the wave directions:

$$D_r(x,y,t,\theta) = \frac{S_r(x,y,t,\theta)}{E_r(x,y,t,\theta)} \overline{D}_r(x,y,t)$$

Both the rollers and the short waves contribute to the radiation stress.

$$S_{xx,w}(x,y,t) = \int \left(n(1+\cos^2\theta) - \frac{1}{2}\right) S_w d\theta$$

$$S_{xy,w} = S_{yx,w} = \int \sin\theta \cos\theta \, (nS_w) d\theta$$

$$S_{yy,w}(x,y,t) = \int \left(n(1+\sin^2\theta) - \frac{1}{2}\right) S_w d\theta$$

Where $n = \frac{c_g}{c}$, and:

$$S_{xx,r}(x,y,t) = \int \cos^2\theta \, S_r d\theta$$

$$S_{xy,r} = S_{yx,r} = \int \sin\theta \cos\theta \, S_r d\theta$$

$$S_{yy,r}(x,y,t) = \int \sin^2\theta \, S_r d\theta$$

Both radiation stress contribution are added to calculate the wave forcing using the radiation stress tensor:

$$F_x(x,y,t) = -\left(\frac{\partial S_{xx,w} + \partial S_{xx,r}}{\partial x} + \frac{\partial S_{xy,w} + \partial S_{xy,r}}{\partial y}\right)$$
$$F_y(x,y,t) = -\left(\frac{\partial S_{xy,w} + \partial S_{xy,r}}{\partial x} + \frac{\partial S_{yy,w} + \partial S_{yy,r}}{\partial y}\right)$$

Shallow water equations

For the low-frequency and mean flows the shallow water equations are used. These are expressed in the form of a depth-averaged Generalised Lagrangian Mean (GLM) formulation to account for wave induced mass flux and subsequent (return) flow. This means that the momentum and continuity equations are expressed in terms of the Lagrangian velocity, u_L, which is defined as the distance a water particle travels in one wave period, divided by that period. The Lagrangian velocity is related to the Eulerian velocity, the short-wave-averaged velocity observed at a fixed point, by: $u^L = u^E + u^S$ and $v^L = v^E + v^S$.

u_S and v_S represent the Stokes drift which is defined as: $u^S = \frac{E_w \cos\theta}{\rho hc}$ and $v^S = \frac{E_w \sin\theta}{\rho hc}$. The momentum and continuity equations take the following form:

$$\frac{\partial u^L}{\partial t} + u^L\frac{\partial u^L}{\partial x} + v^L\frac{\partial u^L}{\partial y} - fv^L - \nu_h\left(\frac{\partial^2 u^L}{\partial x^2} + \frac{\partial^2 u^L}{\partial y^2}\right) = \frac{\tau_{sx}}{\rho h} - \frac{\tau_{bx}^E}{\rho h} - g\frac{\partial \eta}{\partial x} + \frac{F_x}{\rho h}$$

$$\frac{\partial v^L}{\partial t} + u^L\frac{\partial v^L}{\partial x} + v^L\frac{\partial v^L}{\partial y} + fu^L - \nu_h\left(\frac{\partial^2 v^L}{\partial x^2} + \frac{\partial^2 v^L}{\partial y^2}\right) = \frac{\tau_{sy}}{\rho h} - \frac{\tau_{by}^E}{\rho h} - g\frac{\partial \eta}{\partial y} + \frac{F_y}{\rho h}$$

$$\frac{\partial \eta}{\partial t} + \frac{\partial hu^L}{\partial x} + \frac{\partial hv^L}{\partial y} = 0$$

η is the water level, ν_h is the horizontal viscosity, f is the Coriolis coefficient and τ_s and τ_b are the surface and bed shear stresses respectively. The bed shear stress is calculated using the Eulerian velocity, u^E, as experienced by the bed and not the GLM velocity.

Flow friction

Besides the friction by waves, XBeach also includes bottom friction on the flow through the parameter τ_{bx}^E in the shallow water equations. The value of τ is computed according to the approach of Ruessink et al. (2001):

$$\tau = C_f \rho u_E \sqrt{(1.16 u_{rms})^2 + \bar{v}^2}$$

Where C_f is the flow friction factor, u_E is the local Eulerian velocity, u_{rms} is the local orbital velocity and $\bar{v}$ is viscosity.

Sediment transport

The sediment transport in XBeach is modelled with a depth-averaged advection diffusion equation by Galappatti (1983) as cited in Van Thiel de Vries (2009):

$$\frac{\partial hC}{\partial t} + \frac{\partial hC(u^E + u_A \sin\theta_m)}{\partial x} + \frac{\partial hC(v^E + u_A \cos\theta_m)}{\partial y} + \frac{\partial}{\partial x}\left[D_h h \frac{\partial C}{\partial x}\right] + \frac{\partial}{\partial y}\left[D_h h \frac{\partial C}{\partial y}\right] = \frac{hc_{eq} - hC}{T_s}$$

In this formulation h is the water depth, C is the depth-averaged concentration, u_A is a flow velocity related to wave nonlinearity, θ_m is the mean wave direction of incoming waves and T_s is an adaptation time scale for sediment entrainment so that it adapts gradually to changing hydraulic conditions. The time scale is given by an expression containing the local water depth and the sediment fall velocity w_s:

$$T_s = \max\left(0.05\frac{h}{w_s}, T_{s,min}\right)$$

Where $T_{s,min}$ is a user specified minimum adaptation time with a default value of 1 second. The value of T_s becomes small in shallow water which means that the sediment will respond almost instantaneously to changing hydrodynamics. The entrainment of sediment is determined by the mismatch between the actual concentration C and the equilibrium concentration c_{eq}. The equilibrium concentration is calculated with the transport formulation of Van Rijn (2007) which has been extended with near-bed turbulence (Van Thiel de Vries, 2009):

$$c_{eq} = \frac{A_{sb}}{h}\left(\sqrt{\gamma_{flow}u^2 + \gamma_{wave}u_{rms,2}^2} - u_{cr}\right)^{1.5} + \frac{A_{ss}}{h}\left(\sqrt{\gamma_{flow}u^2 + \gamma_{wave}u_{rms,2}^2} - u_{cr}\right)^{2.4}$$

Where A_{sb} and A_{ss} are a bed load and a suspended load coefficient respectively:

$$A_{sb} = \frac{0.015h\rho_s\left(\frac{D_{50}}{h}\right)^{1.2}}{\left((s-1)gD_{50}\right)^{0.75}}$$

$$A_{sb} = \frac{0.012D_{50}\rho_s D_*^{-0.6}}{\left((s-1)gD_{50}\right)^{1.2}}$$

ρ_s is the mass density of sand, D_{50} is the median grain size diameter, D_* is a dimensionless particle size, s is the relative density and in the first equation u is the wave averaged flow, $u_{rms,2}$ is the near-bed wave orbital flow velocity including turbulence ($u_{rms,2} = (u_{rms}^2 + \gamma_{turb}k_b)^{0.5}$ and u_{cr} is the critical flow velocity defined as $u_{cr} = \alpha u_{cr,c} + (1-\alpha)u_{cr,w}$, where $u_{cr,c}$ is the critical flow velocity for steady flows based on Shields and $u_{cr,w}$ is the critical flow velocity for waves following Komar and Miller (1975). α is a weighting coefficient: $u/(u + u_{rms,2}$. k_b is the near-bed turbulence intensity which can be determined with a wave-averaged or a bore-averaged approach.

In the formulation there are three free parameters, namely γ_{flow}, γ_{wave} and γ_{turb}. It was proposed by Van Rijn (2007) to use $\gamma_{flow} = 1$ and $\gamma_{wave} = 0.64$ for irregular waves and 2.56 for regular waves. XBeach is set up with a value of 0.64 since random waves are considered and with $\gamma_{turb} = 1.45$ for the bore-averaged turbulence model and $\gamma_{turb} = 12.4$ for the wave-averaged turbulence model showing that the former model is much more efficient in producing large sediment suspensions (Van Thiel de Vries, 2009). The final transport formulation in XBeach becomes:

$$c_{eq} = \frac{A_{sb}}{h}\left(\sqrt{(u^E)^2 + 0.64u_{rms,2}^2} - u_{cr}\right)^{1.5} + \frac{A_{ss}}{h}\left(\sqrt{(u^E)^2 + 0.64u_{rms,2}^2} - u_{cr}\right)^{2.4}$$

Where u^E is the Eulerian flow velocity.

Bed level change
Gradients in the sediment transport are the main driver for bed level change in the wet area according to:

$$\frac{\partial z_b}{\partial t} = \frac{1}{1-p}\left(\frac{\partial S_x}{\partial x} + \frac{\partial S_y}{\partial x}\right)\gamma_{morf}$$

where p is porosity, γ_{morf} is the morphological multiplication factor for bed level changes and S_x and S_y are computed sediment transport in cross-shore (x) and alongshore direction (y):

$$S_x = hC(u^E + u_A \sin\theta_m) + \frac{\partial}{\partial x}\left(D_h h \frac{\partial C}{\partial x}\right)$$

$$S_y = hC(v^E + u_A \sin\theta_m) + \frac{\partial}{\partial y}\left(D_h h \frac{\partial C}{\partial y}\right)$$

D_h is a sediment diffusion coefficient defined as $D_h = \gamma_{visc}\nu_h$, where γ_{visc} is a calibration factor (default value 1) and ν_h is the horizontal viscosity.

Besides this slumping of the dune or beach face and associated sediment supply is accounted for by an avalanching algorithm, which depends on the exceeding of a critical bed slope:

$$\left|\frac{\partial z_b}{\partial x}\right| > m_{cr}$$

A different value of the critical slope is used for dry and wet areas.

F Recommendations for improvements of XBeach

- **Long wave height mismatch between model and data at offshore boundary:** Measured time series of long wave height were used as boundary condition for the XBeach model. However, analysis of the XBeach results showed that the long wave height at the boundary in XBeach, did not match the measured long wave height at that location for the cases S01, S02 and S04, while it should be an exact match. For case S03 there is an exact match between XBeach and the data at the boundary. It is unclear what causes the mismatch in the other cases, but it might be related to the pre- and post-processing of flow velocity and wave height time series, e.g. the separation into long and short and incoming and reflected waves.

- **Transfer of energy towards long waves before reef slope:**
  The long wave height in XBeach was observed to increase in the region from the boundary until the reef slope. This implies that there is transfer of energy to the long waves, which is not present in the experiment data. The energy transfer is possibly related to the use of measured long wave height and short wave energy time series as a boundary condition. In XBeach the propagation of these two parameters is computed in two different equations which could lead to a small mismatch between the two in such a way that the resulting phase difference induces transfer of energy from the short waves to the long waves.

- **Reef flat seiching:**
  The XBeach model showed a dependency of the magnitude of seiching on bed roughness and water depth, which was not in agreement with the data. In case S01 the effect of bed roughness on the magnitude of seiching was negligible, while in XBeach the seiching is strongly reduced compared to the smooth case S03. Also the seiching in case S04 in XBeach is less strong than in case S03, while in the experiments the opposite was observed.

- **Sediment transport formulation:**
  It was discussed in detail in section 5.4 that the amount of suspension of sediment using the default transport formulation is too small compared to the data.

- **Beach profile development:**
  The beach profile development was not predicted correctly in XBeach. Recommendations to improve this were also provided in chapter 5.

- **XBeach crashes when water level on reef is too low:**
  It was found that lowering the water level on the reef to approximately 1 cm eventually led XBeach to crash. That is why case S02 was not taken into account in the analysis of the XBeach results.

- **Breaker model:**
  It was not possible to get the short wave height transformation completely correct in XBeach using the Daly/Roelvink breaker model. Which could be related to the fact that the breaker model was developed for spilling breakers. To model the plunging breakers of a fringing reef, it is recommended to developed a breaker model for

plunging waves. Additionally, in the Daly/Roelvink model the influence of the gamma2 parameter was not clear, see Figure 5.3.

- **Artificial lowering of water level offshore:**
  The experiments were performed in a flume so a water level increase on the reef, led to a lowered water level offshore because of continuity. In XBeach the water level offshore is maintained constant and extra water is supplied to the model in order to achieve the water level set-up on the reef. To model the water levels offshore correctly, it had to be lowered manually to the mean water level that was measured.

- **Setting of parameter *hmin*:**
  It was found that in order to model the set-up in a scaled model correctly it is necessary to select a sufficiently low value for the parameter *hmin*.